INVESTIGATION ON DYNAMIC PULSE BUCKLING AND DAMAGE BEHAVIOR OF COMPOSITE LAMINATED BEAMS SUBJECT TO AXIAL IMPULSE

by

ZHENG ZHANG

Submitted
in Partial Fulfillment of the Requirements
for the Degree of

Doctor of Philosophy

Major Subject: Civil Engineering

At

DALHOUSIE UNIVERSITY

Halifax, Nova Scotia 2003

Your file Votre référence
ISBN: 0-612-89103-8
Our file Notre référence
ISBN: 0-612-89103-8

DALHOUSIE UNIVERSITY
FACULTY OF ENGINEERING

The undersigned hereby certify that they have examined, and recommend to the Faculty of Graduate Studies for acceptance, the thesis entitled "Investigation on Dynamic Pulse buckling and Damage Behavior of Composite Laminated Beams subject to Axial Impulse" by Zheng Zhang in partial fulfillment of the requirements for the degree of Doctor of Philosophy.

Dated: Oct 10/03

Dr. Farid Taheri, Supervisor

Dr. Neil Pegg, Supervisory committee member

Dr. Gordon Fenton, Supervisory committee member

Dr. Rajamohan Ganesan, External Examiner
Concordia University

DALHOUSIE UNIVERSITY

FACULTY OF ENGINEERING

Dated: Oct. 10. 2003

AUTHOR: Zheng Zhang

TITLE: Investigation on dynamic pulse buckling and damage behavior of composite laminated beams subject to axial impulse

MAJOR SUBJECT: Civil Engineering

DEGREE: Doctor of Philosophy

CONVOCATION: May, 2004

TABLE OF CONTENTS

Page

List of Tables

List of Figures

List of Symbols and Abbreviations

Latin Alphabet

a	length of delamination
A_i	intermediate constants for finite difference method
A	laminate stiffness matrix
b	beam width
$[B]$	laminate stiffness matrix
B_i	intermediate constants for finite difference method
c	wave propagation velocity along the beam length
C	laminate stiffness matrix
C_i	intermediate constants for finite difference method
C_L	damping factor in axial direction of beam,
C_T	damping factor in lateral direction of beam,
C_R	damping factor in rotational (cross section) direction of beam
D	laminate stiffness matrix
E_{11}	elastic modulus in longitudinal direction
E_{22}	elastic modulus in transverse direction
E	laminate stiffness matrix
$F(t)$	impulse force
F_d	failure index of delamination
F_f^T	failure index of fiber in tension mode
F_f^C	failure index of fiber in compressive mode
F	laminate stiffness matrix
FDM	finite difference method
FRP	fiber-reinforced plastics
FS	fixed-end support
FSDT	first-order shear deformation theory
G_{12}	in-plane shear modulus
G_I	mode I strain energy release rate
G_{IC}	mode I critical strain energy release rate
G_{II}	mode II strain energy release rate
G_{IIC}	mode II critical strain energy release rate
G	laminates stiffness matrix
h	thickness of beam
h_s	thickness of upper delaminated region
h_m	thickness of lower delaminated ergion
H	laminate stiffness matrix

HSDT	higher-order shear deformation theory
I	principal moment of inertia or second moment of area
I_1	translational inertia per unit beam width
I_2	rotaional inertia per unit beam width
I_d	delamination index
K_I	mode I stress intensity factor
K_{II}	mode II stress intensity factor
L	beam length
M	mass of impactor
N_x	axial force per unit beam width
M_x	bending moment per unit beam width
M^*	linear combinations of moments from delaminated legs of beam
PS	pinned-end support
$\overline{Q}_{ij}$	transformer stiffnness terms
V	shear force per unit beam width across the section of beam
VCCT	virtual crack closure technique
n	layers
P	axial compressive force
P^*	linear combination of load from delaminated legs of beam
P_c	critical static Euler load
q_n	fourier coefficients of motion equation
SEM	scanning electron microscopy
S_L^+	longitudinal tensile strength
S_L^-	longitudinal compressive strength
S_{LT}	in-plane shear strength
S_T^+	transverse tensile strength
S_T^-	transverse compressive strength
S_{TL}	through-the-thickness shear strength
t	time
u	axial displacement of beam
$\overline{u}$	non-dimensional axial displacement of the beam
w	lateral displacement of the beam
$\overline{w}$	non-dimensional lateral displacement of the beam
U	displacement of impactor
V_o	initial velocity of impactor
$w_0(x)$	initial geometric imperfection
W_0	magnitude of initial geometric imperfection
x	axial coordinate
$\overline{x}$	non-dimensional axial coordinate
y	transverse deflection of the beam
y_o	initial geometric imperfection

z	coordinate axis through beam thickness

Greek Symbols

σ_x	axial stress of each lamina
τ	non-dimensional time
τ_{xy}	shear stress in each lamina
τ_{xz}	inter-laminar shear stress
$\Delta\tau$	non-dimensional time step
ε_x	axial strain of each lamina
γ_{12}	Poisson ratio
γ_{xz}	inter-laminar shear strain
θ	rotation of cross section of beam
$\bar{\theta}$	non-dimensional rotation of cross section of beam
θ_x	rotation of normal about y-axis
θ_y	rotation of normal about x-axis
ρ	mass density of the lamina.
$\Delta\bar{x}$	non-dimensional discretized segment length
ξ	damping coefficinet
ω	natrual frequency
ψ_I	mode I partitioning factor for work done by moment
ψ_{II}	mode II partitioning factor for work done by moment

Acknowledgments

I would like to express my appreciation to my supervisor, Dr. Farid Taheri, professor of Civil Engineering at Dalhousie University, whose knowledge, experience and guidance have been crucial throughout the course of this study. I could always benefit from the discussions I had with Dr. Taheri on various technical issues when I faced a cross-road.

The financial support of NSERC in the form of an operating grant to Dr. Farid Taheri in support of this work is gratefully acknowledged.

I would also thank the technicians of the Civil Engineering Department, Mr. Marc MacDonald and Mr. Balair Nickerson, for their assistances on spcimen preparation and test setup during the experimental investigation period of this work.

Appreciation also goes to the other members of Guiding Committee for their time and interest in reviewing this manuscript.

Lastly, I would thank my wife, Lin, for her great support during my studies.

Abstract

The dynamic behavior, including pulse buckling, damage initiation and delamination growth of slender fiber-reinforced plastic (FRP) laminated beams, having initial geometric imperfections, subjected to an axial impulse was investigated numerically and experimentally.

The dynamic equilibrium equations of slender FRP beams, having initial geometric imperfections were established based on the Timoshenko beam theory, with the consideration of several parameters such as the beam's axial and transverse inertia, transverse shear deformation, and the cross section rotational inertia. The von-Karman nonlinear strain-displacement relationship was used to describe the beam's response. The First-Order and Higher-Order Shear Deformation Theories were used to model the displacement fields of the beams. The dynamic differential equations were solved with the finite difference method. The results obtained from the proposed formulations agree well with those of the finite element analysis.

Pulse buckling, as an instability form (that is, the excessive growth of lateral, or out of plane displacement) can result from a single transient pulse load with a magnitude greater than that of the static Euler buckling load. Several parameters were investigated to assess the effects of initial geometric imperfection, slenderness ratio, curvature and boundary conditions of the beams on its pulse buckling response. A criterion for establishing the onset of the dynamic pulse buckling of the beams was also suggested.

The investigation of dynamic damage behavior of laminated beams was also carried out for understanding the damage initiation mechanism in the beams impacted axially by a moving mass. Hashin's failure criteria was used to predict the likelihood of damage generated in the beams. The experimental work was conducted using a horizontal linear bearing impact setup. Scanning Electron Microscopy was used to analyze the damage mechanism of laminated beams. The influence of fiber angle, lay-up sequence and initial imperfection on the critical energy required for damage initiation was also investigated.

Delamination propagation characteristics of the beam were also investigated numerically and experimentally. Carbon fiber/epoxy specimens with different initial delamination length, located along beams' length and through their thickness, were experimentally tested and numerically analyzed. The strain energy release rate based on the virtual crack closure technique (VCCT) was calculated at the tip of the delaminations. Critical impact energy for delamination growth was predicted numerically as well.

The dynamics pulse-buckling response of carbon/epoxy and E-glass/epoxy laminated composite beams with $[(\pm 67.5)_n]_s$ angle lay-up, subject to axial impact was investigated experimentally and numerically as well. These beams exhibited plasticity like response under axial impact.

1 Introduction

1.1 Overview

In design of engineering structures, three basic criteria must be satisfied. One is the strength criterion, which states that the maximum stresses in the structure must not exceed the allowable stresses under the designated load conditions. The second is the stiffness criterion, which specifies that the maximum deflection of the structure under a specified load case must be lower than that of a specified criterion. This criterion ensures a comfortable and safe feel to the users of the structures, and minimizes undesirable and potentially dangerous behaviors such as fluttering or excessive mechanical vibration, which hinder the normal service. Stability is the third important issue that structural engineers must consider seriously in their design, particularly for thin-walled or slender structural components such as bars, beams, columns, plates and shells, which may fail in some instability mode(s) under compressive load and/or under static or dynamic compressive loading conditions.

The well-known Euler column theory can be used to provide the solution for determining the stability of a slender, perfectly straight and concentrically compressed column with various boundary conditions. For a one end fixed and the other end free column (see Figure 1-1(a)), the smallest critical load causing the member buckling can be determined by

$$P_c = \frac{\pi^2 EI}{4L^2} \tag{1.1}$$

in which E is the elastic modulus, I is the moment inertia of the cross-section and L is the length of the beam. The corresponding buckling mode is shown in Figure 1-1(b).

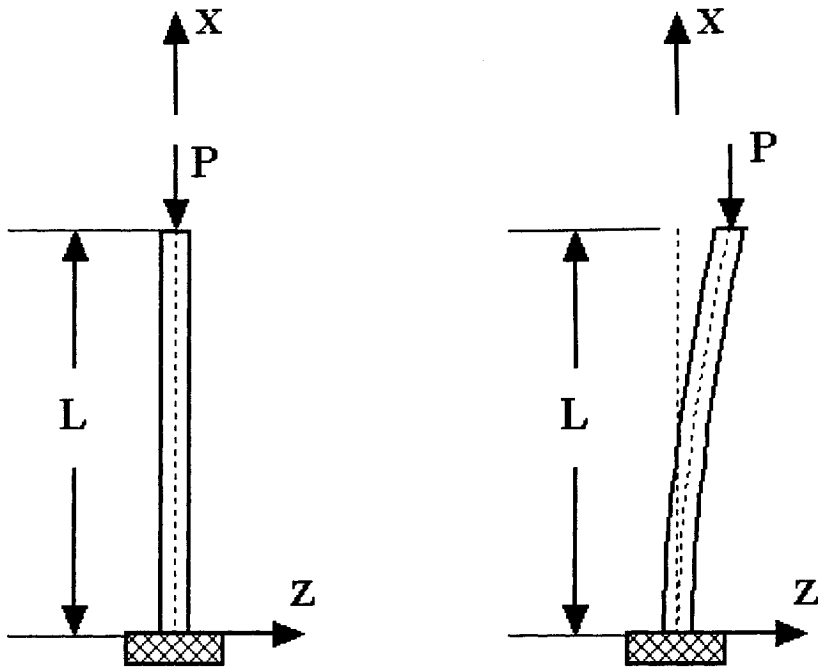

(b)

Figure 1-1 The Euler's column buckling.

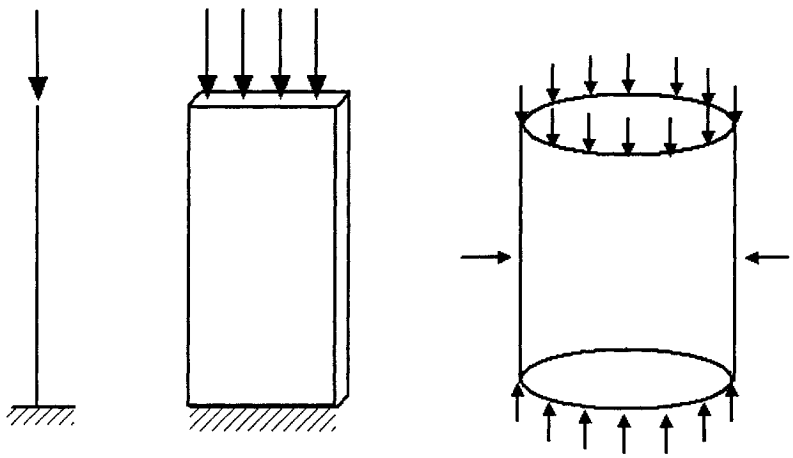

Figure 1-2 Slender and thin-walled structural components may lose their stability under static or dynamic compressive loads.

Thin-walled or slender structural components (Figure 1-2) may lose their stability under static or dynamic load. In the real world, many stability problems are concerned with dynamic loading. For example, airplanes, automobiles and ships have many components that may be subjected to dynamic instability.

Dynamic stability of structures (*i.e.*, dynamic buckling) is a broad topic which includes not only dynamic buckling from oscillatory loads and impact pulse loads, but also those due to the interaction with the media surrounding the structures, such as solid-fluid interaction or fluttering due to wind on tall buildings or on aircraft fuselages. In general, we classify dynamic buckling from oscillatory loads as vibration buckling and dynamic buckling from (transient) impact or pulse loads as dynamic pulse buckling [Lindberg and Florence, 1987].

Vibration buckling, which is defined as unacceptably large vibration amplitudes, is caused by oscillating loads, when the combination of load amplitude, frequency and structural stiffness, mass and damping meet certain criteria for a given structure. Vibration buckling, on the other hand, is caused due to bending moment resulting from an inevitable imperfection. The resonance phenomena, which occurs when the stimulating frequency meets the natural frequency of the structure is well known. But vibration buckling is different from resonant vibration, in that resonant vibration deforms the component in the same direction as the stimulating pulse, however, in vibration buckling, the axial force induces a bending moment and the bending moment in turn causes the lateral deflection of the beam. Figure 1-3(a) is an example of vibration buckling in which a simply supported beam is loaded by an oscillatory force. The critical load of vibration buckling can be either larger or smaller than the Euler buckling load for the same structure, as it depends on the oscillatory frequency and the intrinsic frequency of the structure.

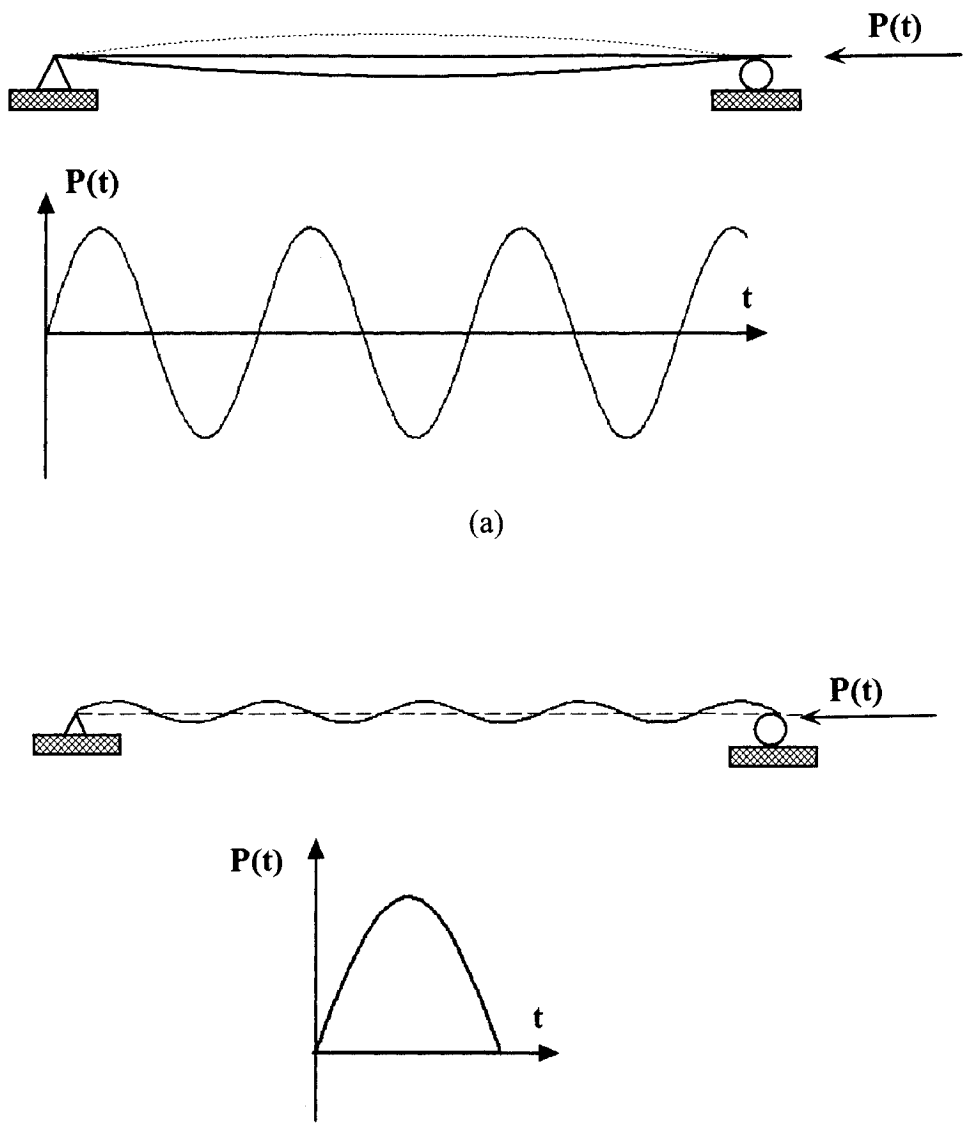

Figure 1-3 Vibration Buckling and Pulse Buckling [Lindberg and Florence, 1987].

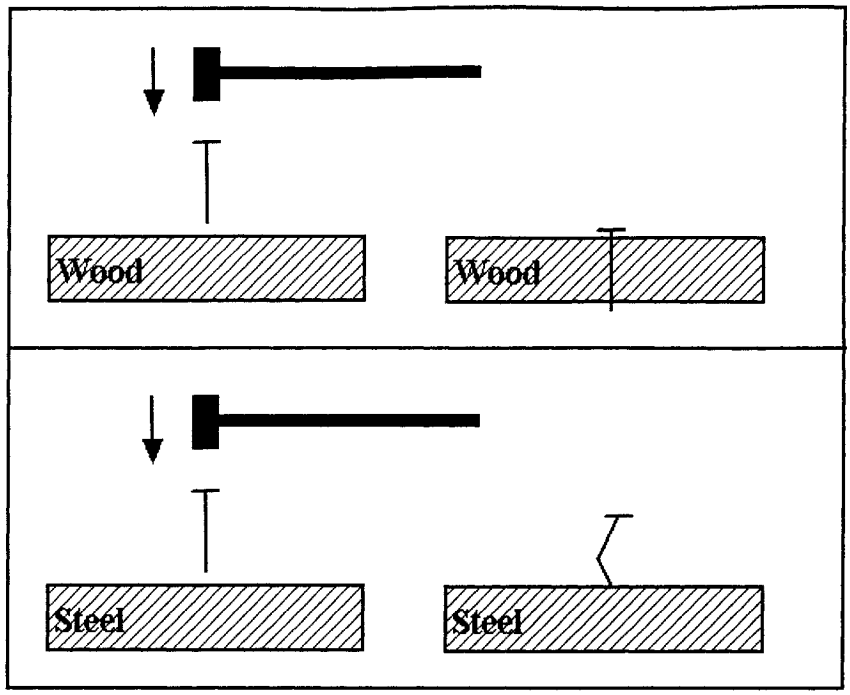

Figure 1-4 A hammer hit a nail and the nail buckled plastically.

Pulse buckling, as an instability phenomenon, that is, the excessive growth of the lateral, or out of plane displacement can result from a transient loading function in the form of a single pulse with a magnitude greater than the static Euler buckling load [Ari-Gur, *et al*, 1982]. A simple example is shown in Figure 1-3(b) that describes a simply supported beam which buckles under pulse load that is much greater than the critical Euler buckling load. The buckling mode depends on the load amplitude, its duration and the intrinsic properties of the beam. Figure 1-3(b) shows a high-order mode caused by a shorter duration, but more intense load. The most simple and easily understood example is that of a hammer impacting a nail, as shown in Figure 1-4. In practical engineering, shock wave from an explosive detonation against a shelled structure (e.g. submarine hull), the force on landing gears of airplanes and crash loads on vehicles are some of the classical examples of impact or pulse loads on structures.

Besides the loading, the component's material significantly also influences the dynamic buckling characteristics.

In the last two decades, due to their high specific strength and stiffness, fiber-reinforced composites have been widely used in industrial applications such as aerospace, automotive, shipbuilding and civil engineering. A large amount of research has been performed on static buckling and post-buckling of composite structures, while relatively less work has been done on their dynamic buckling and post-buckling. On the topic of dynamic buckling and post-buckling, most of the previous works concentrate on vibration buckling of plates/shells (*i.e.*, instability under in-plane periodic loads and transverse periodic loads on cylindrical shells), and some on transverse pulse loads on cylindrical shells [Liaw and Yang, 1991; Balamurugan, *et al*, 1996; Lam and Ng, 1998 for example]. But till now, to the best of author's knowledge, very few works (including analytical, numerical and experimental) have been conducted on investigating pulse buckling and post-buckling behavior of composite laminated slender beams, despite the fact that pulse loads (impact) are very common mode of loading on structures. Although considerable work has been done on pulse buckling characteristics of isotropic structures, because of the difference in response of isotropic and orthotropic materials, the research results on isotropic materials cannot be directly applied to composites. The mechanical properties of fibers, matrix, volume ratios of fibers and matrix, stack sequences, and fiber orientation have significant effects on the response of the laminated composites. To ensure adequate impact resistance, all above factors should be considered when designing thin-walled load bearing composite components.

Initial geometric and material imperfections due to manufacturing and installation of composites are inherent to these materials. They have significant effects on the buckling and damage resistance of composite components.

To investigate the dynamic pulse buckling behavior of laminated composite beams with initial geometric imperfections subject to axial impact, this dissertation will present the details of the analytical and numerical investigation carried out to better understand the behavior of composites.

As stated earlier, composite materials have attracted a wide market in a variety of engineering applications. Their susceptibility to damage resulting from mechanical, physical and chemical factors, however, greatly degrades their stiffness, strength and durability. Impact in particular is one of the main causes of damage in composites, which can cause matrix cracks, laminate delamination and fiber breakage. Often damages generated in FRP (fiber-reinforced plastics) are undetectable to the naked eye, therefore, it is particularly important to understand the damage mechanism (including their initiation and progress) in composite structures. Although a great number of investigations have considered impact characterization of FRP composite materials, most such works [Choi, *et al*,1992; Pavier and Clarke, 2000; Zhou, 1995; Park and Zhou, 2000; Necib and Mili, 2001; Luo, *et al* 2001] have concentrated on the damage due to transversely impacted loads (as the details will be presented in Chapter 5). Only a few works have investigated the response of composite laminates subject to axial or in-plane impact.

Slender, axially loaded structural components are commonly used components found in various structures. These components may easily buckle when subject to static or dynamic loads. Due to manufacturing induced factors, many composite laminates often bear initial imperfections and/or voids. When subjected to axial or in-plane static or dynamic loads, irrespective of occurrence of buckling, such laminates could experience damage, in the form of delamination, fiber breakage and matrix cracking if certain stress or strain components exceed the limiting criterion during the pre- and post-buckling periods. Investigation of damage and damage propagation in laminated composite beams subject to axial impact is another topic of research besides the dynamic pulse buckling

analysis in this dissertation. This dissertation will therefore also investigate the damage behavior of laminated composite beams subject to axial impulse, both numerically and experimentally.

1.2 Organization of this dissertation

The governing equations of motion and their solutions for the beams considered will be presented in Chapter 2. The finite difference solutions of the governing equations based on the first and higher order shear deformation theories will be presented and discussed as well. The state of current literature on dynamic pulse buckling is reviewed and presented in chapter 2.

In Chapter 3, numerical investigations on dynamic pulse buckling and post-buckling of FRP composite laminated beams subject to axial impulse will be discussed. Results obtained by the finite difference method based on the first and higher order shear deformation theories are compared with those of the finite element method. A definition of pulse buckling of beams, a measure for the onset of pulse buckling, stress wave propagation and sensitivity of initial geometric imperfections are discussed, as well.

Chapter 4 presents the details of the experimental program on investigation of dynamic pulse buckling and damage behavior of composite laminated beams subjected to axial impact. Experimental setup, the data acquisition system, specimen preparation and other experimental details are also discussed.

Numerical and experimental investigation of damage initiation of laminated composite beams subject to axial impact will be presented in Chapter 5. The literature on damage analysis of composite materials will be reviewed. Damage criterion and critical energy

for damage initiation as a function of different lay-up sequences will be discussed in that chapter as well.

Chapter 6 will present the analytical model of delaminated beams subject to axial impact. A literature review of delamination buckling and propagation will be presented. The details for the analysis of a delaminated beam model and the comparison of the numerical and experimental results will also be presented.

Chapter 7 will discuss the findings of our experimental results on pulse buckling characteristics of laminated composite beams with $[(\pm 67.5)_n]_s$ lay-up.

Finally, a summary and conclusions of the results will be outlined in Chapter 8. Recommendations for future research are proposed as well.

2 Governing Equations of Motion

A literature review on dynamic pulse buckling analysis is presented in this chapter. Governing equations of motion of slender fiber-reinforced plastic (FRP) composite laminated beams, having initial geometric imperfections, subjected to an axial impulse are established. Solutions based on the first and higher order shear deformation theories are derived. A numerical solution scheme developed based on the finite difference method (FDM) is also presented.

2.1 Literature review

2.1.1 Description of the problem

As described in Chapter 1, dynamic pulse buckling, as an instability form, or in the form of excessive growth of lateral or out of plane displacement, can result from a transient loading function of a single pulse with a magnitude greater than the static Euler buckling load. Considerable progress has been made regarding the dynamic pulse buckling analysis of metallic components (isotropic) since the earlier work of Koning and Taub in 1934. Our investigation considered a beam impacted by a moving mass, as shown in Figure 2-1. The beam is fixed at the left end. The right end is also fixed but is allowed to move in the axial direction. If the beam is perfectly straight and the impact has no eccentricity, it will deform only in the axial direction. If the beam is not perfectly straight, (*i.e.*, the beam has initial geometric imperfections), or the moving mass impacts the beam eccentrically, the beam will deform not only in the axial direction, but also in the lateral direction because the axial force creates a bending moment in the beam. Additionally, the beam's cross section will also rotate. So, the inertia of the beam in the axial and lateral directions, as well as the rotation of cross section play important roles in the movement of the beam when impacted by a pulse. Shear stress distribution through thickness, and

inter-laminar shear stresses are also important factors that affect the behavior of laminated components.

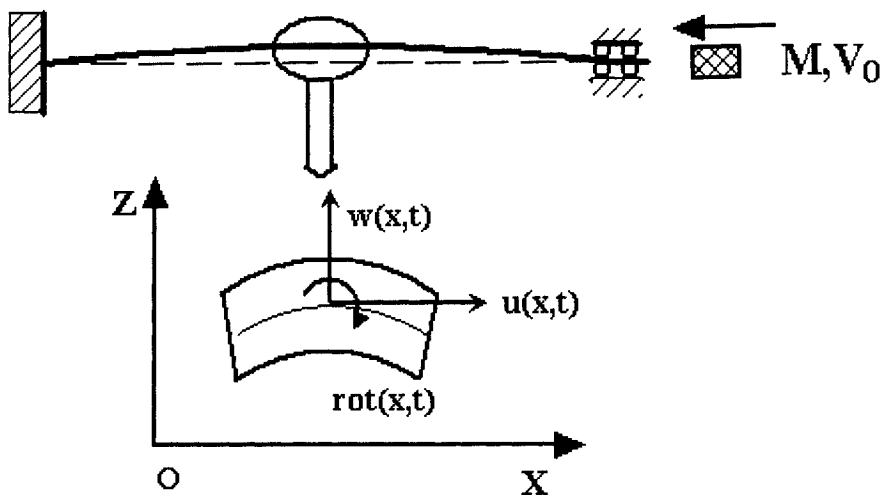

Figure 2-1 Example of a beam impacted by a moving mass.

2.1.2 Impact pulse buckling of isotropic beams

A monograph by Lindberg and Florence [1987] on dynamic pulse buckling characteristics of isotropic materials provided a systematic overview of pulse buckling, both theoretically and experimentally. They developed the dynamic equation of motion for a simply supported beam under a rectangular pulse, as well as determining the lateral displacement amplification function. The concept of "preferred mode" of dynamic buckling was accordingly proposed. In their formulations, the axial stress wave was neglected, hence the axial shortening was ignored, and the shear deformation was not considered either. With reference to Figure 2-2, only the transverse direction was considered, as defined by:

$$EI\frac{\partial^4 y}{\partial x^4} + P\frac{\partial^2}{\partial x^2}(y + y_0) + \rho A\frac{\partial^2 y}{\partial t^2} = 0 \qquad (2.1.1)$$

By assuming the displacement field of the beam as

$$y(x,t) = \sum_{n=1}^{\infty} q_n(\tau) \sin \frac{n\pi x}{L} , \tag{2.1.2}$$

dynamic equation (2.1.1) was solved. The solution of the dynamic equation was related to the dynamic impact load, material properties, beam geometric properties and buckling modal order.

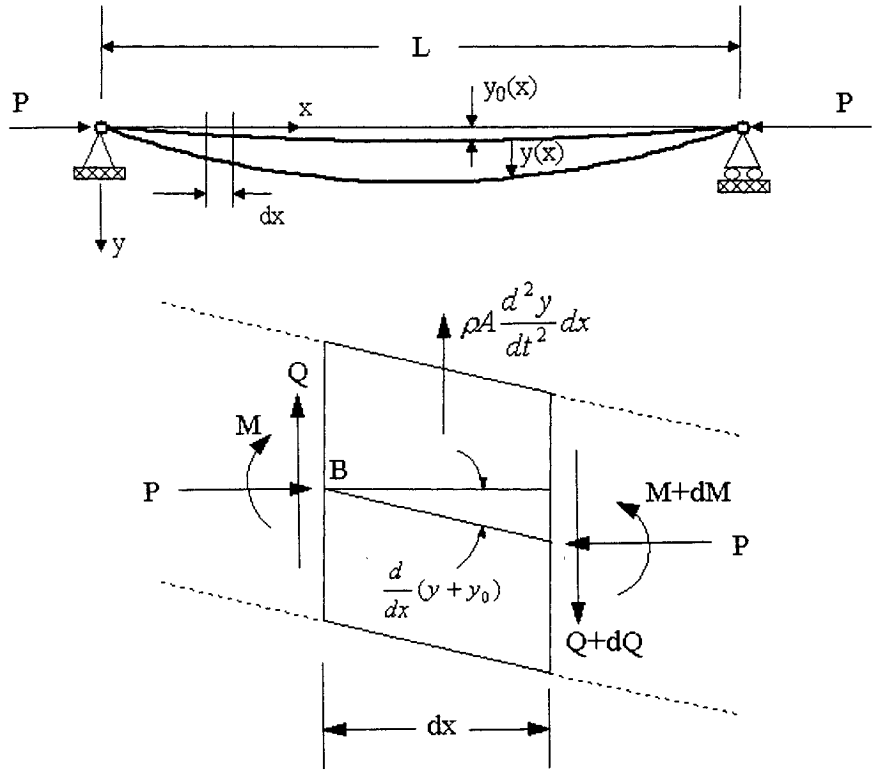

Figure 2-2 Simply supported beam is loaded by a constant load.
[Lindberg and Florence, 1987]

The solution was derived only for a rectangular impulse load, thus, it is not admissible for other types of loading, such as triangle pulse, half-sine pulse, and the case of a known impact mass and velocity. Another key disadvantage of the above work is that no axial

displacement or axial stress wave propagation along the beam length was considered in developing the dynamic equation, although the axial stiffness offers significant resistance to such structures.

Housner and Tso [1962] studied the dynamic response of a pin-ended prismatic structure subjected to a rapidly applied constant axial load, in which both shear deformation and rotary inertia were accounted for in the solution; the axial deformation and inertia were however neglected in their solution. Abrahamson and Goodier [1966] presented their research on dynamic flexural buckling of rods subjected to an axial plastic compressive wave. The dynamic plastic buckling of rods was investigated for a material that exhibited strain-hardening. They also neglected the axial deformation and inertia effect in their studies. Ari-Gur, *et al.* [1982] studied the dynamic response of columns subjected to an axial impact, experimentally and theoretically. A criterion was defined for determining the dynamic buckling loads based on their analytical and experimental results for columns with initial geometric imperfection under an axial impact. In their studies, axial displacement and inertia were considered, while the rotary inertia of the cross section was neglected. Hayashi and Sano [1972a, 1972b] investigated the dynamic instability of pinned end columns subjected to axial impact with the consideration of several factors, such as axial displacement and inertia, rotary inertia of cross section, transverse shear deformation and large deflection. In their solution, the shear stress across the column section was assumed to be uniformly distributed through the thickness of the cross section. Sugiura, *et al.* [1985] analyzed the dynamic instability of axially impacted the columns with the Euler-Bernoulli assumption in which the rotary inertia of the cross section of column and transverse shear deformation effects were neglected. Energy loss of the striking body was introduced to assess the criterion of dynamic buckling. Ari-Gur and Elishakoff [1997] researched the dynamic instability of a transversely isotropic pinned-end column subjected to a compressive pulse, using a numerical method. Their analytical model was based on the Timoshenko beam-column theory in which the axial displacement and inertia effects, rotary inertia effects of cross section, and transverse

shear deformation were included. The shear stress across the column section was also assumed to be uniformly distributed through the thickness of the cross section. Karagiozova and Jones [1996] also studied the dynamic elastic-plastic buckling of a rod under axial impact. A discrete model was proposed to investigate the influence of the axial and lateral inertias. Their numerical results showed that the striking mass played an important role in the development of buckling shape, and it caused different patterns of axial strain distributions at the onset of buckling. The authors stated that there was a strong interaction between the axial inertia (wave propagation) and the lateral inertial effect for the dynamic elastic-plastic buckling of a column with an axially moving and stationary end. Kenny, *et al.* [2000, 2002a, 2002b] presented results from their numerical (both Finite Difference and Finite Element Methods) and experimental investigations, on the dynamic buckling analysis of elastic and plastic slender beams subjected to axial impact. Their analyses demonstrated that only randomly distributed geometric imperfections would trigger the exponential growth of transverse displacement. Moreover, their finite element analysis demonstrated that the nonlinear geometric behavior could be used in considering the coupled axial and transverse displacement terms, for evaluating the effect of load intensity and other related parameters.

2.1.3 Dynamic instability of laminated beams/plates

As stated earlier, in comparison to the work done on dynamic instability of metallic materials, relatively much less research has been performed on characterization of the dynamic buckling response of FRP beams/plates. The mechanical properties and volume ratios of fibers and matrices, fiber angles, and stacking sequence, all have considerable effect on the dynamic buckling response of FRP beams.

Ekstrom [1973] investigated the elastic buckling of a simply supported rectangular orthotropic plate, with initial imperfection, under a compressive pulse load. The shortening of the plate along the load direction and the shear effect through the plate

thickness were not considered in his analysis. Ari-Gur and Simonetta [1997] constructed the analytical dynamic pulse buckling model of rectangular composite plates based on the Kirchhoff thin-plate deformation theory and the assumption of small rotation of the cross-section. The rotary inertia effect was neglected in the equations of dynamic equilibrium. Abramovich and Grunwald [1995] studied the dynamic stability of axially impacted laminated plates experimentally, in which the plates had various aspect ratios and boundary conditions. The Dynamic Load-amplification Factor (DLF) was used as a criterion for dynamic pulse buckling. Wang, *et al.*, [1998] also reported their investigation on the topic of dynamic buckling of laminated composite bars subjected to axial impact. Their governing equations were based on the Timoshenko beam assumption. The total transverse displacement was assumed as the sum of the initial transverse deflection and the transverse deflection due to bending and shearing. The shear stress was assumed uniformly distributed on the cross section and the rotation of cross section due to shear deformation was not included in the governing equations. The proposed solution was valid for a problem in which the beam was impacted with a constant velocity.

The above literature review, on the topic of dynamic pulse buckling of composite laminated beam revealed that very few investigations have considered the pulse buckling of laminate composite. Several areas have been identified that need particular attention, thus additional research on this topic is necessary.

As stated, FRP beams/plates with layer-wise anisotropic characteristics, undergoing dynamic pulse buckling, behave considerably different from their isotropic counterparts. Therefore, when formulating their dynamic equilibrium equations, in view of the resulting large deflection and cross section rotation, one should account for the associated axial shortening and inertia. Moreover, due to susceptibility of FRP to shear deformation, the distribution of shear stress though the thickness of the beam and the rotation of the

cross section should also be considered. Finally, the equations should be admissible for multiple boundary conditions and impact loading types.

In the next section of this chapter, governing equations of motion will be constructed with consideration of the transverse and axial inertias, shear deformation, the cross section's rotational inertia and the axial shortening in the equilibrium equations. The von-Karman nonlinear strain-displacement relationship will be used to model the deformation of the beam. The First & Higher Order Shear Deformation Theories are adopted to model the displacement field of the beam. The kinematic equations are developed and are valid for various boundary conditions and types of impulse.

2.2 Governing equations of motion

2.2.1 Dynamic equilibrium equations

Consider a FRP composite laminated beam with one end compressed by a pulse load as shown in Figure 2-3. The pulse load can be generated by a moving mass (M) with velocity (V_0) or an impulse force ($F(t)$). The boundary conditions of the beam can be a combination of either two ends fixed with one end allowed to move along the axial direction(as shown in Figure 2-3), or, one end pinned and the other end simply supported. The cross section of the beam is rectangular (as shown in the figure), with width b, thickness h, and is made of n layers of laminae. The length of the beam is L. The initial geometric imperfection is $w_0(x)$, which is defined as the initial displacement of the beam in the Z-direction as a function of location x, in the form of one or more sine waves distributed along the beam's length, or it can be randomly distributed, or it can be measured from real structure.

With the Timoshenko beam assumption, the equilibrium equations are constructed for the laminated FRP beam with the consideration of both the axial and flexual inertias, as well as the rotation inertia, and the through thickness shear deformation of the beam,

$$\frac{\partial N_x}{\partial x} - I_1 \frac{\partial^2 u}{\partial t^2} = 0 \tag{2.2.1a}$$

$$\frac{\partial (N_x(\theta - \frac{\partial w_0}{\partial x}))}{\partial x} - \frac{\partial V}{\partial x} + I_1 \frac{\partial^2 w}{\partial t^2} = 0 \tag{2.2.1b}$$

$$-\frac{\partial M_x}{\partial x} + V + I_2 \frac{\partial^2 \theta}{\partial t^2} = 0 \tag{2.2.1c}$$

where $u(x,t)$, unknown, is the axial displacement of the beam in the x direction;

$w(x,t)$, unknown, is the lateral displacement of the beam;

$\theta(x,t)$, unknown, is the rotation of the cross section of the beam;

$$(N_x; M_x) = \int_{-h/2}^{h/2} \sigma_x (1; z) dz \tag{2.2.2a,b}$$

are the axial force and bending moment per unit beam width, respectively, and σ_x is the axial stress of each lamina;

$$V = \int_{-h/2}^{h/2} \tau_{xz} dz \tag{2.2.3}$$

is the shear force per unit beam width across the cross section of beam, and τ_{xz} is the shear stress in each lamina;

$$(I_1; I_2) = \int_{-h/2}^{h/2} \rho (1; z^2) dz \tag{2.2.4a,b}$$

are the translational and rotational inertia per unit beam width, respectively, and ρ is the mass density of each lamina.

Ari-Gui and Elishakoff (1997) derived similar equations of motion for a transversely isotropic column.

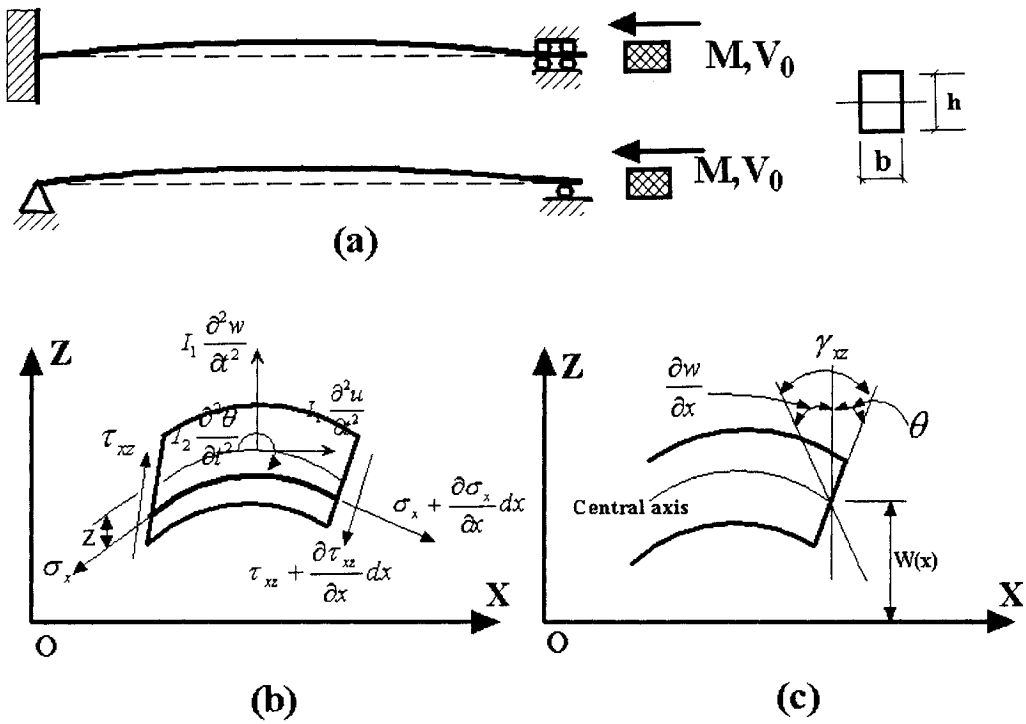

Figure 2-3 The laminated FRP Beam Model.

2.2.2 Constitutive relationship

The strain and stress relationship for the *k*th layer of the laminated beam is,

$$\begin{Bmatrix}\sigma_x\\ \sigma_y\\ \tau_{xy}\end{Bmatrix}=\begin{bmatrix}\overline{Q}_{11} & \overline{Q}_{12} & \overline{Q}_{16}\\ \overline{Q}_{21} & \overline{Q}_{22} & \overline{Q}_{26}\\ \overline{Q}_{61} & \overline{Q}_{62} & \overline{Q}_{66}\end{bmatrix}\begin{Bmatrix}\varepsilon_x\\ \varepsilon_y\\ \gamma_{xy}\end{Bmatrix},\quad \begin{Bmatrix}\tau_{yz}\\ \tau_{xz}\end{Bmatrix}=\begin{bmatrix}\overline{Q}_{44} & \overline{Q}_{45}\\ \overline{Q}_{54} & \overline{Q}_{55}\end{bmatrix}\begin{Bmatrix}\gamma_{yz}\\ \gamma_{xz}\end{Bmatrix} \qquad (2.2.5a, b)$$

where $\overline{Q}_{ij}$ are the transformer stiffness terms [Daniel and Ishai, 1994] . Shear correction factors does not appear in Equation (2.2.5b). This is because shear corrction factors are

used for uniformly distributed shear strain assumptions. In this dissertation, the shear strains are not assumed to be uniformly distributed through beam thickness, as described in section 2.3.

For the slender laminated beam, we can assume $\varepsilon_y = 0$, $\gamma_{xy} = 0$, and $\gamma_{yz} = 0$, then equation (2.2.5) simplifies to

$$\sigma_x = \overline{Q}_{11}\varepsilon_x \tag{2.2.6a}$$

$$\text{and } \tau_{xz} = \overline{Q}_{55}\gamma_{xz} \tag{2.2.6b}$$

2.3 Shear deformation theory solutions

2.3.1 The first order shear deformation theory (FSDT)

We can now solve the differential equation of motion (2.2.1) with the First-Order Shear Deformation Theory (FSDT). The displacement field in the First-Order Shear Deformation Theory is expressed by:

$$u_x(x,z,t) = u(x,t) + z\theta(x,t) \tag{2.3.1a}$$

$$u_z(x,z,t) = w(x,t) - w_0(x) \tag{2.3.1b}$$

where $w_0(x)$ is the initial imperfection of beam.

For the dynamic pulse buckling problem of FRP laminated beams, the von-Karman strain-displacement relationship is used to model the nonlinear relationship between the axial strain, displacement and the deflection of the beam,

$$\varepsilon_x = \frac{\partial u_x}{\partial x} + \frac{1}{2}\left(\frac{\partial w}{\partial x}\right)^2 - \frac{1}{2}\left(\frac{\partial w_0}{\partial x}\right)^2 \tag{2.3.2a}$$

$$\gamma_{xz} = \frac{\partial u_x}{\partial z} + \frac{\partial u_z}{\partial x} \tag{2.3.2b}$$

Substituting equations (2.3.1) into equation (2.3.2), we get,

$$\varepsilon_x = \frac{\partial u}{\partial x} + z\frac{\partial \theta}{\partial x} + \frac{1}{2}(\frac{\partial w}{\partial x})^2 - \frac{1}{2}(\frac{\partial w_0}{\partial x})^2 \tag{2.3.3a}$$

$$\gamma_{xz} = \theta + \frac{\partial w}{\partial x} - \frac{\partial w_0}{\partial x} \tag{2.3.3b}$$

Expanding the definition of axial force, moment and shear force which are defined in equations (2.2.2) and (2.2.3), we obtain:

$$\begin{aligned} N_x &= \int_{-h/2}^{h/2} \sigma_x dz \\ &= \int_{-h/2}^{h/2} \overline{Q}_{11}\varepsilon_x dz \\ &= \int_{-h/2}^{h/2} \overline{Q}_{11}[\frac{\partial u}{\partial x} + z\frac{\partial \theta}{\partial x} + \frac{1}{2}(\frac{\partial w}{\partial x})^2 - \frac{1}{2}(\frac{\partial w_0}{\partial x})^2]dz \\ &= A[\frac{\partial u}{\partial x} + \frac{1}{2}(\frac{\partial w}{\partial x})^2 - \frac{1}{2}(\frac{\partial w_0}{\partial x})^2] + B(\frac{\partial \theta}{\partial x}) \end{aligned} \tag{2.3.4a}$$

$$\begin{aligned} V &= \int_{-h/2}^{h/2} \tau_{xz} dz \\ &= \int_{-h/2}^{h/2} \overline{Q}_{55}(\theta + \frac{\partial w}{\partial x} - \frac{\partial w_0}{\partial x})dz \\ &= F(\theta + \frac{\partial w}{\partial x} - \frac{\partial w_0}{\partial x}) \end{aligned} \tag{2.3.4b}$$

$$\begin{aligned} M_x &= \int_{-h/2}^{h/2} \sigma_x z dz \\ &= \int_{-h/2}^{h/2} \overline{Q}_{11} z[\frac{\partial u}{\partial x} + z\frac{\partial \theta}{\partial x} + \frac{1}{2}(\frac{\partial w}{\partial x})^2 - \frac{1}{2}(\frac{\partial w_0}{\partial x})^2]dz \end{aligned}$$

$$= B[\frac{\partial u}{\partial x} + \frac{1}{2}(\frac{\partial w}{\partial x})^2 - \frac{1}{2}(\frac{\partial w_0}{\partial x})^2] + D(\frac{\partial \theta}{\partial x}) \tag{2.3.4c}$$

where A, B, D, and F in the above equations are defined as,

$$A = \int_{-h/2}^{h/2} \overline{Q}_{11} dz = \sum_{k=1}^{n} \overline{Q}_{11}^{k} (h_k - h_{k-1}) \tag{2.3.5a}$$

$$B = \int_{-h/2}^{h/2} z\overline{Q}_{11} dz = \frac{1}{2}\sum_{k=1}^{n} \overline{Q}_{11}^{k} (h_k^2 - h_{k-1}^2) \tag{2.3.5b}$$

$$D = \int_{-h/2}^{h/2} z^2\overline{Q}_{11} dz = \frac{1}{3}\sum_{k=1}^{n} \overline{Q}_{11}^{k} (h_k^3 - h_{k-1}^3) \tag{2.3.5c}$$

$$F = \int_{-h/2}^{h/2} \overline{Q}_{55} dz = \sum_{k=1}^{n} \overline{Q}_{55}^{k} (h_k - h_{k-1}) \tag{2.3.5d}$$

Taking derivatives of the three equations in (2.3.4) with respect to *x,* gives,

$$\frac{\partial N_x}{\partial x} = A[\frac{\partial^2 u}{\partial x^2} + (\frac{\partial w}{\partial x})(\frac{\partial^2 w}{\partial x^2}) - (\frac{\partial w_0}{\partial x})(\frac{\partial^2 w_0}{\partial x^2})] + B(\frac{\partial^2 \theta}{\partial x^2}) \tag{2.3.6a}$$

$$\frac{\partial V}{\partial x} = F(\frac{\partial \theta}{\partial x} + \frac{\partial^2 w}{\partial x^2} - \frac{\partial^2 w_0}{\partial x^2}) \tag{2.3.6b}$$

$$\frac{\partial M_x}{\partial x} = B[\frac{\partial^2 u}{\partial x^2} + (\frac{\partial w}{\partial x})(\frac{\partial^2 w}{\partial x^2}) - (\frac{\partial w_0}{\partial x})(\frac{\partial^2 w_0}{\partial x^2})] + D\frac{\partial^2 \theta}{\partial x^2} \tag{2.3.6c}$$

Substituting equations (2.3.6) into equation (2.2.1), we get the following differential equations,

$$I_1 \frac{\partial^2 u}{\partial t^2} = A[\frac{\partial^2 u}{\partial x^2} + (\frac{\partial w}{\partial x})(\frac{\partial^2 w}{\partial x^2}) - (\frac{\partial w_0}{\partial x})(\frac{\partial^2 w_0}{\partial x^2})] + B(\frac{\partial^2 \theta}{\partial x^2}) \tag{2.3.7a}$$

$$I_1 \frac{\partial^2 w}{\partial t^2} = \{A[\frac{\partial^2 u}{\partial x^2} + (\frac{\partial w}{\partial x})(\frac{\partial^2 w}{\partial x^2}) - (\frac{\partial w_0}{\partial x})(\frac{\partial^2 w_0}{\partial x^2})] + B(\frac{\partial^2 \theta}{\partial x^2})\}(-\theta + \frac{\partial w_0}{\partial x})$$

$$+\{A[\frac{\partial u}{\partial x}+\frac{1}{2}(\frac{\partial w}{\partial x})^2-\frac{1}{2}(\frac{\partial w_0}{\partial x})^2]+B(\frac{\partial \theta}{\partial x})\}(-\frac{\partial \theta}{\partial x}+\frac{\partial^2 w_0}{\partial x^2})$$

$$+F(\frac{\partial \theta}{\partial x}+\frac{\partial^2 w}{\partial x^2}-\frac{\partial^2 w_0}{\partial x^2}) \qquad (2.3.7b)$$

$$I_2\frac{\partial^2 \theta}{\partial t^2}=B[\frac{\partial^2 u}{\partial x^2}+\frac{\partial w}{\partial x}\frac{\partial^2 w}{\partial x^2}-\frac{\partial w_0}{\partial x}\frac{\partial^2 w_0}{\partial x^2}]+D\frac{\partial^2 \theta}{\partial x^2}-F(\theta+\frac{\partial w}{\partial x}-\frac{\partial w_0}{\partial x}) \qquad (2.3.7c)$$

To non-dimensionalize equations (2.3.7), we define the following non-dimensional variables

$$\bar{u}=\frac{u}{L},\ \bar{w}=\frac{w}{L},\ \bar{x}=\frac{x}{L},\bar{\theta}=\theta,\tau=\frac{c}{L}t, \qquad (2.3.8a, b, c, d, e)$$

where c is the wave propagation velocity along the beam length [Ari-Gur, *et al.*, 1982],

$$c=\sqrt{\frac{A}{I_1}} \qquad (2.3.9)$$

in which A and I_1 are defined in equation (2.3.5a) and (2.2.4a), respectively.

The derivatives in terms of the non-dimensional variables can be expressed by:

$$\frac{\partial u}{\partial x}=\frac{\partial \bar{u}}{\partial \bar{x}},$$

$$\frac{\partial^2 u}{\partial x^2}=\frac{1}{L}\frac{\partial^2 \bar{u}}{\partial \bar{x}^2},$$

$$\frac{\partial w}{\partial x}=\frac{\partial \bar{w}}{\partial \bar{x}},$$

$$\frac{\partial^2 w}{\partial x^2}=\frac{1}{L}\frac{\partial^2 \bar{w}}{\partial \bar{x}^2},$$

$$\frac{\partial \theta}{\partial x} = \frac{1}{L}\frac{\partial \bar{\theta}}{\partial \bar{x}}$$

$$\frac{\partial^2 \theta}{\partial x^2} = \frac{1}{L^2}\frac{\partial^2 \bar{\theta}}{\partial \bar{x}^2}$$

$$\frac{\partial^2 u}{\partial t^2} = \frac{c^2}{L}\frac{\partial^2 \bar{u}}{\partial \tau^2},$$

$$\frac{\partial^2 w}{\partial t^2} = \frac{c^2}{L}\frac{\partial^2 \bar{w}}{\partial \tau^2},$$

$$\frac{\partial^2 \theta}{\partial t^2} = \frac{c^2}{L^2}\frac{\partial^2 \bar{\theta}}{\partial \tau^2}$$

$$\frac{\partial^3 w}{\partial x^3} = \frac{1}{L^2}\frac{\partial^3 \bar{w}}{\partial \bar{x}^3}$$

$$\frac{\partial^3 w_0}{\partial x^3} = \frac{1}{L^2}\frac{\partial^3 \bar{w}_0}{\partial \bar{x}^3} \qquad \text{(2.3.10 a, b, c, d, e, f, g, h, i, j, k)}$$

Substituting (2.3.10) into (2.3.7), equilibrium equations can be rewritten in the non-dimensional form as:

$$\frac{\partial^2 \bar{u}}{\partial \tau^2} = \frac{\partial^2 \bar{u}}{\partial \bar{x}^2} + \frac{\partial \bar{w}}{\partial \bar{x}}\frac{\partial^2 \bar{w}}{\partial \bar{x}^2} - \frac{\partial \bar{w}_0}{\partial \bar{x}}\frac{\partial^2 \bar{w}_0}{\partial \bar{x}^2} + \frac{B}{AL}\frac{\partial^2 \bar{\theta}}{\partial \bar{x}^2} \qquad \text{(2.3.11a)}$$

$$\begin{aligned}\frac{\partial^2 \bar{w}}{\partial \tau^2} = {} & \left(\frac{\partial^2 \bar{u}}{\partial \bar{x}^2} + \frac{\partial \bar{w}}{\partial \bar{x}}\frac{\partial^2 \bar{w}}{\partial \bar{x}^2} - \frac{\partial \bar{w}_0}{\partial \bar{x}}\frac{\partial^2 \bar{w}_0}{\partial \bar{x}^2} + \frac{B}{AL}\frac{\partial^2 \bar{\theta}}{\partial \bar{x}^2}\right)\left(-\bar{\theta} + \frac{\partial \bar{w}_0}{\partial \bar{x}}\right) \\ & + \left[\frac{\partial \bar{u}}{\partial \bar{x}} + \frac{1}{2}\left(\frac{\partial \bar{w}}{\partial \bar{x}}\right)^2 - \frac{1}{2}\left(\frac{\partial \bar{w}_0}{\partial \bar{x}}\right)^2 + \frac{B}{AL}\frac{\partial \bar{\theta}}{\partial \bar{x}}\right]\left(-\frac{\partial \bar{\theta}}{\partial \bar{x}} + \frac{\partial^2 \bar{w}_0}{\partial \bar{x}^2}\right) \\ & + \frac{F}{A}\left(\frac{\partial \bar{\theta}}{\partial \bar{x}} + \frac{\partial^2 \bar{w}}{\partial \bar{x}^2} - \frac{\partial^2 \bar{w}_0}{\partial \bar{x}^2}\right)\end{aligned} \qquad \text{(2.3.11b)}$$

$$\begin{aligned}\frac{\partial^2 \bar{\theta}}{\partial \tau^2} = {} & \left\{\left[\left(\frac{\partial^2 \bar{u}}{\partial \bar{x}^2} + \frac{\partial \bar{w}}{\partial \bar{x}}\frac{\partial^2 \bar{w}}{\partial \bar{x}^2} - \frac{\partial \bar{w}_0}{\partial \bar{x}}\frac{\partial^2 \bar{w}_0}{\partial \bar{x}^2}\right)BL + D\frac{\partial^2 \bar{\theta}}{\partial x^2}\right.\right. \\ & \left.\left. - FL^2\left(\theta + \frac{\partial w}{\partial x} - \frac{\partial w_0}{\partial x}\right)\right]\right\}\frac{I_1}{AI_2}\end{aligned} \qquad \text{(2.3.11c)}$$

The finite difference solution of the above 3 differential equations will be presented in section 2.4.

2.3.2 The higher order shear deformation theory (HSDT)

We can also solve the equation of motion (2.2.1) with Reddy's Higher-Order Shear Deformation Theory [Reddy, 1984].

Displacement fields of laminated plate in the HSDT are defined as:

$$u = u_0(x,y) + z\theta_x + z^2\xi_x + z^3\zeta_x$$
$$v = v_0(x,y) + z\theta_y + z^2\xi_y + z^3\zeta_y$$
$$w = w(x,y) \qquad \text{(2.3.12a, b, c)}$$

in which u, v and w denote the displacements of a point (x, y) on the mid-plane, and θ_x and θ_y are the rotations of normal about the y and x axes, respectively. The functions ξ_x, ξ_y, ζ_x and ζ_y will be determined using the assumption that transverse shear strain ε_{xz} and ε_{yz} vanish at the top and bottom surfaces,

$$\varepsilon_{xz} = \frac{\partial u}{\partial z} + \frac{\partial w}{\partial x} = \theta_x + 2z\xi_x + 3z^2\zeta_x + \frac{\partial w}{\partial x} \qquad \text{(2.3.13a)}$$

$$\varepsilon_{yz} = \frac{\partial v}{\partial z} + \frac{\partial w}{\partial y} = \theta_y + 2z\xi_y + 3z^2\zeta_y + \frac{\partial w}{\partial y} \qquad \text{(2.3.13b)}$$

So, by setting $\varepsilon_{xz} = \varepsilon_{yz} = 0$ at $z = \pm\frac{1}{2}h$ gives

$$\xi_x = \xi_y = 0$$

$$\zeta_x = -\frac{4}{3}\frac{1}{h^2}(\theta_x + \frac{\partial w}{\partial x})$$

$$\zeta_y = -\frac{4}{3}\frac{1}{h^2}(\theta_y + \frac{\partial w}{\partial x}) \qquad (2.3.14a, b, c)$$

Substitute (2.3.14) into (2.3.12) gives the following displacement field equations,

$$u = u_0(x,y) - z\frac{\partial w}{\partial x} + z\theta_x - \frac{4}{3}\frac{z^3}{h^2}\theta_x \qquad (2.3.15a)$$

$$v = v_0(x,y) - z\frac{\partial w}{\partial y} + z\theta_y - \frac{4}{3}\frac{z^3}{h^2}\theta_y \qquad (2.3.16b)$$

The above displacement fields will degrade to the classical theory when θ_x and θ_y (shear rotation) are very small and they indicate cubic variation of the in-plane displacements and a parabolic distribution of the transverse shear strains through the thickness of the plate.

Now, considering the current problem, dynamic pulse buckling of a slender laminated beam with initial geometric imperfection $w_0(x)$, we use the following Higher-Order Shear Deformation Theory (HSDT) displacement field:

$$u_x(x,z,t) = u(x,t) + z(\theta - \frac{\partial w}{\partial x} + \frac{\partial w_0}{\partial x}) - \frac{4z^3}{3h^2}\theta \qquad (2.3.17a)$$

$$u_z(x,z,t) = w(x,t) - w_0(x) \qquad (2.3.17b)$$

Similar to the FSDT solution, we will also use the von-Karman strain-displacement relationship to model the deformed shape of the beam,

$$\varepsilon_x = \frac{\partial u_x}{\partial x} + \frac{1}{2}(\frac{\partial w}{\partial x})^2 - \frac{1}{2}(\frac{\partial w_0}{\partial x})^2$$

$$= \frac{\partial u}{\partial x} + z\frac{\partial \theta}{\partial x} - \frac{4z^3}{3h^2}(\frac{\partial \theta}{\partial x} - \frac{\partial^2 w}{\partial x^2} + \frac{\partial^2 w_0}{\partial x^2}) + \frac{1}{2}(\frac{\partial w}{\partial x})^2 - \frac{1}{2}(\frac{\partial w_0}{\partial x})^2 \quad (2.3.18a)$$

$$\gamma_{xz} = \frac{\partial u_x}{\partial z} + \frac{\partial u_z}{\partial x} = \theta - \frac{4z^2}{h^2}(\theta + \frac{\partial w}{\partial x} - \frac{\partial w_0}{\partial x}) + \frac{\partial w}{\partial x} - \frac{\partial w_0}{\partial x}$$

$$= (1 - \frac{4z^2}{h^2})(\theta + \frac{\partial w}{\partial x} - \frac{\partial w_0}{\partial x}) \quad (2.3.18b)$$

Now the axial force, moment and shear force and their derivatives for a unit width beam can be rewritten as,

$$N_x = \int_{-h/2}^{h/2} \sigma_x dz$$

$$= \int_{-h/2}^{h/2} \overline{Q}_{xx} \varepsilon_x dz$$

$$= \int_{-h/2}^{h/2} \overline{Q}_{xx} [\frac{\partial u}{\partial x} + z\frac{\partial \theta}{\partial x} - \frac{4z^3}{3h^2}(\frac{\partial \theta}{\partial x} - \frac{\partial^2 w}{\partial x^2} + \frac{\partial^2 w_0}{\partial x^2}) + \frac{1}{2}(\frac{\partial w}{\partial x})^2 - \frac{1}{2}(\frac{\partial w_0}{\partial x})^2] dz$$

$$= A[\frac{\partial u}{\partial x} + \frac{1}{2}(\frac{\partial w}{\partial x})^2 - \frac{1}{2}(\frac{\partial w_0}{\partial x})^2] + B\frac{\partial \theta}{\partial x} - \frac{4E}{3h^2}(\frac{\partial \theta}{\partial x} + \frac{\partial^2 w}{\partial x^2} - \frac{\partial^2 w_0}{\partial x^2}) \quad (2.3.19a)$$

$$V = \int_{-h/2}^{h/2} \tau_{xz} dz$$

$$= \int_{-h/2}^{h/2} \overline{Q}_{55}(1 - \frac{4z^2}{h^2})(\theta + \frac{\partial w}{\partial x} - \frac{\partial w_0}{\partial x}) dz$$

$$= (F - \frac{4}{h^2}G)(\theta + \frac{\partial w}{\partial x} - \frac{\partial w_0}{\partial x}) \quad (2.3.19b)$$

$$M_x = \int_{-h/2}^{h/2} \sigma_x z dz$$

$$= \int_{-h/2}^{h/2} \overline{Q}_{xx} z[\frac{\partial u}{\partial x} + z\frac{\partial \theta}{\partial x} - \frac{4z^3}{3h^2}(\frac{\partial \theta}{\partial x} + \frac{\partial^2 w}{\partial x^2} - \frac{\partial^2 w_0}{\partial x^2}) + \frac{1}{2}(\frac{\partial w}{\partial x})^2 - \frac{1}{2}(\frac{\partial w_0}{\partial x})^2]dz$$

$$= B[\frac{\partial u}{\partial x} + \frac{1}{2}(\frac{\partial w}{\partial x})^2 - \frac{1}{2}(\frac{\partial w_0}{\partial x})^2] + D\frac{\partial \theta}{\partial x} - \frac{4H}{3h^2}(\frac{\partial \theta}{\partial x} - \frac{\partial^2 w}{\partial x^2} + \frac{\partial^2 w_0}{\partial x^2}) \quad (2.3.19c)$$

and

$$\frac{\partial V}{\partial x} = (F - \frac{4}{h^2}G)(\frac{\partial \theta}{\partial x} + \frac{\partial^2 w}{\partial x^2} - \frac{\partial^2 w_0}{\partial x^2}) \quad (2.3.20a)$$

$$\frac{\partial N_x}{\partial x} = A[\frac{\partial u^2}{\partial x^2} + \frac{\partial w}{\partial x}\frac{\partial^2 w}{\partial x^2} - \frac{\partial w_0}{\partial x}\frac{\partial^2 w_0}{\partial x^2}] + B\frac{\partial^2 \theta}{\partial x^2} - \frac{4E}{3h^2}(\frac{\partial^2 \theta}{\partial x^2} + \frac{\partial^3 w}{\partial x^3} - \frac{\partial^3 w_0}{\partial x^3}) \quad (2.3.20b)$$

$$\frac{\partial M_x}{\partial x} = B[\frac{\partial^2 u}{\partial x^2} + \frac{\partial w}{\partial x}\frac{\partial^2 w}{\partial x^2} - \frac{\partial w_0}{\partial x}\frac{\partial^2 w_0}{\partial x^2}]$$

$$+ D\frac{\partial^2 \theta}{\partial x^2} - \frac{4H}{3h^2}(\frac{\partial^2 \theta}{\partial x^2} + \frac{\partial^3 w}{\partial x^3} - \frac{\partial^3 w_0}{\partial x^3}) \quad (2.3.20c)$$

where E, G, and H in the above equations are defined,

$$E = \int_{-h/2}^{h/2} z^3 \overline{Q}_{11} dz = \frac{1}{4}\sum_{k=1}^{n} \overline{Q}_{11}^k (h_k^4 - h_{k-1}^4) \quad (2.3.21a)$$

$$G = \int_{-h/2}^{h/2} z^2 \overline{Q}_{55} dz = \frac{1}{3}\sum_{k=1}^{n} \overline{Q}_{55}^k (h_k^3 - h_{k-1}^3) \quad (2.3.21b)$$

$$H = \int_{-h/2}^{h/2} z^4 \overline{Q}_{11} dz = \frac{1}{5}\sum_{k=1}^{n} \overline{Q}_{11}^k (h_k^5 - h_{k-1}^5) \quad (2.3.21c)$$

Now substitute (2.3.20) into equations (2.2.1), we get,

$$I_1 \frac{\partial^2 u}{\partial t^2} = A[\frac{\partial u^2}{\partial x^2} + \frac{\partial w}{\partial x}\frac{\partial^2 w}{\partial x^2} - \frac{\partial w_0}{\partial x}\frac{\partial^2 w_0}{\partial x^2}] + B\frac{\partial^2 \theta}{\partial x^2} - \frac{4E}{3h^2}(\frac{\partial^2 \theta}{\partial x^2} + \frac{\partial^3 w}{\partial x^3} - \frac{\partial^3 w_0}{\partial x^3}) \quad (2.3.22a)$$

$$I_1\frac{\partial^2 w}{\partial t^2}=\{A[\frac{\partial u^2}{\partial x^2}+\frac{\partial w}{\partial x}\frac{\partial^2 w}{\partial x^2}-\frac{\partial w_0}{\partial x}\frac{\partial^2 w_0}{\partial x^2}]+B\frac{\partial^2\theta}{\partial x^2}-$$

$$\frac{4E}{3h^2}(\frac{\partial^2\theta}{\partial x^2}+\frac{\partial^3 w}{\partial x^3}-\frac{\partial^3 w_0}{\partial x^3})\}(-\theta+\frac{\partial w_0}{\partial x})+$$

$$\{A[\frac{\partial u}{\partial x}+\frac{1}{2}(\frac{\partial w}{\partial x})^2-\frac{1}{2}(\frac{\partial w_0}{\partial x})^2]+B\frac{\partial\theta}{\partial x}-$$

$$\frac{4E}{3h^2}(\frac{\partial\theta}{\partial x}+\frac{\partial^2 w}{\partial x^2}-\frac{\partial^2 w_0}{\partial x^2})\}(-\frac{\partial\theta}{\partial x}+\frac{\partial^2 w}{\partial x^2})+$$

$$(F-\frac{4G}{h^2})(\frac{\partial\theta}{\partial x}+\frac{\partial^2 w}{\partial x^2}-\frac{\partial^2 w_0}{\partial x^2}) \qquad (2.3.22b)$$

$$I_2\frac{\partial^2\theta}{\partial t^2}=-B[\frac{\partial^2 u}{\partial x^2}+\frac{\partial w}{\partial x}\frac{\partial^2 w}{\partial x^2}-\frac{\partial w_0}{\partial x}\frac{\partial^2 w_0}{\partial x^2}]-D\frac{\partial^2\theta}{\partial x^2}+$$

$$\frac{4H}{3h^2}(\frac{\partial^2\theta}{\partial x^2}+\frac{\partial^3 w}{\partial x^3}-\frac{\partial^3 w_0}{\partial x^3})+(F-\frac{4G}{h^2})(\theta+\frac{\partial w}{\partial x}-\frac{\partial w_0}{\partial x}) \qquad (2.3.22c)$$

Similar to the earlier procedure (in the FSDT), we can non-dimensionalize the equation, as:

$$\frac{\partial^2\bar{u}}{\partial\tau^2}=(\frac{\partial^2\bar{u}}{\partial\bar{x}^2}+\frac{\partial\bar{w}}{\partial\bar{x}}\frac{\partial^2\bar{w}}{\partial\bar{x}^2}-\frac{\partial\bar{w}_0}{\partial\bar{x}}\frac{\partial^2\bar{w}_0}{\partial\bar{x}^2})+\frac{B}{AL}\frac{\partial^2\bar{\theta}}{\partial\bar{x}^2}-\frac{4E}{3ALh^2}(\frac{\partial^2\bar{\theta}}{\partial\bar{x}^2}+\frac{\partial^3\bar{w}}{\partial\bar{x}^3}-\frac{\partial^3\bar{w}_0}{\partial\bar{x}^3}) \qquad (2.3.23a)$$

$$\frac{\partial^2\bar{w}}{\partial\tau^2}=[(\frac{\partial^2\bar{u}}{\partial\bar{x}^2}+\frac{\partial\bar{w}}{\partial\bar{x}}\frac{\partial^2\bar{w}}{\partial\bar{x}^2}-\frac{\partial\bar{w}_0}{\partial\bar{x}}\frac{\partial^2\bar{w}_0}{\partial\bar{x}^2})+\frac{B}{AL}(\frac{\partial^2\bar{\theta}}{\partial^2\bar{x}}+\frac{\partial^3\bar{w}}{\partial\bar{x}^3}-\frac{\partial^3\bar{w}_0}{\partial\bar{x}^3})-\frac{4E}{3ALh^2}\frac{\partial^2\bar{\theta}}{\partial\bar{x}^2}]\bar{\theta}$$

$$+\frac{4E}{3ALh^2}(\frac{\partial\bar{\theta}}{\partial\bar{x}}+\frac{\partial^2\bar{w}}{\partial\bar{x}^2}-\frac{\partial^2\bar{w}_0}{\partial\bar{x}^2})](-\frac{\partial\bar{\theta}}{\partial\bar{x}}+\frac{\partial^2 w_0}{\partial x^2})$$

$$-\frac{F-\frac{4G}{h^2}}{A}(\frac{\partial\bar{\theta}}{\partial\bar{x}}+\frac{\partial^2\bar{w}}{\partial\bar{x}^2}-\frac{\partial^2\bar{w}_0}{\partial\bar{x}^2}) \qquad (2.3.23b)$$

$$\frac{\partial^2\bar{\theta}}{\partial t^2}=[-(\frac{\partial^2\bar{u}}{\partial\bar{x}^2}+\frac{\partial\bar{w}}{\partial\bar{x}}\frac{\partial^2\bar{w}}{\partial\bar{x}^2}-\frac{\partial\bar{w}_0}{\partial\bar{x}}\frac{\partial^2\bar{w}_0}{\partial\bar{x}^2})BL-D\frac{\partial^2\bar{\theta}}{\partial x^2}$$

$$+\frac{4H}{3Lh^2}\left(\frac{\partial^2\bar{\theta}}{\partial\bar{x}^2}+\frac{\partial^3\bar{w}}{\partial\bar{x}^3}-\frac{\partial^3\bar{w}_0}{\partial\bar{x}^3}\right)-L^2\left(F-\frac{4G}{h^2}\right)\left(\bar{\theta}+\frac{\partial\bar{w}}{\partial\bar{x}}-\frac{\partial\bar{w}_0}{\partial\bar{x}}\right)\Bigg]\frac{I_1}{AI_2} \quad (2.3.23c)$$

2.4 Finite difference equations

The differential equations (2.3.11) and (2.3.23) are solved with the Finite Difference Method (FDM) to evaluate the dynamic buckling response of the FRP laminated beam. The analysis model was discretized into n segments with equal length $\Delta\bar{x}$ along the beam's length and the solution was carried out with m time steps with the interval (time step) of $\Delta\tau$. The explicit central difference scheme with accuracy order of $O(h^2)$ was used to compute the solution of u, w and θ of the j^{th} spatial grid of beam at $(k+1)^{th}$ time step. The selection of time step $\Delta\tau$ should be with the consideration of ensuring numerical stability and the spatial discretization of the beam should be such to promote convergence.

To configure the finite difference equations to solve the differential equations (2.3.11) for the First-Order Shear Deformation solution and (2.3.22) for the Higher-Order Shear Deformation solution, we define,

spatial step as $\Delta\bar{x}$, thus, for step j, $\bar{x} = j \cdot \bar{\Delta}x$

time step as $\Delta\tau$, thus, for step k, $\tau = k \cdot \Delta\tau$

The central difference formulae can be expressed as,

$$\frac{\partial\bar{u}}{\partial\bar{x}} = \frac{\bar{u}_{j+1,k} - \bar{u}_{j-1,k}}{2\Delta\bar{x}}$$

$$\frac{\partial^2\bar{u}}{\partial\bar{x}^2} = \frac{\bar{u}_{j+1,k} - 2\bar{u}_{j,k} + \bar{u}_{j-1,k}}{\Delta\bar{x}^2}$$

$$\frac{\partial^2 \bar{u}}{\partial \tau^2} = \frac{\bar{u}_{j,k+1} - 2\bar{u}_{j,k} + \bar{u}_{j,k-1}}{\Delta \tau^2}$$

$$\frac{\partial \bar{w}}{\partial \bar{x}} = \frac{\bar{w}_{j+1,k} - \bar{w}_{j-1,k}}{2\Delta \bar{x}}$$

$$\frac{\partial \bar{w}_0}{\partial \bar{x}} = \frac{\bar{w}_{j+1,0} - \bar{w}_{j-1,0}}{2\Delta \bar{x}}$$

$$\frac{\partial^2 \bar{w}}{\partial \bar{x}^2} = \frac{\bar{w}_{j+1,k} - 2\bar{w}_{j,k} + \bar{w}_{j-1,k}}{\Delta \bar{x}^2}$$

$$\frac{\partial^2 \bar{w}_0}{\partial \bar{x}^2} = \frac{\bar{w}_{j+1,0} - 2\bar{w}_{j,0} + \bar{w}_{j-1,0}}{\Delta \bar{x}^2}$$

$$\frac{\partial^3 \bar{w}}{\partial \bar{x}^3} = \frac{\bar{w}_{j+2,k} - 2\bar{w}_{j+1,k} + 2\bar{w}_{j-1,k} - \bar{w}_{j-2,k}}{2(\Delta \bar{x}^3)}$$

$$\frac{\partial^3 \bar{w}_0}{\partial \bar{x}^3} = \frac{\bar{w}_{j+2,0} - 2\bar{w}_{j+1,0} + 2\bar{w}_{j-1,0} - \bar{w}_{j-2,0}}{2(\Delta \bar{x}^3)}$$

$$\frac{\partial^2 \bar{w}}{\partial \tau^2} = \frac{\bar{w}_{j,k+1} - 2\bar{w}_{j,k} + \bar{w}_{j,k-1}}{\Delta \tau^2}$$

$$\frac{\partial \bar{\theta}}{\partial \bar{x}} = \frac{\bar{\theta}_{j+1,k} - \bar{\theta}_{j-1,k}}{2\Delta \bar{x}}$$

$$\frac{\partial^2 \bar{\theta}}{\partial \bar{x}^2} = \frac{\bar{\theta}_{j+1,k} - 2\bar{\theta}_{j,k} + \bar{\theta}_{j-1,k}}{\Delta \bar{x}^2}$$

$$\frac{\partial^2 \bar{\theta}}{\partial \tau^2} = \frac{\bar{\theta}_{j,k+1} - 2\bar{\theta}_{j,k} + \bar{\theta}_{j,k-1}}{\Delta \tau^2} \qquad \text{(2.4.1a - l)}$$

Substitute Equations (2.4.1a-l) into equations (2.3.11), and with the help of constants (A_3 , B_5 , C_6 , and $E_i (i = 1,6)$) defined in Appendix A, the following finite difference formulae for the solution of FSDT can be obtained,

$$\bar{u}_{j,k+1} = E_1 (\Delta \tau)^2 - A_3 \qquad \text{(2.4.3a)}$$

$$\bar{w}_{j,k+1} = E_2 (\Delta \tau)^2 - B_5 \qquad \text{(2.4.3b)}$$

$$\bar{\theta}_{j,k+1} = E_3(\Delta\tau)^2 - C_6 \tag{2.4.3c}$$

Similarly way, we get the finite difference formulae for the solution of HSDT,

$$\bar{u}_{j,k+1} = E_4(\Delta\tau)^2 - A_3 \tag{2.4.4a}$$

$$\bar{w}_{j,k+1} = E_5(\Delta\tau)^2 - B_5 \tag{2.4.4b}$$

$$\bar{\theta}_{j,k+1} = E_6(\Delta\tau)^2 - C_6 \tag{2.4.4c}$$

2.5 Boundary conditions and initial conditions

The boundary conditions for the problems considered in this dissertation can be pinned or fixed supports or any reasonable combinations with the impacted end allowed to move freely along the axial direction of the beam. The impact can be due to a known impulse force time history *F(t)*, known mass M with initial velocity V_0 of the impact body, or other types of impact contact model. In the numerical analysis of pulse buckling, the initial geometric imperfection of the beam is assumed as a half sine form,

$$w_0(x) = W_0 \sin(\frac{\pi x}{L}) \tag{2.5.1}$$

In the damage and delamination propagation analysis, the initial geometric imperfection of the beam was measured based on the actual shape of each specimen. The beam is assumed to be initially at rest.

Two types of impact loads will be considered,

(i) A known impact force time history $F(t)$;

(ii) A known impact mass M with velocity V_0.

Also, two types of boundary conditions will be considered,

(i) The left end ($x=0$) is fixed and the right end ($x=L$) of the beam is restrained laterally, but it can move in the x direction at the right end.

(ii) The beam is simply supported, i.e., the left end ($x=0$) is pinned, and the right end ($x=L$) is restrained in the normal direction, but the beam can move in the x direction.

2.5.1 Fixed support - case a

For this kind of boundary condition, both the left end ($x=0$) and right end ($x=L$) of the beam are fixed, but the beam can move in the x direction at the right end. Then we have,

$$\text{(i)} \quad w = \frac{\partial w}{\partial x} = \theta = 0 \qquad \text{at} \quad x = 0, \quad x = L \tag{2.5.2a}$$

$$\text{(ii)} \quad u = 0 \qquad \text{at} \quad x = 0 \tag{2.5.2b}$$

The initial conditions for this case are

$$\text{(i)} \quad w(x)\big|_{t=0} = w_0(x), \; \theta(x)\big|_{t=0} = -\frac{\partial w_0}{\partial x} \tag{2.5.3a}$$

$$\text{(ii)} \quad \left.\frac{\partial w}{\partial t}\right|_{t=0} = \left.\frac{\partial \theta}{\partial t}\right|_{t=0} = u\big|_{t=0} = \left.\frac{\partial u}{\partial t}\right|_{t=0} = 0 \tag{2.5.3b}$$

2.5.2 Pinned support – case b

The beam is simply supported, i.e., the left end ($x=0$) is pinned, and the right end ($x=L$) is restrained in normal direction, the beam can move in the x-direction at the right end,

(i) $$w = \frac{\partial^2 w}{\partial x^2} = \frac{\partial \theta}{\partial x} = 0 \text{ at } x = 0, \quad x = L \tag{2.5.4.a}$$

(ii) $$u = 0 \text{ at } x = 0 \tag{2.5.4.b}$$

The initial conditions for this case are

(i) $$w(x)\big|_{t=0} = w_0(x),\ \theta(x)\big|_{t=0} = 0 \tag{2.5.5a}$$

(ii) $$\left.\frac{\partial w}{\partial t}\right|_{t=0} = \left.\frac{\partial \theta}{\partial t}\right|_{t=0} = u\big|_{t=0} = \left.\frac{\partial u}{\partial t}\right|_{t=0,x<L} = 0 \tag{2.5.5b}$$

(iii) $$\left.\frac{\partial u}{\partial t}\right|_{t=0} = V_0 \qquad (x = L) \tag{2.5.5c}$$

2.5.3 Impact force time history *F(t)*

For the case of knowing the impact force time history, we assume that the external impact force is transferred to the impacted end without loss, that is,

$$N_x(t) = F(t) \qquad (x = L) \tag{2.5.6}$$

For the solutions based on the FSDT, we have

$$N_x = A[\frac{\partial u}{\partial x} + \frac{1}{2}(\frac{\partial w}{\partial x})^2 - \frac{1}{2}(\frac{\partial w_0}{\partial x})^2] + B(\frac{\partial \theta}{\partial x}) \tag{2.5.7}$$

Considering the boundary conditions of the impacted end for both types of support conditions, we have

$$\frac{\partial u}{\partial x}|_{x=L} = \frac{F(t)}{A} \tag{2.5.8}$$

Using a similar method, we can get the solution of the HSDT.

2.5.4 Impact mass *M* and velocity V_0

This impact model is based on Ari-Gur's work [1982]. At the moment when the moving mass (M) traveling at velocity (V_0) begins to impact the beam's end, we assume the displacement of the mass along the axial direction of the beam is defined as

$$U_{t=0} = 0 \tag{2.5.9}$$

and the velocity of the moving mass is,

$$V_{t=0} = \dot{U}_{t=0} = V_0 \tag{2.5.10}$$

The mass is decelerated by the repulsive force bN_x at the impacted end of the beam ($x = L$), where b is the beam's width. According to the "Momentum Balance" theory, we have,

$$M[V(t) - V_0] = b\int_0 N_x(t)dt \tag{2.5.11}$$

Divide both sides of equation (2.5.11) by M and move the terms involving V_0 to the right side, we would get,

$$V(t) = V_0 + \frac{b}{M}\int_0 N_x|_{x=L}\, dt \tag{2.5.12}$$

From Equation (2.5.6) and (2.5.8), we have,

$$N_x|_{x=L} = A\frac{\partial u}{\partial x}|_{x=L} = A\varepsilon_x|_{x=L} \tag{2.5.13}$$

Substitute (2.5.13) into (2.5.12), we get,

$$V(t) = V_0 + \frac{b}{M}A\int_0^t \varepsilon_x|_{x=L}\,dt \tag{2.5.14}$$

The displacement of the moving mass can be obtained by

$$U(t) = \int_0^t V(t)dt\,. \tag{2.5.15}$$

Equation (2.5.14) indicates that the velocity $V(t)$ of the impact mass M can be obtained through the strain accumulation at the right end of the beam (x=L), from beginning of the event to time t. We also assume that during the impact period:

$$u(t) = U \qquad \text{at } x = L \tag{2.5.16}$$

where U is the displacement of the impact mass, and also the displacement of the impacted end of the beam.

2.6 Evaluation of the solution methodologies

2.6.1 Convergence tests of FDM Solutions

2.6.1.1 Mesh Sensitivity analysis the of Finite Difference Solution

An E-glass/epoxy laminated composite beam with $[0^0]_8$ lay-up was impacted by a moving mass at the right end of the beam, in which the beam was restrained according to the boundary conditions described in equation (2.5.3). The geometry and physical properties of the beam are as follows: Length=0.25m, Width=0.0185m, Thickness=0.0014m. The initial geometric imperfection was assumed as a sine form, with the amplitude equal to 100% of the beam thickness (*i.e.*, 0.0014m). The mechanical properties were $E_{11}=39x10^9$ Pa, $E_{22}=3.9x10^9$ Pa, $G_{12}=3.9x10^9$ Pa, and Density $=2100Kg/m^3$. The mass of the impacter was 0.175Kg, and the velocity of the moving mass was at 5.0 m/sec.

Figure 2-4 shows the deflection at the mid-span of the beam vs. time for different mesh densities in terms of the aspect ratio. The aspect ratio is defined as the ratio of the element length over thickness of the beam. From Figure 2-4, we can observe that the results converge when the aspect ratio is smaller than or equal to 0.893.

2.6.1.2 Time Step Sensitivity analysis of the Finite Difference Solution

The same problem used to test the mesh sensitivity was used for this test. The geometry was analyzed with 80 segments along the beam length, but the time step was taken differently. From Figure 2-5 we observe that the analysis results are the same for non-diverging time steps.

The comparison of the results with LS-DYNA will be shown in the next chapter.

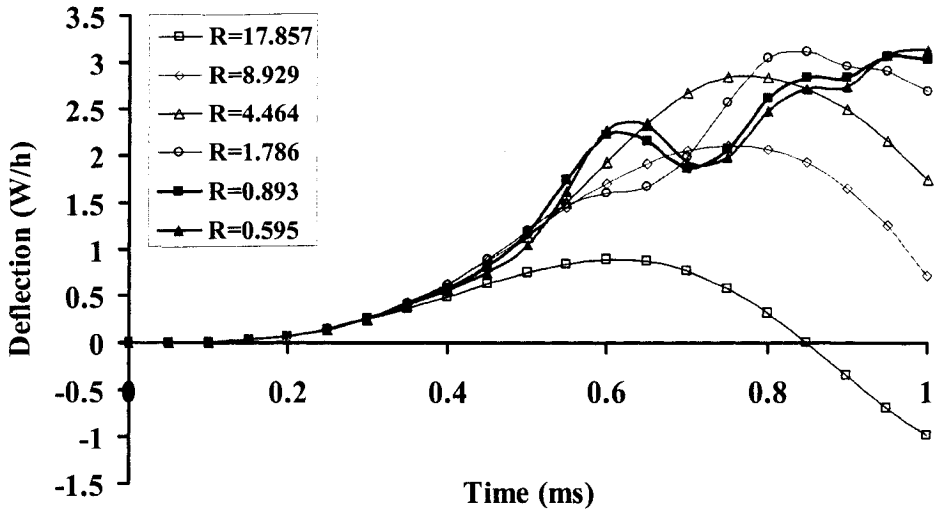

Figure 2-4 Grid Sensitivity Analysis – Deflection at mid-span of beam vs time history for different beam aspect ratios (R).

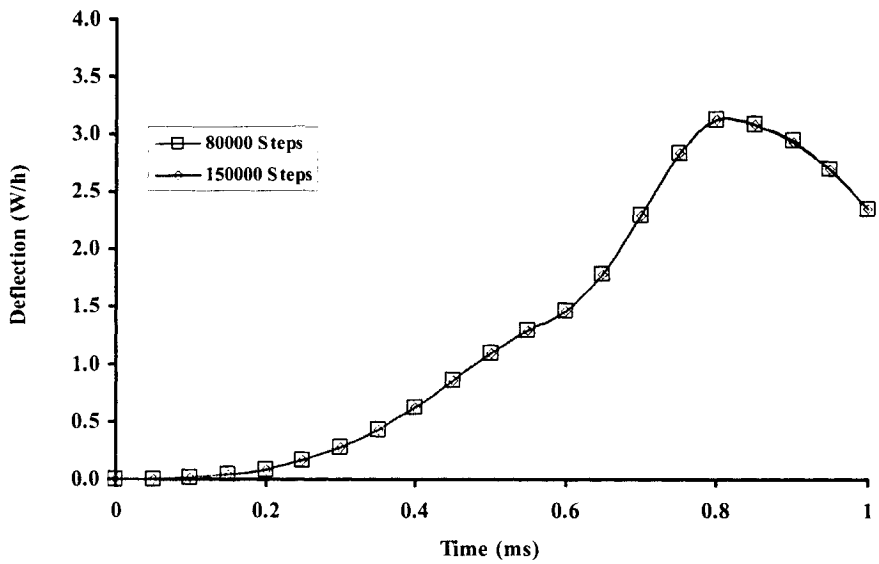

Figure 2-5 Time Step Sensitivity Analysis.

3 Pulse buckling Analysis

Numerical studies on dynamic pulse buckling and post-buckling response of FRP beams subject to axial impulse will be presented in this chapter. Results of the finite difference analyses based on the first and higher order shear deformation theories are compared with those of the finite element method obtained using LS-DYNA [LSTC, 1999]. Definition of pulse buckling of beams, establishing a measuring criterion for the onset of pulse buckling, stress wave propagation and sensitivity will be discussed.

3.1 Problem description

Two types of problems will be discussed in this chapter. One is a simply supported Kevlar/epoxy laminated beam impacted by a rectangular impact force, another is an E-glass/epoxy laminated beam with a fixed boundary condition subject to an impact by a moving mass.

The purpose of these problems is to investigate the dynamic buckling response of the beams subject to an impact force with short time duration and impact of a moving mass And further more, it is also targeted to establish a mean to establish the onset of pulse buckling criterion and perform sensitivity analysis in terms of slenderness ratio, magnitude of initial geometric imperfection, beam curvature and fiber angle.

3.1.1 Simply supported beam

An 8-layer simply supported Kevlar/epoxy laminated beam impacted by a rectangular pulse force is considered as shown in Figure 3.1. The lay-up of the laminated beam is $[(0)_8]$. The force magnitude is 1115 N. The initial geometric imperfection of the beam is

assumed to have a half sine wave form. The geometrical and material properties are tabulated in Table 3.1.

Table 3-1 Geometric and material properties of the simply supported beam.

Length (m)	Width (m)	Thickness (m)	Imperfection W_0 (m) ($W_0 \sin(\pi x/L)$)	E_{11} (N/m^2)	E_{22} (N/m^2)	G_{12} (N/m^2)	γ_{12}	Density (Kg/m^3)
0.762	0.0127	0.0003175	Factor * thickness	87×10^9	55×10^8	22×10^8	0.34	1380

Table 3-2 Geometric and material properties of the fixed support beam.

Length (mm)	Width (mm)	Thickness (mm)	Imperfection W_0(mm) ($W_0 \sin(\pi x/L)$)	E_{11} (N/m^2)	E_{22} (N/m^2)	G_{12} (N/m^2)	γ_{12}	Density (Kg/m^3)
300	20	1.6	Factor * thickness	39×10^9	86×10^8	38×10^8	0.28	2100

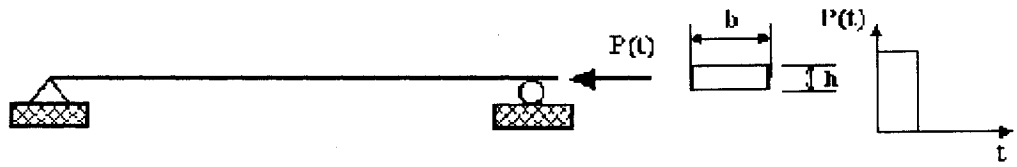

Figure 3-1 A slender beam is impacted by a pulse force.

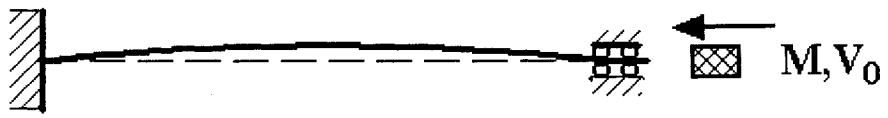

Figure 3-2 A slender beam is impacted by a moving mass.

3.1.2 Fixed-pinned beam

An 8-layer E-glass/epoxy laminated beam with the boundary condition shown in Figure 3.2 is considered. The initial geometric imperfection of the beam is assumed to have a half sine wave form. The lay-up of this beam is $[(0)_8]$. The right end of the beam is

impacted by a moving mass (see Figure 3-2). The geometrical and material properties are tabulated in Table 3.2.

3.2 Verification of the solutions

3.2.1 Comparison between FDM solution based on FSDT with FEM

3.2.1.1 Axial displacement at impacted end

Figure 3.3 shows the time history results (time range 0-0.001 second) of the axial displacement at the impacted end of the simply supported beams described in Section 3.1.1 obtained by the finite difference method (FDM) and finite element method (FEM) of LS-DYNA [LSTC, 1999], a commercial FEM code. In the FEM model, the beam is modeled as an orthotropic elastic laminated plate with the Belytschko-Tsay shell element. The load time duration is 5.0 microseconds.

For the fixed beam described in Section 3.1.2, the results obtained by the finite difference solution (FDM) of the First Order Shear Deformation Theory solution are compared with those of the FEM. The amplitude of the initial geometric imperfect half-sine wave was 10 percent of the thickness of the laminated beam. The beam was impacted by a moving rigid body with mass M=0.10 kg and initial velocity V_0=10.0 m/s. Figure 3.4 shows the results of axial displacement at the impacted end of beam.

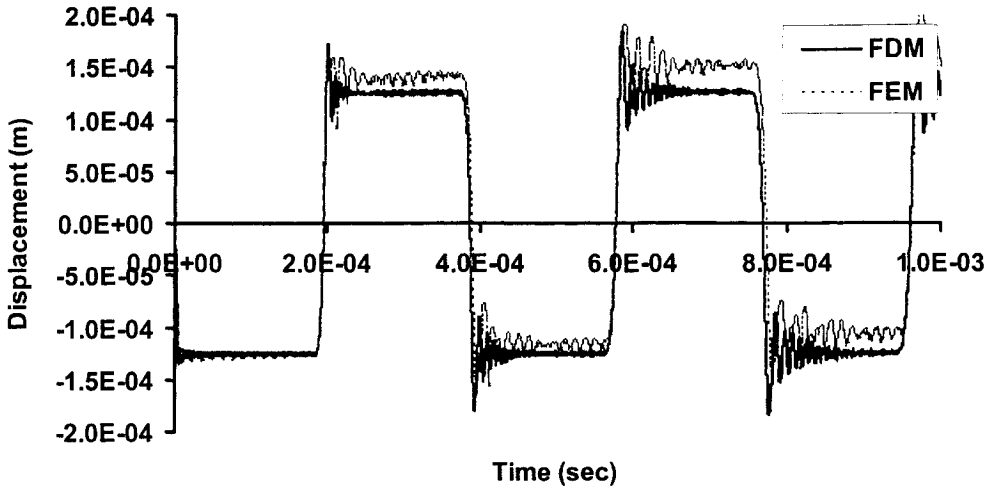

Figure 3-3 Axial Displacement of the impacted end of the simply supported beam.

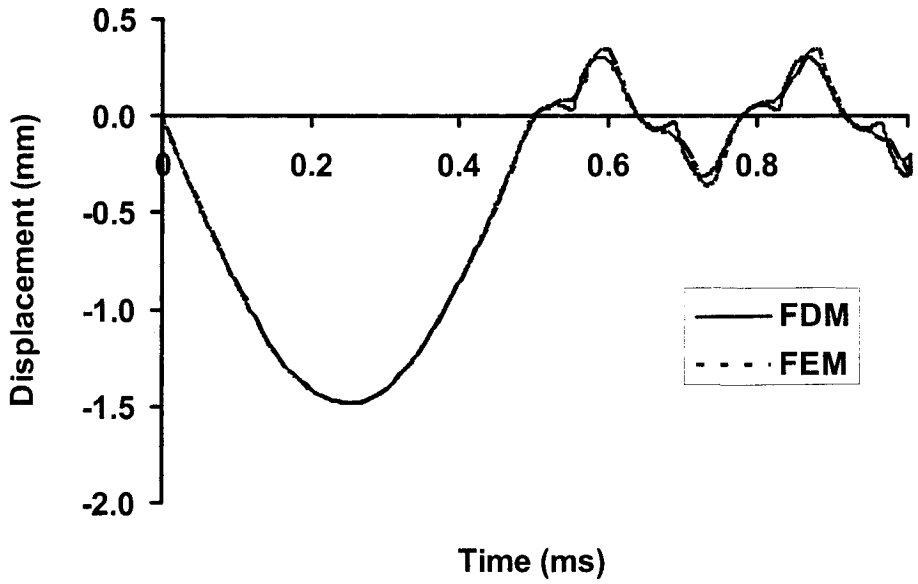

Figure 3-4 Axial Displacement of the impacted end of the fixed-pinned beam.

3.2.1.2 Compressive strain and stress wave propagation

Stress wave propagation is an important issue in dynamic buckling analysis. In this dissertation, we evaluate the stress wave in terms of strain wave. Figure 3.5 shows the comparison of strain wave results (time range 0-0.0001 seconds) of the simply supported beam obtained by proposed FDM and LS-DYNA FEM. From Figure 3.5, we can see that the FDM results agree well with the FEM results. Figure 3.6 shows the strain wave propagation at different stations along the beam obtained by FDM. With the help of Equation (2.3.9), we calculate the wave propagation velocity to be 7970 m/sec. The time for the stress wave to travel half of the beam length is $0.5*0.762/7970=4.78\text{x}10^{-5}$ seconds; this is graphically illustrated in Figure 3.6, as the time period between the first and third peaks ($7.57\ \text{x}10^{-5} - 2.71\ \text{x}10^{-5} = 4.86\ \text{x}10^{-5}$).

The minor discrepancies observed in the graphs of Figure 3.5 can be due to the differences in the formulations of the FDM and FEM. As stated, the proposed formulation accounts for the effects of axial and lateral deformation of the beam on the axial behavior (compressive shortening) by the von-Karman Strain-Displacement nonlinear relationship, as shown in Equation (2.3.2a). During the post-impact response of the beam, the increase in lateral deflection weakens the axial compressive endurance of the beam. Moreover, the Belytschko-Tsay shell element of LS-DYNA [LSTC, 1999] used in the analysis adopts an hourglass control algorithm to induce proper bending effect. It can be seen from Figure 3.5 that the FEM predictions become larger than that of FDM after the first compressive strain peak. The nonlinear relationship of strain and displacement can also be seen from Figure 3.6, in which the strain wave decreases as it travels from the impacted end to the fixed end, as the lateral deflection of the beam increases. This increase in deflection reduces the compressive strain as per Equation (2.3.2a). This is also consistent with the dynamic pulse buckling phenomenon, in that the axial load capacity does not increase as it will be described in the next section.

Similar phenomenon was obtained for the beam with fixed support, impacted by a moving mass, as described in section 3.1.2. Figure 3-7 shows the comparison of strain wave results of the fixed support beam obtained by proposed FDM and LS-DYNA FEM. Figure 3-8 shows the strain wave propagation at different stations along the beam obtained by the FDM.

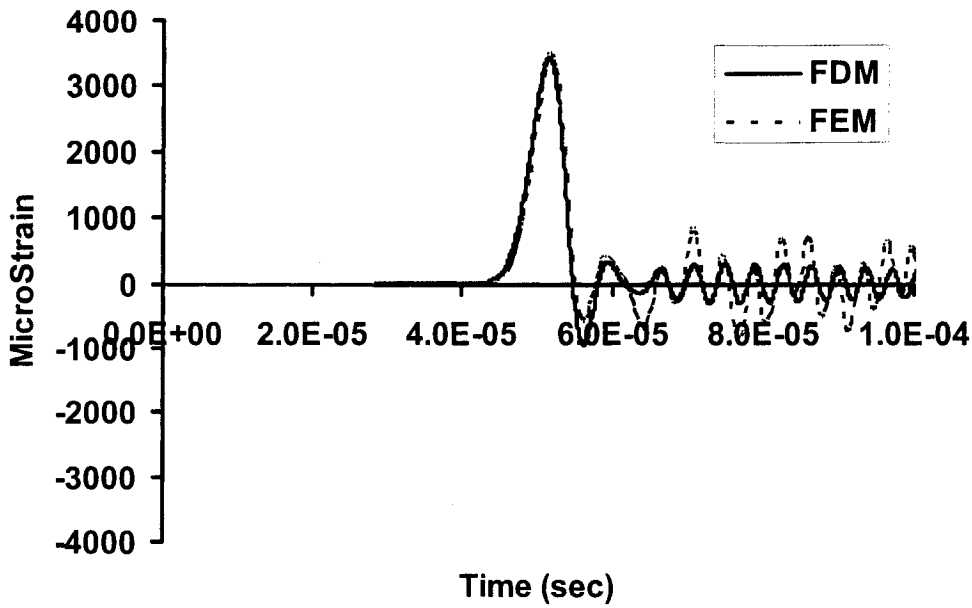

Figure 3-5 Time history results of compressive strain taken at the neutral axis of the simply supported beam's mid-span.

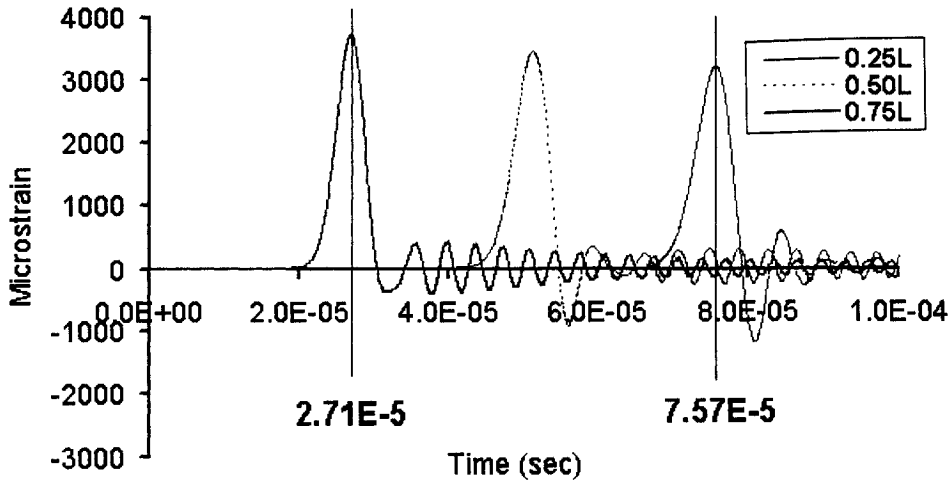

Figure 3-6 Strain Wave Propagation of the simply supported beam by FDM.

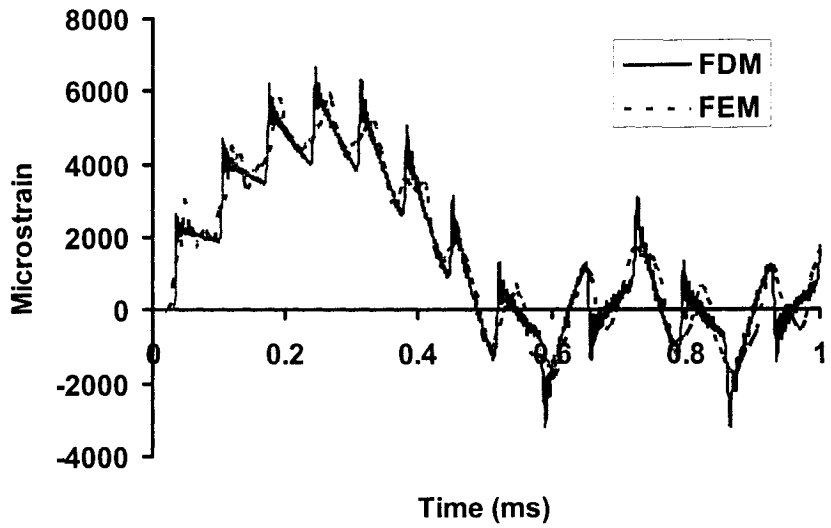

Figure 3-7 Time history results of compressive strain taken at the neutral axis of the fixed supported beam's mid-span.

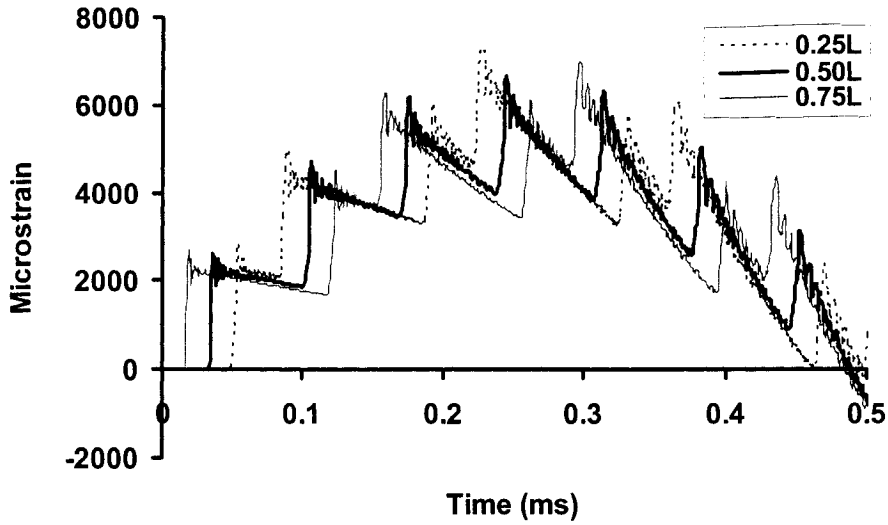

Figure 3-8 Strain Wave Propagation of the fixed supported beam by FDM.

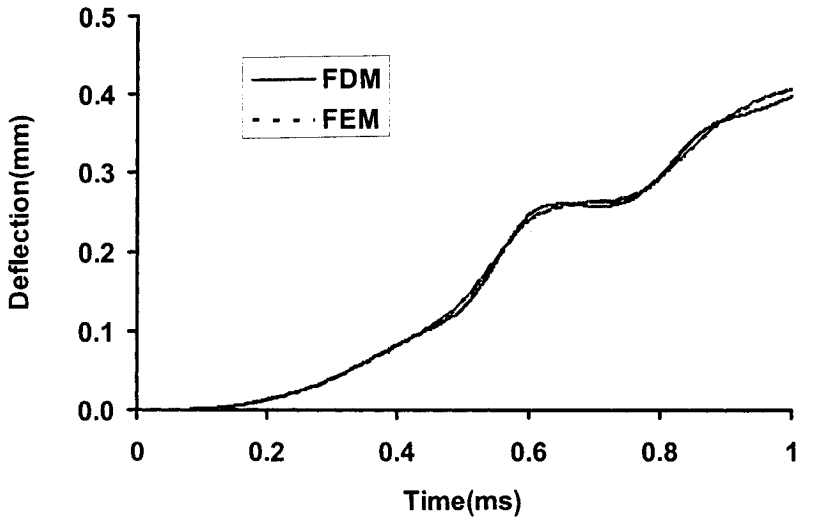

Figure 3-9 Deflection at mid-span of the fixed beam.

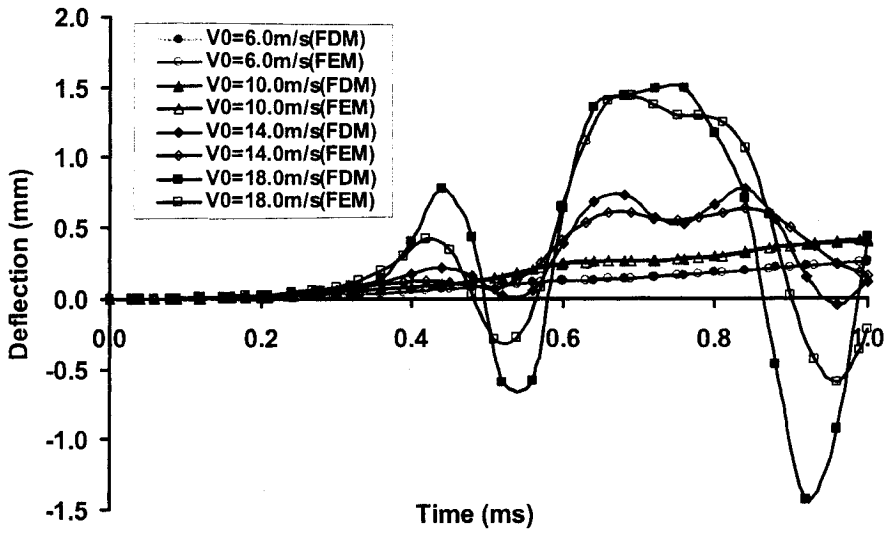

Figure 3-10 Comparison of the mid-span deflection at different impact velocities.

3.2.2 Comparison of the FDM-HSDT with FDM-FSDT and 3D-FEM results

The results obtained by the finite difference solution (FDM) of the higher order shear deformation theory (HSDT) are compared with those predicted by the Kirchhoff thin plate theory, the first order shear deformation theory (FSDT) in section 3.2.1 and those of 3-dimensional finite element (3D-FEM) produced by LS-DYNA [LSTC, 1999]. In the analysis with Kirchhoff thin plate theory, the rotational inertia of the cross section of the beam is not considered. In the FEM analysis, the beam was modeled as an orthotropic elastic solid with 8-node, 3D elements. The 3D solid element used was a 3D fully integrated quadratic 8-node element with nodal rotations. This element type has 48 degrees-of-freedom (LS-DYNA, 1999). It should be noted that with the ability to accommodate the rotational degrees of freedom, the behavior of this element is not as stiff as the conventional 3D element (which accommodates only the degrees of freedom at each node), when modeling behavior of plates and beams.

3.2.2.1 Axial displacement at impacted end

Figure 3-11 shows the results of the axial displacement sampled at the impacted end of the beam when the beam is impacted by a moving rigid body with a mass of M=0.10 kg at an initial velocity of V_0=10.0 m/s. The boundary condition was taken as a fixed support as shown in Figure 3-2. The amplitude(W_0) of the initial geometric imperfect half-sine wave was taken as 10% of the thickness (h) of the laminated beam. From Figure 3-11, one can see that the axial displacement results of the FDM-HSDT analysis agree very well with the results obtained from FDM-FSDT, 3D-FEM and the Kirchhoff thin plate theory.

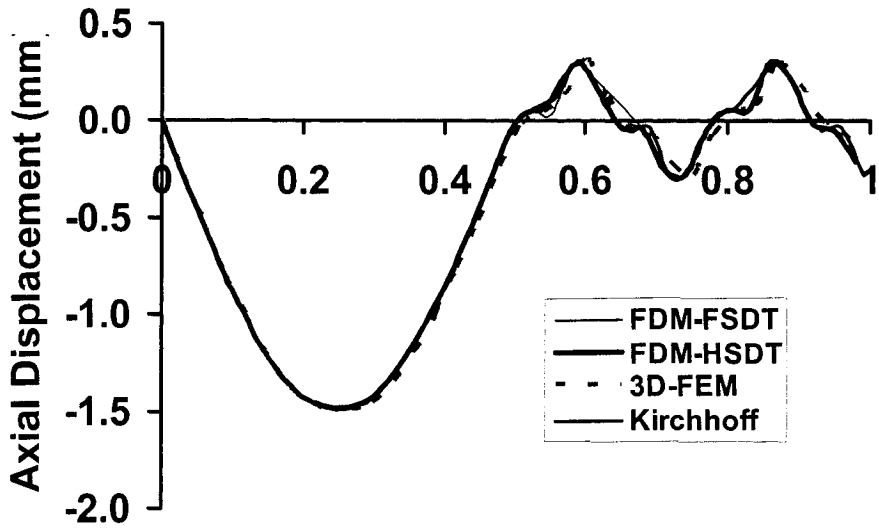

Figure 3-11 Comparison of the FDM-HSDT, FDM-FSDT and 3D-FEM results – Axial displacement at the impacted end.

3.2.2.2 Lateral deflection and compressive strain at mid-span of the beam

For the deflection of the beam (Figure 3-12), the FDM-HSDT results agree more closely to the 3D-FEM results than that of FDM-FSDT during the period when the mid-span deflection reaches its first peak. Without consideration of the rotation of the cross section of the beam, however, the Kirchhoff thin plate theory predicts a lower transverse deflection than other theories. From Figure 3-13, one can also see that in predicting the peak compressive strains at the neutral axis, the HSDT prediction is closer to the 3D-FEM results than the other two theories. This demonstrates that the solution of the HSDT is more accurate than that of FSDT in depicting the lateral displacement and strains of the beam in this type of dynamic problem.

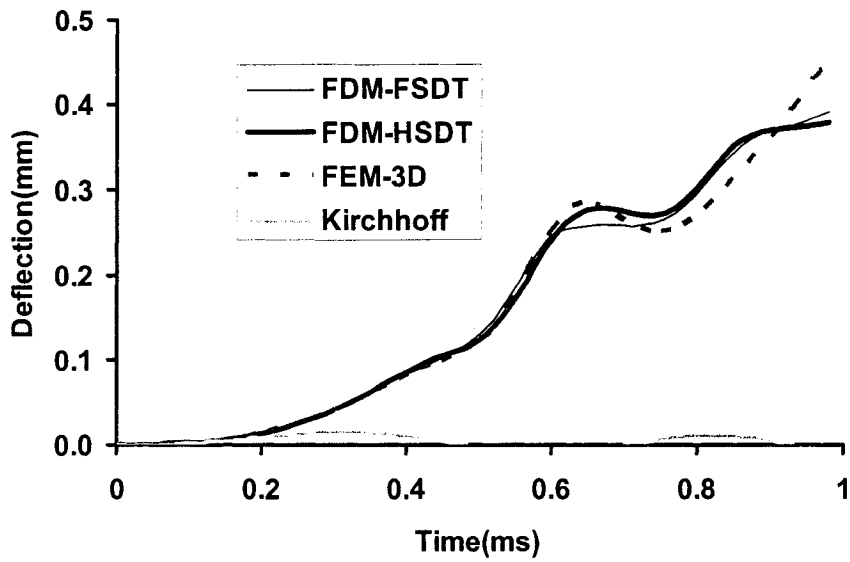

Figure 3-12 Comparison of the FDM-HSDT, FDM-FSDT and 3D-FEM results – mid-span deflection of the beam.

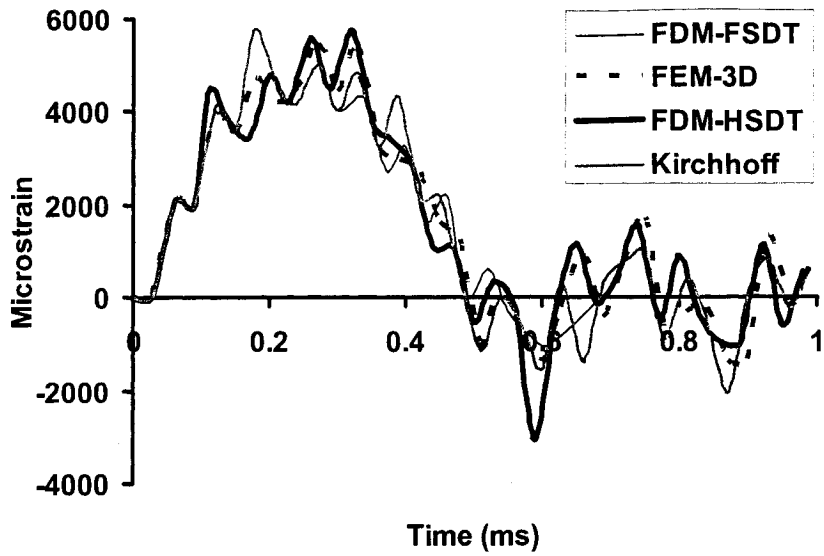

Figure 3-13 Comparison of the FDM-HSDT, FDM-FSDT and 3D-FEM results - compressive strain at the neutral axis of the beam mid-span.

3.3 Pulse buckling response and momentum

As mentioned earlier, dynamic pulse buckling, as an instability phenomenon, is characterized with excessive growth of the lateral, or out of plane displacement while the load capacity of the structure remains relatively unchanged. For the problem of simply supported beams described in Section 3.1.1, the right end of the beam is loaded by a constant force. In such a case, the dynamic response of the beam varies with the force time duration. When the force time duration is increased to the vicinity of some 'critical value', the deflection of the beam would increase drastically with a small increase of force time duration while the compressive strain of the beam remains relatively constant. Figure 3-14 shows the results of maximum lateral deflection of the beam versus the maximum compressive strain taken at the neutral axis of the beam's mid-span. The maximum deflection is chosen as the maximum lateral displacement of the beam and the

maximum compressive strain is chosen as the maximum compressive strain during the period of impact. Figure 3-15 shows the results of maximum deflection as a function of impulse (product of the force amplitude and force time duration). Figures- 3-14 and 3-15 show that after the impulse reaches a critical value, a small increase of the impulse causes the beam to buckle dynamically. The axial load capacity (see from the axial compressive strain diagram), however, does not increase as much as the deflection.

For the fixed beam described in Section 3.1.2, the beam is impacted by a moving mass. In such a case, the dynamic response of the beam varies with the different impact velocity of the moving mass. When the velocity of the moving mass is increased to the vicinity of some 'critical value', with a small increase of impact velocity (i.e., momentum of the moving mass), the deflection of the beam increases dramatically (see Figure 3-16), while the axial displacement and compressive strain of the beam have relatively smaller variation.

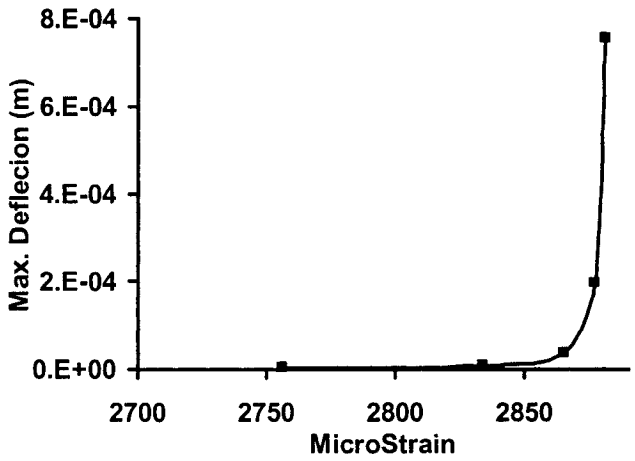

Figure 3-14 Dynamic pulse buckling response of beam (Length = 0.762m) with initial geometric imperfection amplitude $W_0 = 0.10h$. Maximum deflection at mid-span of beam versus maximum axial compressive strain taken at the neutral axis of the beam's mid-span.

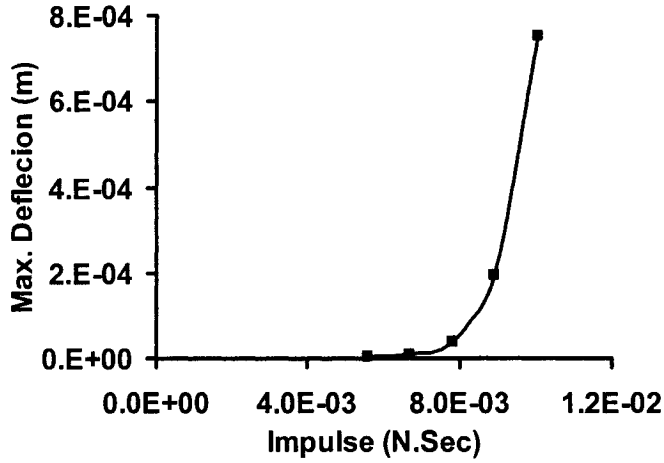

Figure 3-15 Dynamic pulse buckling response of beam (Length = 0.762m) with initial geometric imperfection amplitude $W_0 = 0.10h$. Maximum deflection at the mid-span of beam as a function of impulse.

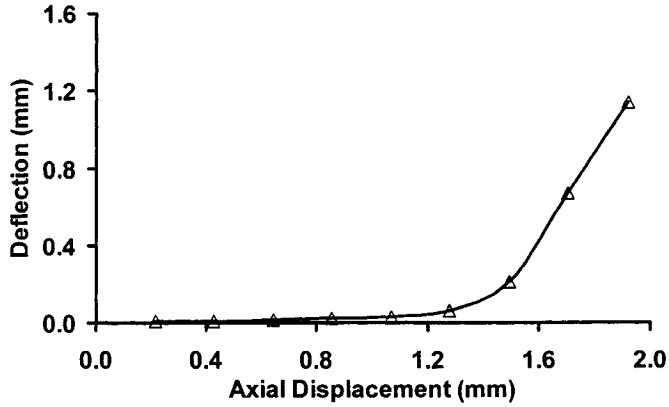

(a)

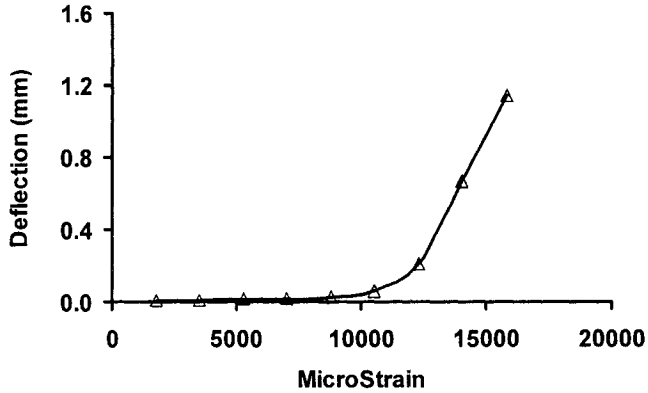

(b)

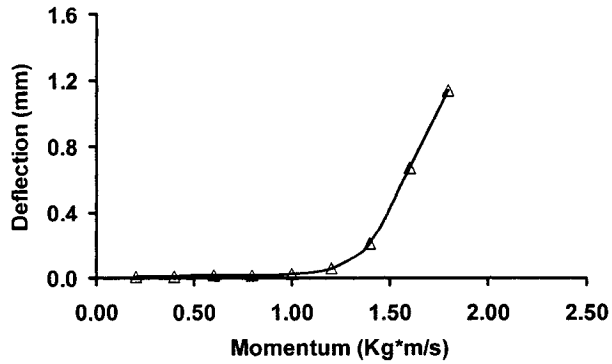

(c)

Figure 3-16 Dynamic pulse buckling response of the beams with Length = 150 mm, width = 20 mm, initial geometric imperfection $W_0 = 0.01h$ – (a) mid-span deflection versus maximum axial displacement at the impacted end, (b) mid-span deflection of beam versus compressive strain at the neutral axis of the beam's mid-span, and (c) mid-span deflection versus impact momentum.

3.4 Sensitivity analysis

3.4.1 Sensitivity analysis of initial geometric imperfection

3.4.1.1 Simply supported beam loaded by a constant force

To investigate the effect of initial geometric imperfection of the beam on the critical impulse, (i.e., the sensitivity of imperfection,) four beams with length of 0.762m and different initial geometric imperfections of $W_0 = 0.01h$, $W_0 = 0.05h$, $W_0 = 0.10h$, and $W_0 = 0.15h$ were analyzed with varying load time duration. Figure 3-17(a) shows the maximum deflection of the beams versus the compressive strain taken at the neutral axis of the mid-span of the beam. Figure 3-17(b) shows the maximum deflection of the beam as a function of impulse. It is obvious that the bigger the initial geometric imperfection, the smaller the critical impulse and axial load capacity (i.e., axial compressive strain). Similar phenomenon occurs for the other beams with different lengths (0.6096m and 0.4572m).

3.4.1.2 Fixed beam impacted by a moving mass

To investigate the influence of initial geometric imperfection of the beam on the critical momentum, three beams with lengths of 450mm, 300 mm and 150 mm, each with width of 20 mm, and different initial geometric imperfections of $W_0 = 0.001h$, $W_0 = 0.01h$, and $W_0 = 0.10h$, were analyzed subject to varying impact velocities. The resulting lateral deflection at the mid-span of the beam versus the maximum axial displacement at the impacted end is shown in Figure 3-18(a). Figure 3-18(b) shows the resulting mid-span deflection versus the maximum compressive strain (taken during the period of impact), for the 450 mm long beams. In Figure 3-18(c), the resulting deflection is plotted as a function of impact momentum (product of the impact mass and velocity). It is obvious that the larger the initial geometric imperfection, the smaller the critical momentum and

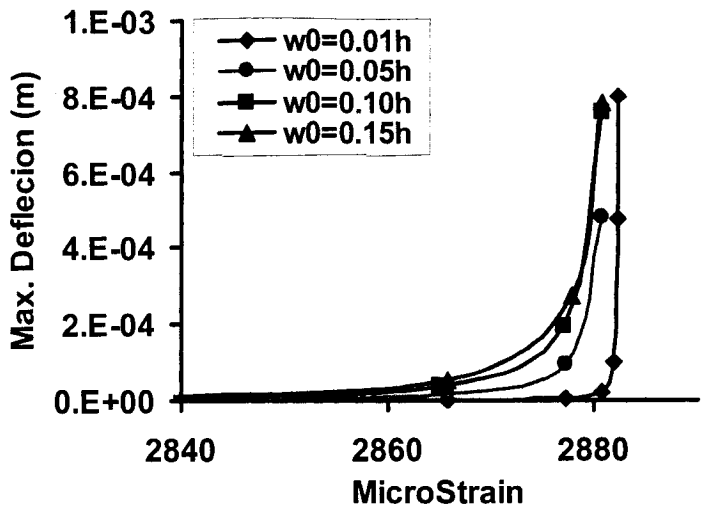

(a)

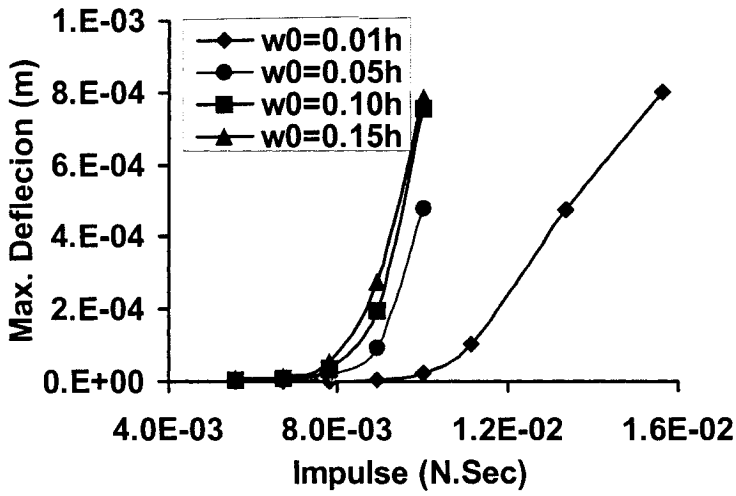

(b)

Figure 3-17 Dynamic pulse buckling of beam (Length=0.762m) for different initial geometric imperfections. (a) maximum deflection versus compressive strain; (b) maximum deflection as a function of impulse.

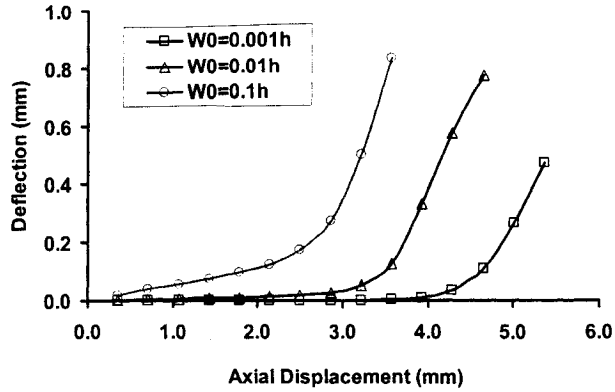

(a)

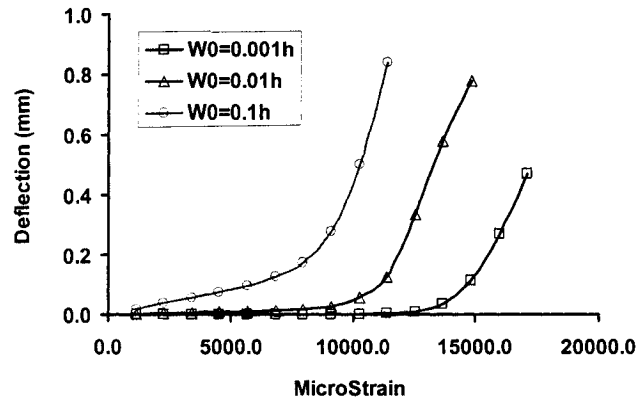

(b)

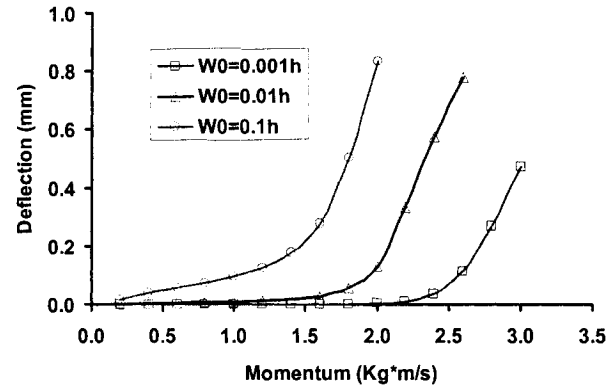

(c)

Figure 3-18 Dynamic pulse buckling response of the beams with Length = 450 mm, Width = 20 mm, for different initial geometric imperfection – (a) mid-span deflection versus maximum axial displacement at the impacted end, (b) mid-span deflection of beam versus compressive strain at the neutral axis of the beam's mid-span, and (c) mid-span deflection versus impact momentum.

axial load capacity (i.e., axial displacement and axial compressive strain). Similar responses are exhibited for the other beams with different lengths (300 mm, and 150 mm), as shown in Figures 3-19 and 3-20, respectively. Figure 13-18(c) also indicates that regardless of the initial imperfection amplitude, once the momentum reaches a critical value, with a minor increase in the momentum, the beams undergo dynamic buckling (*i.e.*, the lateral deflection increases rapidly and excessively). The axial load capacity (seen from the axial displacement and axial compressive strain diagram), however, does not increase as significantly as the lateral deflection. In Section 3.5, we will see the momentum can be viewed as a mean for detecting the onset of pulse buckling for beams.

3.4.2 Sensitivity analysis of slenderness ratio

Under static and quasi-static loading conditions, the Euler critical buckling load increases with the decrease of slenderness ratio. This, however, does not hold in dynamic pulse buckling.

Figure 3-21(a) shows the variation of maximum deflection versus maximum compressive strain for beams with different lengths (0.4572m, 0.6096m and 0.7620m) and with an initial geometric imperfection $W_0 = 0.10h$ for the simply supported beams described in Section 3.1.1. Figure 3-21(b) shows the variation of maximum deflection as a function of impulse for the same beams. From Figure 3-21, we observe that for a specific initial imperfection, the buckling critical impulse and compressive strain (i.e., the axial load capacity) decrease as the length decreases (i.e., the decrease of slenderness). Similar phenomenon occurs for the other beams with different imperfection magnitudes ($W_0 = 0.05h$, and $W_0 = 0.15h$).

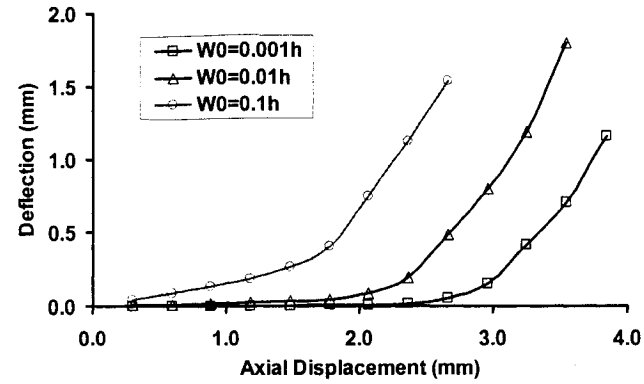

(a)

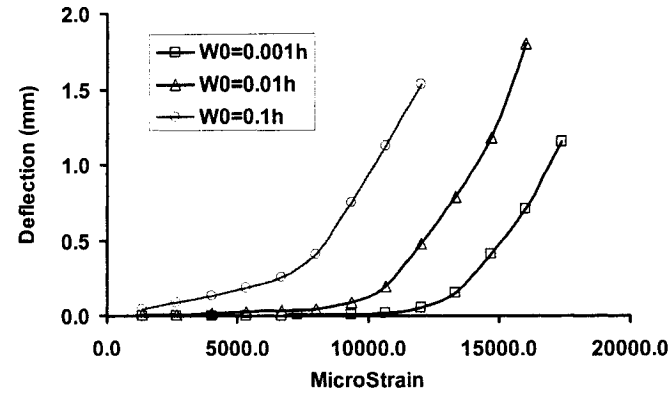

(b)

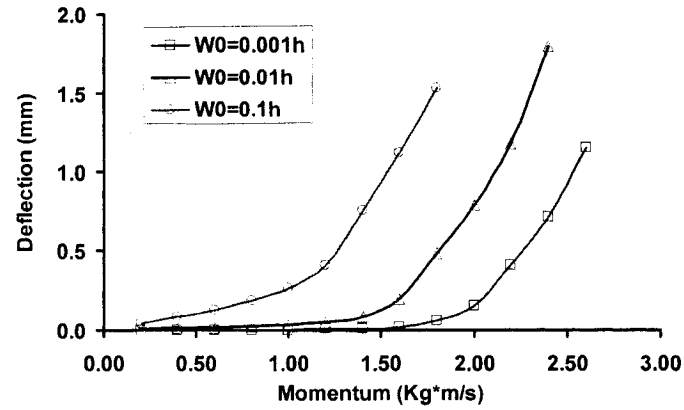

(c)

Figure 3-19 Dynamic pulse buckling response of the beams with Length = 300 mm, Width = 20 mm, for different initial geometric imperfection – (a) mid-span deflection versus maximum axial displacement at the impacted end, (b) mid-span deflection of beam versus compressive strain at the neutral axis of the beam's mid-span, and (c) mid-span deflection versus impact momentum.

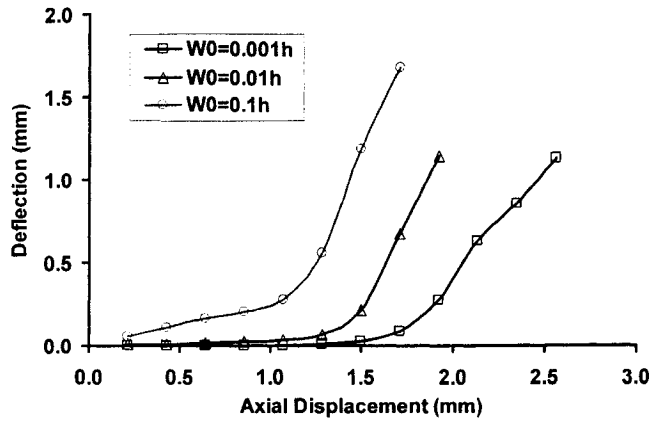

(a)

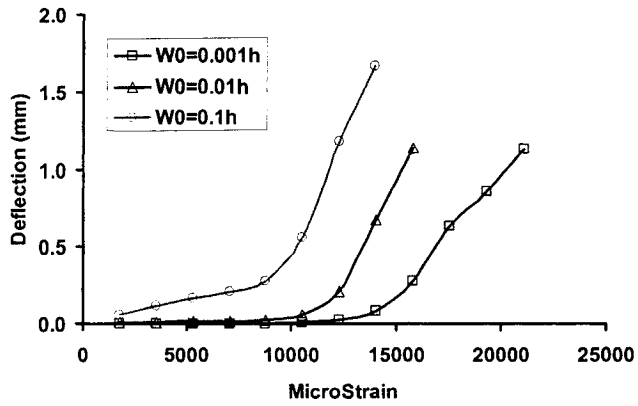

(b)

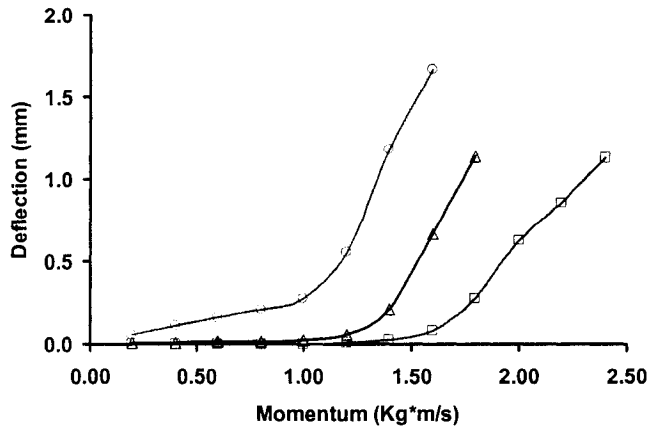

(c)

Figure 3-20 Dynamic pulse buckling response of the beams with Length = 150 mm, Width = 20 mm, for different initial geometric imperfection – (a) mid-span deflection versus maximum axial displacement at the impacted end, (b) mid-span deflection of beam versus compressive strain at the neutral axis of the beam's mid-span, and (c) mid-span deflection versus impact momentum.

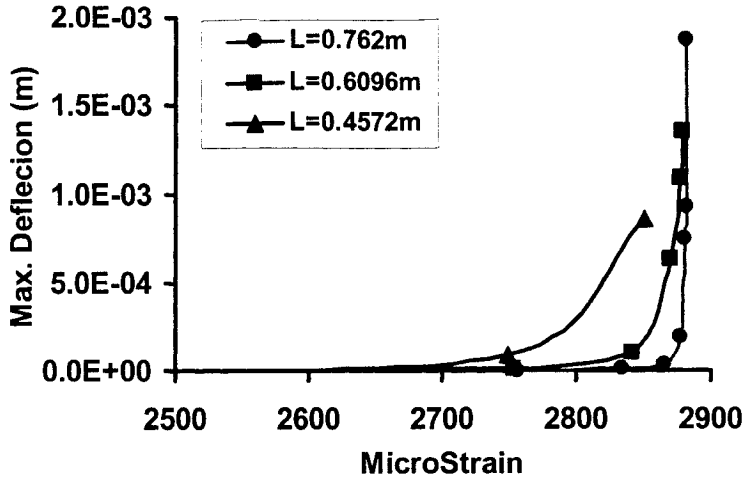

(a)

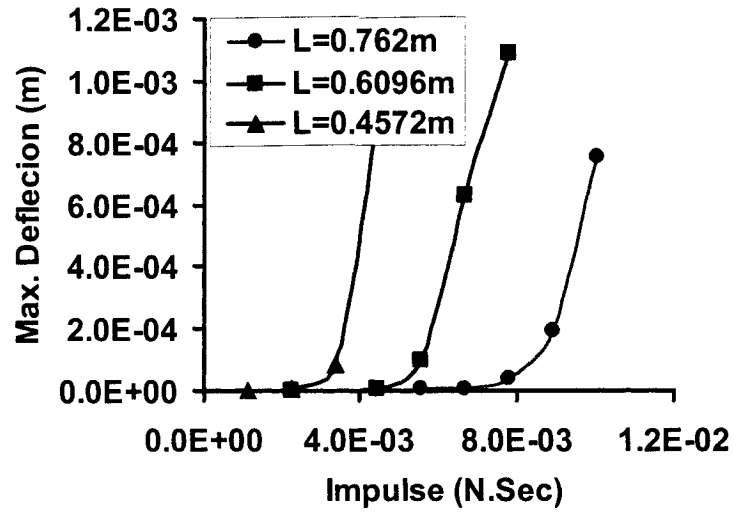

(b)

Figure 3-21 Variation of the maximum deflection for different beam lengths.
(a) deflection versus maximum compressive strain;
(b) deflection as a function of impulse.

Considering the momentum graphs (Fig. 3-18(c), 3-19(c), and 3-20(c)) of the fixed beams described in Section 3.1.2, one would observe that shortening the beam length does not necessarily increase the buckling momentum.

The response depicted by the above plots presents a contradictory response, in that, the beams undergo sudden instability as the slenderness ratio decreases (i.e., as the length gets shorter), for all of the initial imperfection values tested. This is opposite to what common sense would indicate, as one would expect that the critical buckling capacity should increase as the slenderness ratio decreases. Such a response is due to the fact that for a specific imperfection amplitude, the shorter the beam, the larger the curvature of the beam. With the realization that the bending moment is proportional to the curvature, therefore, the larger the curvature, the higher the bending moment. This phenomenon is also validated by the response shown in Figure 3-22 and Figure 3-23. One can therefore state that the curvature of the imperfect beam plays a more significant role than the beam's slenderness ratio.

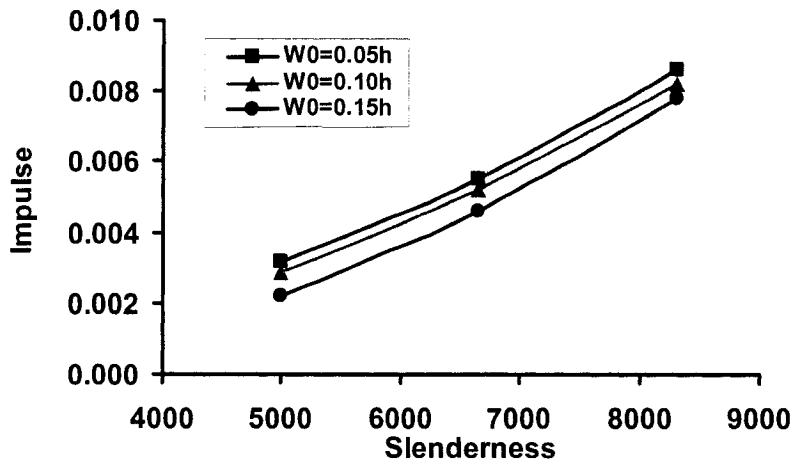

Figure 3-22 The critical buckling impulse as a function of slenderness ratio for different initial geometric imperfections.

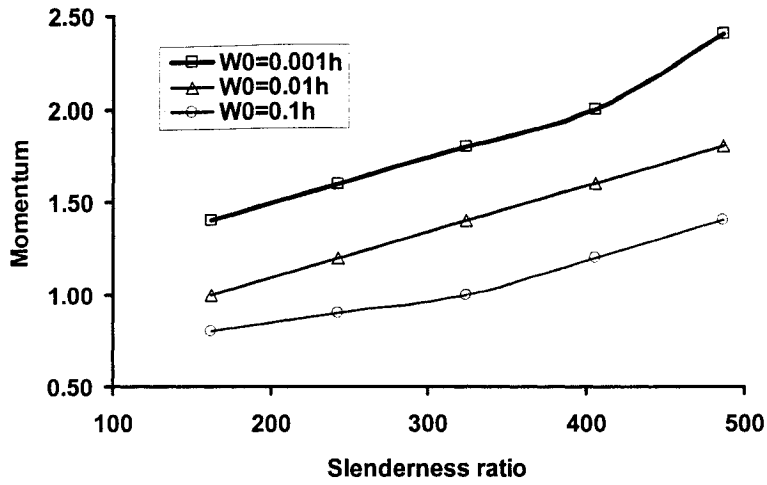

Figure 3-23 Variation of buckling momentum as a function of slenderness ratio.

3.4.3 Effect of the beam's curvature

Figure 3-24 and Figure 3-25 show the variation of buckling impulse/momentum as a function of maximum curvature of the beam for different initial geometric imperfections. From the diagrams, one can predict the critical impulse/momentum of a beam for a specific imperfection and slenderness ratio based on the maximum curvature of the beam.

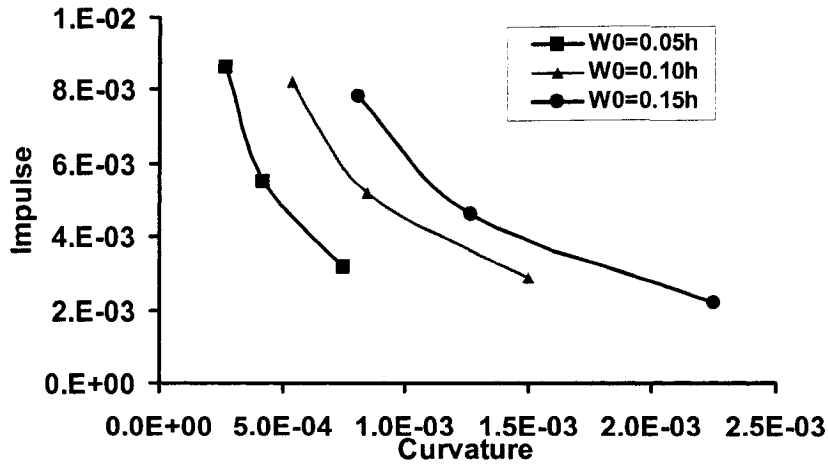

Figure 3-24 Buckling impulse as a function of curvature for different initial geometric imperfections for the simply supported beam subject to a constant force with a short time duration.

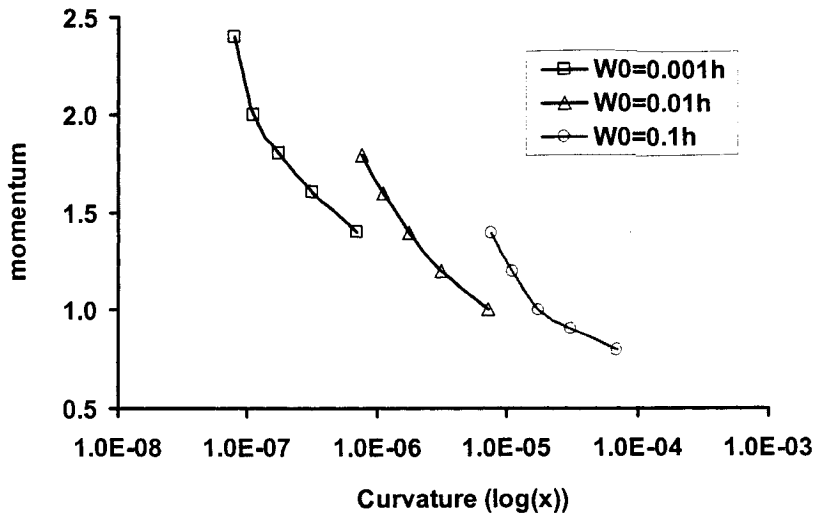

Figure 3-25 Critical buckling momentum as a function of curvature for different initial geometric imperfections for the fixed beam subject to impact of a moving mass.

3.4.4 Effects of fiber angle

For FRP laminated beams, the fiber angle has an important effect on the critical buckling impulse. Beams with imperfection of $W_0 = 0.10h$, and different fiber angles were analyzed. Figure 3-26(a) shows the maximum deflection at the mid-span of the beams as a function of impulse, while Figure 3-26(b) shows the maximum axial displacement at the impacted end of the beams as a function of impulse. From Figure 3-26, we can see that the increase in stiffness in transverse direction and relative decrease in longitudinal stiffness would increase the dynamic buckling capacities of the beams. It is also noted that increase in stiffness in the transverse direction would result in an increase of maximum axial displacement. Figure 3-27 shows the critical buckling impulse as a function of the ratio of longitudinal to transverse stiffness (A_{11} / A_{22}).

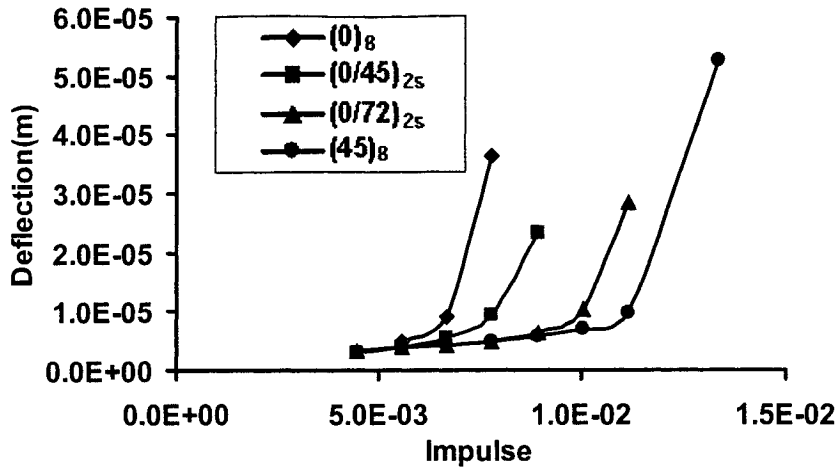

(a)

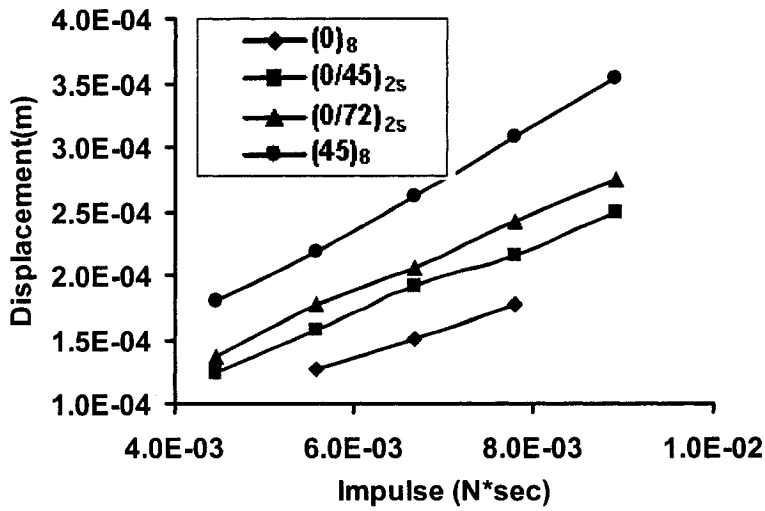

(b)

Figure 3-26 Dynamic pulse buckling response for beams with different fiber angle layup.

(a) maximum deflection as a function of impulse;

(b) maximum axial displacement as a function of impulse.

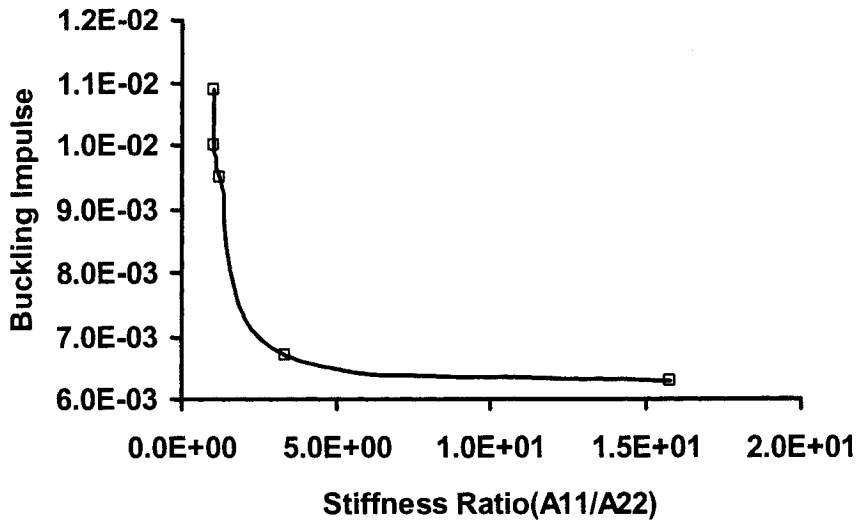

Figure 3-27 Critical buckling impulse as a function of stiffness ration of longitudinal and lateral stiffness A_{11} / A_{22}.

3.4.5 Comparison of effects of boundary conditions

As stated earlier, to investigate the influence of boundary conditions on the pulse buckling and postbuckling responses of the beams, two types of boundary conditions were considered: (i) fixed-end support (FS) and (ii) pinned-end support (PS), as shown in Figure 3-28.

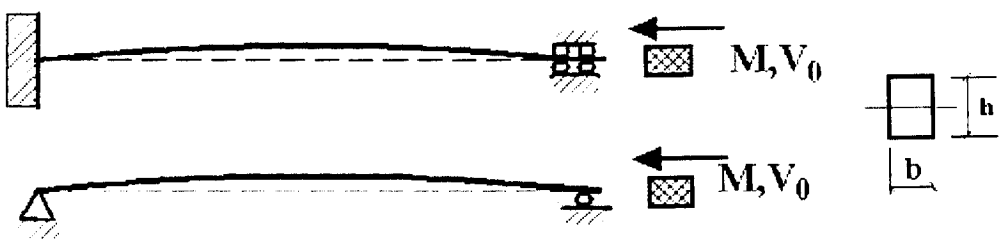

Figure 3-28 The Laminated FRP beam model with different boundary conditions (fixed and simply supported).

3.4.5.1 The influence of axial displacement, axial compressive strain and deflection

Figure 3-29 shows the results of the axial displacement, axial compressive strain and deflection for different boundary conditions when the beam was impacted by a moving rigid body with a mass of M=0.10 kg and initial velocity of V_0=10.0 m/s. The amplitude (W_0) of the initial geometric imperfect half-sine wave was taken as 10 percent of the thickness (h) of the laminated beam. From Figure 3-29, we can see that during the impact period (approximately 0.0~0.5ms), the transverse boundary conditions had no influence on the response. In general, the axial displacement was much larger than the lateral deformation of the beam. Considering the one-dimensional wave propagation equation of a perfect beam as

$$\frac{\partial^2 \bar{u}}{\partial \tau^2} = \frac{\partial^2 \bar{u}}{\partial \bar{x}^2} \tag{3-1}$$

one can forecast that the axial component of the boundary condition controls the axial wave propagation. During the post impact period, however, the deflection for the simply-support case becomes larger than that of the fixed-pinned support beam, as shown in Figure 3-29(b). This is mainly due to the fact that the PS provides no rotational constraint to the beam.

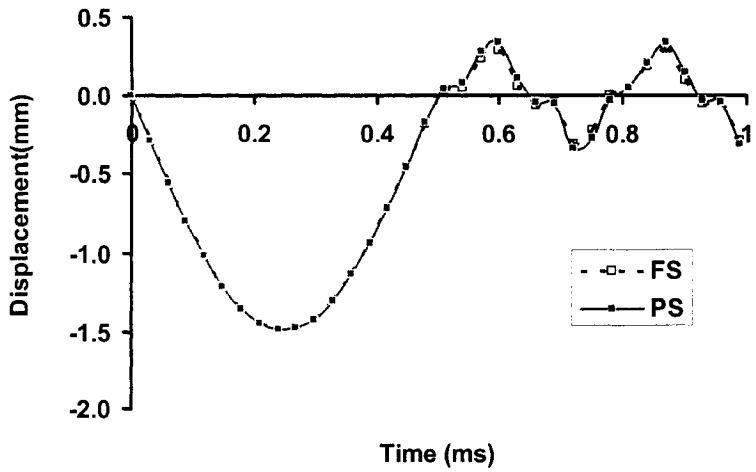

(a)

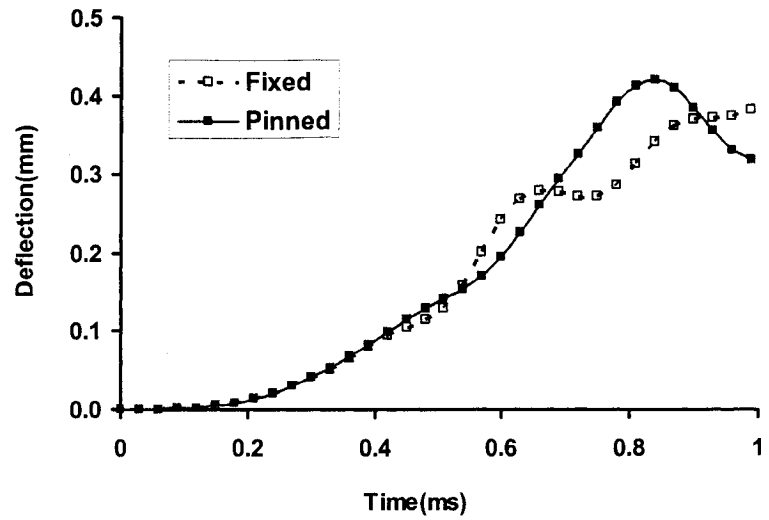

(b)

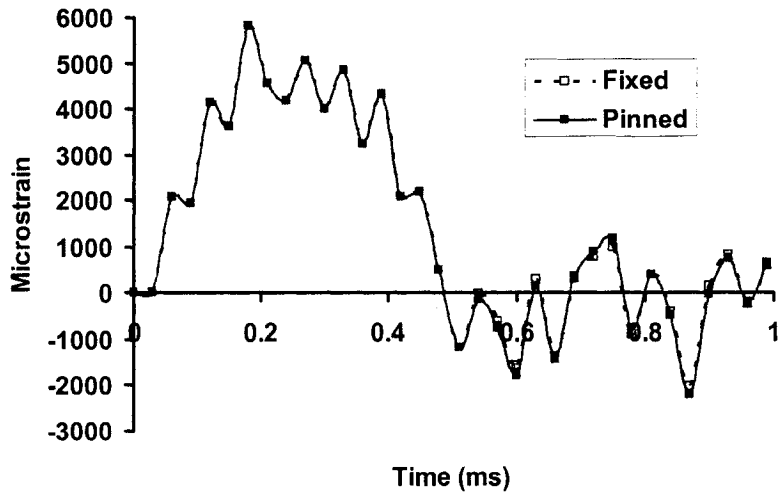

(c)

Figure 3-29 Comparison of the influence of fixed-pinned support (FS) and pinned-end support (PS) on: (a) axial displacement at the impacted end; (b) mid-span deflection of the beam; (c) compressive strain at the neutral axis of the beam mid-span.

3.5 Pulse buckling criterion

3.5.1 Momentum as a dynamic pulse buckling criterion

Momentum (M_t), defined as the product of mass (M) and impact velocity (V_0) of the moving mass, can be considered as a parameter that predicts dynamic instability. It is assumed that the investigated beams experienced dynamic instability when their momentum approached a critical value. Figure 3-30 shows the resulting deflection as a function of momentum, in which four curves were plotted for the fixed beam with $W_0 = 0.001h$ and L=300mm impacted by a moving mass, $M = 0.1Kg$, with velocities of $V_0 = 6.0m/s$, $V_0 = 8.0m/s$. Figure 3-31 and Figure 3-32 illustrate the graphs for the beams with $W_0 = 0.01h$ and $W_0 = 0.1h$, respectively.

These plots illustrate that the critical buckling momentum for a beam with a given initial imperfection is a stationary value, irrespective of variation of the impact mass and velocity. Therefore, momentum may be used as a reasonable mean for predicting the onset of dynamic pulse buckling of FRP laminated beams subjected to axial impact of a moving mass.

3.5.2 Effects of boundary conditions

3.5.2.1 Buckling criteria

As mentioned earlier, dynamic pulse buckling, as an instability phenomenon, is characterized with unbounded growth of the lateral, or out of plane displacement, while the load bearing capacity of the component remains relatively unchanged. In our investigation, the beams with different boundary conditions were impacted by a moving mass. In such a case, the dynamic response of the beams varied with the impact velocity

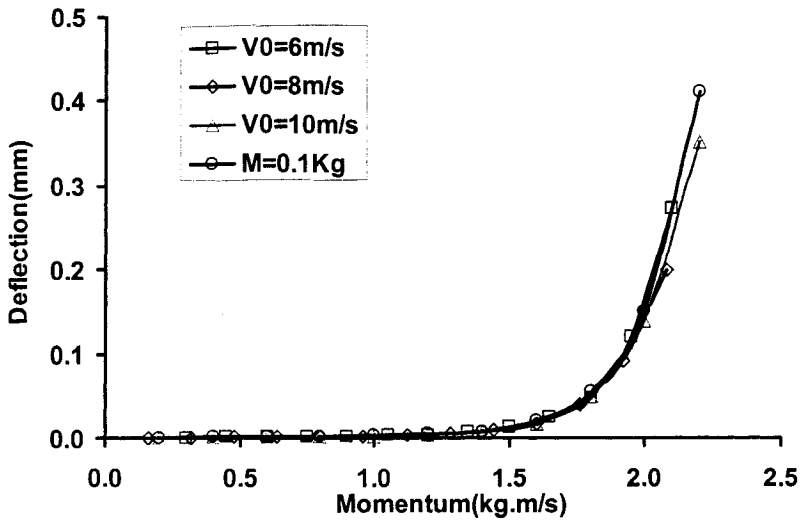

Figure 3-30 Variation of the mid-span deflection as a function of impact momentum for various combinations of velocity and initial imperfection ($W_0 = 0.001h$, L=300mm).

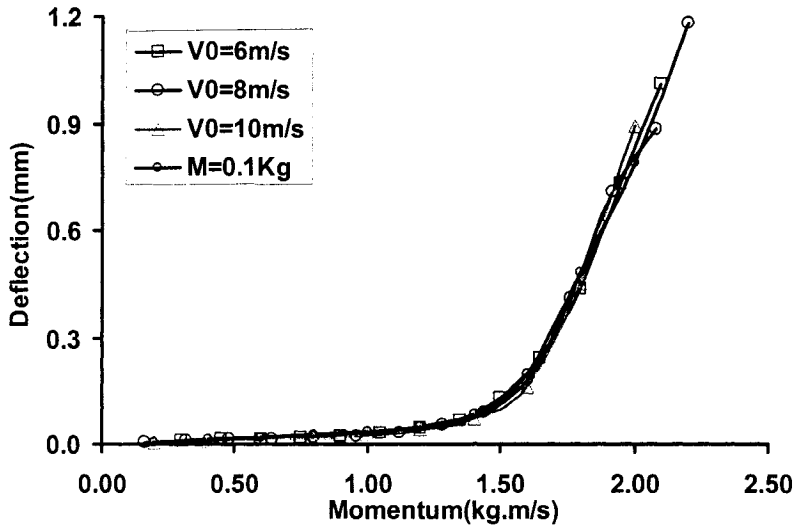

Figure 3-31 Variation of the mid-span deflection as a function of impact momentum for various combinations of velocity and initial imperfection ($W_0 = 0.01h$, L=300mm).

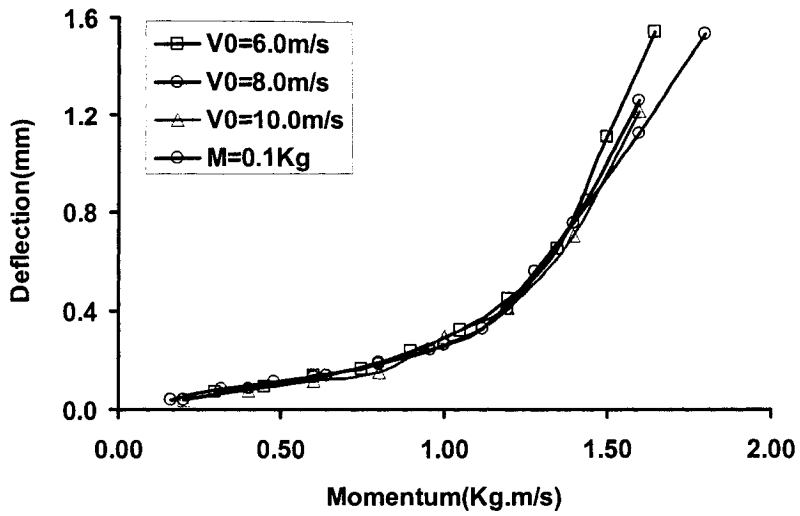

Figure 3-32 Variation of the mid-span deflection as a function of impact momentum for various combinations of velocity and initial imperfection ($W_0 = 0.10h$, L=300mm).

of the moving mass. When the velocity of the moving mass was increased to the vicinity of a 'critical value', the deflection of the beams increased dramatically, while the compressive strain of the beams remained relatively unchanged. As discussed in section 3.5.1 and by Zhang and Taheri [2002b, 2002c], the momentum (product of mass and velocity) could be used as a mean for predicting the onset of dynamic pulse buckling of FRP laminated beams subjected to axial impact of a moving mass. To further validate our hypothesis, we examined the variation of mid-span deflection of beams as a function of momentum for beams having various initial geometric imperfections, restrained by various boundary conditions, as shown in Figure 3-33. One can clearly see from the figure that for both types of supports, the larger the magnitude of the initial geometric imperfection, the smaller the critical buckling momentum. This is consistent with the earlier findings of Zhang and Taheri [2002a, 2002b, 2002c] and the discussion outlined in Section 3.4.1. Figure 3-33 indicates that the influence of boundary conditions on the critical pulse buckling momentum is relatively negligible. This phenomenon can also be seen from the time history results of mid-span deflection of the beams impacted with

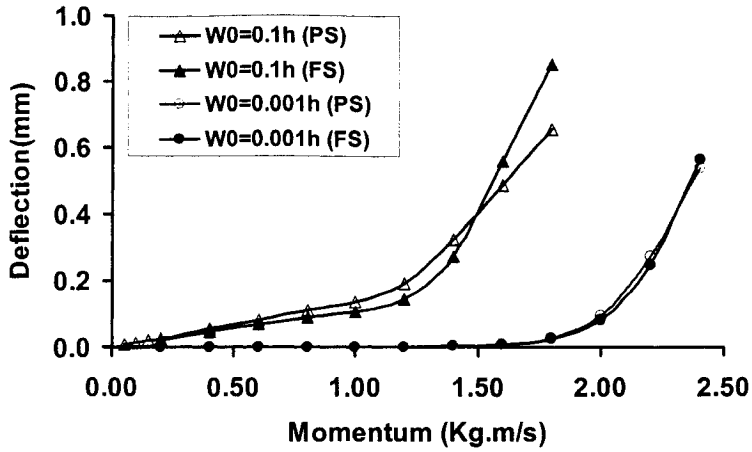

Figure 3-33 Dynamic pulse buckling response of beams having different initial geometric imperfections and boundary conditions - mid-span deflection versus impact momentum.

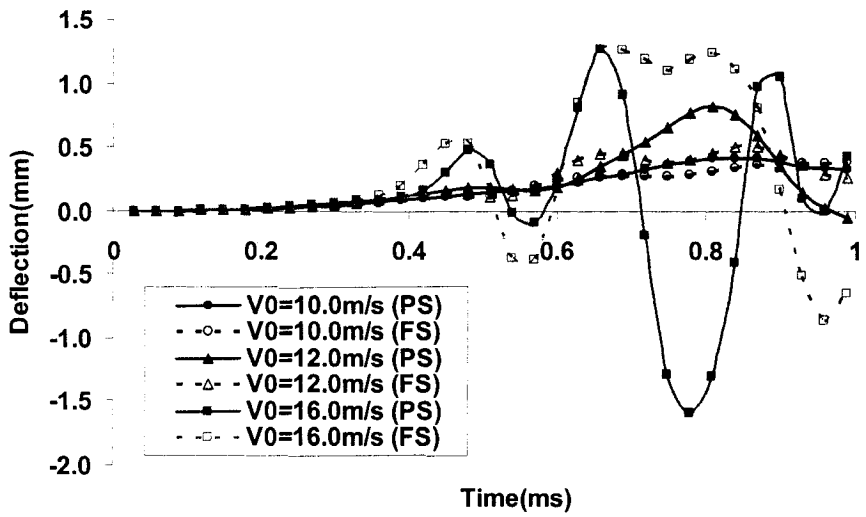

Figure 3-34 Time history results of mid-span deflection for different impact velocities.

different impact velocities, as shown in Figure 3-34. The magnitude of initial geometric imperfection was taken as $W_0 = 0.1h$. Although the lateral response of beams is different depending on the boundary conditions, the critical impact velocity is very similar. From Figure 3-33, we can also see that the critical buckling momentum for the initial geometric imperfection of $W_0 = 0.1h$ is about 1.2 Kg.m/s, which corresponds to the impact velocity of 12.0 m/s for a striker mass of 0.1Kg. The same trend can be seen from the deflection curves of Figure 3-34, in which the lateral deflection for the 12.0m/s velocity is much larger than that at a velocity of 10.0m/s, particularly for the simply supported beam.

3.5.2.2 Buckling profile

Beam buckling profile is an important concern in buckling analysis. The position of the maximum deflection of the beam plays an important role in such analysis. Figure 3-35 shows the buckling profiles of the beams under the critical impact velocity of V_0=12.0m/s restrained by PS and FS boundary conditions. One can see that the maximum deflection occurs at the impacted end of the beam at the onset of pulse buckling.

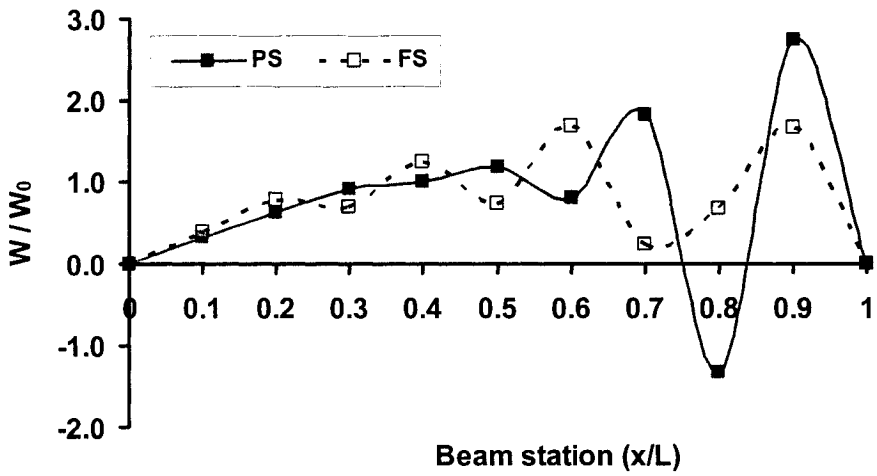

Figure 3-35 Buckling profiles of the beams under the critical impact velocity (V_0=12.0m/s) for both types of boundary conditions.

3.6 Post-buckling analysis

Figure 3-36 shows the dynamic profile (lateral deflection), and axial displacement along the pinned supported beam, before and after the onset of pulse buckling. The beam was impacted by a critical momentum, corresponding to the impact velocity of 12.0m/s. One can see from the graphs that the onset of buckling occurred at 0.5ms during the event. The beam then oscillated in high modes, with deflection larger than its pre-buckling state. The axial displacement reached a maximum before the beam buckled, and then kept oscillating with a lower magnitude after buckling. Similar phenomenon occurred for the fixed support beam, as shown in Figure 3-37. Comparing Figures 3-36 and 3-37, one observes that the vibration amplitude of the PS beam is larger than the FS beam, when beams are subjected to the same momentum.

3.7 Conclusions

Dynamic pulse buckling of FRP laminated slender beams with initial geometric imperfections, subject to impulse loads were numerically investigated. Several factors, such as the beam's axial and transverse inertia, transverse shear deformation, the non-uniform distribution of shear stress across the beam section, and the cross section's rotational inertia, were considered in the equilibrium equations, as described in Chapter 2. The von-Karman nonlinear Strain-Displacement relationship was used to model the deformation of the beam. The First-Order Shear Deformation (FSDT) and Higher-Order Shear Deformation (HSDT) theories were adopted to model the displacement field of the beam. The kinematics equations were developed and demonstrated to be valid for various boundary conditions and types of impulse. The parameters investigated in the study (through sensitivity analysis) included the effect of initial geometric imperfection, slenderness ratio and curvature of the beam on the pulse buckling response. The effects of boundary conditions on the pulse buckling and postbuckling responses were also

numerically investigated and discussed. A mean for predicting the onset of the dynamic pulse buckling was established.

The following summaries and conclusions are reached:

(i) The results obtained from the proposed finite difference formulations agree well with the results obtained from the 3D finite element analyses. The results based on the HSDT solution are closer to those of FEA.

(ii) Momentum may be considered as a viable parameter for predicting the dynamic pulse buckling limit of beams.

(iii) The onset of dynamic pulse buckling may be predicted from the graph of momentum/impulse versus curvature.

(iv) It is apparent that critical buckling momentum decreases with the increase in initial geometric imperfection amplitude. The amplitude of initial geometric imperfection plays a more significant sole in promoting dynamic pulse buckling than the slenderness ratio of the beam.

(v) As the ratio of the transverse to longitudinal stiffness increases, the critical dynamic buckling capacity also increases, thereby indicating the influence of fiber angle or layup sequence.

(vi) It is evident that pulse buckling response is mainly controlled by the axial component of the restraints, while the rotational restraints produce minimal influence.

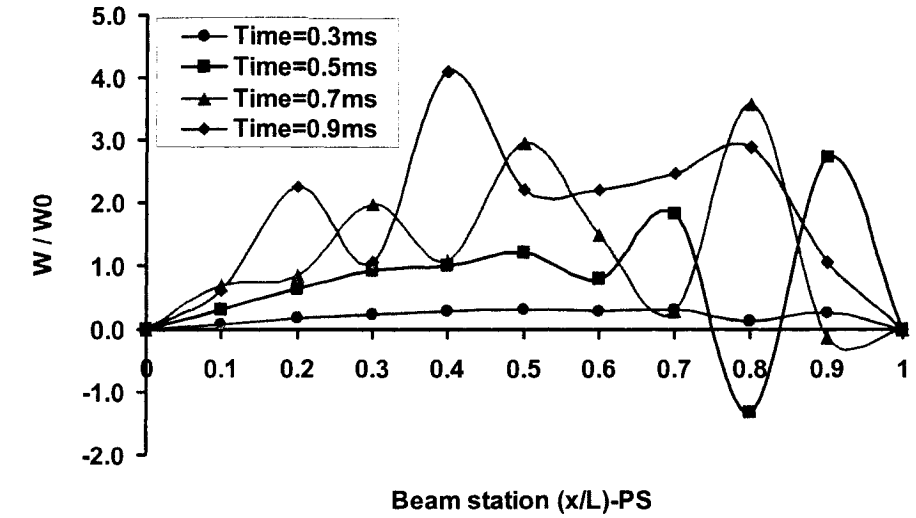

(a)

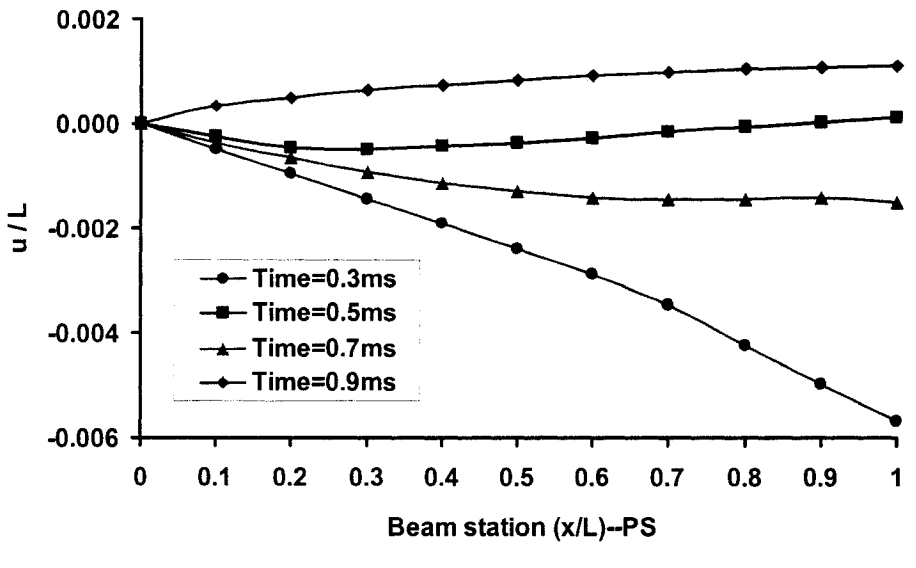

(b)

Figure 3-36 Dynamic profile of the beam and distribution of the axial displacement along the beam length, before and after the onset of buckling, for the pinned support condition.

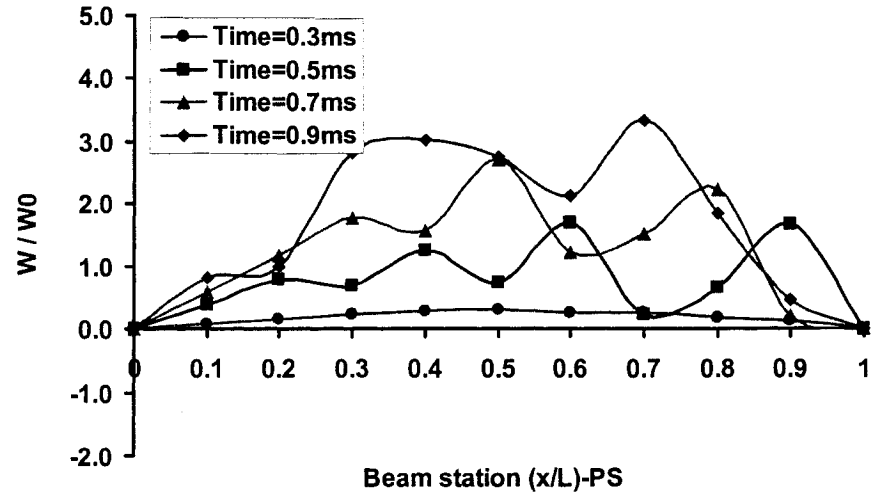

(a)

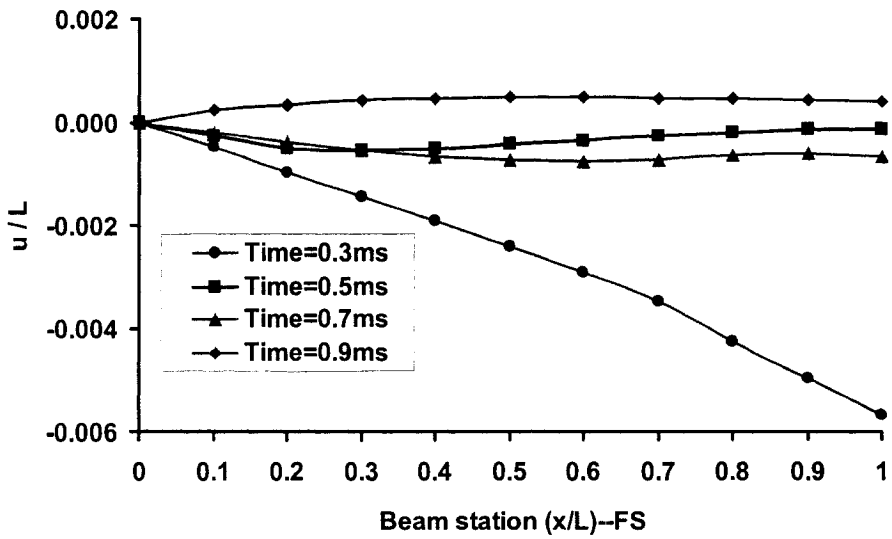

(b)

Figure 3-37 Dynamic profile of the beam and distribution of the axial displacement along the beam length, before and after the onset of buckling, for the fixed support condition.

4 Experimental Program

Relatively few experimental investigations have addressed the dynamic buckling, postbuckling and damage behavior of FRP composite laminated beams subjected to axial impact. As reviewed in Chapter 2, most of the analytical and experimental research on pulse buckling of slender beams were concentrated on those made of isotropic materials. Also, as will be discussed in Chapters 5 and 6, most of the works on composite damage investigation is about that induced by transverse impact or dynamic load.

In this chapter, an experimental program on investigation of dynamic pulse buckling and damage behavior of composite laminated beams subjected to axial impact will be presented. Experimental setup, data acquisition system and specimen preparation will be discussed. Experimental procedure will be presented in detail. The experimental results will be discussed in the next three chapters.

4.1 Experimental setup

The drop-weight setup is a common means of applying impact load for dynamic testing, as reported in several experimental works [Choi, *et al*, 1992; Christoforrou and Yigit, 1994; Sohn, *et al*, 2000; Necib and Mili, 2001; Olsson, 2001; Kenny, 2000]. The disadvantage of a drop-weight setup is that it is difficult to eliminate the rebound impact. To overcome this problem, a new impact setup was designed and fabricated, as shown in Figures 4-1 and 4-2. The major components include a pendulum, a guiding tube with linear bearings along its full length, specimen support fixtures and an impactor. The linear bearings are horizontally fixed on a strand. The linear bearing, fixture and specimen were calibrated horizontally so that the impact contact would be collinear. When the impactor is hit by the pendulum, it would travel through the tube on the

bearings. In this system, the impactor rebound and will not impact the specimen more than once. The impactor's mass can be adjusted according to the experimental requirement. The pendulum's mass can also be adjusted. By lifting the pendulum to different heights, various speeds can be applied to the impactor. The velocity of the impactor is monitored by two non-contact optical sensors (*Omron Model E2S-Q13*). The first optical sensor also acts as a trigger for the data acquisition card, which then collects the data. When the impactor passes the leading sensor, the data acquisition system is triggered by the output signal. The time gap can be recorded on the data acquisition system when the impactor passes the two sensors, so that the velocity of the impactor before it impacts the specimen can be obtained.

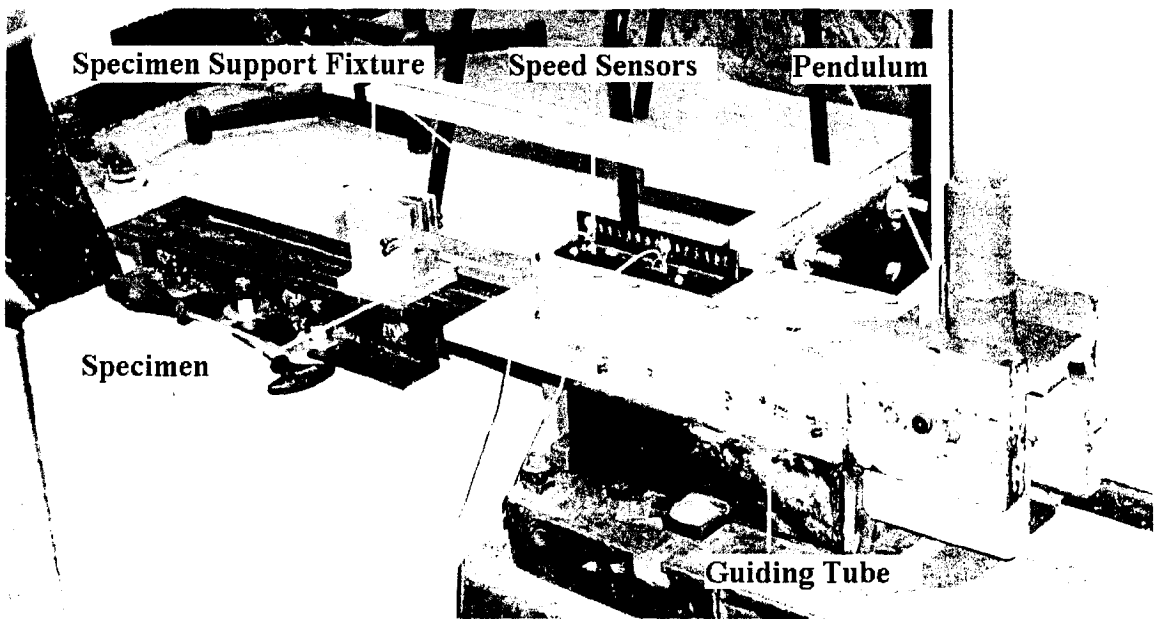

Figure 4-1 Test setup for dynamic axial impact experiment.

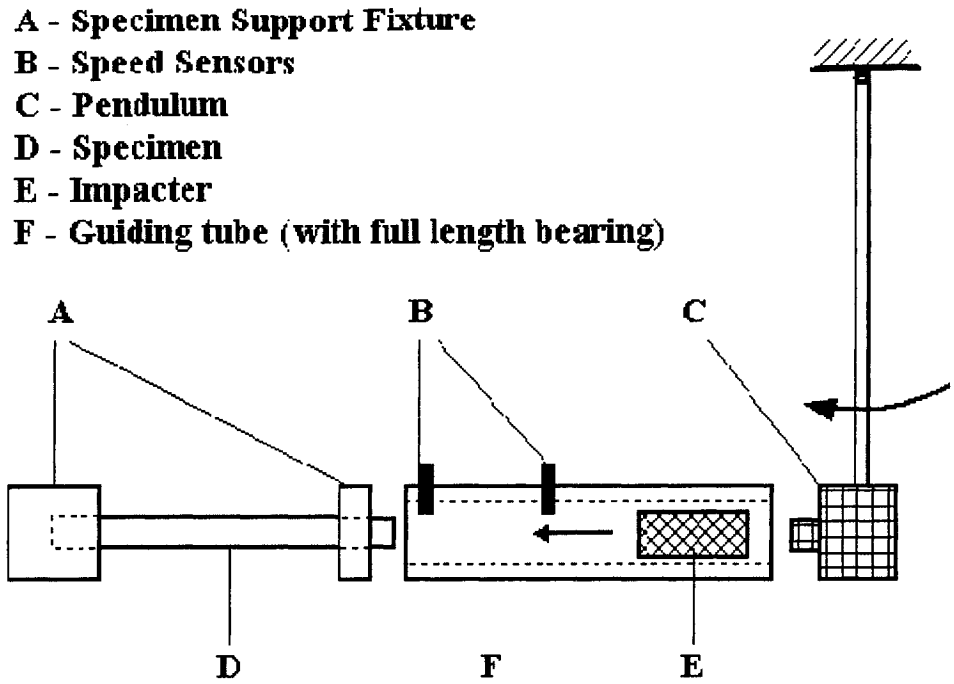

Figure 4-2 Test setup schemes for dynamic axial impact experiment.

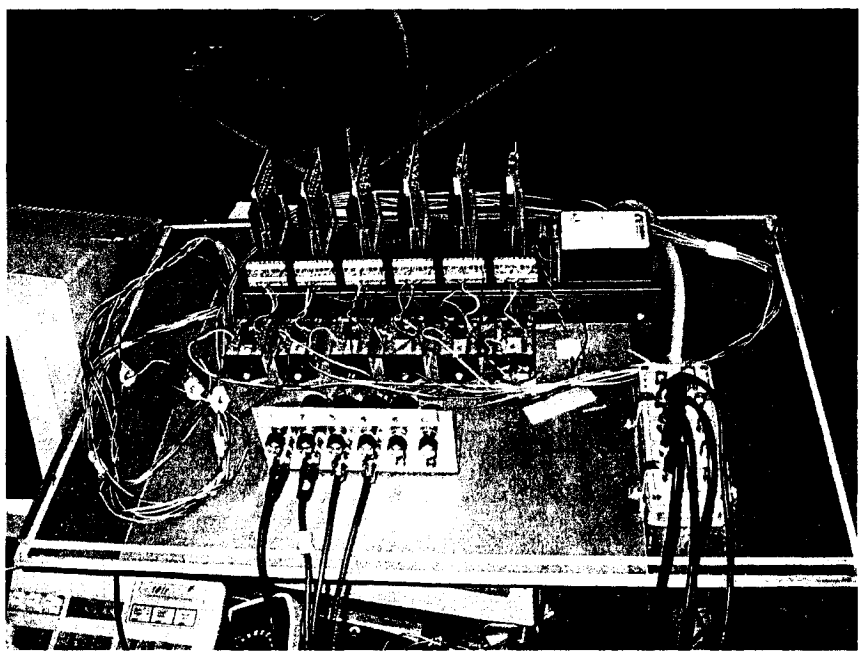

Figure 4-3 OM2-165/BE 490 Data Acquisition System

The strain gages used in this work were pre-wired strain gages made by KYOWA (Model KFRP-5-350-C1-1L5M3R). Strain data, as well as the signal from the non-contact optical sensors were collected by the OM2-165/BE490 Data Acquisition system, which was assembled in-house. Figure 4-3 shows the OM2-165/BE490 Data Acquisition system.

4.2 Specimen preparation

Both carbon/epoxy and E-glass/epoxy materials were used in this study. The laminates used for the study were hand-made in the lab of the Department of Civil Engineering, Dalhousie University.

4.2.1 Carbon/Epoxy laminate

The carbon fiber material used in this study was TENAX/R6376 carbon fiber/epoxy pre-preg by HEXCEL. R6376 is a high performance tough matrix formulated for the fabrication of primary aircraft structures. It offers high impact resistance and damage tolerance. Figure 4-4 shows the typical lay-up sequence for bagging operations. When the lay-up procedure was finished, vacuum machine was used to vacuum the bag to a vacuum of 700 KN/m^2 pressure according to the manufacturer's specification. Then the laminate panel was cured for 2 hours at 175^0C temperature with heating rate of 2^0C to 5^0 C per minute in an oven, as recommended by the manufacturer, as well. Thermocouples were inserted in the bag for monitoring the temperature. For the purpose of delamination growth test, Teflon strips with thickness of 0.001" with appropriate width and length were inserted into the laminate during the lay-up, so that control delaminations could be formed.

4.2.2 E-Glass/Epoxy laminates

The lay-up and cure of E-glass/epoxy fiber laminates was performed under room temperature. The laminate panels were then cut into beams.

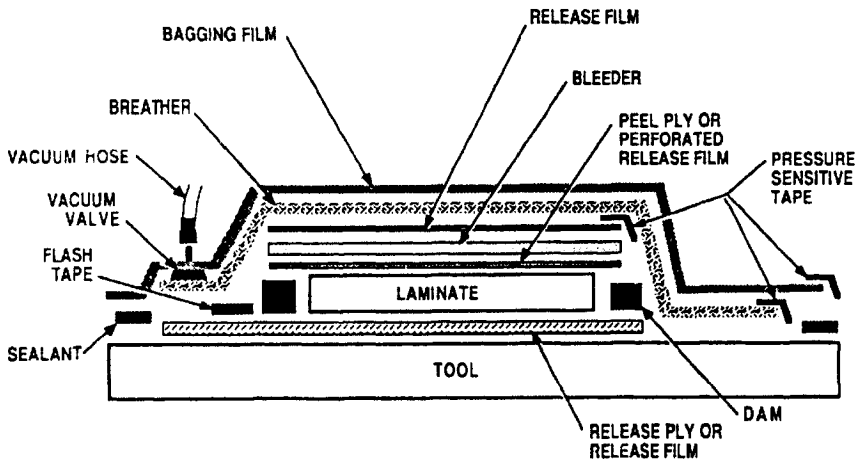

Figure 4-4 Lay-up sequence for bagging operations.
(Richmond Aircraft Product Inc., 2000)

The mechanical properties of the laminates were evaluated according to ASTM D3039, ASTM D5467, ASTM D5379 [1999] test methods. The critical energy release rate was estimated according to the ASTM D5528-94a [1999] standard test method as well.

4.3 Experimental contents

Two categories of tests were performed. One was a dynamic damage initiation test. The other was a delamination propagation test. The purpose of the damage initiation test was to investigate the damage initiation behavior of laminated composite beams subjected to

axial impact. The objective of delamination propagation test was to study the delamination propagation characteristics of delaminated composite beams subject to axial impact.

4.3.1 Damage initiation

To investigate the damage initiation behavior of carbon/epoxy composite laminated beams with initial geometric imperfections subject to axial impact of a moving mass, several groups of beams with different lay-up configurations were fabricated and tested. The lay-up configurations in this study were $[0_{12}]$, $[(\pm 22.5)_3]_s$, $[(\pm 45)_3]_s$, $[(\pm 67.5)_3]_s$, $[(0/90)_3]_s$ and $[(0/90)_2/0_2]_s$. The initial geometric imperfection was measured before each test for every specimen. The support condition of the beam is fixed at the left, and the right end is also fixed but is allowed to move in the axial direction, as shown in Figure 2-3. The mechanical properties of the laminate and geometric properties of the beams are listed in Table 4-1. The damping coefficient of the beam was determined to be 0.04 approximately by a Grindo*Sonic* MK5 "Industrial" instrument [Lemmens, 2001]. The extent of damage in the specimens was inspected visually and by Scanning Electron Microscopy (SEM) fractography. Experimental results and associated numerical analysis will be discussed in Chapter 5.

4.3.2 Delamination growth

The critical energy release rate was estimated according to ASTM D5528-94a [1999] as G_I =411.0 J/m^2 and G_{II} =1007.0 J/m^2. Tsai, *et al* [2001] stated that the dynamic delamination fracture toughness in unidirectional polymeric composites was basically equal to the static fracture toughness and was not significantly affected by crack speed up to 1100 m/s. We will use these values in our numerical investigation.

In total 7 groups of specimens with different delamination lengths and locations along the beams' length and through the thickness were tested. Each specimen was impacted once by a steel impactor with a mass of 0.518 Kg. The impactor's velocity was different for every event. The purpose of this test was to investigate the delamination growth of laminated beams with different delamination situations under axial impact. Microscope was used to visualize the delamination position and growth. Detailed information of each group of specimens and the associated experimental results, as well as the numerical analysis results will be presented and discussed in Chapter 6.

Table 4-1 Physical and mechanical properties of carbon/epoxy and E-glass/epoxy laminated beams.

Material Types	Carbon/Epoxy	Glass/Epoxy
Specimen Length (mm)	105~148	145
Specimen Width (mm)	15.93~16.43	15.68~18.20
Specimen Thickness (mm)	1.6	3.65~3.95
Imperfection Magnitude W_0 (mm)	Measured from initial geometry of beams	
Longitudinal Modulus E_{11} (GPa)	1.18×10^2	21.97
Transverse Modulus E_{22} (GPa)	5.54	4.13
In-plane Shear Modulus G_{12} (GPa)	4.77	0.518
Major Poisson's Ratio (v_{12})	0.27	0.31
Density (Kg/m^3)	1512	2100
Longitudinal Tensile Strength S_L^+ (MPa)	1094.8	560
Longitudinal Compressive Strength S_L^- (MPa)	712.9	255
Transverse Tensile Strength S_T^+ (MPa)	26.44	9.13
Transverse Compressive Strength S_T^- (MPa)	84.33	50.5
In-plane Shear Strength S_{LT} (MPa)	84.42	33.3
Through-the-thickness Shear Strength S_{TL} (MPa)	65.36	42.0

5 Damage Initiation

The dynamic damage initiation of fiber-reinforced plastic (FRP) composite laminated beams, having initial geometric imperfections, subject to an axial impact is investigated numerically and experimentally in this chapter. The dynamic equilibrium equations presented in Chapter 2 are updated with the consideration of damping effects. Based on our findings in Chapter 3 (in that the Higher-Order Shear Deformation Theory produced more accurate results), the HSDT solution was adopted to model the nonlinearly distributed shear strain across the beam thickness. Hashin's failure criteria was used to predict the damage of beams. The experiments were performed on the horizontal linear bearing impact setup. The Scanning Electron Microscopy (SEM) fractographic technique was used to identify the extent of damage in the laminated beams. Effect of fiber angle, lay-up sequence and initial geometric imperfections on the critical energy of damage initiation, were also investigated.

5.1 Literature review on damage analysis

As reviewed in Chapters 1 and 2, due to their high specific stiffness and strength, fiber-reinforced plastic (FRP) laminated composites have been widely used in industrial applications such as aerospace, automobile, shipbuilding, marine and civil infrastructures. However, their susceptibility to damage resulting from mechanical, physical and chemical factors can greatly degrade their stiffness, strength and durability. Impact is particularly one of the important damage sources, which can cause matrix cracking, laminate delamination and fiber breakage. Often damage generated in FRP is undetectable to the naked eye, therefore, it is particularly important to understand the damage mechanism in FRP (including its initiation and propagation).

Although a great number of investigations have considered FRP impact characterization, most works [Choi, *et al*, 1992; Christoforou and Yigit, 1994; Pavier and Clarke, 1995; Zhou, 1995; Sohn, *et al*, 2000; Park and Zhou, 2000; Franz, 2001; Necib B and Mili, 2001; Luo, *et al*, 2001; Olsson, 2001] considered damage due to transverse impact. Choi, *et al* [1992] conducted analytical and experimental investigations of damage initiation of graphite/epoxy composite plates subject to transverse line-loading impact, in which the effects of laminate lay-up sequence and impactor's mass were the prime focus. Pavier and Clarke [1995] proposed an experimental technique which could be used to replicate the damage of composite laminates, which was transversely impacted by a drop-weight. Zhou [1995] conducted tests on thick glass-fiber-reinforced laminates under transverse impact by a flat-ended impactor. Damage mechanism was investigated by post-impact visual inspection and ultrasonic C-scanning techniques. Sohn, *et al* [2000] performed drop-weight impact damage tests of carbon-fiber/epoxy composites and used several characterization techniques, such as cross-section fractography, scanning acoustic microscopy, and scanning electron microscopy (SEM), to observe and assess the damage due to impact. Park and Zhou [2000] investigated the transverse impact response and damage in composite laminates by obtaining time history results of contact force, displacement and energy absorption on a three-point bend fixture in a split Hopkinson pressure bar. With the photo elastic stress coating technique, Franz [2001] established an experimental method for investigating dynamic response and damage behavior of composite plates due to impact load. Necib and Mili [2001] experimentally investigated the dynamic behavior of various E-glass/epoxy laminates subject to a drop weight impacting the specimens on their transverse side. Luo, *et al* [2001] proposed an approach to evaluate the impact damage initiation and propagation in composite plates, both experimentally and numerically. The plates were impacted transversely by a controlled drop weight, and the damage and propagation were inspected with an optical microscope and X-ray chamber. Olsson [2001] suggested an analytical model for predicting the impact damage initiation and growth of composite laminates; critical loads and energies for damage initiation and growth were also discussed.

As the above literature review indicates, most of the experimental and analytical works have been based on transverse impact of composite laminates using the so called 'drop-weight' method of testing. In comparison, only a few investigations have been reported by which the response of composite laminates subject to axial or in-plane impact was investigated.

Slender, axially loaded bearing structural components are commonly found in various structures. These components may easily buckle when subjected to static or dynamic loads [Zhang and Taheri, 2002a, 2002b, 2002c]. Due to manufacturing induced factors, many composite laminates bear initial imperfections and/or voids. When subject to axial or in-plane static or dynamic loads, regardless of the occurrence of buckling, such laminates could experience damage, in the form of delamination, fiber breakage and matrix cracking if certain stress or strain components exceed the limiting criterion during the pre- and post-buckling periods.

Using a falling weight impact system, Hsiao and Daniel [1998] investigated the strain rate effect on the compressive and shear behavior of carbon/epoxy composite laminates. Bogdanovich and Friedrich [1994] predicted the initial failure and ply-by-ply failure processes of composite laminates under dynamic loading. Abrate [2001] introduced models for simulating impact on composite structures. An energy-balance model, spring-mass model and a complete model were used to simulate the impact of composite laminates.

It can be seen that damage characterization in axial composite members, subject to impulse loading, has not been thoroughly investigated. The scarcity of such experimental data motivated the present investigation.

The purpose of this chapter is to experimentally investigate the damage initiation mechanism and types of damage in fiber-reinforced composite laminated beams subject

to axial impulse. The objective is also to predict and simulate such damage mechanism by computational simulations.

5.2 Numerical model of damage analysis

To analytically investigate the dynamic behavior of composite laminated beams subject to axial impulse, the analytical model developed in Chapter 2, was further developed by including damping effects in the dynamic equilibrium equations. We consider a *n*-layer FRP composite laminated beam with one end impacted by a pulse load as shown in Figure 5-1. The cross section of the beam was rectangular with width *b* and thickness *h*. The length of the beam is *L*. The initial geometric imperfection is $w_0(x)$, which is defined as the initial displacement of the beam in the Z-direction as a function of location *x*.

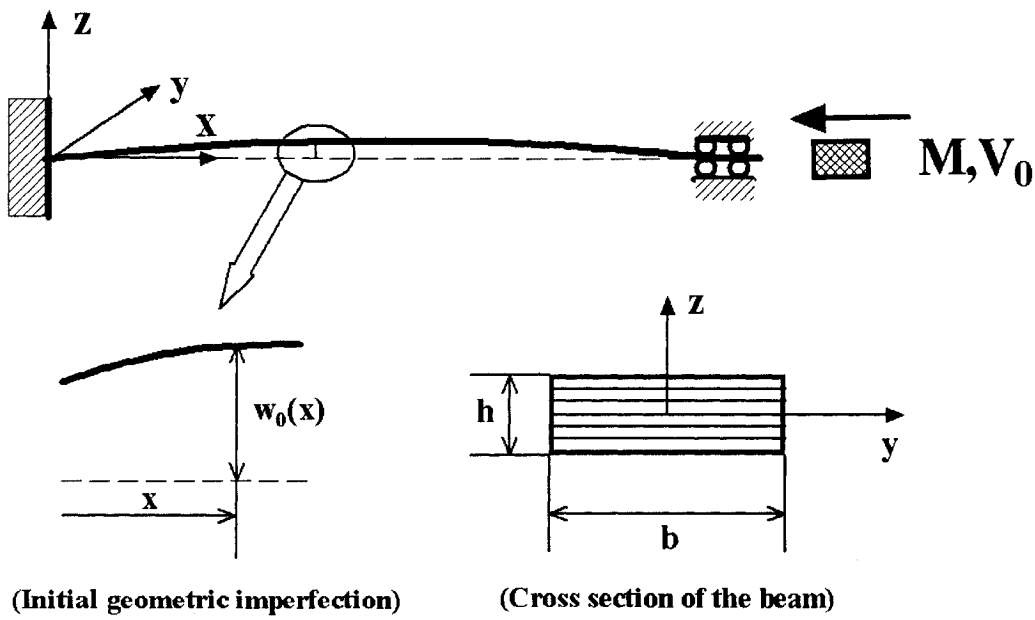

Figure 5-1 Schematics of a FRP beam being impacted by a moving mass.

With the Timoshenko beam assumption, the equilibrium equations were constructed for the FRP laminated beam. The formulation includes the axial, lateral and rotational inertias of the beam, the shear deformation through the thickness of the beam, and the damping effects in the axial, lateral and rotational directions as follows:

$$I_1 \frac{\partial^2 u}{\partial t^2} = \frac{\partial N_x}{\partial x} - C_L \frac{\partial u}{\partial t} \tag{5-1a}$$

$$I_1 \frac{\partial^2 w}{\partial t^2} = \frac{\partial V}{\partial x} - \frac{\partial (N_x(\theta - \frac{\partial w_0}{\partial x}))}{\partial x} - C_T \frac{\partial w}{\partial t} \tag{5-1b}$$

$$I_2 \frac{\partial^2 \theta}{\partial t^2} = \frac{\partial M_x}{\partial x} - V - C_R \frac{\partial \theta}{\partial t} \tag{5-1c}$$

where $u(x,t)$, $w(x,t)$, $\theta(x,t)$, N_x, M_x, V, I_1 and I_2 are defined in Chapter 2.

C_L, C_T, C_R are damping factors in the axial, lateral and rotational directions of the beam, respectively, which are defined as follows.

For a single degree of freedom (DOF) system, the free vibration equation with damping is,

$$\ddot{y} + \frac{c}{m}\dot{y} + \frac{k}{m} y = 0 \tag{5-2}$$

We define,

$$\frac{c}{m} = 2\xi\omega \tag{5-3}$$

in which ξ is the damping coefficient and ω is the natural frequency. Then damping factor can be represented by:

$$c = 2\xi\omega m \tag{5-4}$$

5.3 Damage criterion

Three failure modes in forms of fiber failure, matrix failure and delamination can be expected to occur in the composite laminated beams subject to the dynamic load. For the one-dimensional laminated beams subject to axial impact, we will not consider the matrix failure along the width of the beam and, therefore, only fiber failure and delamination through the thickness of the beam will be considered in simulation of the laminated beams in this investigation.

5.3.1 Fiber failure

5.3.1.1 Tension fiber mode

As Hashin [1980] stated, both tensile stress, σ_{11}^{+} and shear stress, τ_{13} of the fibers affect their failure. Fiber failure occurs if the tensile stress σ_{11}^{+} and shear stress τ_{13} of fibers satisfy the following equations,

$$F_f^T = (\frac{\sigma_{11}^{+}}{S_L^{+}})^2 + (\frac{\tau_{13}}{S_{LT}})^2 \geq 1.0 \qquad (5\text{-}5)$$

in which, F_f^T is the failure index of fiber in a tension mode, the S_L^{+} is the tension strength of lamina and S_{LT} is the shear strength of the lamina in the 1-3 plane.

5.3.1.2 Compressive fiber mode

Under compressive situation, fibers are assumed to fail in microbuckling and/or kinking. Rosen [1965] stated that fibers under axial compression buckle in a shear mode when the

volume fraction of fibers is higher than a certain limit (*e.g.*, ≈ 60% for carbon/epoxy). The shear and compressive stresses both contribute to the compressive failure of fibers. The deviatoric strain energy theory, known as Tsai-Hill criterion [Azzi and Tsai, 1965; Hill, 1948], is similar to Hashin's failure criteria for fibers in tension, that is:

$$F_f^C = (\frac{\sigma_{11}^-}{S_L^-})^2 + (\frac{\tau_{13}}{S_{LT}})^2 \geq 1.0 \tag{5-6}$$

in which, F_f^C is the failure index of fiber in the compressive states, S_L^- is the compressive strength of fiber, and the σ_{11}^- is the compressive stress.

5.3.2 Delamination

Delamination in laminates occurs due to normal and inter-laminar shear stresses. As described by the differential equations, the normal and through-the-thickness stresses are ignored for the current one-dimensional laminated beam subject to axial impulse. The failure criteria is described as,

$$F_d = (\frac{\tau_{31}}{S_{TL}})^2 \geq 1.0 \tag{5-7}$$

in which, F_d is the failure index of delamination and S_{TL} is the through-the-thickness shear strength of the lamina.

5.4 Results and discussion

To investigate the damage initiation behavior of carbon/epoxy composite laminated beams with initial geometric imperfections subject to axial impact of a moving mass,

several groups of beams with different lay-up configurations were fabricated and tested, and also analyzed numerically. The lay-up configurations in this study were $[0_{12}]$, $[(\pm 22.5)_3]_s$, $[(\pm 45)_3]_s$, $[(\pm 67.5)_3]_s$, $[(0/90)_3]_s$, and $[(0/90)_2/0_2]_s$. The initial geometric imperfections were measured before testing for every specimen. The support condition of the beam is shown in Figure 5-1. The mechanical properties of the laminate and the geometric properties of beams are listed in Table 4-1 in Chapter 4. The damping coefficient of the beam is approximately 0.04, as measured by a Grindo*Sonic* MK5 "Industrial" instrument [Lemmens, 2001], and as mentioned in Chapter 4.

5.4.1 Strain records

Figure 5-2 shows typical strain values recorded by two strain gages mounted on the top and bottom surfaces, at the mid-span of the beam. When a geometrically imperfect beam is impacted axially, it would vibrate in both axial and transverse directions. From Figure 5-2, we can see that both top and bottom surfaces experience compressive strain at the beginning of the event, because the beam is deformed axially due to the impacting compressive load. As the stress wave propagates along the beam, the beam experiences combined bending and axial compressive loading, in which the top surface of the beam is in a compressive state, and the bottom is in tension. Due to the damping effect, the vibration diminishes gradually. From this figure, we can see the maximum strain or stress that occurred during the first transverse vibration cycle. Considering the dynamic pulse-buckling phenomenon [Zhang and Taheri, 2002c], the damage may occur during pre- and/or post-buckling phases.

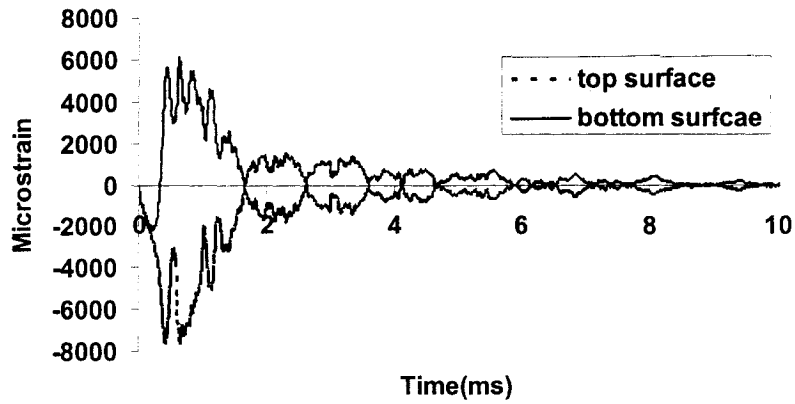

Figure 5-2 Typical strain records.

5.4.2 Damage investigation

The damage mechanism of axially impacted FRP beams differs from damage from transverse impact in the latter of which delamination, fiber breakage and matrix cracking mainly occurs around the contact area of the impacted region [Zhou, 1995; Sohn, *et al*, 2000; Park and Zhou, 2000]. Under axial impact, the damage occurs at a location in part or along the whole length of the beam. Damage location through the beam thickness varies depending on lay-up configurations. When impacted axially, the beams with initial geometric imperfections deform transversely and axially. The maximum tension and/or compression strains occur at the outer plies. According to the higher order shear deformation theory, the shear strain through the beam thickness varies in a parabolic distribution and the maximum occurs at the beam's mid-plane. This phenomenon was demonstrated in Figure 5-3. Figure 5-3 represents a typical delamination and matrix damage. Initial voids due to manufacturing are not negligible, the delamination and matrix cracking occurs usually in the weak regions. For all tested specimens except those with $[0_{12}]$ and $[(\pm 67.5)_3]_s$ layups, delamination and matrix cracking dominated the

damage mechanism. Matrix damage, normal to the fiber direction, occurred in most of the $[0_{12}]$ lay-up beams.

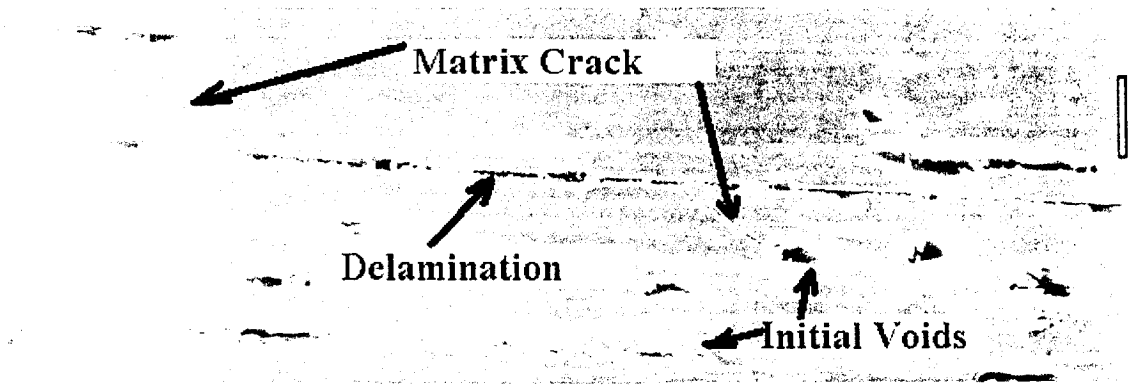

Figure 5-3 Typical delamination and matrix crack damage.

No delamination and matrix cracking were observed after impact in most of the $[(\pm 67.5)_3]_s$ lay-up beams, but their deformed shape remained after impact due to the plastic deformation of the matrix, as shown in Figure 5-4(a) and 5-4(b). The details of the mechanism and a prediction method will be presented in Chapter 7.

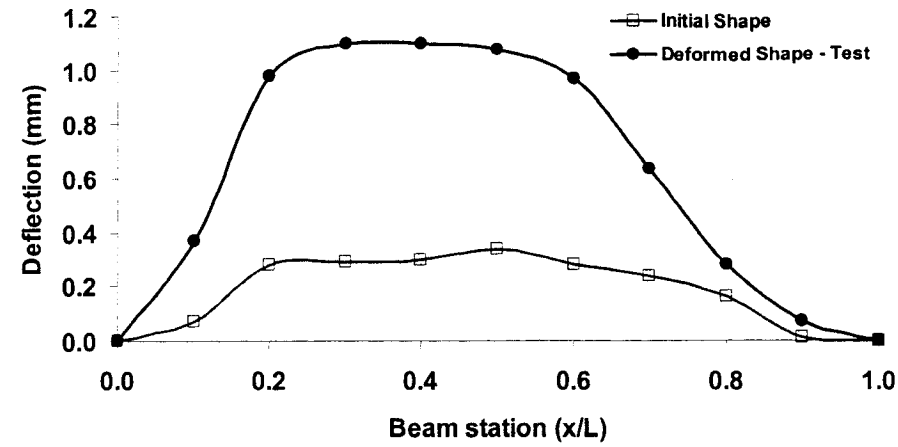

(a)

(b)

Figure 5-4 Initial and deformed beam shape of one of the beams with $[(\pm 67.5)_3]_s$ lay-up.

5.4.2.1 Damage analysis of beams with $[(\pm 22.5)_3]_s$ *Lay-up*

Three groups of beams, having a lay up sequence of $[(\pm 22.5)_3]_s$ had three different lengths (105 mm, 128mm and 148 mm). Each group had 4 specimens and each specimen was impacted with different impact energy. Damage, mostly in the form of delamination, was observed between plies 6 and 7. Some of the delaminations extended along the whole length of the beams, but was limited between the two restrained ends. Figures 5-5(a) and 5-5(b) show the time history results of axial displacement and lateral deflection at station 0.7 of the beam (0.7 indicates $^7/_{10}L$ distance from the fixed support end of the beam), obtained through our numerical analyses for one of the specimens. Figure 5-5(c)

shows the lateral deformed shape at time 0.4ms compared with the initial shape of the beam. Figures 5-6(a) and 5-6(b) show the failure indices of fiber breakage for each layer, and delamination failure for each inter-laminar interface at station 0.7 of the beam, obtained though equations (5-5, 5-6, and 5-7). From the figures, we can see that all fiber failure indices are less than 1.0, which indicates that the fibers do not break; Some of the delamination failure indices are however greater than 1.0, indicating that delamination should have occurred. Further analysis of Figure 5-6(b) indicated that even though failure indices of interface 5-6 and 7-8 were greater than 1.0, visual observation did not confirm such a mechanism. This was because the interface 6-7, which was at the beam's mid-plane, met the delamination criterion before the other interfaces. In this case the other interfaces did not have the opportunity to delaminate, even though the failure factors were greater than 1.0.

5.4.2.2 Damage analysis of beams with $[(\pm 45)_3]_s$ *Lay-up*

Unlike beams with a $[(\pm 22.5)_3]_s$ lay-up in which delamination dominated the damage mechanism, extending along the whole length of beam, delamination in these beams occurred at some discrete stations along the beam length and was accompanied by matrix cracking. Figure 5-7 illustrates a typical illustration of delamination and matrix cracking in those beams. Figure 5-8 shows another example of this beam group, showing a major delamination occurring between plies 6 and 7, which was also connected to another delamination (between ply 3 and 4) by a matrix crack, which facilitated through an initial void. Figure 5-9 illustrates a typical matrix cracking of this group.

In summary, most of the delaminations in $[(\pm 22.5)_3]_s$ and $[(\pm 45)_3]_s$ beams occurred at the beam mid-spans, extending though the beams' thickness. The specimens having $[(0/90)_3]_s$ lay-up, however exhibited different failure patterns, discussed as follows.

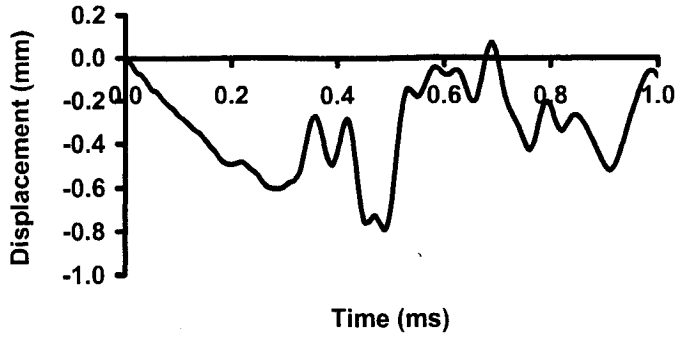

(a)

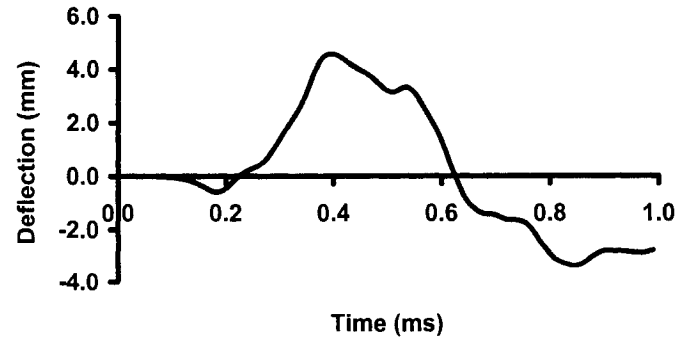

(b)

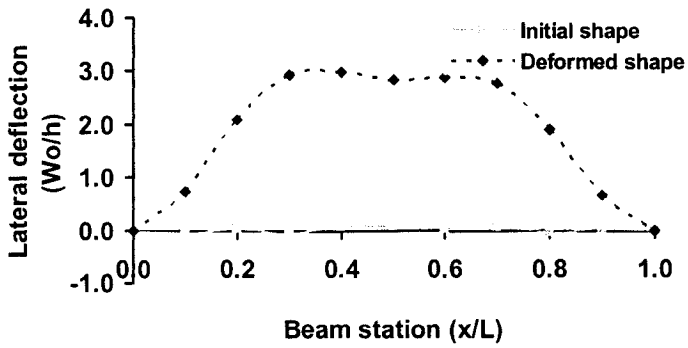

(c)

Figure 5-5 Numerical results: (a) time history of axial displacement at station 0.7 of the beam; (b) time history of deflection at station 0.7 of the beam; (c) initial and deformed shape and initial shape of the beam.

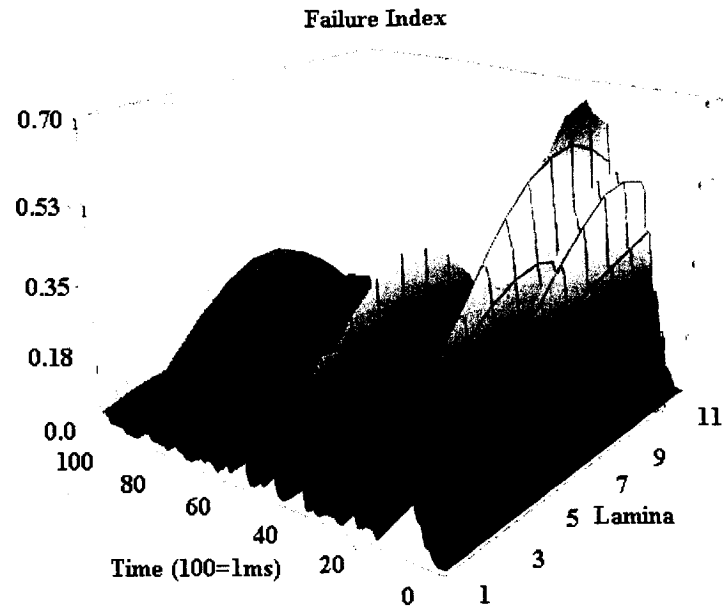

(a)

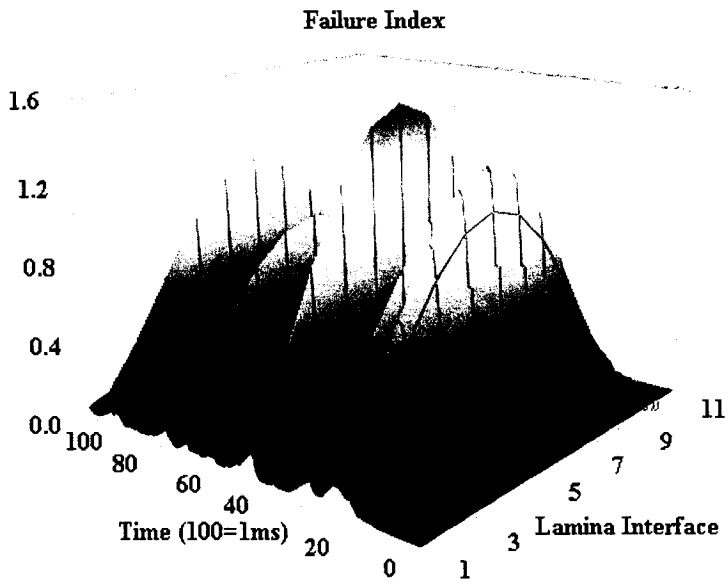

(b)

Figure 5-6 Numerical results of the failure indices.
(a) failure index for fiber breakage. (b) failure index for delamination.

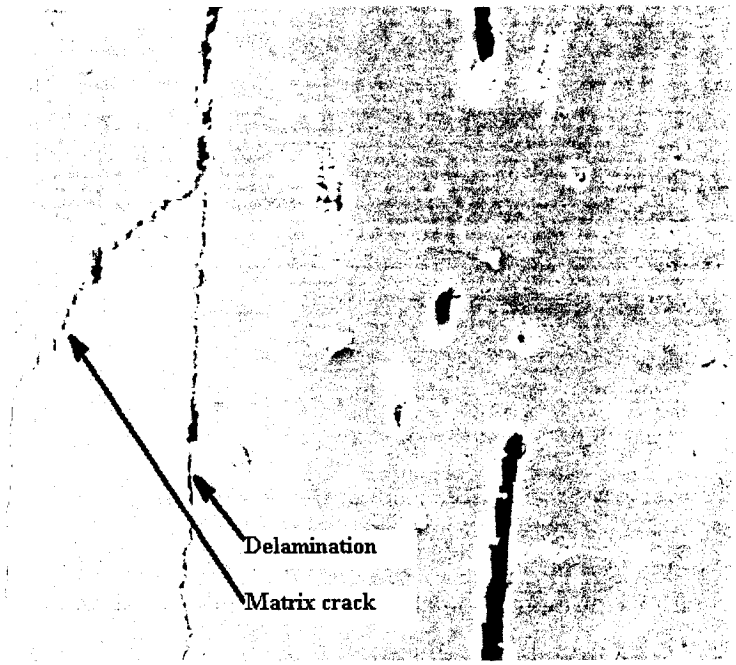

Figure 5-7 SEM fractograph showing typical delamination and matrix crack of a $[(\pm 45)_3]_s$ specimen.

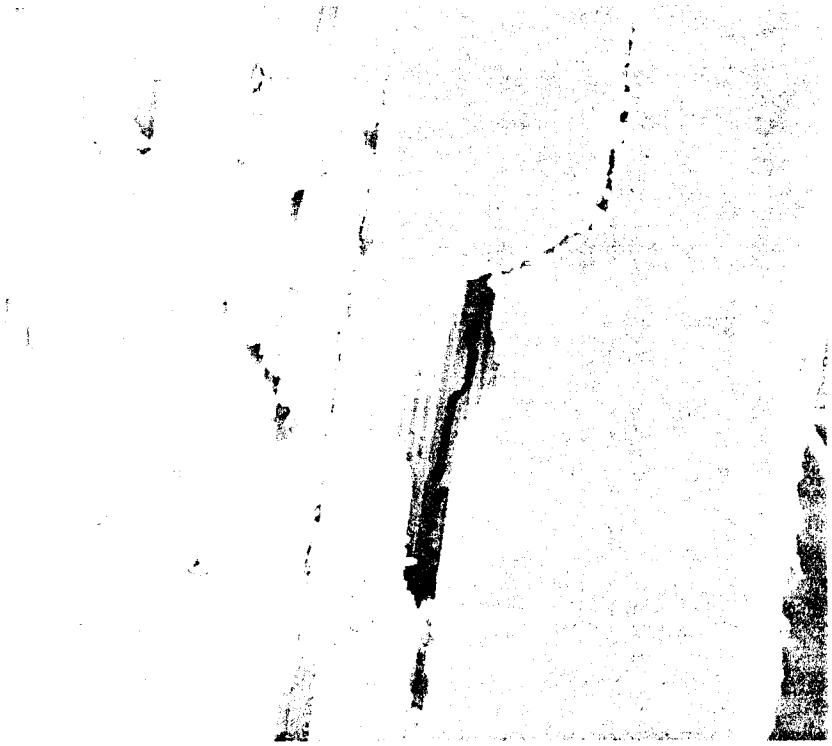

Figure 5-8 SEM fractograph showing typical interfacing of two delaminations.

Figure 5-9 SEM fractograph of a typical matrix crack.

5.4.2.3 Damage analysis of beams with $[(0/90)_3]_s$ *Lay-up*

In this group of beams, the two 90^0 plies in their mid-plane did not contribute much in carrying the axial force. During the transverse deformation stage, the outer plies endured most of the tensile and compressive loads. Moreover, the 3^{rd}, 5^{th}, 8^{th} and 10^{th} 0^0 plies would have endured the maximum shear strain. Therefore, it is reasonable to expect to see that delaminations would occur between plies 1-2, 11-12, 5-6 and 7-8, as was the case. Furthermore, a matrix crack, running through plies 6 and 7, linked the 5-6 delamination to the 7-8 delamination. Figure 5-10(a) is an example of delamination between plies 1 and 2, while Figure 5-10(b) shows the connection of the two delaminations, as described above.

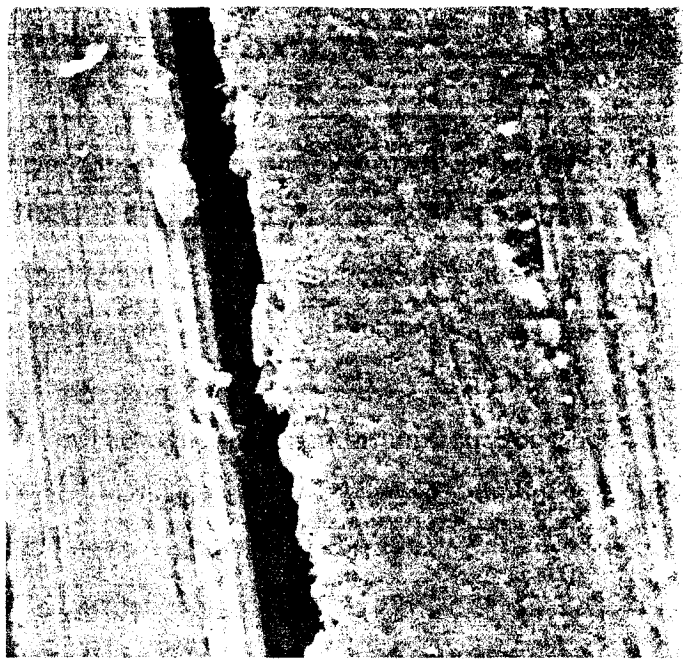

(a)

(b)

Figure 5-10 SEM fractographs. (a) showing delamination between ply 1 and 2. (b) showing delamination between plies 5 and 6 connected to delamination between plies 7 and 8 by a matrix crack.

5.4.2.4 Damage analysis of beams with $[(0/90)_2/0_2]_s$ *Lay-up*

Four specimens were tested within this group. Similarly, delamination dominated the damage mechanism. The most delaminations occurred at the mid-plane. Similarly, delamination modes were very similar to those discussed earlier.

5.4.3 Location of damage initiation

When a damage criterion is exceeded, the damage (fiber breakage, delamination and or matrix crack) will initiate due to excessive stresses. According to the visual inspection and the associated numerical analysis for the test specimens, delamination and matrix cracks are the dominating damage mechanism observed in the imperfect beams that were subject to axial impact. Once the delamination and or matrix crack occurs, the energy absorbed by the beam is partially released by generation of the damage, delamination propagation then depends on the amount of energy absorbed by the beam. This phenomena will be discussed in Chapter 6. Here we discuss the location of delamination initiation (*i.e.*, location along the beam and through inter-laminar interfaces). Visual and microscopic inspection of the tested specimens suggested that most delaminations occurred between the supports. Numerical analysis results for all the tested specimens predicted that initial geometric imperfections had a significant effect on the delamination initiation position along the beam. Figure 5-11(a) and 5-11(b) are histograms showing the density of the delaminations based on their relative distance along the beam, and their interface location. From Figure 5-11, one can see that besides the local damages initiated at station 0.0 (fixed end) and 1.0 (impacted end) along the beam, most damages took place around stations 0.3 ~ 0.4 (near the fixed end) and 0.7, near the impacted end. The delamination positions through the thickness were at inter-laminar 4, 5 and 6. The distribution of shear strain through the beam thickness is maximum at the beam mid-span, and minimum at the top and bottom surfaces of the beams. Due to the different ply

orientations, however, the center plies did not necessarily experience the maximum stress, therefore, a certain amount of delaminations occurred at 4-5 interface.

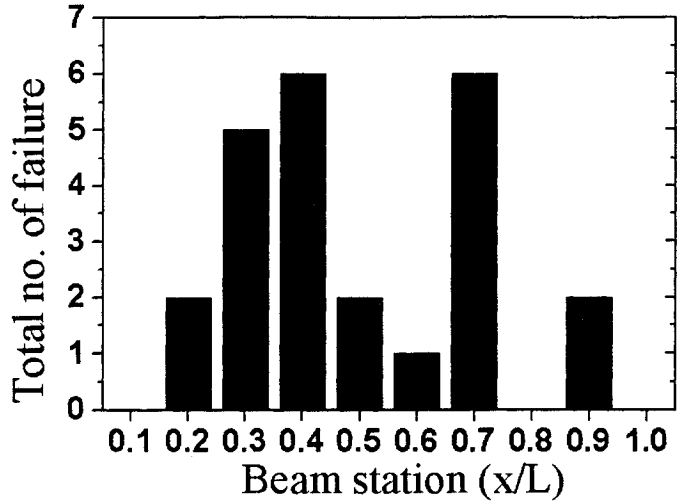

(a)

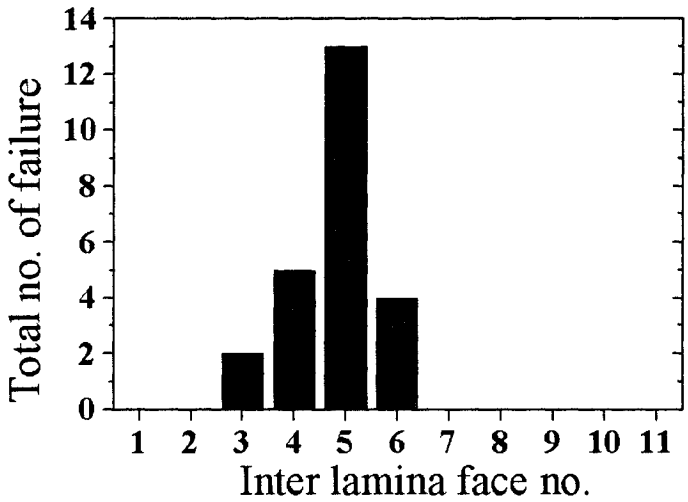

(b)

Figure 5-11 Histograms from all specimens illustrating (a) location of delamination initiation failure in the FRP beams; (b) total number of interface failure.

Initial geometric shapes of beams were either sinusoidal or random. Some of the typical initial geometric imperfections measured before impact tests are shown in Figure 5-12. Observation of the experimental results also indicated that beams having relatively large

imperfection; (i.e., $W_0/h > 0.2$), failed mostly at their ends; otherwise, failure occurred along the length of the beams.

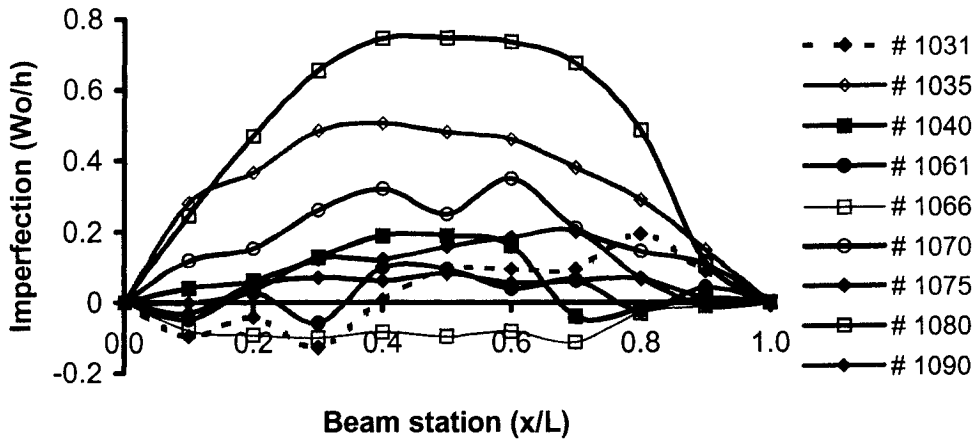

Figure 5-12 Initial out of plane geometric shapes of tested specimens.

5.4.4 Critical energy for damage initiation

When addressing the damage initiation of FRP laminated beams subject to axial impulse load, one should consider the critical energy used for damage initiation, an unavoidable phenomenon. The angle ply laminates with relatively large axial and bending stiffness will endure greater axial and transverse deformation resistance when subject to impact, and thus would endure larger stresses; the reverse is true for laminates which have smaller axial and bending stiffness. Moreover, the larger the slenderness ratios, the larger the energy required to initiate the damage. This can be seen from Figure 5-13, which was constructed based on the inspection of the experimental results. The axial stiffness (along the x-axis) is normalized relative to that of the zero degree (uniaxial) layers.

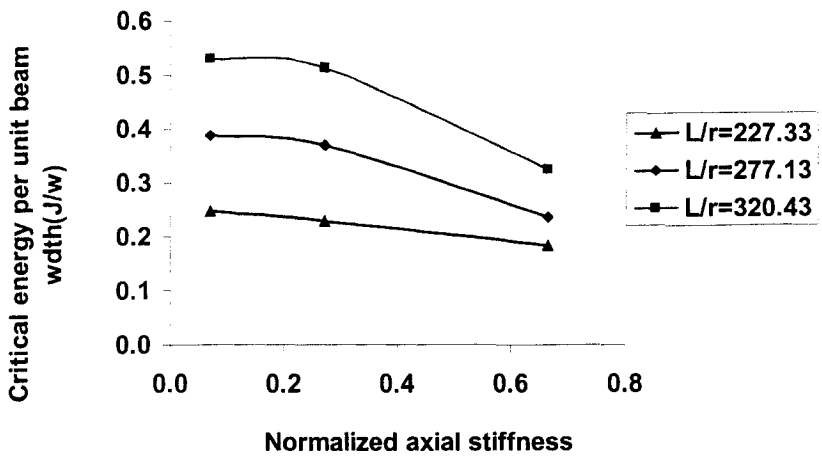

Figure 5-13 Variation of the critical energy for damage initiation as a function of the axial stiffness and slenderness ratio.

5.5 Summary

Dynamic damage behavior of FRP laminated slender beams, having various lay-ups, subject to axial impact was investigated experimentally and numerically. Several factors, such as the beam's axial transverse inertia, cross section's rotational inertia, the non-uniform distribution of shear stress across the beam cross-section, damping effect, and the nonlinear strain-displacement relationship between axial strain and transverse displacement, were all accounted for in the numerical solution.

Axial impact experiments were performed on carbon/epoxy laminated beams with different lay-up and slenderness ratios. From the results of the numerical and experimental analyses, the following conclusions can be drawn,

(i) Delamination and matrix cracking were the dominant damage mechanism in the carbon/epoxy laminated beams subjected to axial impulse.

(ii) The density and length of delaminations depended on the lay-up sequences.

(iii) Delamination position and interlaminar interface locations of the delaminations were mainly concentrated at stations 0.4 and 0.7, and at layers 4 and 5 interface, respectively. The damage mechanism was also strongly dependent on the nature of the initial geometric imperfections.

(iv) The critical energy for damage initiation varied with the lay-up and slenderness ratio.

6 Delamination Growth

In this chapter, the dynamic delamination growth behavior of fiber-reinforced plastic (FRP) composite laminated beams subject to axial impulse was investigated experimentally and numerically. The impact experiments were performed on a horizontal linear bearing impact setup as described in Chapter 4. Carbon fiber/epoxy specimens with different initial delamination length and position along the beam length and through its thickness were tested. The dynamic equilibrium equations derived in Chapter 5 were applied to each region of the delaminated beam (including the intact and delaminated parts) to develop the solutions. The strain energy release rate at the tips of each end of the delamination was calculated based on the virtual crack closure technique (VCCT), through a numerical analysis. The evaluation was performed for every increment of the delamination growth (at every time step). Critical impact energy for delamination growth was also evaluated numerically. The numerical analysis results obtained for each specimen group were compared to the experimental results.

6.1 Introduction

In Chapter 5, numerical and experimental investigations of damage initiation of laminated composite beam subjected to axial impact were presented. As a continuation of dynamic damage behavior analysis, delamination propagation of a laminated composite beam with initial delamination subjected to axial impact will be presented in this chapter.

Delamination and its growth in composite laminated structures can greatly degrade the integrity and durability of a FRP structural component. Since the earlier works of Whitcomb [1981] and Chai [1981], research on delamination propagation of laminates under in-plane or out-of-plane loads attracted considerable attention. Whitcomb [1981] performed a numerical investigation on the effects of delamination length, depth, applied

load and lateral deflection on the stress distribution and strain energy release rate of post-buckled laminates with through-width delamination. He also experimentally investigated the delamination growth of composites under cyclic loads. Chai [1981] introduced the 'thin-film' and 'general' models for characterizing delamination buckling and growth. He stated that a delamination may propagate stably, unstably or unstably and then stably. To examine the unstable growth of delamination, Gaudenzi, *et al* [2001] proposed an incremental-iterative method in their numerical investigation of the response of composite panels having a through-width delamination. Cochelin and Patier-Ferry [1992] proposed a numerical model to treat buckling and delamination growth in composite laminates with circular delamination. He concluded that Griffith's type criterion (without mode separation), derived based on the J-integral theory, could provide a reasonable means for predicting the onset of delamination growth, but it was inadequate for predicting the growth of delamination. Delamination geometry and position, and fiber orientation were found to have crucial effect on the buckling response and delamination growth. Kruger, *et al* [1996] demonstrated that the mixed mode of energy release rate was extremely sensitive to the geometry of the delamination through their numerical and experimental investigations of the delamination growth of carbon fiber reinforced epoxy laminates, having embedded delaminations. Kyoung and Kim [1995] also stated that delamination location and size had pronounced effects on the buckling loads and growth of delamination through examination of one-dimensional delaminated beam-plates. Nilsson, *et al* [2001], through their investigation on buckling and growth of delaminations in a slender composite panel, observed that the delaminated panels failed by delamination growth at a slightly lower load than that of an intact panel. They also investigated the stability of the delamination growth as a function of the through-thickness location of delamination.

Due to the anisotropic nature of composite laminates, fiber orientation of plies plays an important role in the distribution of strain energy release rate on the delamination front. The development of a suitable simulation scheme that could predict the delamination

growth could therefore be a worthy contribution. For instance, Shen, *et al* [2001] demonstrated that for circular delaminated plates, one quarter of the model is inadequate to simulate the entire model when predicting delamination growth. To predict the growth of delamination, the critical energy release rate is a very effective criterion. Many researchers [Ricco, *et al*, 2001; Tsai , *et al,* 2001; Yin ,1993; Hwang , *et al*, 2001; Suo and Hutchinson, 1990; Williams, 1988; Whitcomb, 1986; Zou, 2001; Sheinman and Kardomateas, 1997; Park and Sankar, 2002; Rybicki and Kanninen, 1977; Robinson and Besant, 1998] have expended effort in calculating the strain energy release rate associated with crack/delamination growth. Many workers have also used other schemes, such as numerical modeling, to predict the propagation. To simulate the degradation influence on the stiffness of laminates due to the delamination progress, Sun, *et al* [2001] used the moving mesh scheme for simulating the progressive failure analysis of laminated plates with delaminations. Wagner, *et al* [2001] used a stress based criterion to predict the critical points of the delamination interface by using a non-vanishing layer in their investigation of delamination propagation. Luo, *et al* [2001] used delamination strength, instead of critical energy release rate to determine whether the delamination propagation would occur in their investigation of a composite plate impacted transversely by a rigid ball.

It should be noted that the research into delamination buckling of composite laminates and resulting delamination growth reported in most of the above mentioned references have considered the cases of in-plane static or quasi-static loads. However, structures in most real engineering situations are subjected to dynamic loads. Axial or in-plane dynamic loads on plate/shell and beam/column components can cause dynamic buckling and/or pulse buckling [Ari-Gur, *et al*, 1982; Lindberg and Florence, 1987; Kenny, 2000; Kenny, *et al*, 2000, 2001, 2002a and 2002b; Zhang and Taheri, 2002a, 2002b, 2002c, and 2003], delamination growth and/or other types of damages, such as fiber breakage and matrix crack as reported in Chapter 5. To the best of the author's knowledge, most of the reported works on damage/delamination growth of composite laminated plates/beams

have considered laminates subjected to transverse force or impact. The lack of information and experimental data in characterizing delamination growth in laminates subject to axial impulse (impact), therefore, constitutes a major motivating reason for the work of this chapter.

As stated, the research examining the delamination growth of laminate composites subjected to impact loading is relatively scarce. Kusaka, *et al* [2001] proposed a method for estimating the mixed mode interlaminar fracture toughness of composite laminates subjected to a transversely applied low velocity impact load. Li, *et al* [2001a, 2002b] presented their FEM model and experimental investigation of laminate damages induced by transverse low-velocity impact of a rigid body into a plate. Sankar and Hu [1991] modeled the dynamic delamination propagation of composite beams subjected to transverse impact load. Their delaminated beam was modeled as two beams, idealizing the laminates above and below the delamination plane, while the uncracked portion was modeled as a spring element.

To further enhance the available limited bank of experimental data and research in delamination growth characterization of composite laminates, this chapter will therefore investigate the delamination growth of laminated composite beams subject to axial impact, experimentally and numerically.

6.2 Delaminated beam model and strain energy release rate

6.2.1 Differential equations of motion

The delaminated composite beam considered herein, with a delamination through its width subject to axial impact is shown in Figure 6-1(a). The beam is divided into four regions as shown in Figure 6-1(b), including two intact and two delaminated parts. The

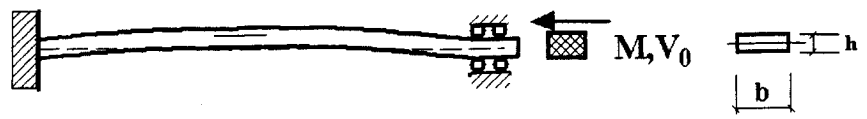

(a)

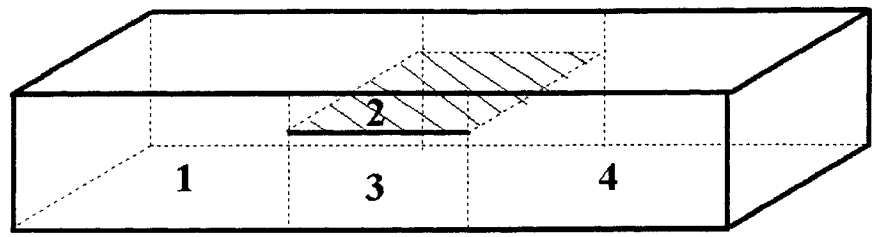

(b)

Figure 6-1 Delamination growth model of an imperfect composite beam. (a) the beam is impacted by a moving mass, (b) the beam modeled into four regions.

cross section of this n-layered FRP composite laminated beam is rectangular with width b and thickness h. The length of the beam is L, and the delamination length is a, the thickness of the upper delaminated region (2) is h_s, the thickness of the lower part (3) is h_m.The initial geometric imperfection is $w_0(x)$. To analytically investigate the dynamic delamination growth behavior of composite laminated beams subject to axial impulse, we adopt the dynamic equilibrium equations developed in Chapter 5, in which the response of a FRP laminated beam subject to axial impact was considered. The formulation accounts for the beam's axial, lateral and rotational inertias, the through thickness shear deformation, and the damping effects in axial, lateral and rotational directions with the following equations:

$$I_1^{(i)} \frac{\partial^2 u^{(i)}}{\partial t^2} = \frac{\partial N_x^{(i)}}{\partial x} - C_L^{(i)} \frac{\partial u^{(i)}}{\partial t} \tag{6-1a}$$

$$I_1^{(i)} \frac{\partial^2 w^{(i)}}{\partial t^2} = \frac{\partial V^{(i)}}{\partial x} - \frac{\partial (N_x^{(i)} (\theta^{(i)} - \frac{\partial w_0^{(i)}}{\partial x}))}{\partial x} - C_T^{(i)} \frac{\partial w^{(i)}}{\partial t} \tag{6-1b}$$

$$I_2^{(i)} \frac{\partial^2 \theta^{(i)}}{\partial t^2} = \frac{\partial M_x^{(i)}}{\partial x} - V^{(i)} - C_R^{(i)} \frac{\partial \theta^{(i)}}{\partial t} \tag{6-1c}$$

where (i=1, 2, 3 and 4), represents each region of the beam as shown in Figure 6-1(b); $u^{(i)}(x,t)$ is the axial displacement of the region i in the x-direction (an unknown), $w^{(i)}(x,t)$ is the lateral displacement of the region i (also an unknown), $\theta^{(i)}(x,t)$, also an unknown, is the rotation of the cross section of the beam region i; and

$$(N_x^{(i)}; M_x^{(i)}) = \int_{-h^{(i)}/2}^{h^{(i)}/2} \sigma_x^{(i)}(1; z) dz \tag{6-2a,b}$$

are the axial force and bending moment, respectively, per unit beam width, for the i^{th} region; $\sigma_x^{(i)}$ is the axial stress in the i^{th} region; and

$$V^{(i)} = \int_{-h^{(i)}/2}^{h^{(i)}/2} \tau^{(i)}{}_{xz} dz \tag{6-3}$$

is the shear force per unit beam width across the cross-section in the i^{th} region, τ_x is the shear stress of each lamina in the i^{th} region, and finally

$$(I_1^{(i)}; I_2^{(i)}) = \int_{-h^{(i)}/2}^{h^{(i)}/2} \rho^{(i)}(1; z^2) dz \tag{6-4a,b}$$

are the translational and rotational inertia per unit width of the beam, respectively. $\rho^{(i)}$ is the mass density of the i^{th} region and $C_L^{(i)}, C_T^{(i)}, C_R^{(i)}$ are the axial, lateral and rotational damping factors, respectively, of the i^{th} region. These latter three factors vary with the delamination length during the impact event.

The solution of the equilibrium equations is based on the von Karman strain-displacement relationship and Reddy's higher order shear deformation theory, as described in Chapter 2.

6.2.2 Delamination growth in delaminated beams

Evaluation of delamination growth is believed to be the key step in characterizing the response of composite laminated beams subject to axial impact. Strain energy release rate is an effective criterion for predicting the delamination growth. It is assumed that the growth of delamination is dependent on the comparison of strain energy release rate of the crack tip when exceeding a critical value.

In consideration of the current problem, when the beam is impacted by a moving mass, the beam would deform dynamically in both axial and transverse directions. The delamination is assumed to grow if the strain energy release rate at the delamination front exceeds the critical value, so that the strain energy of the beam is released. The strain energy release rate is calculated at the tip of the delamination and the evaluation is performed for the growth of delamination for every time step of the analysis. With the virtual crack closure technique (VCCT) [Rybicki and Kanninen, 1977], the strain energy release rate of Mode I and Mode II can be calculated. The discretized model is shown in Figure 6-2. In the current problem, the mode III fracture resulting from the out-of-plane deflection (in Z-direction) is not considered; thus the energy release rates can be expressed by:

$$G_I = \frac{1}{2\Delta a} \cdot \frac{(V_i \Delta w_m + V_j \Delta w_n + \psi_I (M_i \Delta \theta_m + M_j \Delta \theta_n))}{2} \tag{6-5a}$$

$$G_{II} = \frac{1}{2\Delta a} \cdot \frac{(P_i \Delta u_m + P_j \Delta u_n + \psi_{II} (M_i \Delta \theta_m + M_j \Delta \theta_n))}{2} \tag{6-5b}$$

in which, ψ_I and ψ_{II} are mode separation factors for work done by moment (details are given in the next section).

During the delamination analysis, the dimensional dynamic equations (2.3.22) based on HSDT are solved, instead of the non-dimensional equations (2.3.23). This is because during the delamination procedure, the beam segment length ($L^{(i)}$) of regions 1,2,3 and 4 vary, thus making the solution based on the non-dimensional variables, such as $\bar{u} = \frac{u}{L^{(i)}}$ complicated, consuming unnecessary calculation time and computer resources.

The critical energy release rates, G_I (Mode I) and G_{II} (Mode II) of the tested laminates were experimentally obtained based on the ASTM standard test methods [ASTM, 1999b and Johnson, 1985]. The following criterion was used to evaluate whether the delamination growth would occur,

$$I_d = \left(\frac{G_I}{G_{IC}}\right)^2 + \left(\frac{G_{II}}{G_{IIC}}\right)^2 \geq 1.0 \tag{6-6}$$

in which I_d is the delamination index; the assumption being if $I_d \geq 1.0$, then the delamination would grow.

The delamination growth index is evaluated for both ends of the delamination, on every time step.

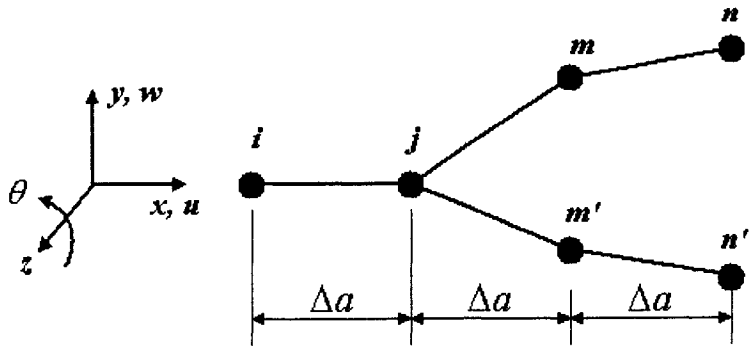

Figure 6-2 The discrete half model of the delamination beam for calculation of strain energy release rate of Mode I and Mode II.

6.2.3 Mode partitioning factors

Bending moment can cause either mode I or mode II, or mixed mode delamination in composite beams. Mode partitioning factors described in section 6.2.2 were derived based on the work of Kardomates [1993] and Suo and Hutchinson [1991].

Stress intensity factors of Mode I and Mode II are expressed by Karmodates [1993],

$$K_I = \frac{1}{\sqrt{2}}\left[\frac{P^*}{\sqrt{A^* h_s}}\cos\omega + \frac{M^*}{\sqrt{I^* h_s^3}}\sin(\omega+\gamma)\right] \tag{6.7a}$$

$$K_{II} = \frac{1}{\sqrt{2}}\left[\frac{P^*}{\sqrt{A^* h_s}}\sin\omega - \frac{M^*}{\sqrt{I^* h_s^3}}\cos(\omega+\gamma)\right] \tag{6.7b}$$

in which, P^* and M^* are linear combinations of loads from delaminated legs of beam, and A^*, I^*, ω and γ are defined as follows,

$$A^* = \frac{1}{1+4\eta+6\eta^2+3\eta^3} \tag{6.8a}$$

$$I^* = \frac{1}{12(1+\eta^3)} \tag{6.8b}$$

$$\sin\gamma = 6\eta^2(1+\eta)\sqrt{A^* I^*} \tag{6.8c}$$

$$\omega = 52.1^0 - 3^0\eta \tag{6.8d}$$

$$\eta = h_s / h \tag{6.8e}$$

where h_s and h are thicknesses of the upper delaminated region and intact region, respectively.

From Equation (6.7), one can see that the coefficients of stress intensity factors contributed by bending moment are $\sin(\omega+\gamma)$ and $\cos(\omega+\gamma)$. Considering our current problem, we define the mode separation factors for work done by the bending moment as follows,

$$\psi_I = \frac{\sin(\omega+\gamma)}{\sin(\omega+\gamma)+\cos(\omega+\gamma)} \tag{6.9a}$$

$$\psi_{II} = \frac{\cos(\omega+\gamma)}{\sin(\omega+\gamma)+\cos(\omega+\gamma)} \tag{6.9b}$$

6.3 Experimental results

6.3.1 Specifications of the specimens

The details of the experimental set up, intact specimen preparation, curing cycle and other physical and geometrical specifications were described in Chapter 4. To generate the desired delamination, a 0.001" thick strip of Teflon was embedded in between the laminae during laying-up of the laminates. The cured laminates were then cut into strips. The mechanical properties of each laminate were evaluated experimentally and provided in Chapter 4. The experimentally measured critical energy release rates were determined

to be G_I =411.0 J/m^2 and G_{II} =1007.0 J/m^2. Tsai, *et al* [2001] observed that the dynamic delamination fracture toughness of the unidirectional polymeric composites that they tested was basically the same as their static fracture toughness, and it was not significantly affected by crack speed of up to 1100 m/s. In the current numerical investigation, therefore, the values of the strain energy release rates obtained experimentally under static condition will be used for the purpose of dynamic analysis.

A total of 7 groups of specimens were tested, and each group had 6 specimens, except group A, which had 5 specimens. Each group of specimens had different delamination length and locations (with respect to the beam length and thickness). Table 6-1 lists the specifications of each groups of specimens. For all beams, the length between two supports was 150mm. Each specimen was impacted only once by a 0.518 Kg steel impactor. The impactor's velocity, however, was different for each impact event. The main objective of the investigation was to study the growth of delamination in the laminated beams subject to varying conditions. The initial geometric imperfection of each specimen was measured for the numerical analysis.

Table 6-1 Delamination specifications of each group of specimens.

Sepcimen Groups	Delamination Length (mm)	Delamination Location	
		Along Beam (mm)*	Through Thickness
A	10.0	75.0	$[0_8 // 0_8]$
B	20.0	75.0	$[0_8 // 0_8]$
C	30.0	75.0	$[0_8 // 0_8]$
D	20.0	75.0	$[0_5 // 0_{11}]$
E	20.0	75.0	$[0_2 // 0_{14}]$
F	20.0	35.0	$[0_8 // 0_8]$
G	20.0	115.0	$[0_8 // 0_8]$

Note: * Along beam means distance from the delamination center to the fixed end of beam.

6.3.2 Results of groups A, B and C with different delamination lengths

These three groups of specimens had the same lay-up $[0_8 // 0_8]$, but different initial delamination lengths, 10mm, 20mm and 30mm, located at the mid-span of the beams. The '//' indicates delamination location through the beam thickness. Table 6-2 lists the test results of delamination growth for group A with an initial delamination length of 10 mm, including geometric data and delamination growth of both left end (Dlm_LG) and right end (Dlm_RG) of the delaminations, total delamination growth (Dlm_TG), impactor mass and velocity, and the derived impactor momentum, energy and delamination growth per unit momentum and energy. Table 6-3 and 6-4 tabulate the test results for group B and C, for initial delamination lengths of 20mm and 30mm, respectively. Due to the brittle nature of carbon/epoxy laminates and the variation in the mechanical properties, including the elastic modulus, and in particular the critical energy release rate and impact velocity for each individual specimen, the delamination growth due to axial impact were found to vary inconsistently from specimen to specimen. Considering the amount of delamination growth due to the impact, Tables 6-2, 6-3 and 6-4 indicate an average growth per unit impact energy of the impactor as follows: (a) an average growth of 11.9 mm for group A (this group had a 10 mm long initial delamination); (b) an average growth of 14.4 mm for group B (this group had a 20mm long initial delamination); (c) while only an average of 8.9 mm growth was observed for group C (the beams of this group had 30 mm long initial delamination). A similar trend exists when considering growth per unit momentum of the impactor as well. That is, the amount of delamination growth per unit impact energy did not increase monotonously for the beams tested. This phenomenon can also be seen when analyzing the relation between critical impact energy and delamination growth, as presented in section 6.4.3.

Table 6-2 Delamination specifications of Group A: Delamination Length =10mm, located in the mid-span of beam.

Specimen No.	A1	A2	A3	A4	A5	Average
Width (mm)	17.02	17.36	17.31	17.37	16.87	17.19
Thickness (mm)	2.24	2.28	2.25	2.24	2.31	2.26
Dlm_LG (mm)	63.35	67.40	60.85	55.10	51.65	59.67
Dlm_RG (mm)	28.70	15.60	63.95	26.70	9.60	28.91
Dlm_TG (mm)	92.05	83.00	124.80	81.80	61.25	88.58
Mass (Kg)	0.518	0.518	0.518	0.518	0.518	0.518
Velocity (m/s)	5.480	5.230	5.630	5.270	5.200	5.362
Momentum (Kg.m/s)	2.838	2.710	2.917	2.729	2.692	2.777
Energy (J)	7.772	7.089	8.211	7.186	6.993	7.450
Delam. Growth Per Unit Momentum	32.435	30.627	42.784	29.974	22.753	31.895
Delam. Growth per Unit Energy	11.844	11.708	15.199	11.383	8.759	11.890

Table 6-3 Delamination specifications of Group B: Delamination Length =20mm, located in the mid-span of beam.

Specimen No.	B1	B2	B3	B4	B5	B6	Average
Width (mm)	17.12	17.40	17.20	17.30	17.38	17.45	17.31
Thickness (mm)	1.91	2.02	1.89	1.99	1.99	2.03	1.97
Dlm_LG (mm)	58.55	27.25	54.65	30.90	48.50	49.50	44.89
Dlm_RG (mm)	50.35	51.05	19.00	29.80	58.40	27.30	39.32]
Dlm_TG (mm)	108.90	78.30	73.65	60.70	106.90	76.80	84.21
Mass (Kg)	0.518	0.518	0.518	0.518	0.518	0.518	0.518
Velocity (m/s)	5.330	4.480	4.790	4.710	4.700	4.510	4.753
Momentum (Kg.m/s)	2.759	2.318	2.480	2.438	2.435	2.337	2.461
Energy (J)	7.347	5.188	5.938	5.736	5.722	5.274	5.868
Delam. Growth Per Unit Momentum	39.471	33.779	29.698	24.897	43.901	32.863	34.215
Delam. Growth per Unit Energy	14.822	15.093	12.403	10.582	18.682	14.562	14.352

Table 6-4 Delamination specifications of Group C: Delamination Length =30mm, located in the mid-span of beam.

Specimen No.	C1	C2	C3	C4	C5	C6	Average
Width (mm)	17.48	16.81	17.31	17.04	17.48	17.21	17.22
Thickness (mm)	2.27	2.27	2.33	2.31	2.35	2.31	2.31
Dlm_BP	57.00	21.20	57.00	59.65	58.00	9.60	43.74
Dlm_EP	10.40	55.00	25.00	13.55	10.15	30.10	24.03
Dlm_TP	67.40	76.20	82.00	73.20	68.15	39.70	67.78
Mass (Kg)	0.518	0.518	0.518	0.518	0.518	0.518	0.518
Velocity (m/s)	5.300	5.550	5.490	4.860	5.110	4.560	5.146
Mom.(Kg.m/s)	2.747	2.874	2.846	2.518	2.649	2.360	2.666
Engy.(J)	7.286	7.975	7.816	6.119	6.771	5.374	6.890
Delam Growth Per Unit Momentum	11.302	26.509	28.816	29.072	25.730	16.825	23.042
Delam Growth per Unit Energy	4.262	9.554	10.491	11.962	10.064	7.387	8.953

6.3.3 Results of groups D and E with different delamination positions through beam thickness

These two groups (D and E) of specimens had different lay-ups: $[0_5 // 0_{11}]$ and $[0_2 // 0_{14}]$, hosting a 20 mm long delamination located at their mid-span. The purpose of the tests was to investigate the influence of the through thickness position of delamination and lay up sequence on delamination growth. Tables 6-5 and 6-6 tabulate the delamination growth information for group D and E, respectively. Comparing the average growth per unit impact energy of group D, E and B, we can see that delamination growth of group E with $[0_2 // 0_{14}]$ lay-up is smaller than that of group D with $[0_5 // 0_{11}]$lay-up and group B with $[0_8 // 0_8]$lay-up. That is, the closer the delamination is to the outer surface, the more energy it takes for it to grow.

Table 6-5 Delamination specifications of Group D: Delamination Length =20mm, located in the mid-span of beam.

Specimen No.	D1	D2	D3	D4	D5	D6	Average
Width (mm)	16.58	16.33	16.61	16.58	16.50	16.47	16.51
Thickness (mm)	2.33	2.30	2.29	2.08	2.27	2.25	2.25
Dlm_LG (mm)	51.13	35.39	25.29	28.53	41.42	27.85	34.94
Dlm_RG (mm)	66.74	46.20	30.95	54.89	28.62	36.54	43.99
Dlm_TG (mm)	117.87	81.59	56.24	83.42	70.04	64.39	78.93
Mass (Kg)	0.518	0.518	0.518	0.518	0.518	0.518	0.518
Velocity (m/s)	5.490	4.240	4.500	4.510	4.520	4.300	4.593
Momentum (Kg.m/s)	2.844	2.196	2.331	2.336	2.341	2.227	2.379
Energy (J)	7.806	4.656	5.245	5.268	5.291	4.789	5.465
Delam. Growth Per Unit Momentum	41.45	37.15	24.13	35.71	29.91	28.91	33.17
Delam. Growth per Unit Energy	15.10	17.52	10.72	15.83	13.24	13.45	14.44

Table 6-6 Delamination specifications of Group E: Delamination Length =20mm, located in the mid-span of beam.

Specimen No.	E1	E2	E3	E4	E5	E6	Average
Width (mm)	16.35	16.77	16.53	16.83	16.56	16.88	16.65
Thickness (mm)	2.25	2.03	2.08	2.14	2.16	2.17	2.14
Dlm_LG (mm)	5.03	7.51	3.37	10.04	12.34	12.84	8.52
Dlm_RG (mm)	3.82	6.52	16.41	16.14	15.2	38.36	16.08
Dlm_TG (mm)	8.85	14.03	19.78	26.18	27.54	51.20	24.60
Mass (Kg)	0.518	0.518	0.518	0.518	0.518	0.518	0.518
Velocity (m/s)	4.550	4.980	4.880	4.960	4.920	5.200	4.915
Momentum (Kg.m/s)	2.357	2.580	2.528	2.569	2.549	2.694	2.546
Energy (J)	5.362	6.423	6.168	6.372	6.269	7.003	6.257
Delam. Growth Per Unit Momentum	3.75	5.44	7.82	10.19	10.81	19.01	9.66
Delam. Growth per Unit Energy	1.65	2.18	3.21	4.11	4.39	7.31	3.93

6.3.4 Results of groups F and G with different delamination positions along beam length

These two groups of specimens had the same lay-ups $[0_8 // 0_8]$, and the same initial delamination length of 20mm, but with delamination at different locations along the beam length, as listed in Table 6-1. The purpose of these two groups of tests was to investigate the influence of the longitudinal location of delaminations on their growth. Table 6-7 and 6-8 list the delamination growth data for Group F and G. In these tables, the centre locations of delaminations with respect to the fixed end of the beams were 35mm and 115 mm, for Group F and G, respectively. Comparing the average growth per unit impact energy of the beams, one can see that for Group F (with delamination center located at 35 mm from the fixed end of the beams), the growth length was larger than that of group G (with delamination center located at 115 mm to the fixed end of the beams); both groups showed lower growth than that of Group B, in which the delamination was located at the mid-span of beam.

6.4 Numerical results

6.4.1 Delamination growth

Numerical analysis was performed for every specimen of Group B and for a model representing the 'average' of all specimens in Group B (i.e., with average geometry, average initial geometric imperfections, and average impact velocity). Group B had a 20-mm delamination located at the mid-span of each beam with $[0_8 // 0_8]$ lay-up, subject to impact by a moving mass with different velocities. Figures 6-3(a) and 6-3(b) show the delamination index (Equation 6-6) calculated for the left end and right end of the delamination of the 'average' beam, impacted by a moving mass of M=0.518Kg, with an

Table 6-7 Delamination specifications of Group F: Delamination Length =20mm, delamination center located at 35mm from fixed end of beam.

Specimen No.	F1	F2	F3	F4	F5	F6	Average
Width (mm)	16.81	16.82	17.08	16.60	16.81	17.02	16.86
Thickness (mm)	2.19	2.21	2.20	2.19	2.19	2.25	2.21
Dlm_LG (mm)	13.87	5.43	8.31	19.94	17.56	15.04	13.36
Dlm_RG (mm)	93.15	7.54	30.62	33.03	26.07	58.14	41.43
Dlm_TG (mm)	107.02	12.97	38.93	52.97	43.63	73.18	54.78
Mass (Kg)	0.518	0.518	0.518	0.518	0.518	0.518	0.518
Velocity (m/s)	5.620	5.490	5.440	5.690	5.470	5.530	5.540
Momentum (Kg.m/s)	2.912	2.846	2.817	2.947	2.834	2.866	2.870
Energy(J)	8.187	7.816	7.662	8.382	7.750	7.929	7.954
Delam. Growth Per Unit Momentum	36.751	4.557	13.820	17.974	15.395	25.534	19.086
Delam. Growth per Unit Energy	13.072	1.659	5.081	6.319	5.630	9.229	6.887

Table 6-8 Delamination specifications of Group G: Delamination length =20mm, delamination center located at 115 mm from fixed end of beam.

Specimen No.	G1	G2	G3	G4	G5	G6	Average
Width (mm)	16.31	16.89	16.87	16.22	17.03	16.66	16.66
Thickness (mm)	2.27	2.24	2.26	2.23	2.28	2.26	2.26
Dlm_LG (mm)	26.44	13.88	6.90	6.07	16.94	14.04	14.05
Dlm_RG (mm)	23.39	30.10	19.73	16.25	17.51	21.39	21.40
Dlm_TG (mm)	49.83	43.98	26.63	22.32	34.45	35.44	35.44
Mass (Kg)	0.518	0.518	0.518	0.518	0.518	0.518	0.518
Velocity (m/s)	5.110	5.110	5.070	4.880	5.050	5.043	5.044
Momentum (Kg.m/s)	2.645	2.649	2.624	2.527	2.617	2.613	2.613
Energy (J)	6.753	6.771	6.647	6.166	6.612	6.590	6.590
Delam. Growth Per Unit Momentum	18.839	16.602	10.149	8.833	13.164	13.561	13.566
Delam. Growth per Unit Energy	7.379	6.495	4.006	3.620	5.210	5.377	5.378

average velocity of 4.75m/s. This 'average' beam was supported as fully fixed at its left side and impacted at its right end as shown in Figure 6-1(a). From Figure 6-3(a), one can see that the delamination growth began at the right end of the delamination, which was closer to the impacted end (right end). Figure 6-3(b) illustrates the details of the delamination index between time steps 1800 to 2200. The stress wave started from the right end and then propagated to the left, and then, the stress wave met the fixed support end and reflected back; as a result, the delamination growth of the left end of the delamination dominated the growth.

Numerical analyses results of group B are also compared with the experimental results, as tabulated in Table 6-9. The table lists the values of growth of the left and right ends of the delaminations, as well as the total growth amounts. One can see the discrepancy when comparing the numerical results with the individual experimental results. However, when one compares the numerical results with the average of the experimental results for groups A to G, as tabulated in Table 6-10, one can see much less discrepancy (in the order of 10%), with the experimental results.

6.4.2 Strain energy release rate

Figures 6-4(a) and 6-4(b) show the Mode I (G_I) and Mode II (G_{II}) strain energy release rates for the left and right ends of the delaminations for the 'average' beam of group B. The values of the critical strain energy release rates are also illustrated in the figures. The unit for the strain energy release rates in the figures is in J/mm^2. One can see from the figures that for the examined axially impacted beams, the mode II strain energy release rates are considerably larger than the mode I values.

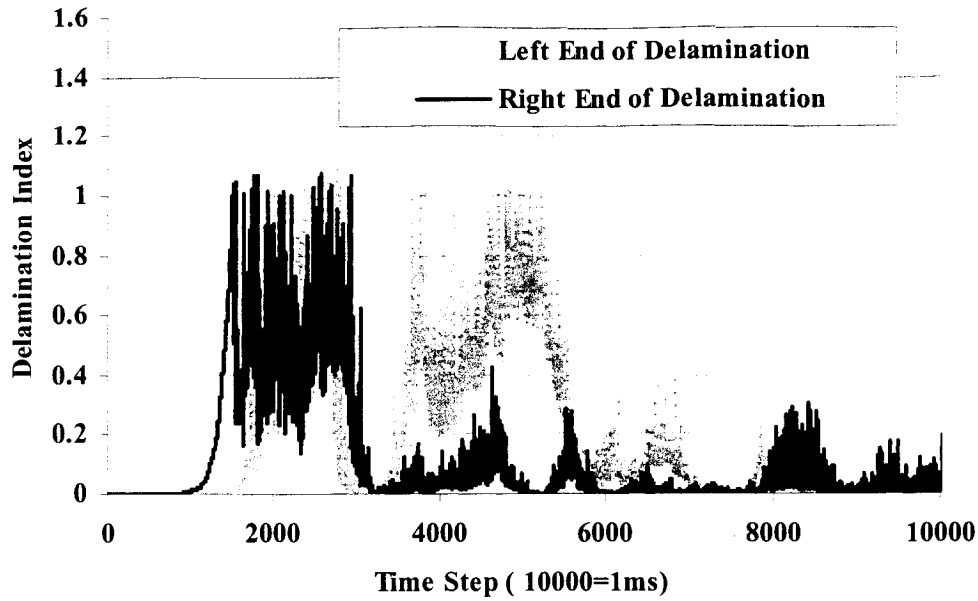

(a)

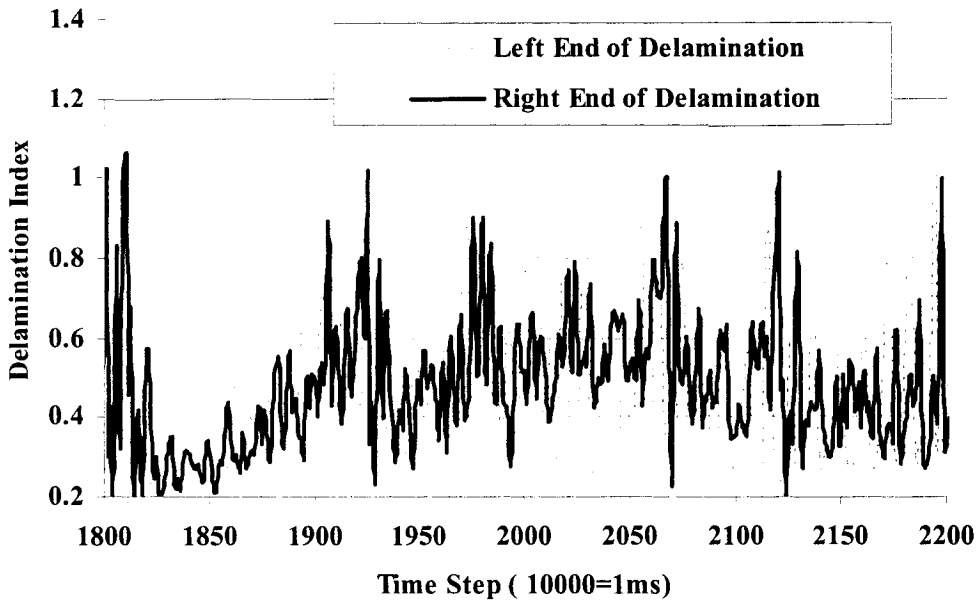

(b)

Figure 6-3 Delamination index of left and right ends of delamination. (a) time steps 0-10000 (1ms); (b) time steps 1800-2200.

Table 6-9 Comparison between the numerical and experimental results of delamination growth of Group B (Delamination Length =20mm, located in the mid-span of beam).

Specimen No.	B1	B2	B3	B4	B5	B6	Average	
Dlm_LG_E (mm)	58.55	27.25	54.65	30.90	48.50	49.50	44.89	
Dlm_LG_N (mm)	21.00	22.50	65.25	42.75	42.75	23.25	36.25*a*	42.00*b*
Dlm_RG_E (mm)	50.35	51.05	19.00	29.80	58.40	27.30	39.32	
Dlm_RG_N (mm)	64.50	32.25	45.00	32.25	32.25	31.50	39.63*a*	34.50*b*
Dlm_TG_E (mm)	108.90	78.30	73.65	60.70	106.90	76.80	84.21	
Dlm_TG_E (mm)	85.50	54.75	110.25	75.00	75.00	54.75	75.88*a*	76.50*b*

Note: Dlm_LG_N is for numerical results, Dlm_LG_E is for experimental results.
a results are the average of each specimens,
b results are calculated based on the average geometry of the specimens and subjected to the average impact velocity.

Table 6-10 Summary of comparison between numerical and experimental results.

Sepcimen Groups	Average Delamination Growth					
	Left End Growth (mm)		Right End Growth (mm)		Total Growth (mm)	
	Exp.	Num.	Exp.	Num.	Exp.	Num.
A	59.67	36.00	28.91	45.00	88.58	81.00
B	44.89	42.00	39.32	34.50	84.21	76.50
C	43.74	32.25	24.03	29.25	67.77	61.50
D	34.94	47.25	43.99	27.75	78.93	75.00
E	8.52	8.25	16.08	6.75	24.60	15.00
F	13.36	25.50	41.43	35.25	54.79	60.75
G	14.05	35.35	21.40	20.89	35.45	56.24

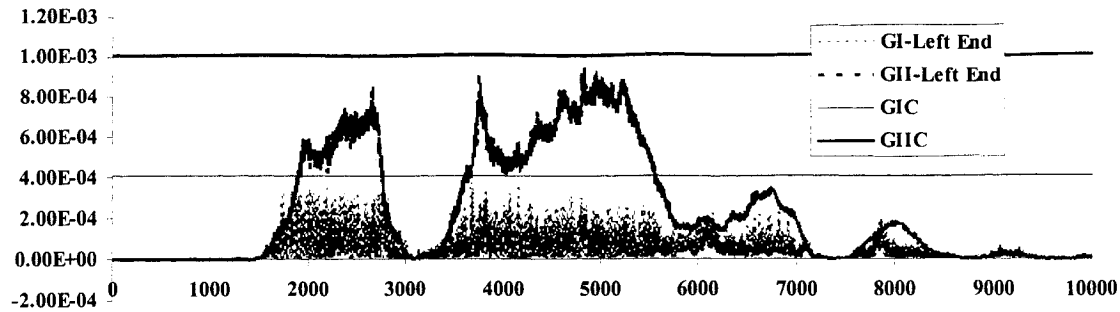

(a)

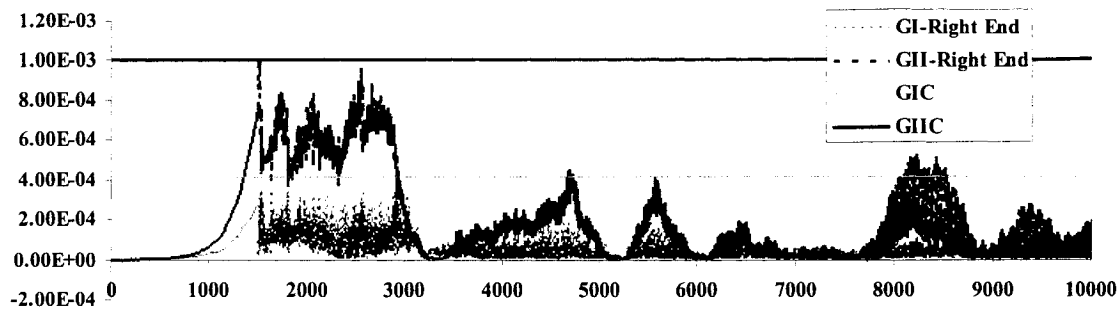

(b)

Figure 6-4 Strain energy release rate of modes I and II.
(a) left end of delamination; (b) right end of delamination.

6.4.3 Critical impact energy of delamination growth

The average critical impact energy causing delamination growth obtained for all beam series are illustrated in Figures 6-5(a-c). The results are organized into three charts. The chart in Figure 6-5(a) summarizes the results of groups A, B, and C, with their specifications tabulated in Table 6-1. One can see from the figure that the critical impact energy for the delaminations grew for the three beam groups (having 10mm, 20mm and 30mm long delaminations). Interestingly, their critical energies do not decrease, as the common sense would have indicated (in that, the critical impact energy should have decreased as the delamination length increased). This finding is indeed consistent with

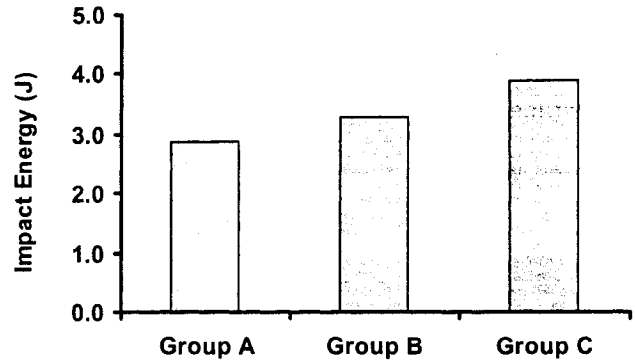

(a)

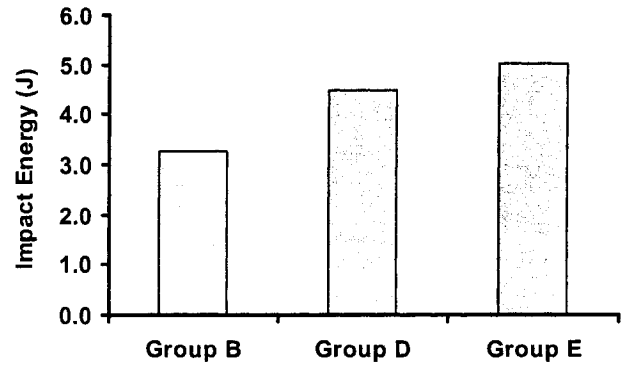

(b)

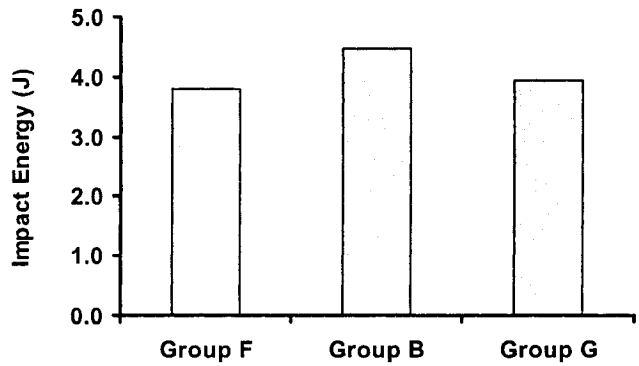

(c)

Figure 6-5 Critical impact energy of delamination growth. (a) groups A, B, and C with delamination at the same location but with different length of 10mm, 20mm, and 30mm; (b) groups B, D, and E with same delamination length of 20mm, but at different position through beam thickness $[0_8 // 0_8]$, $[0_5 // 0_{11}]$, and $[0_2 // 0_{14}]$; (c) groups F, B, and G with same delamination length of 20mm, but at and different position along beam length, 35mm, 75mm and 115 mm, respectively.

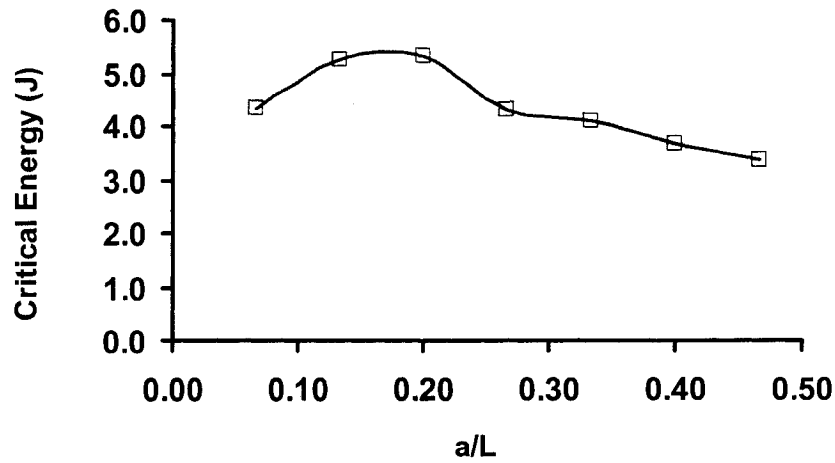

Figure 6-6 Variation of critical impact energy as a function of the delamination length.

the experimental results described in Section 6.3.2, which showed that the amount of delamination growth per unit outer impact energy did not monotonously increase with the delamination length. To further analyze the effect of delamination length on the critical impact energy, a group of beams with assumed sinusoidal geometric imperfection (i.e., $W_0(x) = 0.1h\sin(\pi x / L)$), having different delamination length, subject to axial impact, were numerically analyzed. Figure 6-6 shows the critical impact energy at the onset of delamination propagation as a function of delamination length. One can see from the figure that the critical impact energy did not vary monotonously with the increase in delamination length.

Figure 6-5(b) shows the variation of the critical impact energy as a function of the through-thickness location of delamination (i.e., as the delamination moves from the mid-plane to toward the surfaces). One can see that the critical impact energy were larger when delamination was located near the surface. This is also consistent with the phenomenon described in section 6.3.3, in that more energy was required for delamination growth when the delamination was closer the surface.

Figure 6-5(c) illustrates the variation of the critical impact energy as a function of the lengthwise location of delamination (i.e., as the delamination moves from the center of the beam toward the beam-ends). One can see that the critical impact energy was lower when the delamination was located near the either ends of the beams. This is also consistent with our findings as discussed in section 6.3.4, in that the experimental values of the energy required for the delamination growth near the ends were larger than that required for the delaminations near the mid-span.

6.5 Conclusions

Dynamic delamination growth behavior of FRP laminated beams, with various delamination lengths located at various positions along the span and through the thickness of the beams, subject to axial impact was investigated experimentally and numerically in this chapter. The experiments were performed on delaminated carbon/epoxy beams. The numerical and experimental results led us to draw the following conclusions:

(i) Unlike common sense would have indictated, the delamination growths per unit impact energy and the critical impact energy required for delamination growth of the beams tested did not monotonously increase as the delamination length was increased.

(ii) More energy was required for a delamination to grow when the delaminations were located near the beam surfaces, than when the delamination was located at the mid-plane of a beam. This phenomenon was also consistent when examining the beams' critical impact energy.

(iii) The critical impact energy was lower when the delamination was located near the fixed-end or the impacted-end of the beams than that located at the mid-span.

7 Dynamic Pulse-buckling of Plasticity-like FRP Beams

In this chapter, dynamic pulse-buckling response of carbon/epoxy and E-glass/epoxy laminated composite beams with $[(\pm 67.5)_n]_s$ angle lay-up, subjected to axial impact is investigated experimentally and numerically. These FRP beams behaved like ductile metal, exhibiting plasticity like behavior. Both types of FRP beams had residual deformed shapes after axial impact, while no obvious delamination was evident. Numerical investigation was also performed for the two category beams.

7.1 Introduction

As described in the previous chapters, dynamic pulse buckling, as a response to axial impact, has been a research topic since the early work of Koning and Taub [1934]. Due to their anisotropic and layer-wise nature of composite components, lay-up sequence and angle of lamina have a crucial effect on the buckling behavior of axial components when subject to axial impact [Zhang and Taheri, 2002a], as described in Chapter 3. The damage behavior of composite laminated beams subject to axial impact is also different from that of the isotropic materials. As stated in Chapter 5, the laminated beams with $[(\pm 67.5)_3]_s$ lay-up showed different deformation and damage characteristic in comparison with beams with other lay-up sequences when subjected to axial impact. The beams exhibited a pronounced residual deformation after impact. In this chapter, dynamic pulse-buckling behavior of the laminated beams with $[(\pm 67.5)_n]_s$ lay-up subject to axial impact will be investigated. Two categories of composites were tested: E-glass/epoxy laminates and carbon/epoxy laminates.

7.2 Experimental specimens

A total of 3 groups (CA, CB and CC) of carbon/epoxy beams, each with 4 specimens were tested. For the E-glass/epoxy fiber laminated beams, two groups (GA, GB) were tested; group GA had 10 specimens and GB had 4 specimens. The mechanical properties of the carbon/epoxy and E-glass/epoxy laminates were listed in Table 4-1 along with the geometric properties of the beams.

7.3 Experimental results and discussion

7.3.1 Carbon/Epoxy laminated beams

Three groups (CA, CB and CC), each having 4 specimens were tested. As described in Chapter 5, the specimens with lay-ups of $[0_{12}]$, $[(\pm 22.5)_3]_s$, $[(\pm 45)_3]_s$ and $[(0/90)_3]_s$ showed damage in the form of matrix crack, delamination and fiber breakage when impacted by a moving mass. However, most of the specimens with $[(\pm 67.5)_3]_s$ lay-up had no obvious damage, but they remained in a deformed shape after impact. Figures 7-1(a), 7-1(b), and 7-1(c) show the deformed shapes of these beams (group CA, CB and CC). This phenomenon is consistent with plastic pulse buckling of isotropic beams, as demonstrated by Abrahamson and Goodier [1966] and Kenny [2000], and Figure 7-2 presents the post-buckled profile of aluminum beams impacted by a moving mass obtained by Kenny [2000]. Comparing Figures 7-1(a), 7-1(b) and 7-1(c) with Figure 7-2, one can observe that the laminated beams with $[(\pm 67.5)_3]_s$ lay-up showed 'plasticity' like behavior.

Table 7-1 summarizes the impact information of specimens in each group of carbon/epoxy laminated beams, including specimen length, impact velocity and energy,

Table 7-1 Specifications of carbon/epoxy laminated beams.

Specimen	Beam Length(mm)	Velocity	Energy	Wmax/Wo
CA1	105	3.92	3.98	0.694
CA2	105	4.11	4.38	0.688
CA3	105	4.84	6.06	0.963
CA4	105	5.46	7.72	1.381
CB1	128	5.21	7.02	1.267
CB2	128	4.92	6.26	1.140
CB3	128	5.36	7.44	1.150
CB4	128	6.36	10.48	1.784
CC1	148	6.00	9.32	1.236
CC2	148	6.30	10.28	1.138
CC3	148	5.98	9.26	0.900
CC4	148	5.75	8.56	0.939

and ratio of the maximum deflection over beam thickness. W_{max} is the measured maximum deflection of a beam with one buckled crest, or sum of the crest deflections of a beam with two or more crests. The impactor mass was 0.518 Kg. The typical deformed shape, (i.e., the buckled profiles and the initial shapes) of specimens of groups CA, CB and CC are shown in Figures 7-3(a-d), 7-4(a-d), and 7-5(a-d). Comparing these figures, one can see that there is only one buckle crest for each beam of group CA with length of 105 mm, while other beams in groups CB and CC exhibited 2 or more crests. Figure 7-6 summarizes the relationship between the normalized residual maximum deflection versus impact energy for beams with various slenderness ratios. One can observe from the figure that most of the specimens with slenderness ratios of (L/r=227 and 277) developed only one crest once they buckled, as shown in Figures 7-3 and 7-4, with a linear relationship between their residual maximum deflections and impact energies. The beams with slenderness ratio (L/r=320), however, developed two or more crests in their buckled profile. For beams with this kind of lay-up ($[(\pm 67.5)_3]_s$), the axial and bending stiffness are much lower than those of beams with $[0_{12}]$, $[(\pm 22.5)_3]_s$,$[(\pm 45)_3]_s$ lay-ups, as shown

in Figure 7-7. The matrix of beams with $[(\pm 67.5)_n]_s$ lay-up, being epoxy and an inherently a brittle matrix, easily failed and the beams thus lost their elasticty and could not rebound back to their original position. As a result the beams retained their deformed shapes after impact. Figure 7-8 shows the time history results for the transverse stress component (σ_2 , the stress normal to the fiber direction) taken at the mid-span of specimen CA1 which was impacted by a moving mass of $M = 0.518Kg$ with velocity of $V_0 = 3.92m/s$. From the figure one can observe that both top and bottom surfaces of this specimen experienced σ_2 stress exceeding the ultimate tensile strength of the matrix.

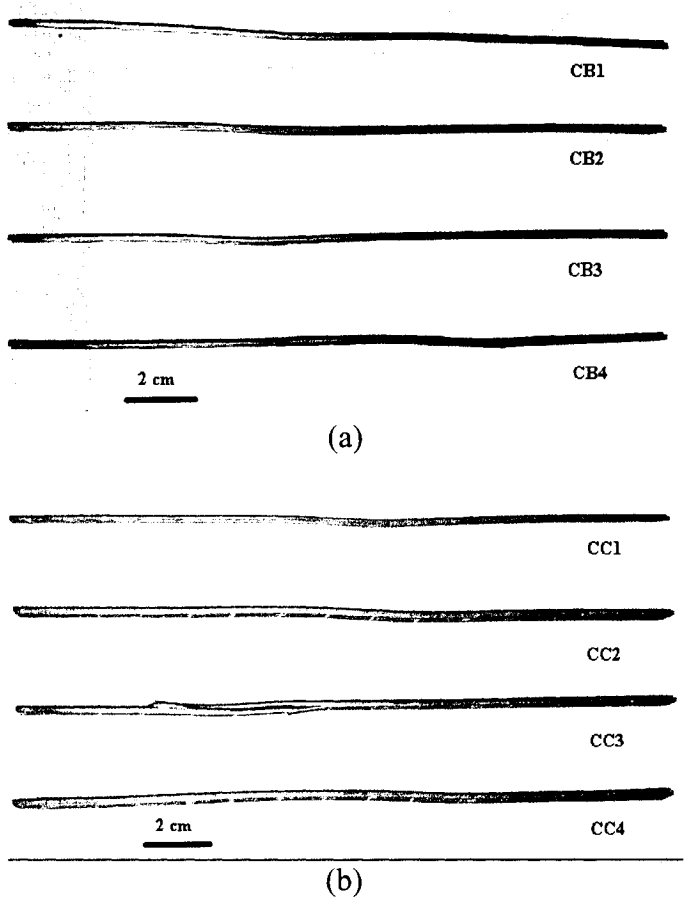

Figure 7-1 Residual deformed shape of carbon/epoxy laminated beams after impact. Group CA; (b) Group CB; (c) Group CC.
(continued in the next page)

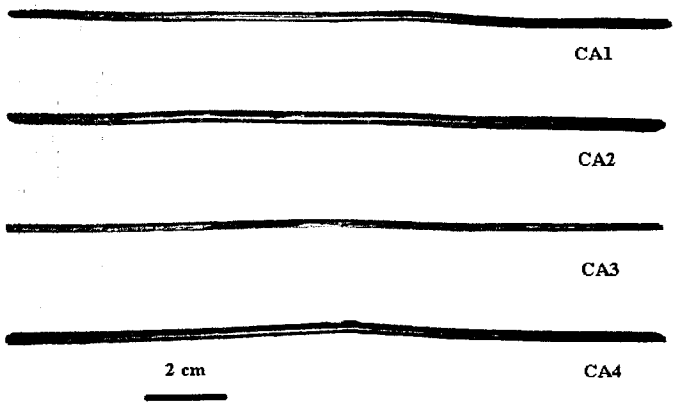

(c)

Figure 7-1 continued.

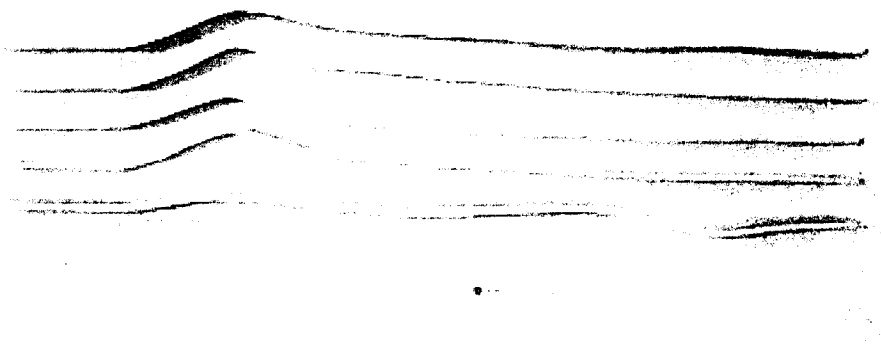

Figure 7-2 Deformed Buckled Profiles of aluminum beams subjected to axial impact [Kenny, 2000].

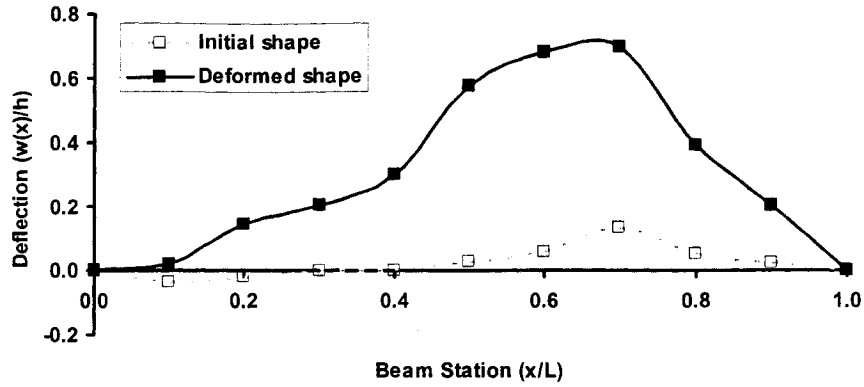

(a)

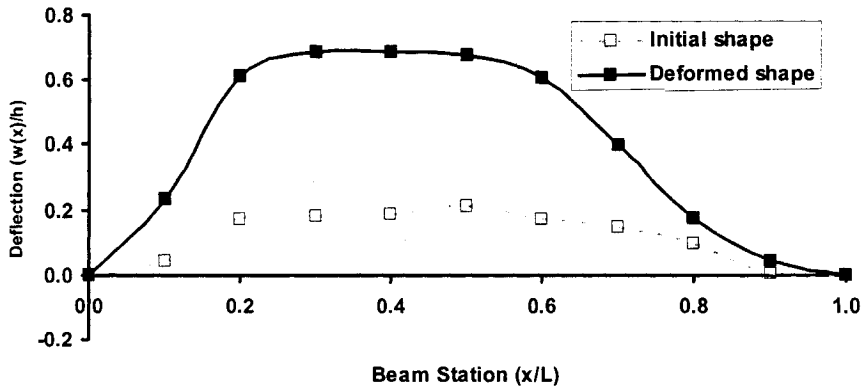

(b)

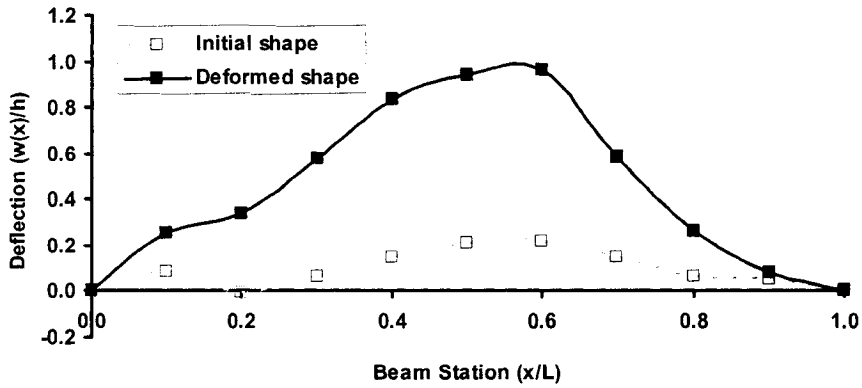

(c)

Figure 7-3 Initial shape and buckled profile of specimens of Group CA.
(continued in the next page)

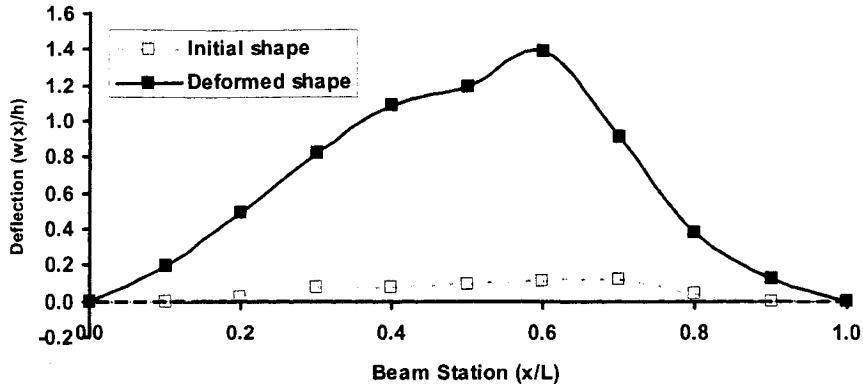

(d)

Figure 7-3 continued.

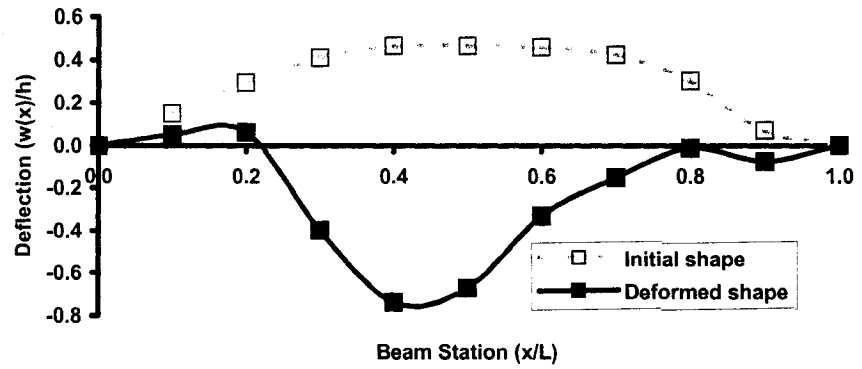

(a)

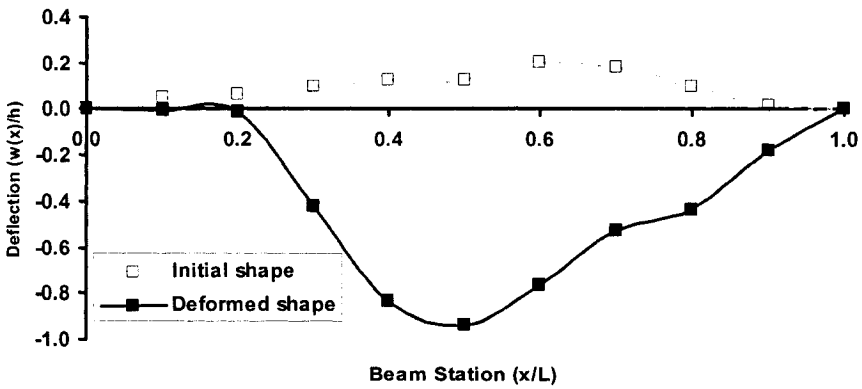

(b)

Figure 7-4 Initial shape and buckled profile of specimens of Group CB.
(continued in the next page)

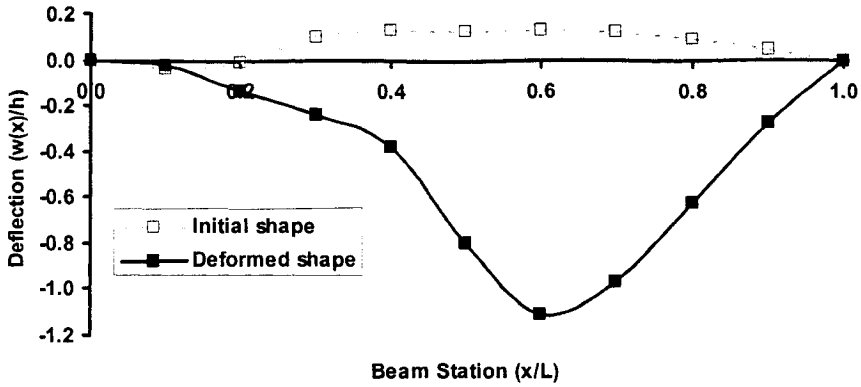

(c)

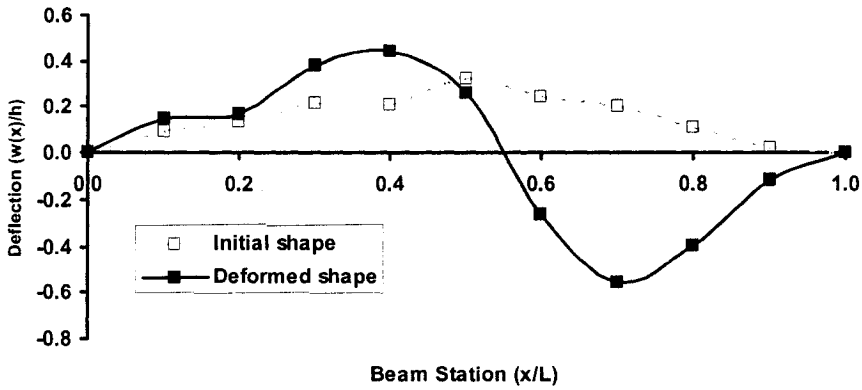

(d)

Figure 7-4 continued.

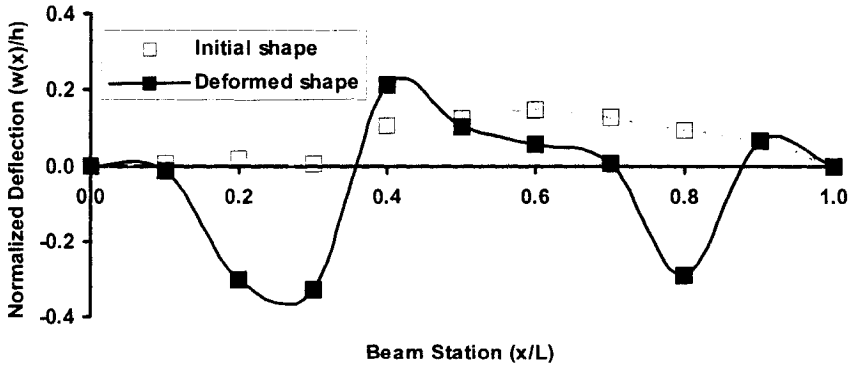

(a)

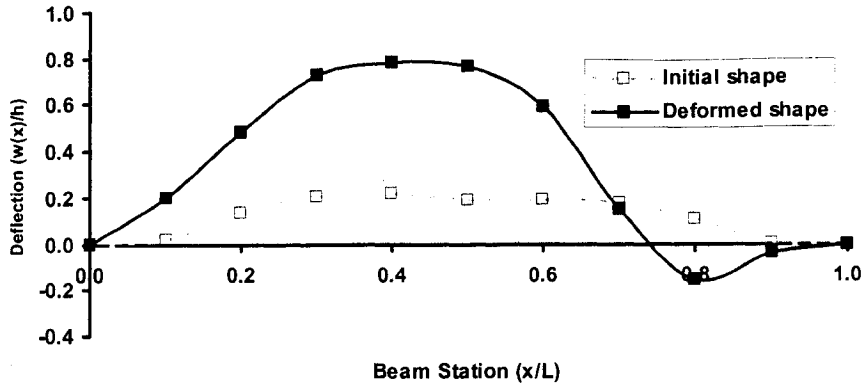

(b)

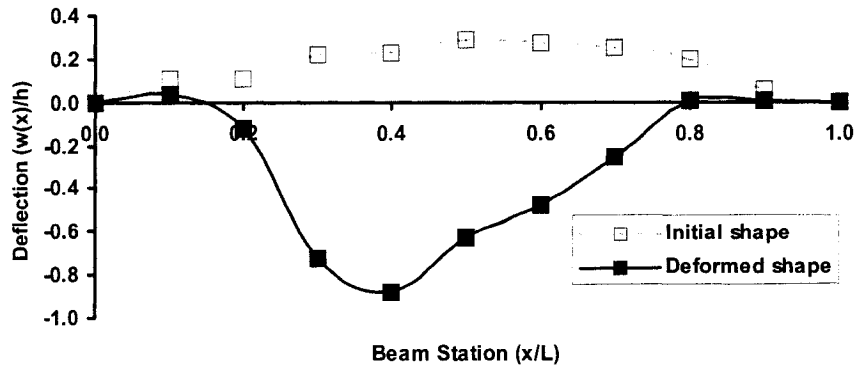

(c)

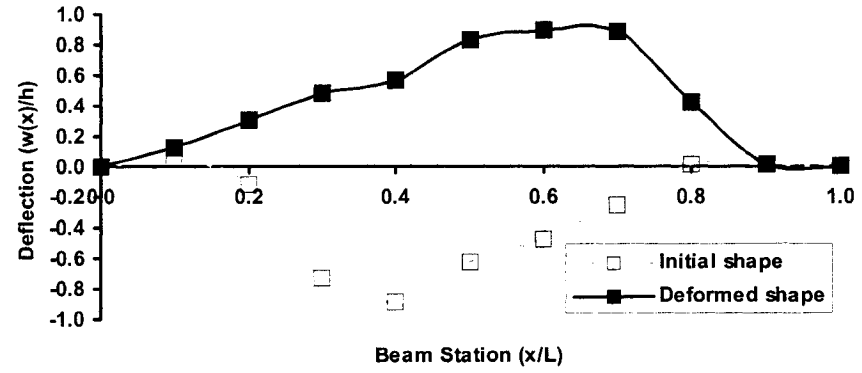

(d)

Figure 7-5 Initial shape and buckled profile of specimens of Group CC.

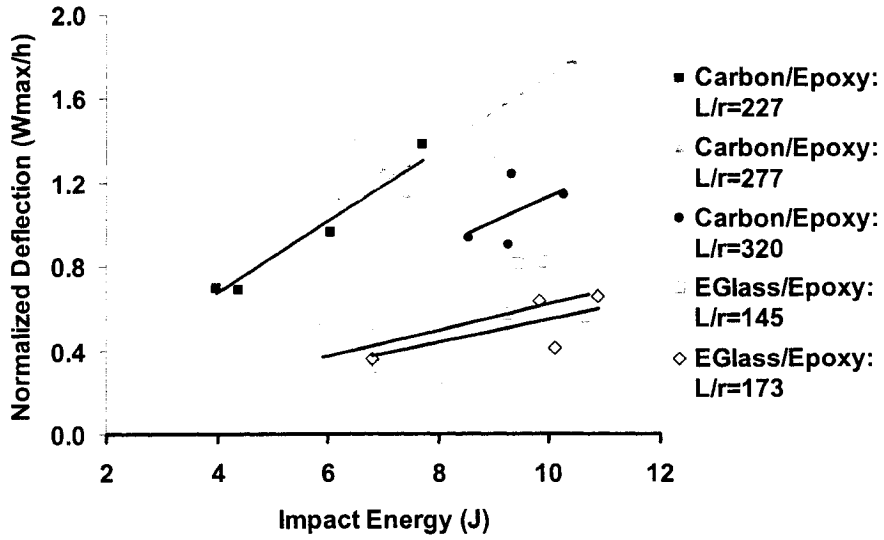

Figure 7-6 Variation of residual deflection versus impact energy.

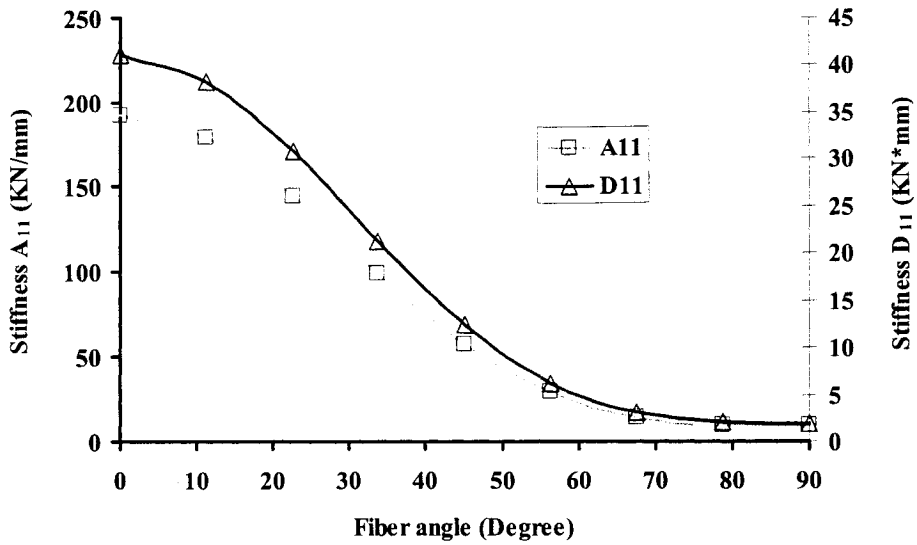

Figure 7-7 The axial and bending stiffnesses versus fiber angle for beams with $[(\pm\theta)_3]_s$ lay-up.

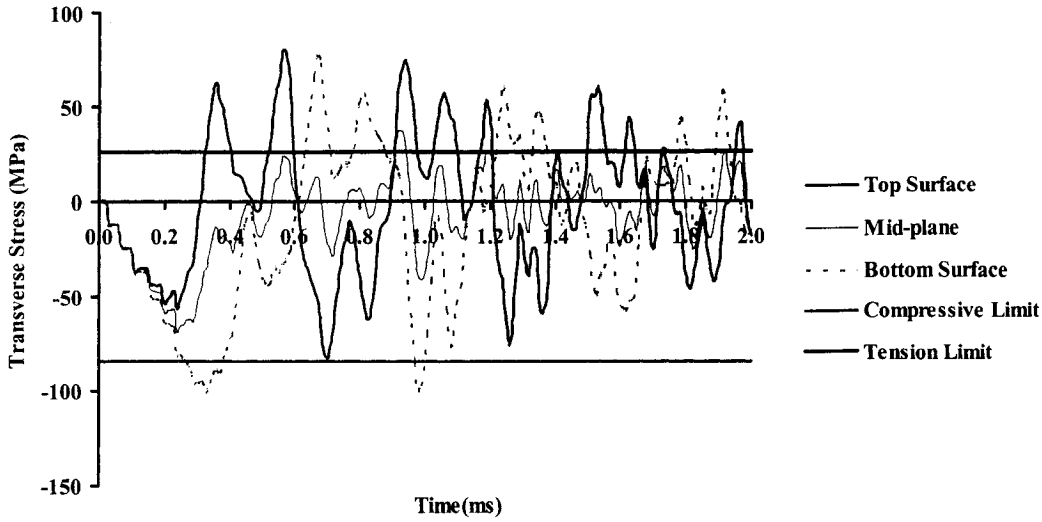

Figure 7-8 Time history results of the transverse stress component (σ_2) taken at the beam mid-span for specimen CA1, impacted by a moving mass of $M = 0.518Kg$ with velocity of $V_0 = 3.92m/s$.

7.3.2 E-Glass/Epoxy laminated beams

To further verify the dynamic behavior of laminated beams with lay-up of $[(\pm 67.5)_n]_s$ subjected to axial impact, 2 groups (GA and GB) of E-glass/epoxy laminated beams were tested. These specimens also exhibited residual deformed shapes after being impacted by a moving mass, similar to the phenomenon experienced by the carbon/epoxy laminate beams. Figure 7-9(a) and 7-9(b) show typical deformed shapes of these two groups. Table 7-2 summarizes the impact information of specimens in each group. The comparison of typical deformed and undeformed shapes of specimens of group GA and GB are shown Figure 10(a-j) and 11(a-d). The relationship between the residual deformation of these beams as a function of the impact energy for various slenderness ratios is also presented in Figure 7-6. A linear relationship exists between the residual deformation and impact energy for beams with slenderness ratio of L/r=145 and 173. Figure 7-12 shows the time history results of the σ_2 stress component taken at the beam

mid-span for specimen GA1 which was impacted by a moving mass of $M = 0.518Kg$ with a velocity of $V_0 = 5.04m/s$. One can see that both top and bottom surface laminae experienced tensile stress exceeding the matrix's ultimate tensile strength. This behavior is consistent with those of the carbon/epoxy laminate beams.

7.4 Summary

Dynamic pulse-buckling response of carbon/epoxy and E-glass/epoxy laminated composite beams with angle lay-up of $[(\pm 67.5)_n]_s$ subject to axial impact was investigated experimentally and numerically. Both types of laminates exhibited post-impact residual deformation, while no obvious delamination was observed. The crest deflection of the beam was linearly proportional to the impact energy. The numerical investigation showed that both the top and bottom surfaces of the beams failed due to excessive transverse stress.

Table 7-2 Specifications of E-glass/epoxy laminated beams.

Specimen	Beam Length(mm)	Velocity	Energy	Wmax/Wo
GA01	145	5.04	6.579	0.39
GA02	145	4.78	5.918	0.50
GA03	145	5.17	6.923	0.32
GA04	145	5.27	7.193	0.18
GA05	145	5.15	6.869	0.53
GA06	145	5.59	8.093	0.27
GA07	145	6.19	9.924	0.82
GA08	145	5.98	9.262	0.57
GA09	145	6.43	10.708	0.56
GA10	145	6.04	9.449	0.81
GB01	173	5.12	6.790	0.36
GB02	173	6.48	10.876	0.66
GB03	173	6.25	10.117	0.41
GB04	173	6.16	9.828	0.63

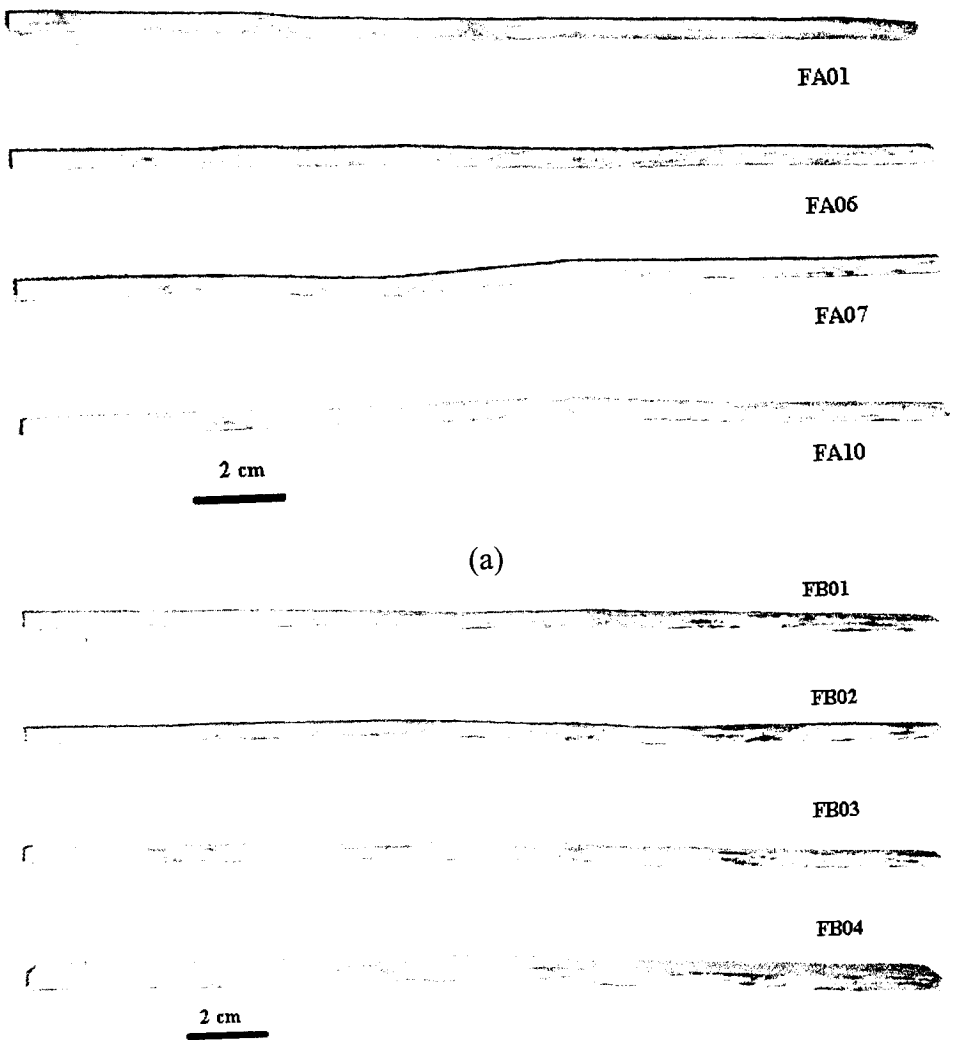

Figure 7-9 Residual deformed shape of Eglass/epoxy laminated beams after impact. Group GA; (b) Group GB.

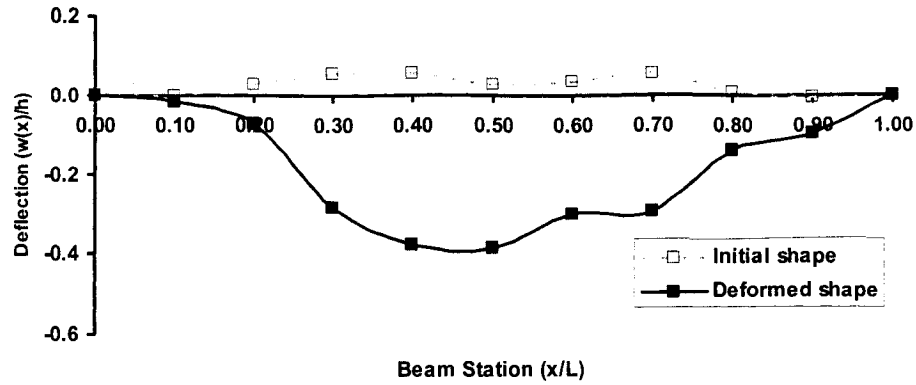

(a)

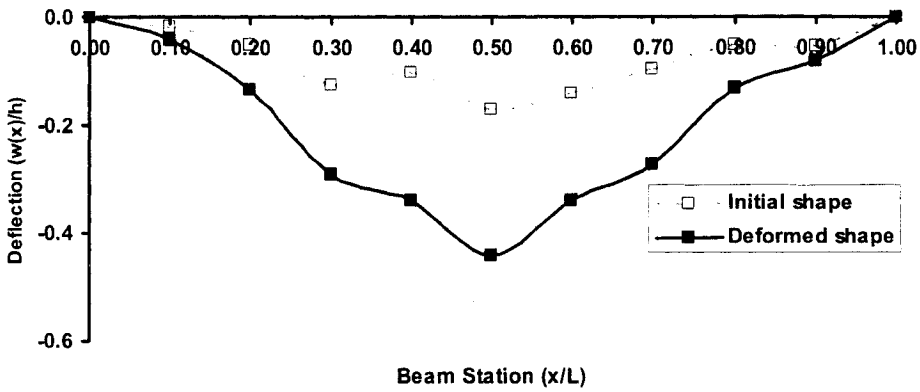

(b)

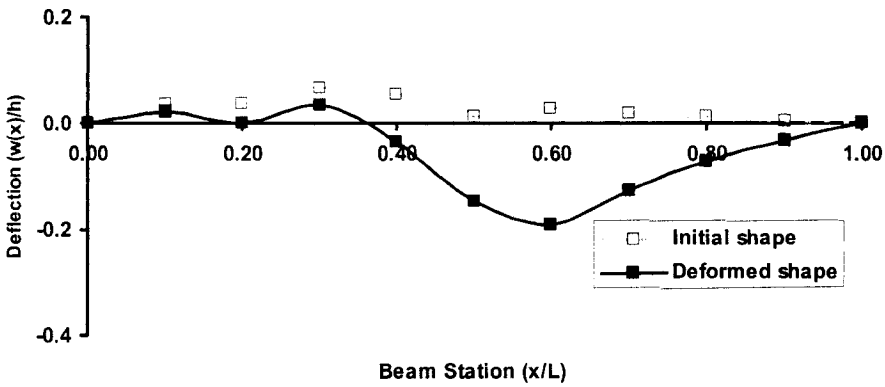

(c)

Figure 7-10 Initial and pulse buckled profiles of the E-glass/epoxy Specimens of group GA (continued in the next page)

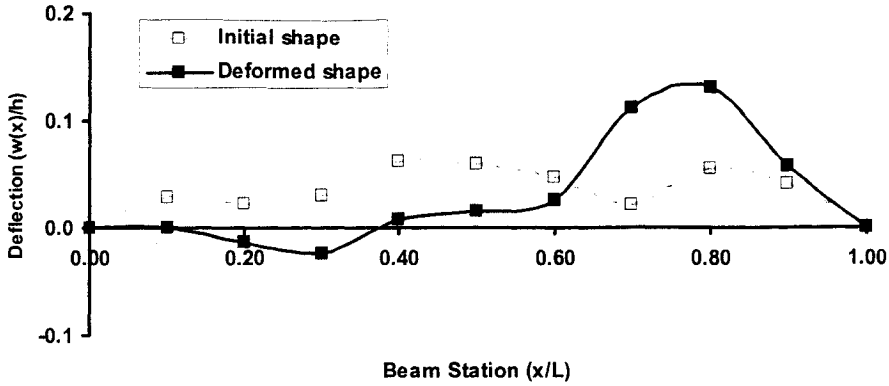

(d)

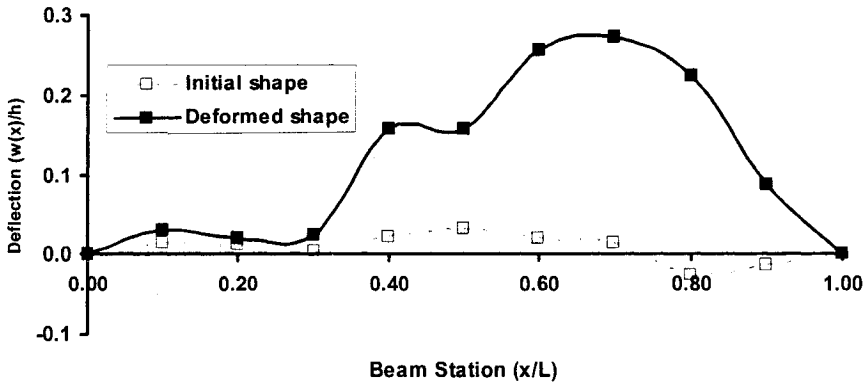

(e)

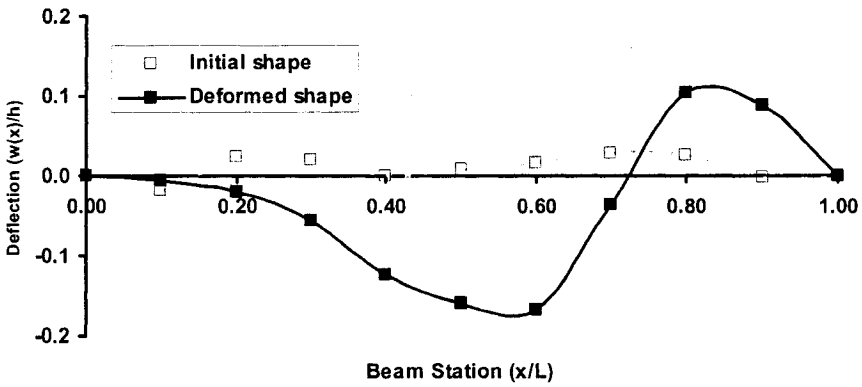

(f)

Figure 7-10 continued.

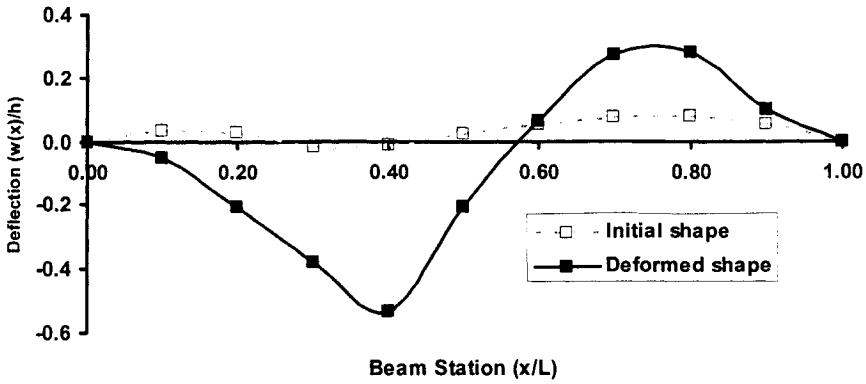

(g)

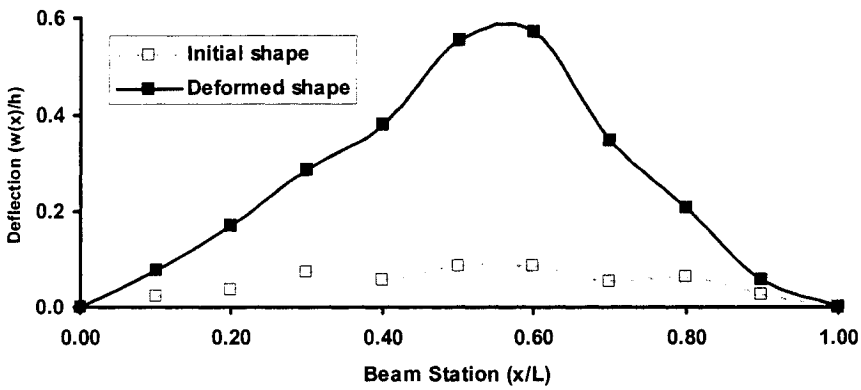

(h)

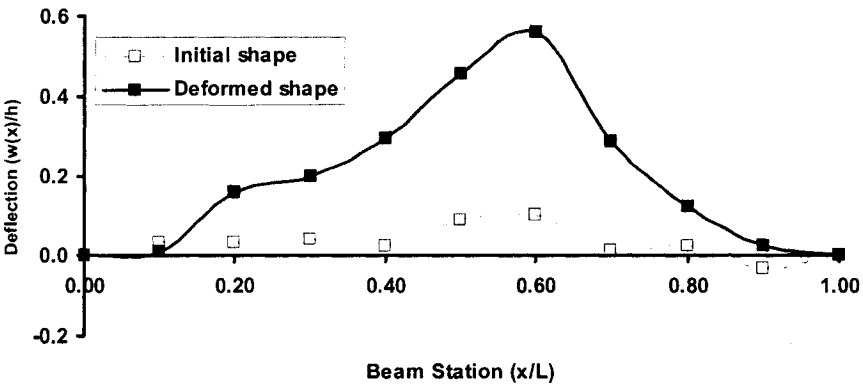

(i)

Figure 7-10 continued.

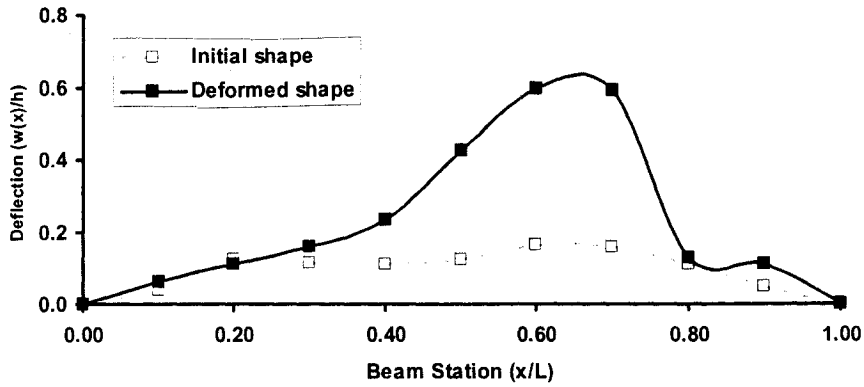

(j)

Figure 7-10 continued.

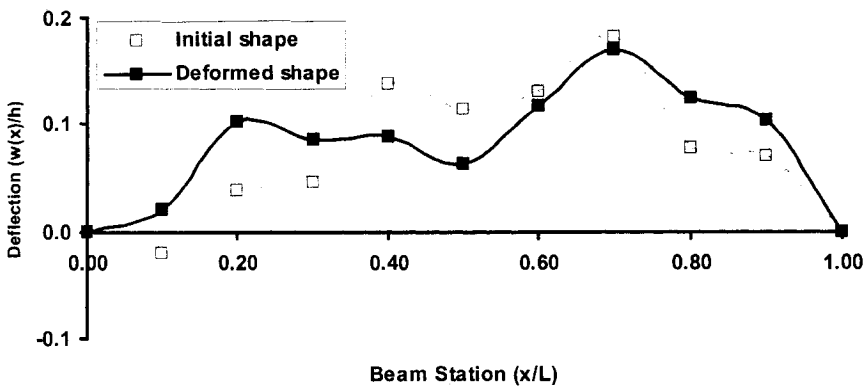

(a)

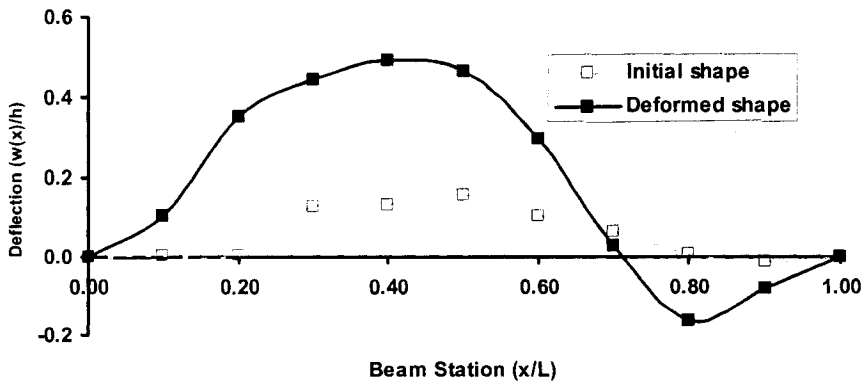

(b)

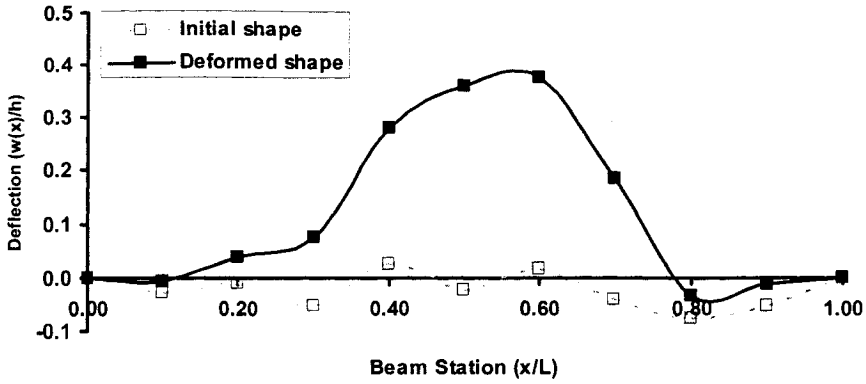

(c)

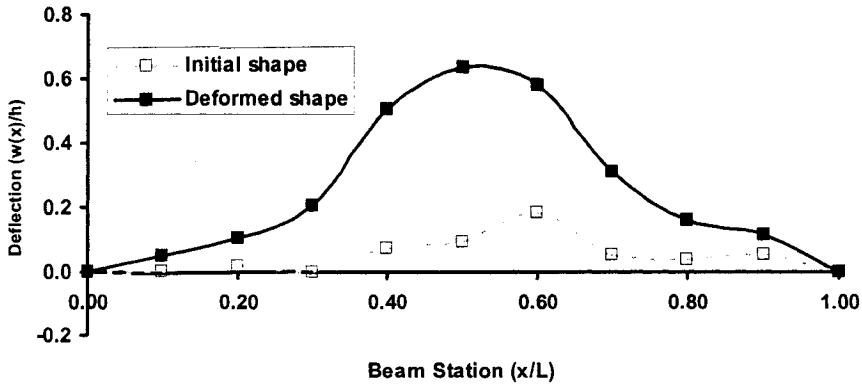

(d)

Figure 7-11 Initial and pulse buckled profiles of the E-glass/epoxy Specimens of group GB.

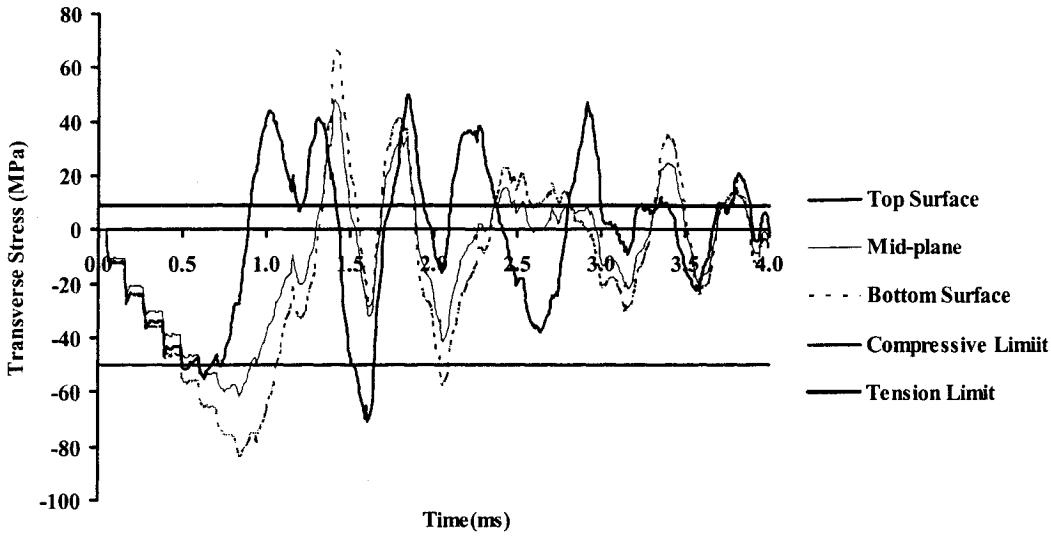

Figure 7-12 Stress-time history of the transverse component (σ_2), at the beam mid-span for specimen GA1, impacted by a moving mass of $M = 0.518Kg$ with velocity of $V_0 = 5.04m/s$.

8 Summary and Conclusion

In this dissertation, the dynamic behavior, including pulse buckling response, damage initiation and delamination growth of slender fiber-reinforced plastic (FRP) composite laminated beams, having initial geometric imperfections, subject to an axial impact was investigated numerically and experimentally.

This chapter provides a summary of the work and conclusions in this dissertation. Recommendations for future work are proposed.

8.1 Numerical model

When a beam with initial geometric imperfections is impacted axially, it will deform in both axial and lateral directions. The cross section of the beam will also rotate about the neutral axis. When the beam is impacted axially, the inertia in the axial and lateral directions, as well as the rotation of the cross section would have significant effects on the beam's deformation. To evaluate the complete and accurate dynamic behavior of a beam under such a case, one should not ignore the effects of these factors. For laminated components, shear stress distribution through the thickness, and inter-laminar shear stresses are important factors that affect the behavior of laminated components.

In this dissertation, the dynamic equilibrium equations of slender fiber-reinforced plastic (FRP) composite laminated beams, having initial geometric imperfections, subjected to an axial impulse, were established based on Timoshenko beam theory with the consideration of all above mentioned parameters. During the deformation of such beams, there exists a nonlinear relationship between the axial and lateral displacement of beams. The von-Karman nonlinear strain-displacement relationship was therefore employed to describe such relationships. To best describe the shear stress distribution through the

beam thickness, the First-Order and Higher-Order Shear Deformation Theories were used to model the displacement fields of the beam, respectively, and the results were compared based on these two theories. The central difference method was used to solve the developed dynamic equations. The integrity of the numerical results were verified with those of the finite element analysis obtained from commercial codes, and good agreement was observed.

8.2 Dynamic pulse buckling

Pulse buckling, as an instability form, that is, as excessive and sudden growth of lateral, or out of plane displacement, can result from the application of a transient loading function of a single pulse with a magnitude greater than the static Euler buckling load. Numerical analysis for both the FSDT and HSDT were performed for FRP laminated slender beams with initial geometric imperfections subject to an impulse load. The dynamic pulse buckling phenomenon was identified as the variation of lateral deflection versus the axial deformation, axial compressive strain and impact momentum/impulse. It was demonstrated that the momentum/impulse could be taken as a viable parameter for predicting the onset of dynamic pulse buckling. The parameters investigated in this study (through sensitivity analysis), included the effect of initial geometric imperfection, slenderness ratio and curvature of the beam on the pulse buckling response. The proposed kinematic equations were developed and demonstrated to be valid for various boundary conditions and types of impulse through several numerical cases.

8.3 Damage initiation

Fiber-reinforced composites' susceptibility to damage resulting from mechanical, physical and chemical factors adversely affect their stiffness, strength and durability. Impact is one of the most significant sources of damage that can cause matrix cracking,

laminate delamination and fiber breakage. The study of dynamic damage behavior of laminated beams was performed numerically and experimentally. Hashin's failure criteria was used to predict a damage mechanism in the beams. Scanning Electron Microscopy was also used to analyze the damage mechanism. The influence of fiber angle, lay-up sequence and initial geometric imperfection on the critical energy causing damage initiation was also investigated.

Delamination and matrix cracking were the two dominating damage mechanisms in the carbon/epoxy laminated beams subjected to axial impulse. The density and length of delamination(s) depended on the lay-up sequences. The damage mechanism was also observed to be strongly dependent on the nature of the initial geometric imperfections. The critical energy for damage initiation varied with the lay-up and slenderness ratio.

8.4 Delamination propagation

Delamination propagation in the beams was investigated numerically and experimentally. The strain energy release rate based on the virtual crack closure technique (VCCT) was calculated at the tips of the delamination. Carbon fiber/epoxy specimens having various size delamination, located along the beams' length and through the thickness, subjected to impact were tested and analyzed. The critical impact energy for delamination growth was predicted numerically as well. It was observed that the delamination growth per unit impact energy and the critical impact energy to propagate the delamination did not consistently increase as the delamination length was increased. The closer the delamination to the outer surface, the more energy would be consumed to grow the delamination; the same was observed for the critical impact energy. The critical impact energy was lower when the delamination was located near the fixed end or the impacted end of the beams.

8.5 Pulse buckling behavior of plasticity-like angle ply laminated beams

Dynamic pulse-buckling response of carbon/epoxy and E-glass/epoxy laminated composite beams with $[(\pm 67.5)_n]_s$ lay-up, subjected to axial impact was investigated experimentally and numerically. For both types of materials (carbon/epoxy and E-glass/epoxy), the $[(\pm 67.5)_n]_s$ laminated beams exhibited post-impact residual deformed shape, while no obvious delamination was evident. The crest deflection of the beams was linearly proportional to the impact energy. The numerical investigation showed that both the top and bottom surfaces failed due to excessive transverse tensile stress (normal to the fiber direction).

8.6 Recommendations for future research

Based on the numerical and experimental investigations conducted during the work of this thesis and the outcoming results, the following recommendations are offered.

The initial geometric imperfection of the beams was assumed to be a sinusoidal shape in the pulse buckling investigation. Experimental and numerical investigations should be performed to verify the findings of our sensitivity analysis conducted in Chapter 3 by investigating beams having randomly distributed initial geometric imperfections.

To further the current research, it is recommended to expand the scope of materials investigated; ceramics, metal or ceramic matrix composite materials, and their hybrids should be considered. Smart sensors (Piezoelectric), optical fibers, high-speed imaging and other advanced experimental techniques would also constitute a suitable research auxiliary. Besides one-dimensional structural components, other slender and thin-walled structural components, such as plates and cylindrical geometries (to simulate submarine

hulls), subject to in-plane dynamic loads should be investigated for their stability and damage behavior. To further understand the mechanics of damage and propagation, the effects of strain rate on the strain energy release rate of composite materials should be considered as well.

References

Abrahamson GR and Goodier JN, (1966), Dynamic flexural buckling of rods within an axial plastic compression wave, J Appl Mech, vol. 33, pp. 241-247.

Abramovich H and Grunwald A, (1995), Stability of axially impacted composite plates, Compos Struct, vol.32, pp. 151-158

Abrate S, (2001), Modeling of impacts on comosite structures, J Compos Struct, vol. 51, pp. 129-138.

Ari-Gur J, Weller T, and Singer, J, (1982), Experimental and theoretical studies of columns under axial impact. Int. J. Solids and Structures, vol.18, No.7, pp. 619-641.

Ari-Gui J and Elishakoff I, (1997), Dynamic instability of a transversely isotropic column subjected to a compression pulse, Comput & Struct, vol. 62, No.5, pp.811-815

Ari-Gur J and Simonetta SR, (1997), Dynamic pulse buckling of rectangular composite plates, *Composites Part B.* vol. 28B, pp. 301-308

ASTM D3039-95a, (1999a), Standard test Method for Tensile properties of Polymer Matrix Composite Materials.

ASTM D5528-94a, (1999b), Standard test Method for Mode I interlaminar fracture toughness of unidirectional fiber-reinforced polymer matrix composites.

Azzi VD and Tsai SW, (1965), Anisotropic strength of composites, Exp Mech, vol.5, No.9, pp. 283-288.

Balamurugan V, Ganapathi M and Varadan TK, (1996), Nonlinear dynamic instability of laminated composite plates using finite element method, Comput Struct, v60, No. 1, pp. 125-130.

Bogdanovich, A and Friedrich K (1994), Initial and progressive failure analysis of laminated composite structures under dynamic loading, J Compos Struct, vol. 27, pp. 439-456.

Choi HY, Wang HS and Chang GK, (1992), Effect of laminate configuration and impactor's mass on trhe initial impact damage of graphite/epoxy composite plates due to line-loading impact. J Compos Mater; vol. 26, pp. 805-827.

Chai H, Babcock CD, and Knauss WB, (1981), One-dimensional modeling of failure in laminated plates by delamination buckling, Int J Solids Struct,; vol. 17, pp. 1069-1083.

Christoforou AP and Yigit AS, (1994), Normalized impact response and damage in a thin thin composite laminate supported by a rigid substrate. J Compos Mater, vol. 28, pp. 1553-1573.

Cochelin B and Potier-Ferry M, (1992), A numerical model for buckling and growth of delamination in composite laminates, Comp Meth App Mech Engng, vol. 89, pp. 361-380.

Davidson BD, (1991), Delamination Buckling: Theory and Experiment, J Compos Mater, vol. 25, pp. 1351-1378.

Daniel IM and Ishai O, (1994), *Engineering Mechanics of Composite Materials*, Oxford University Press.

Ekstrom RE, (1973), Dynamic buckling of a rectangular orthotropic plate, AIAA J, vol. 11, No.12, pp. 1655-1659.

Franz T, (2000), Photoelastic study of the mechanic behavior of orthotropic composite plates subject to impact, J Compos Struct, vol. 54, pp. 169-178.

Gaudenzi P, Perugini P and Riccio A, (2001), Post-buckling behavior of composite panels in the presence of unstable delamination, Compos Struct, vol. 51, pp. 301-309.

Gu H. Chattopaddhyay A, (1999), An experimental investigation of delamination buckling and postbuckling of composite laminates, Compos Sci Tech, vol. 59, pp. 903-910.

Hayashi T, and Sano Y, (1972a), Dynamic buckling of elastic bars, 1st Report, The case of low velocity impact, Bulletin of the JSME, vol. 15, No.88, pp. 1167-1175.

Hayashi T, Sano Y, (1972b), Dynamic buckling of elastic bars, 2nd Report, The case of high velocity impact, Bulletin of the JSME, vol. 15, No.88, pp. 1176-1184.

Hill R, (1948), A theory of the yielding and plastic flow of anisotropic metals, Proceedings of the Royal Society A, Vol. 193.

Housner GW and Tso WK, (1962), Dynamic behavior of supercritically loaded struts, J Engrg Mech Div, ASCE, vol. 88, EM5, pp. 41-65.

Hsiao HM and Daniel IM, (1998), Strain rate behavior of composite materials. J Compos B, vol. 29, pp. 521-533.

Hwang Shun-Fa, Liu Guu-Huann, (2001), Buckling behavior of composite laminates with multiple delaminations under uniaxial compression, *Composite Structures*, vol. 53, pp. 235-243.

Johnson WS, (1985), Delamination and debonding of materials, ASTM STP 876.

Karagiozova D. and Jones N, (1996), Dynamic elastic-plastic buckling phenomena in a rod due to Axial impact, Int J of Imp Engrg, vol.18, No.7-8, pp. 919-947.

Kardomateas GA, (1990), Postbuckling characteristics in delaminated kevlar/epoxy laminates, An experimental study, J Compos Tech Res, vol. 12 No. 2, pp. 85-90.

Kenny SP, (2000), Dynamic elastic buckling of slender beams with geometric imperfection subject to an axial impulse, Doctoral thesis, Dalhousie University

Kenny S, Pegg N and Taheri F, (2000), Dynamic elastic buckling of a slender beam with geometric imperfection subject to an axial impulse, Finite Elements in Analysis and Design vol. 35, pp. 227-246.

Kenny S, Taheri F, and Pegg N, (2002a) Experimental Investigations on the Dynamic Plastic Buckling of a Slender Beam Subject to Axial Impact, Int J of Imp Engrg, vol. 27, No. 1, pp. 1-17.

Kenny S, Taheri F, and Pegg N, (2002b) Finite element investigations on the dynamic plastic buckling of a slender beam subject to axial impact, Int J of Imp Engrg, vol. 27, No. 2, pp. 179-195.

Koning C and Taub J, (1934), Impact buckling of thin bars in the elastic range hinged at both ends, Technical MemorandumsNumber 748, National Advisory Committee For Aeronautics, Washington, D.C., p32.

Kruger R, Rinderknecht S, Hansel C and Konig M, (1996), Computational structural analysis and tesing: an approach to understabd delamination growth, Key engiieering Materials, vol. 121-122, pp. 181-202.

Kusaka T, Horikawa N, Masuda M, and Adachi S, (2001), Estimation method for mixed mode(I+II) interlaminar fracture toughness of composite laminatyes under low-velocity impact loading, J Soc Mat Sci, Japan, vol. 50, pp. 235-241.

Kyoung WM, Kim CG , (1995), Delamination buckling and growth of composite laminated plates with transverse shear deformation, J Compos Mater, vol. 29. pp. 2047-2068.

Kyoung WM, Kim CG, (1995), Delamination buckling and growth of composite laminated plates with transverse shear deformation, J Compos Mater, vol. 29, No. 15, pp. 2047-2068.

Lemmens J.W., Inc., (2001), Operating instructions for the Grindo*Sonic* MK5 "Industrial" instrument, http://www.grindosonic.com.

Li FC, Hu N, Yin YJ, Sekine H, and Fukunaga H, (2002), Low-velocity impact-induced damage of continuous fiber-reinforced composite laminates, Part I. An FEM numerical model, Composites Part A, vol. 33, pp. 1055-1062.

Li FC, Hu N, Yin YJ, Sekine H, and Fukunaga H, (2002), Low-velocity impact-induced damage of continuous fiber-reinforced composite laminates, Part II. Verification and numerical investigation, Composites Part A, vol. 33, pp. 1063-1072.

Lindberg HE and Florence AL, (1987), *Dynamic Pulse Buckling Theory and Experiment,* Dordrecht: Martinus Nijhoff Publishers.

Liaw DG and Yang TY, (1990), Symmetric and asymmetric dynamic buckling of laminated thin shells with the effect of imperfection and damping, J Compos Mater, vol. 24, pp. 188-207.

LSTC, (1999), Keyword User's Manual, LS-DYNA Version 950, Livermore Software Technology Corporation (http://www.lstc.com).

Luo RK, Green ER, Morrison CJ, (2001), An approarch to evaluate the impact damage initiation and propagation in composite plates, Composites Part B, vol. 32, pp. 513-520.

Necib B and Mili F, (2001), Impact behavior of cross-ply laminated composite plates under low velicities. J Compos Struct, vol. 51, pp. 237-244.

Nilsson KF, Asp LE, Alpman JE, Nystedt L, (2001), Delamination buckling and growth for delaminations at different depths in a slender composite panel, Int J Solids and Structures, vol. 38, pp. 3039-3071.

Olsson R, (2001), Analytical prediction of large mass impact damage in composite laminates, J Compos A, vol. 32, pp. 1207-1215.

Park O and Sankar B, (2002), Crack-tip force method for computing energy release rate in delaminated plates, Compos Struct, vol. 55, pp. 429-434.

Park SW and Zhou M, (2000), Time-resolved impact response and damage of fiber-reinirced composite laminates. J Compos Mater, vol. 34, pp. 879-904.

Pavier MJ and Clarke MP, (1995), Experimental techniques for the investigation of the effects of impact damage on carbon-fiber composites, Compos Sci Tech, vol. 55, pp. 157-169.

Reddy JN, (1984), A simple higher-order theory for laminated composite plates, J App. Mech, vol. 51, pp. 745-752

Ricco A, Scarmuzzino F, Perugini, P, (2001), Embedded delamination growth in composite panels under compressive load, Composite Part B: Engineering, vol. 32. pp. 209-218.

Richmond Aircraft Product Inc., (2000), Product Line(http://www.richmondaircraft.com).

Robinson P, and Besant T, (1998), Delamination fracture mechanics for composite materials, S555/005.

Rybicki EF, and Kanninen MF, (1977), A finite element calculation of stress intensity factors by a modified crack closure integral, Engineering Fracture Mechanics, vol. 9, pp. 931-938.

Sankar BV and Hu SF, (1991), Dynamics delamination propagation in composite beams, J Compos Mater; vol. 25, pp. 1414-1426.

Shen F, Lee KH, and Tay TE, (2001), Modeling delamination growth in laminated composites, Compos Sci Tech, vol. 61, pp. 1239-1251.

Sheinman I and Kardomateas G, (1997), Energy release rate and stress intensity factors for delaimated composite laminates, Int J Solids Structures, vol. 34, No.4, pp. 451-459.

Sohn MS, Hu XZ, Kim JK and Wlker L, (2000), Impact damage characterization of carbon fiber/epoxy exompoasite with multi-layer reinfotrcement. J Compos B, vol. 31, pp. 681-691.

Sugiura K and Mizuno E, and Fukumoto Y, (1985), Dynamic instability analysis of axially impacted columns, J Engrg Mech, vol. 111, No. 7, pp. 893-908.

Sun XN, Tong L, and Chen HR, (2001), Progressive failure analysis of laminated plates with delamination, J Reinforces plastics and composites, vol. 20, pp. 1370-1389.

Suo Z, Hutchinson JW, (1990), Interface crack between two elastic layers, *Int. Journal of Fracture* vol. 43, pp. 1-18.

Tsai JL, Guo C, Sun CT, (2001), Dynamic delamination fracture toughness in unidirectional polymeric composites, Composites Science and technology, vol. 61, pp. 87-94.

Wagner W, Gruttmann F, and Sprenger W, (2001), A finite element formulation for the simulation of propagating delaminations in layered composite structures, Int J Numer Meth Engng, vol. 51, pp. 1337-1359.

Wang D, Chen TY, Xin GN, (1998), Dynamic buckling of laminated composite bars subjected to axial impact, China Ocean Engrg, vol:12, No. 2, pp. 127-134.

Whitcomb JD, (1981), Finite element analysis of instability related delamination growth, J Compos Mater, vol. 15, pp. 403-426.

Whitcomb JD, (1986), Parametric analytical study of instability-related delamination growth, Compos Sci Tech, vol. 25, pp. 19-48.

Williams JG, (1988), On calculation of energy release rates for cracked laminates, *Int. J. of Fracture*, vol. 36, pp. 101-119.

Yin WL, (1993), Energy balance and the speed of crack growth in a compressed plate with delamination, Int J Solids and Structures, vol. 30, pp. 2041-2055.

Zhang Z, Taheri F, (2002a), A Numerical Investigation on Dynamic Pulse Buckling of Slender FRP Composite Laminated Beams Subject to an Axial Impulse, Developments in Theoretical and Applied Mechanics, Vol. XXI, 40th Anniversary Conference, pp:237-246, 2002.

Zhang Z, Taheri F, (2002b), Dynamic Pulse Buckling Analysis of FRP Composite Laminated Beams Using LS-DYNA, in the Proceedings of the 7th International LS-DYNA Users Conference, 2002

Zhang Z, Taheri F, (2002c), Numerical Studies on Dynamic Pulse Buckling of FRP Composite Laminated Beams Subject to an Axial Impact, Compos Struct, vol. 56, pp. 269-277.

Zhang Z, Taheri F, (2003), Dynamic Pulse Buckling of laminated Composite Beam Using Higher Order Theory, Composites B, vol. 34, pp. 391-398.

Zhou G, (1995), Damage mechanisms in composite laminates impacted by a flat-ended impactor. Composite Science and Technology, vol. 54, pp. 267-273.

Zou Z, Reid SR, Soden PD, and Li S, (2001), Mode separation of energy release rate for delamination in composite laminates using sublaminates, Int J Solids Structures, vol. 38, pp. 2597-2613.

Appendix A: Constants of Finite Difference Solutions

Constants Definitions

$$A_1 = \frac{\partial \overline{u}}{\partial \overline{x}} = \frac{\overline{u}_{j+1,k} - \overline{u}_{j-1,k}}{2\Delta \overline{x}} \tag{A-1a}$$

$$A_2 = \frac{\partial^2 \overline{u}}{\partial \overline{x}^2} = \frac{\overline{u}_{j+1,k} - 2\overline{u}_{j,k} + \overline{u}_{j-1,k}}{\Delta \overline{x}^2} \tag{A-1b}$$

$$A_3 = -2\overline{u}_{j,k} + \overline{u}_{j,k-1} \tag{A-1c}$$

$$B_1 = \frac{\partial \overline{w}}{\partial \overline{x}} = \frac{\overline{w}_{j+1,k} - \overline{w}_{j-1,k}}{2\Delta \overline{x}} \tag{A-2a}$$

$$B_2 = \frac{\partial \overline{w}_0}{\partial \overline{x}} = \frac{\overline{w}_{j+1,0} - \overline{w}_{j-1,0}}{2\Delta \overline{x}} \tag{A-2c}$$

$$B_4 = \frac{\partial^2 \overline{w}_0}{\partial \overline{x}^2} = \frac{\overline{w}_{j+1,0} - 2\overline{w}_{j,0} + \overline{w}_{j-1,0}}{\Delta \overline{x}^2} \tag{A-2d}$$

$$B_5 = -2\overline{w}_{j,k} + \overline{w}_{j,k-1} \tag{A-2e}$$

$$B_6 = \frac{\partial^3 \overline{w}}{\partial \overline{x}^3} = \frac{\overline{w}_{j+2,k} - 2\overline{w}_{j+1,k} + 2\overline{w}_{j-1,k} - \overline{w}_{j-2,k}}{2(\Delta \overline{x}^3)} \tag{A-2f}$$

$$B_7 = \frac{\partial^3 \overline{w}_0}{\partial \overline{x}^3} = \frac{\overline{w}_{j+2,0} - 2\overline{w}_{j+1,0} + 2\overline{w}_{j-1,0} - \overline{w}_{j-2,0}}{2(\Delta \overline{x}^3)} \tag{A-2g}$$

$$C_1 = \frac{\partial \overline{\theta}}{\partial \overline{x}} = \frac{\overline{\theta}_{j+1,k} - \overline{\theta}_{j-1,k}}{2\Delta \overline{x}} \tag{A-3a}$$

$$C_2 = \frac{\partial^2 \overline{\theta}}{\partial \overline{x}^2} = \frac{\overline{\theta}_{j+1,k} - 2\overline{\theta}_{j,k} + \overline{\theta}_{j-1,k}}{\Delta \overline{x}^2} \tag{A-3b}$$

$$C_3 = -\vartheta + \frac{\partial \overline{w}_0}{\partial \overline{x}} = -\theta_{j,k} + B_2 \tag{A-3c}$$

$$C_4 = -\frac{\partial \theta}{\partial x} + \frac{\partial^2 \overline{w}_0}{\partial \overline{x}^2} = -C_1 + B_4 \tag{A-3d}$$

$$C_5 = \vartheta + \frac{\partial \overline{w}}{\partial \overline{x}} - \frac{\partial \overline{w}_0}{\partial \overline{x}} = \theta_{j,k} + B_1 - B_2 \tag{A-3d}$$

$$C_6 = -2\overline{\theta}_{j,k} + \overline{\theta}_{j,k-1} \tag{A-3e}$$

$$C_7 = \overline{\theta}_{j,k} \tag{A-3f}$$

$$D_1 = \frac{B(1,1)}{A(1,1)L} \tag{A-4a}$$

$$D_2 = \frac{F(2,2)}{A(1,1)} \tag{A-4b}$$

$$D_3 = B(1,1)L \tag{A-4d}$$

$$D_4 = D(1,1) \tag{A-4e}$$

$$D_5 = F(2,2)L^2 \tag{A-4f}$$

$$D_6 = \frac{I_1}{A(1,1)I_2} \tag{A-4g}$$

$$D_7 = \frac{4E(1,1)}{3A(1,1)L(\Delta\tau)^2} \tag{A-4h}$$

$$D_8 = \frac{4G(1,1)L^2}{\Delta\tau} \tag{A-4i}$$

$$D_9 = (F(2,2) - \frac{4G(1,1)}{(\Delta\tau)^2}) / A(1,1) \tag{A-4j}$$

$$D_{10} = \frac{4H(1,1)}{3L(\Delta\tau)^2} \tag{A-4k}$$

$$D_{11} = L^2(F(2,2) - \frac{4G(1,1)}{(\Delta\tau)^2}) \tag{A-4l}$$

$$E_1 = A_2 + B_1B_3 - B_2B_4 + D_1C_2 \tag{A-5a}$$

$$E_2 = (A_2 + B_1B_3 - B_2B_4 + D_1C_2)C_3 + (A_1 + 0.5B_1B_1 - 0.5B_2B_2 + D_1C_1)C_4 + D_2(C_1 + B_3 - B_4) \tag{A-5b}$$

$$E_3 = (A_2 + B_1B_3 - B_2B_4)D_3 + D_4C_2 - D_5C_5)D_6 \tag{A-5c}$$

$$E_4 = (A_2 + B_1B_3 - B_2B_4 + D_1C_2) - D_7(C_2 + B_6 - B_7) \quad \text{(A-5d)}$$

$$E_5 = [(A_2 + B_1B_3 - B_2B_4) + D_1(C_2 + B_6 - B_7) - D_7C_2]C_7 + D_7(C_1 + B_3 - B_4)C_4 - D_9(C_1 + B_3 - B_4)]C_7 \quad \text{(A-5e)}$$

$$E_6 = [(A_2 + B_1B_3 - B_2B_4)D_3 + D_4C_2 - D_{10}(C_2 + B_6 + B_7) - D_{11}C_5]D_6 \quad \text{(A-5f)}$$

Appendix B: Procedures of Making Laminates with Pre-pregs

1. **Preparation**
   a. Determine the dimensions of the laminate and lay-up sequence, including layers and ply-angle.
   b. Cut the following materials to size:
      - Bagging film - one sheet, larger than the double size of the laminate, used for folding and seal,
      - Release film - two sheets, larger than the size of the laminate,
      - Bleeder and breather- two sheets, larger than the size of the laminate,
      - Peel ply – one sheet, larger than the size of the laminate,
      - Pre-preg
   c. Place the pre-preg in freezer.
2. **Sequence of bagging operation**
   a. Lay-up sequence
      1) Bagging film
      2) Tool (plate)
      3) Peel ply
      4) Release film (perforated)
      5) Pre-preg
      6) Thermal couples on the surface of laminate
      7) Release film (perforated)
      8) Bleeder and Breather (one sheet)
      9) Peel ply
      10) Bleeder and Breather (one sheet)
      11) Tool (plate)
      12) Put the connector on the plate
      13) Bagging film
      14) Use sealant tape to seal the bagging films
   b. Vacuum the bag
      1) Vacuum test the bag to make sure the seal works well
      2) Put the bag into the oven
      3) Connect the hose with the connector in the bag
      4) Vacuum
   c. Cure cycle
      1) Heat up the oven according to the cure cycle of the prepreg, using thermocouple to monitor the temperature variation.
      2) For Carbon R6376, cure for 2 hours at 175^0C and 700kN/m pressure with heating up rate 2^0C to 5^0C/min

Appendix C: Source Code of Dynamic Response of Slender Beam Subject to Axial Impact

```
      PROGRAM FRP_BEAM_PULSE_BUCKLING
      CALL INPUT
      CALL ABDEFH
      CALL SOLVE
      STOP
      END

      SUBROUTINE INPUT
      INCLUDE 'COMMON.INC'
      CALL OPEN_FILES
      CALL READ_DATA
      END


      SUBROUTINE OPEN_FILES
      INCLUDE 'COMMON.INC'
      CHARACTER*20 FINP,FOUT,FDIS,FVEL,FACC,FSTS,FSTR,
     &                    FCMP,TEMP_STRING
      CHARACTER*20 FFU1,FFW1,FFC1,FFU2,FFW2,FFC2
      CHARACTER*20 FHU1,FHW1,FHC1,FHU2,FHW2,FHC2
      CHARACTER*20 FFC,FHC
      CHARACTER  TEMP_CH
      INTEGER LEN_STRING
      I_FLAG=0
      DO WHILE(I_FLAG.EQ.0)
      CALL GETARG(1,FINP)
      LEN_STRING=LEN_TRIM(FINP)
      TEMP_CH=FINP((LEN_STRING-3):(LEN_STRING-3))
      IF((LEN_STRING.LE.4) .OR. (TEMP_CH. NE.'.')) THEN
            WRITE(*,*) 'Your file name is bad, input again,'
            WRITE(*,*) 'Remember: The style is: abcd.xyz'
      ELSE
        I_FLAG=1
      ENDIF
      END DO
      FDIS='.DIS'
      FVEL='.VEL'
      FACC='.ACC'
      FSTS='.STS'
      FSTR='.STR'
```

```
FCMP='.CMP'
FOUT='.OUT'
FFU1='.FU1'
FFW1='.FW1'
FFC1='.FC1'
FFU2='.FU2'
FFW2='.FW2'
FFC2='.FC2'
FHU1='.HU1'
FHW1='.HW1'
FHC1='.HC1'
FHU2='.HU2'
FHW2='.HW2'
FHC2='.HC2'
FFC ='.FFC'
FHC ='.FHC'
FDIS=FINP(1:(LEN_STRING-4))//FDIS
FVEL=FINP(1:(LEN_STRING-4))//FVEL
FACC=FINP(1:(LEN_STRING-4))//FACC
FSTS=FINP(1:(LEN_STRING-4))//FSTS
FSTR=FINP(1:(LEN_STRING-4))//FSTR
FCMP=FINP(1:(LEN_STRING-4))//FCMP
FOUT=FINP(1:(LEN_STRING-4))//FOUT
FFU1=FINP(1:(LEN_STRING-4))//FFU1
FFW1=FINP(1:(LEN_STRING-4))//FFW1
FFC1=FINP(1:(LEN_STRING-4))//FFC1
FFU2=FINP(1:(LEN_STRING-4))//FFU2
FFW2=FINP(1:(LEN_STRING-4))//FFW2
FFC2=FINP(1:(LEN_STRING-4))//FFC2
FHU1=FINP(1:(LEN_STRING-4))//FHU1
FHW1=FINP(1:(LEN_STRING-4))//FHW1
FHC1=FINP(1:(LEN_STRING-4))//FHC1
FHU2=FINP(1:(LEN_STRING-4))//FHU2
FHW2=FINP(1:(LEN_STRING-4))//FHW2
FHC2=FINP(1:(LEN_STRING-4))//FHC2
FFC =FINP(1:(LEN_STRING-4))//FFC
FHC =FINP(1:(LEN_STRING-4))//FHC
IFINP=1
IFDIS=2
IFVEL=3
IFACC=4
IFSTS=5
IFSTR=6
IFCMP=7
```

```
      IFOUT=8
      IFFU1=9
      IFFW1=10
      IFFC1=11
      IFFU2=12
      IFFW2=13
      IFFC2=14
      IFHU1=15
      IFHW1=16
      IFHC1=17
      IFHU2=18
      IFHW2=19
      IFHC2=20
      IFFC =21
      IFHC =22
      IPOS=23
      OPEN(IFINP,FILE=FINP,STATUS='OLD')
      OPEN(IFDIS,FILE=FDIS,STATUS='UNKNOWN')
      OPEN(IFVEL,FILE=FVEL,STATUS='UNKNOWN')
      OPEN(IFACC,FILE=FACC,STATUS='UNKNOWN')
      OPEN(IFSTS,FILE=FSTS,STATUS='UNKNOWN')
      OPEN(IFSTR,FILE=FSTR,STATUS='UNKNOWN')
      OPEN(IFCMP,FILE=FCMP,STATUS='UNKNOWN')
      OPEN(IFOUT,FILE=FOUT,STATUS='UNKNOWN')
      OPEN(IFFU1,FILE=FFU1,STATUS='UNKNOWN')
      OPEN(IFFW1,FILE=FFW1,STATUS='UNKNOWN')
      OPEN(IFFC1,FILE=FFC1,STATUS='UNKNOWN')
      OPEN(IFFU2,FILE=FFU2,STATUS='UNKNOWN')
      OPEN(IFFW2,FILE=FFW2,STATUS='UNKNOWN')
      OPEN(IFFC2,FILE=FFC2,STATUS='UNKNOWN')
      OPEN(IFHU1,FILE=FHU1,STATUS='UNKNOWN')
      OPEN(IFHW1,FILE=FHW1,STATUS='UNKNOWN')
      OPEN(IFHC1,FILE=FHC1,STATUS='UNKNOWN')
      OPEN(IFHU2,FILE=FHU2,STATUS='UNKNOWN')
      OPEN(IFHW2,FILE=FHW2,STATUS='UNKNOWN')
      OPEN(IFHC2,FILE=FHC2,STATUS='UNKNOWN')
      OPEN(IFFC,FILE=FFC,STATUS='UNKNOWN')
      OPEN(IFHC,FILE=FHC,STATUS='UNKNOWN')
      OPEN(IPOS,FILE='POSPLY.DAT',STATUS='UNKNOWN',
     &  ACTION='WRITE', POSITION='APPEND')
      END

      SUBROUTINE READ_DATA
      INCLUDE 'COMMON.INC'
```

```
      CHARACTER SYM_FLAG
      INTEGER I,J,N_DEG,HALF_LAYERS,N_DEG_0,N_MAT
      REAL(8) DEG,TEM_MAT(10,20)
      READ(IFINP,*) A_LEN,B_WID,LAYERS,H_THK
      WRITE(IFOUT,*)'      BEAM LENGTH = ', A_LEN
      WRITE(IFOUT,*)'      BEAM  WIDTH = ', B_WID
      WRITE(IFOUT,*)'     TOTAL LAYERS = ', LAYERS
      WRITE(IFOUT,*)'THICKNESS OF BEAM  = ', H_THK
      READ(IFINP,*) N_STACK
      N_DEG_0=0
      DO 10 I=1,N_STACK
      READ(IFINP,*) DEG, N_DEG, N_MAT
      WRITE(IFOUT,*) ' DEG = ', DEG,' N_DEG=',N_DEG,' N_MAT=',N_MAT
      DO 5 J=1,N_DEG
      L_ANG(J+N_DEG_0)=DEG
5     L_MAT(J+N_DEG_0)=N_MAT
      N_DEG_0=N_DEG_0+N_DEG
10    CONTINUE
      READ(IFINP,*) SYM_FLAG
      IF (SYM_FLAG=='S') THEN
        IF ( MOD(LAYERS,2) .EQ. 1) THEN
                  WRITE(*,*) ' Your model is symmetric, but your layers
     &                        is not even, check your input file!'
        STOP
      ENDIF
      HALF_LAYERS=LAYERS/2
      DO 20 I=1,HALF_LAYERS
      L_MAT(HALF_LAYERS+I)=L_MAT(HALF_LAYERS+1-I)
20    L_ANG(HALF_LAYERS+I)=L_ANG(HALF_LAYERS+1-I)
      END IF
      READ(IFINP,*) I_MAT
      DO 25 I=1,I_MAT
      READ(IFINP,*) TEM_MAT(I,1),TEM_MAT(I,2),TEM_MAT(I,3),
     &              TEM_MAT(I,4)
      READ(IFINP,*) TEM_MAT(I,5),TEM_MAT(I,6),TEM_MAT(I,7)
      READ(IFINP,*) TEM_MAT(I,8),TEM_MAT(I,9),TEM_MAT(I,10)
25    READ(IFINP,*) TEM_MAT(I,11),TEM_MAT(I,12),TEM_MAT(I,13)
      DO 30 I=1,LAYERS
      HZ(I)=(I-1)*H_THK/LAYERS-0.5*H_THK
      DO J=1,13
      MAT(I,J)=TEM_MAT(L_MAT(I),J)
      ENDDO
      WRITE(IFOUT,9)I,L_ANG(I),HZ(I),(MAT(I,J),J=1,13)
9     FORMAT(I3,' ', 1F5.2,' ', 14ES11.3)
```

```
30      CONTINUE
        L_ANG(0)=0
        DO J=1,7
        MAT(0,J)=0.0
        ENDDO
        HZ(LAYERS+1)=H_THK*0.5
        WRITE(IFOUT,*)    'HZ(LAYERS+1)= ',HZ(LAYERS+1)
        WRITE(IFOUT,*)' THICKNESS OF THE PLATE = ', H_THK
        READ(IFINP,*) BND_TYPE
        READ (IFINP,*) IMP_TYPE
        SELECT CASE (IMP_TYPE)
        CASE (1)
          READ(IFINP,*) MASS,VEL_0
          WRITE(IFOUT,*) 'The impacter mass is:', MASS
          WRITE(IFOUT,*) 'The impacter velcity is:', VEL_0
        CASE (2)
          READ(IFINP, *) IFORCE
          IF(IFORCE.EQ.1) THEN
            READ(IFINP,*) F_MAG, F_DUR
                    WRITE(IFOUT,*) 'The constant force magnitude is:', F_MAG
                    WRITE(IFOUT,*) 'The force time duration is:', F_DUR
          ELSEIF(IFORCE.EQ.2) THEN
                READ(IFINP,*) MASS,VEL_0
              ENDIF
        CASE (3)
          READ(IFINP,*) N_VSTEPS
              WRITE(IFOUT,*) 'Total time steps:', N_VSTEPS
          DO I=1,N_VSTEPS
              READ(IFINP,*) VEL(I), V_TIME(I)
              WRITE(IFOUT,50) VEL(I), V_TIME(I)
50      FORMAT(2X,F12.4,3X,F10.6)
          ENDDO
        END SELECT
        READ(IFINP,*) NX_STEP,NT_STEP,T_END
        WRITE(IFOUT,*) 'Total steps in    X direction : ', NX_STEP
        WRITE(IFOUT,*) 'Total steps in Time direction : ', NT_STEP
        WRITE(IFOUT,*) 'Time duration is from 0 sec to ', T_END, 'sec'
        WRITE(IFOUT,*) 'Initial Gemetric Imperfection'

        DO I=0,NX_STEP
        READ(IFINP,*) W_INI(I)
        WRITE(IFOUT,*) W_INI(I)
        END DO
        READ(IFINP,*) NX_OUT_STEP,NT_OUT_STEP,BETA
```

```
      WRITE(IFOUT,*) 'The analysis results are output by '
      WRITE(IFOUT,*) 'every ', NX_OUT_STEP,'s in X-tirection'
      WRITE(IFOUT,*) 'every ', NT_OUT_STEP,'s in T-tirection'
      WRITE(IFOUT,*) ' Analysis Type for hiogher order shear deformation'
      WRITE(IFOUT,*) ' Beta = ', BETA
      READ(IFINP,*) N_STR
      DO I=0,N_STR
      READ(IFINP,*) X_STR(I)
      ENDDO
     WRITE(IFOUT,*) ' You have total ', N_STR,
&          '+1 postions to output strains'
     DO I=0,N_STR
      WRITE(IFOUT,*) X_STR(I)
      ENDDO
      READ(IFINP,*) CIL,CIT,CIR
      WRITE(IFOUT,*)  'Damping Factors are:', CIL,CIT,CIR
     END

      SUBROUTINE ABDEFH
      INCLUDE 'COMMON.INC'
      CALL A_MATRIX
      CALL B_MATRIX
      CALL D_MATRIX
      CALL E_MATRIX
      CALL F_MATRIX
      CALL G_MATRIX
      CALL H_MATRIX
      CALL DI1_MATRIX
      CALL DI2_MATRIX
      CALL DAMPINGS
      END

      SUBROUTINE Q_MATRIX(Q,I)
      INCLUDE 'COMMON.INC'
      REAL(8) M,N,M4,N4,M2N2,M3N,MN3,Q(3,3)
      REAL(8) QXX,QYY,QXY,QXS,QYS,QSS
      REAL(8) POYX
      INTEGER I
      POYX=MAT(I,4)*MAT(I,2)/MAT(I,1)
      Q(1,1)=MAT(I,1)/(1-MAT(I,4)*POYX)
      Q(2,2)=MAT(I,2)/(1-MAT(I,4)*POYX)
      Q(1,2)=POYX*Q(1,1)
      Q(2,1)=Q(1,2)
      Q(3,3)=MAT(I,3)
```

```
Q(1,3)=0
Q(2,3)=0
Q(3,1)=0
Q(3,2)=0
M=COSD(L_ANG(I))
N=SIND(L_ANG(I))
M4=M*M*M*M
N4=N*N*N*N
M2N2=M*M*N*N
M3N=M*M*M*N
MN3=M*N*N*N
M2=M*M
N2=N*N
QXX=M4*Q(1,1)+N4*Q(2,2)+2*M2N2*Q(1,2)+4*M2N2*Q(3,3)
QYY=N4*Q(1,1)+M4*Q(2,2)+2*M2N2*Q(1,2)+4*M2N2*Q(3,3)
QXY=M2N2*Q(1,1)+M2N2*Q(2,2)+(M4+N4)*Q(1,2)-4*M2N2*Q(3,3)
QXS=M3N*Q(1,1)-MN3*Q(2,2)+(MN3-M3N)*Q(1,2)+2*(MN3-M3N)*Q(3,3)
QYS=MN3*Q(1,1)-M3N*Q(2,2)+(M3N-MN3)*Q(1,2)+2*(M3N-MN3)*Q(3,3)
QSS=M2N2*Q(1,1)+M2N2*Q(2,2)-2*M2N2*Q(1,2)+(M2-N2)**2*Q(3,3)
Q(1,1)=QXX
Q(1,2)=QXY
Q(1,3)=QXS
Q(2,1)=QXY
Q(2,2)=QYY
Q(2,3)=QYS
Q(3,1)=Q(1,3)
Q(3,2)=Q(2,3)
Q(3,3)=QSS
END

SUBROUTINE QQ_MATRIX(QQ,I)
INCLUDE 'COMMON.INC'
REAL(8) QQ(2,2)
INTEGER I
QQ(1,1)=MAT(I,5)
QQ(2,2)=MAT(I,6)
QQ(1,2)=0.0
QQ(2,1)=0.0
END

SUBROUTINE A_MATRIX
INCLUDE 'COMMON.INC'
REAL(8) Q(3,3),TEMP
INTEGER I,J,K
```

```
      DO 10 I=1,3
      DO 10 J=1,3
10    A(I,J)=0.0
      DO 20 K=1,LAYERS
      TEMP=HZ(K+1)-HZ(K)
      CALL Q_MATRIX(Q,K)
       DO 20 I=1,3
      DO 20 J=1,3
      A(I,J)=A(I,J)+Q(I,J)*TEMP
20    CONTINUE
      END

      SUBROUTINE B_MATRIX
      INCLUDE 'COMMON.INC'
      REAL(8) Q(3,3),TEMP
      INTEGER I,J,K
      DO 10 I=1,3
      DO 10 J=1,3
10    B(I,J)=0.0
      DO 20 K=1,LAYERS
      CALL Q_MATRIX(Q,K)
      TEMP=(HZ(K+1)**2-HZ(K)**2)*0.5
      DO 20 I=1,3
      DO 20 J=1,3
20    B(I,J)=B(I,J)+Q(I,J)*TEMP
      END

      SUBROUTINE D_MATRIX
      INCLUDE 'COMMON.INC'

      REAL(8) Q(3,3),TEMP
      INTEGER I,J,K
      DO 10 I=1,3
      DO 10 J=1,3
10    D(I,J)=0.0
      DO 20 K=1,LAYERS
      CALL Q_MATRIX(Q,K)
      TEMP=(HZ(K+1)**3-HZ(K)**3)/3.0
      DO 20 I=1,3
      DO 20 J=1,3
20    D(I,J)=D(I,J)+Q(I,J)*TEMP
      END

      SUBROUTINE E_MATRIX
```

```
      INCLUDE 'COMMON.INC'
      REAL(8) Q(3,3),TEMP
      INTEGER I,J,K
      DO 10 I=1,3
      DO 10 J=1,3
10          E(I,J)=0.0
      DO 20 K=1,LAYERS
      CALL Q_MATRIX(Q,K)
      TEMP=(HZ(K+1)**4-HZ(K)**4)/4.0
      DO 20 I=1,3
      DO 20 J=1,3
20    E(I,J)=E(I,J)+Q(I,J)*TEMP
      END

      SUBROUTINE F_MATRIX
      INCLUDE 'COMMON.INC'
      REAL(8) QQ(2,2),TEMP
      INTEGER I,J,K
      DO 10 I=1,2
      DO 10 J=1,2
10    F(I,J)=0.0
      DO 20 K=1,LAYERS
      CALL QQ_MATRIX(QQ,K)
      TEMP=HZ(K+1)-HZ(K)
      DO 20 I=1,2
      DO 20 J=1,2
20    F(I,J)=F(I,J)+QQ(I,J)*TEMP
      END

      SUBROUTINE G_MATRIX
      INCLUDE 'COMMON.INC'
      REAL(8) QQ(2,2),TEMP
      INTEGER I,J,K
      DO 10 I=1,2
      DO 10 J=1,2
10    G(I,J)=0.0
      DO 20 K=1,LAYERS
      CALL QQ_MATRIX(QQ,K)
      TEMP=(HZ(K+1)**3-HZ(K)**3)/3.0
      DO 20 I=1,2
      DO 20 J=1,2
20    G(I,J)=G(I,J)+QQ(I,J)*TEMP

      END
```

```
      SUBROUTINE H_MATRIX
      INCLUDE 'COMMON.INC'
      REAL(8) Q(3,3),TEMP
      INTEGER I,J,K
      DO 10 I=1,3
      DO 10 J=1,3
10    H(I,J)=0.0
      DO 20 K=1,LAYERS
      CALL Q_MATRIX(Q,K)
      TEMP=(HZ(K+1)**5-HZ(K)**5)/5.0
      DO 20 I=1,3
      DO 20 J=1,3
20    H(I,J)=H(I,J)+Q(I,J)*TEMP
      END

      SUBROUTINE DI1_MATRIX
      INCLUDE 'COMMON.INC'
      REAL(8) TEMP
      INTEGER K
      DO 20 K=1,LAYERS
      TEMP=HZ(K+1)-HZ(K)
      DI1=DI1+MAT(K,7)*TEMP
20    CONTINUE
      END

      SUBROUTINE DI2_MATRIX
      INCLUDE 'COMMON.INC'
      REAL(8) TEMP
      INTEGER K
      DO 20 K=1,LAYERS
      TEMP=(HZ(K+1)**3-HZ(K)**3)/3.0
      DI2=DI2+MAT(K,7)*TEMP
20    CONTINUE
      END

      SUBROUTINE DAMPINGS()
      INCLUDE 'COMMON.INC'
      REAL(8) OMEGA_T,OMEGA_L
      OMEGA_T=4.0*3.14159**2*SQRT(D(1,1)/(MAT(1,7)*H_THK))/A_LEN**2
      CT=2.0*CIT*OMEGA_T*DI1
      OMEGA_L=SQRT(2.0*A(1,1)/(H_THK*MAT(1,7)))/A_LEN
      CL=2.0*CIL*OMEGA_L*DI1
      CR=0.5*CT
```

```
 END

 SUBROUTINE SOLVE
 INCLUDE 'COMMON.INC'
 INTEGER status
 REAL(8), ALLOCATABLE :: UWC_OUT(:,:,:)
 REAL(8), ALLOCATABLE :: STR_OUT(:,:,:)
 REAL(8), ALLOCATABLE :: STS_OUT(:,:,:)
 REAL(8), ALLOCATABLE :: FFC_OUT(:,:,:)
 REAL(8), ALLOCATABLE :: FHC_OUT(:,:,:)
 REAL(8) XA(20,4),XB(7,4),XC(9,4),H2,Q(3,3),QQ(2,2)
 REAL(8) TEMP01,TEMP02,TEMP03,TEMP04,TEMP05,TEMP06
 REAL(8) TEMP07,TEMP08,TEMP09,TEMP_SXX_H,TEMP_SXX_F
 REAL(8) TEMP61,TEMP62,TEMP63,TEMP64,TEMP65,TEMP66
 REAL(8) TEMP11,TEMP12,TEMP13,TEMP14,TEMP15,BAL11
 REAL(8) TEMP21,TEMP22,TEMP23,TEMP24,TEMP25
 REAL(8) TEMP31,TEMP32,TEMP33,TEMP34,TEMP35,TEMP36,
&          TEMP37,TEMP38
 REAL(8) TEMP41,TEMP42,TEMP43,TEMP44,TEMP45,TEMP46,
&          TEMP47,TEMP48
 REAL(8) TEMPF
 NX=INT((NX_STEP-1)/NX_OUT_STEP)+1
 NT=INT((NT_STEP-1)/NT_OUT_STEP)+1
 ALLOCATE(UWC_OUT(0:NX,0:NT,12),STAT=status)
 IF(status /=0) THEN
        WRITE(*,*) ' Allocation mem for UWC_OUT failed !'
        STOP
 ENDIF
 NOUT=4*(LAYERS+1)
 NOUTF=2*LAYERS-1
 ALLOCATE(STR_OUT(0:NT,0:NOUT,0:N_STR),STAT=status)
 IF(status /=0) THEN
        WRITE(*,*) ' Allocation mem for STR_OUT failed !'
        STOP
 ENDIF
 ALLOCATE(STS_OUT(0:NT,0:NOUT,0:N_STR),STAT=status)
 IF(status /=0) THEN
        WRITE(*,*) ' Allocation mem for STS_OUT failed !'
        STOP
 ENDIF

 ALLOCATE(FFC_OUT(0:NT,0:NOUTF,0:N_STR),STAT=status)
 IF(status /=0) THEN
        WRITE(*,*) ' Allocation mem for FFC_OUT failed !'
```

```
        STOP
      ENDIF
      ALLOCATE(FHC_OUT(0:NT,0:NOUTF,0:N_STR),STAT=status)
      IF(status /=0) THEN
        WRITE(*,*) ' Allocation mem for FHC_OUT failed !'
        STOP
      ENDIF
      UWC=0.0
      UWCK_1=0.0
      UWCK_2=0.0
      BAL11=B(1,1)/(A(1,1)*A_LEN)
      UJK_1=0.0
      CALL NON_DIMENSION
      H2=HT**2
      ICONTACT=1
      IPF=1
      IF(MOD(LAYERS,2).EQ.0) THEN
        LAYERS_HALF=LAYERS/2
      ELSE
        LAYERS_HALF=0
      ENDIF
      CALL BND_INI
      N=NT_STEP
      M=NX_STEP
      IB=0

      DO 10 JJ=0,NX-1
      DO 10 I=1,12
      IF(MOD(I,3).EQ.2) THEN
        TEMP01=UWC(JJ*NX_OUT_STEP,I)-W_INI(JJ*NX_OUT_STEP)
        UWC_OUT(JJ,0,I)=TEMP01*A_LEN
      ELSE
        UWC_OUT(JJ,0,I)=UWC(JJ*NX_OUT_STEP,I)
      ENDIF
10    CONTINUE
      DO 15 I=1,12
15    UWC_OUT(NX,0,I)=UWC(NX_STEP,I)
      DO 20 K=1,N
      DO 18 I=1,4
18    UMK_2(I)=UWCK_1(NX_STEP,3*I-2)

      UWCK_1=UWCK_2
      UWCK_2=UWC
      DO 20 J=IB,M
```

```
      CALL X_ABC(J,K,XA,XB,XC)
      TEMP11=XB(1,1)+XC(1,1)*XA(8,1)+XC(7,1)
      TEMP12=XB(7,1)+XC(1,1)*XA(7,1)
      TEMP13=XC(2,1)*XB(5,1)-XC(8,1)
      TEMP14=XB(1,1)*XC(3,1)+XC(4,1)*XA(8,1)
      TEMP15=XC(5,1)*XB(6,1)-XC(9,1)
      TEMP21=XB(1,2)+XC(1,2)*XA(8,2)
      TEMP22=XB(7,2)+XC(1,2)*XA(7,2)
      TEMP23=XC(2,2)*XB(5,2)
      TEMP24=XB(1,2)*XC(3,2)+XC(4,2)*XA(8,2)
      TEMP25=XC(5,2)*XB(6,2)
      TEMP31=XB(1,3)+XC(1,3)*XA(8,3)
      TEMP32=BETA*XA(15,3)*XB(2,3)+XC(7,3)
      TEMP33=(XC(2,3)-BETA*XA(16,3))*XB(5,3)-XC(8,3)
      TEMP34=BETA*XA(15,3)*XB(5,3)
      TEMP35=XB(7,3)+XC(1,3)*XA(7,3)
      TEMP36=XB(1,3)*XC(3,3)+XC(4,3)*XA(8,3)
      TEMP37=BETA*XA(17,3)*XB(2,3)-XC(9,3)
      TEMP38=XC(5,3)-BETA*XC(6,3)
      TEMP41=XB(1,4)+XC(1,4)*XA(8,4)
      TEMP42=BETA*XA(15,4)*XB(2,4)
      TEMP43=(XC(2,4)-BETA*XA(16,4))*XB(5,4)
      TEMP44=BETA*XA(15,4)*XB(5,4)
      TEMP45=XB(7,4)+XC(1,4)*XA(7,4)
      TEMP46=XB(1,4)*XC(3,4)+XC(4,4)*XA(8,4)
      TEMP47=BETA*XA(17,4)*XB(2,4)
      TEMP48=XC(5,4)-BETA*XC(6,4)
      UWC(J,1)=TEMP11*H2-XA(9,1)
      UWC(J,7)=(TEMP31-TEMP32)*H2-XA(9,3)
      UWC(J,4)=TEMP21*H2*(1-0.5*XB(3,2)**2)-XA(9,2)
      UWC(J,10)=(TEMP41-TEMP42)*H2*(1-0.5*XB(3,4)**2)-XA(9,4)
      UWC(J,2)=(TEMP11*XB(3,1)+TEMP12*XB(4,1)+TEMP13)*H2-XA(10,1)
      UWC(J,8)=((TEMP31-TEMP32)*XB(3,3)+
     &    (TEMP35-TEMP34)*XB(4,3)+TEMP33)*H2-XA(10,3)
      UWC(J,5)=(TEMP21*XB(3,2)+TEMP22*XB(4,2)+TEMP23)*H2-XA(10,2)
      UWC(J,11)=((TEMP41-TEMP42)*XB(3,4)+
     &     (TEMP45-TEMP44)*XB(4,4)+TEMP43)*H2-XA(10,4)
      UWC(J,3)=(TEMP14-TEMP15)*H2/XA(18,1)-XA(11,1)
      UWC(J,6)=(TEMP24-TEMP25)*H2/XA(18,2)-XA(11,2)

      UWC(J,9)=(TEMP36-TEMP37-TEMP38*XB(6,3))*H2/XA(18,3)-XA(11,3)
      UWC(J,12)=(TEMP46-TEMP47-TEMP48*XB(6,4))*H2/XA(18,4)-XA(11,4)
      IF(J.EQ.0) THEN
      UWC(J,1)=0.0
```

```
      UWC(J,4)=0.0
      UWC(J,7)=0.0
      UWC(J,10)=0.0
      ENDIF
      IF((J.EQ.M).OR.(J.EQ.0)) THEN
      UWC(J,2)=0.0
      UWC(J,5)=0.0
      UWC(J,8)=0.0
      UWC(J,11)=0.0
      ENDIF
       IF (J.EQ.M) THEN
      DO I=1,4
      CALL LEFTENDU(I,K)
      ENDDO
      ENDIF
      IF ((MOD(K,NT_OUT_STEP).EQ.0).AND.(MOD(J,NX_OUT_STEP).EQ.0)
&                 .AND.(J.LT.M)) THEN
        JJ=INT(J/NX_OUT_STEP)
        KK=INT(K/NT_OUT_STEP)
        UWC_OUT(JJ,KK,1)=UWC(J,1)*A_LEN
        UWC_OUT(JJ,KK,2)=(UWC(J,2)-W_INI(J))*A_LEN
        UWC_OUT(JJ,KK,3)=UWC(J,3)
        UWC_OUT(JJ,KK,4)=UWC(J,4)*A_LEN
        UWC_OUT(JJ,KK,5)=(UWC(J,5)-W_INI(J))*A_LEN
        UWC_OUT(JJ,KK,6)=UWC(J,6)
        UWC_OUT(JJ,KK,7)=UWC(J,7)*A_LEN
        UWC_OUT(JJ,KK,8)=(UWC(J,8)-W_INI(J))*A_LEN
        UWC_OUT(JJ,KK,9)=UWC(J,9)
        UWC_OUT(JJ,KK,10)=UWC(J,10)*A_LEN
        UWC_OUT(JJ,KK,11)=(UWC(J,11)-W_INI(J))*A_LEN
        UWC_OUT(JJ,KK,12)=UWC(J,12)
      ENDIF
      IF ((MOD(K,NT_OUT_STEP).EQ.0).AND.(J.EQ.M)) THEN
        KK=INT(K/NT_OUT_STEP)
        UWC_OUT(NX,KK,1)=UWC(J,1)*A_LEN
        UWC_OUT(NX,KK,2)=(UWC(J,2)-W_INI(J))*A_LEN
        UWC_OUT(NX,KK,3)=UWC(J,3)
        UWC_OUT(NX,KK,4)=UWC(J,4)*A_LEN
        UWC_OUT(NX,KK,5)=(UWC(J,5)-W_INI(J))*A_LEN
        UWC_OUT(NX,KK,6)=UWC(J,6)
        UWC_OUT(NX,KK,7)=UWC(J,7)*A_LEN
        UWC_OUT(NX,KK,8)=(UWC(J,8)-W_INI(J))*A_LEN
        UWC_OUT(NX,KK,9)=UWC(J,9)
        UWC_OUT(NX,KK,10)=UWC(J,10)*A_LEN
```

```
      UWC_OUT(NX,KK,11)=(UWC(J,11)-W_INI(J))*A_LEN
      UWC_OUT(NX,KK,12)=UWC(J,12)
    ENDIF
IF (MOD(K,NT_OUT_STEP).EQ.0) THEN
      KK=INT(K/NT_OUT_STEP)
  DO I1=0,N_STR
      IX=INT(X_STR(I1)/GX)
          IF(J.EQ.IX) THEN

                STR_OUT(KK,0,I1)=K*T_END/NT_STEP
                STS_OUT(KK,0,I1)=K*T_END/NT_STEP
        FFC_OUT(KK,0,I1)=K*T_END/NT_STEP
                FHC_OUT(KK,0,I1)=K*T_END/NT_STEP
                IF(J.EQ.M) THEN
                      TEMP04=(UWC(J,1)-UWC(J-1,1))/(1.0*GX)
                      TEMP05=(UWC(J,2)-UWC(J-1,2))/(1.0*GX)
                      TEMP07=(UWC(J,3)-UWC(J-1,3))/(1.0*GX*A_LEN)
                      TEMP06=(W_INI(J)-W_INI(J-1))/(1.0*GX)
                ELSE
                      TEMP04=(UWC(J+1,1)-UWC(J-1,1))/(2.0*GX)
                      TEMP05=(UWC(J+1,2)-UWC(J-1,2))/(2.0*GX)
                      TEMP07=(UWC(J+1,3)-UWC(J-1,3))/(2.0*GX*A_LEN)
                      TEMP06=(W_INI(J+1)-W_INI(J-1))/(2.0*GX)
                ENDIF
                DO I=0,LAYERS
                TEMP08=(I*H_THK/LAYERS-0.5*H_THK)*TEMP07
                STR_OUT(KK,I+1,I1)=TEMP04+TEMP08+
&               (TEMP05+TEMP06)*(TEMP05-TEMP06)*0.5
                STR_OUT(KK,I+1,I1)=1000000*STR_OUT(KK,I+1,I1)
        STR_OUT(KK,LAYERS+2+I,I1)=UWC(J,3)+TEMP05-TEMP06
STR_OUT(KK,LAYERS+2+I,I1)=1000000*STR_OUT(KK,LAYERS+2+I,I1)

                IF(I.EQ.0) THEN
                      QQ(2,2)=0.0
                ELSE
                      CALL QQ_MATRIX(QQ,I)
                ENDIF
                TEMPF=STR_OUT(KK,LAYERS+2+I,I1)
        STS_OUT(KK,LAYERS+1+I,I1)=TEMPF*QQ(2,2)/1000
                ENDDO
        DO I=1,LAYERS
        TEMP_SXX_F=0.5*(STR_OUT(KK,I,I1)+STR_OUT(KK,I+1,I1))
        CALL Q_MATRIX(Q,I)
        STS_OUT(KK,I,I1)=TEMP_SXX_F*Q(1,1)/1000
```

```
      ENDDO
       DO I=1,LAYERS
       IF(STS_OUT(KK,I,I1).GT.0.0) THEN
       FFC_OUT(KK,I,I1)=(STS_OUT(KK,I,I1)/MAT(I,8))**2+
&      ((STS_OUT(KK,LAYERS+I,I1)+STS_OUT(KK,LAYERS+1+I,I1))
&      /(2*MAT(I,13)))**2
       ELSE
       FFC_OUT(KK,I,I1)=(STS_OUT(KK,I,I1)/MAT(I,9))**2+
&      ((STS_OUT(KK,LAYERS+I,I1)+STS_OUT(KK,LAYERS+1+I,I1))
&      /(2*MAT(I,13)))**2
      ENDIF
      ENDDO

       DO I=1,LAYERS-1
       FFC_OUT(KK,LAYERS+I,I1)=4.0*(STS_OUT(KK,LAYERS+1+I,I1)/
&      MAT(I,13))**2
       ENDDO


      IF(J.EQ.M) THEN
        TEMP04=(UWC(J,7)-UWC(J-1,7))/(1.0*GX)
        TEMP05=(UWC(J,8)-UWC(J-1,8))/(1.0*GX)
        TEMP07=(UWC(J,9)-UWC(J-1,9))/(1.0*GX*A_LEN)
        TEMP06=(W_INI(J)-W_INI(J-1))/(1.0*GX)
        TEMP61=(UWC(J,8)-2.0*UWC(J-1,8)+UWC(J-
&                       2,8))/(GX*GX*A_LEN)
        TEMP62=(W_INI(J)-2.0*W_INI(J-1)+W_INI(J-
&                       2))/(GX*GX*A_LEN)
        ELSE
        TEMP04=(UWC(J+1,7)-UWC(J-1,7))/(2.0*GX)
        TEMP05=(UWC(J+1,8)-UWC(J-1,8))/(2.0*GX)
        TEMP07=(UWC(J+1,9)-UWC(J-1,9))/(2.0*GX*A_LEN)
        TEMP06=(W_INI(J+1)-W_INI(J-1))/(2.0*GX)
        TEMP61=(UWC(J+1,8)-2.0*UWC(J,8)+UWC(J-
&             1,8))/(GX*GX*A_LEN)
        TEMP62=(W_INI(J+1)-2.0*W_INI(J)+W_INI(J-
&                       1))/(GX*GX*A_LEN)
        ENDIF
        DO I=0,LAYERS
        TEMP09=I*H_THK/LAYERS-0.5*H_THK
        TEMP08=TEMP09*TEMP07
        TEMP63=4.0*TEMP09**3*BETA/(3.0*H_THK**2)
        TEMP64=TEMP63*(TEMP07-TEMP61+TEMP62)
        TEMP65=(TEMP05+TEMP06)*(TEMP05-TEMP06)*0.5
```

```
      STR_OUT(KK,2*LAYERS+3+I,I1)=TEMP04+TEMP08-
     &                  TEMP64+TEMP65
      TEMP64=1.0-4.0*TEMP09**2*BETA/H_THK**2
      STR_OUT(KK,3*LAYERS+4+I,I1)=TEMP64*(UWC(J,9)+TEMP05-
     &                                    TEMP06)
       STR_OUT(KK,2*LAYERS+3+I,I1)=1000000
     &  *STR_OUT(KK,2*LAYERS+3+I,I1)
      STR_OUT(KK,3*LAYERS+4+I,I1)=1000000
     &  *STR_OUT(KK,3*LAYERS+4+I,I1)
      CALL QQ_MATRIX(QQ,I)
      IF(I.EQ.0) THEN
            QQ(2,2)=0.0
            ENDIF
     STS_OUT(KK,3*LAYERS+2+I,I1)=QQ(2,2)
     &  *STR_OUT(KK,3*LAYERS+4+I,I1)/1000
            ENDDO
     DO I=1,LAYERS
            TEMP_SXX_H=0.5*(STR_OUT(KK,2*LAYERS+2+I,I1)
    ,&   +STR_OUT(KK,2*LAYERS+3+I,I1))
     CALL Q_MATRIX(Q,I)
     STS_OUT(KK,2*LAYERS+1+I,I1)=TEMP_SXX_H*Q(1,1)/1000
            ENDDO
      DO I=1,LAYERS
            IF(STS_OUT(KK,2*LAYERS+1+I,I1).GT.0.0) THEN

      TEMPF1=(STS_OUT(KK,2*LAYERS+1+I,I1)/MAT(I,8))**2
      TEMPF2=STS_OUT(KK,3*LAYERS+1+I,I1)+STS_OUT(KK,3*LAYE
      RS+2+I,I1)
                  TEMPF2=(TEMPF2/(2*MAT(I,13)))**2
                  FHC_OUT(KK,I,I1)=TEMPF1+TEMPF2
            ELSE
      TEMPF1=(STS_OUT(KK,2*LAYERS+1+I,I1)/MAT(I,9))**2
      TEMPF2=STS_OUT(KK,3*LAYERS+1+I,I1)+
     &          STS_OUT(KK,3*LAYERS+2+I,I1)
      TEMPF2=(TEMPF2/(2*MAT(I,13)))**2
      FHC_OUT(KK,I,I1)=TEMPF1+TEMPF2
       ENDIF
      ENDDO

      DO I=1,LAYERS-1
            TEMPF=STS_OUT(KK,3*LAYERS+2+I,I1)/MAT(I,13)
            FHC_OUT(KK,LAYERS+I,I1)=4.0*TEMPF**2
            IF(IPF.EQ.1) THEN
            IF(FHC_OUT(KK,LAYERS+I,I1).GT.1.0) THEN
```

```
                        WRITE(IPOS,19)
                        FHC_OUT(KK,LAYERS+I,I1),X_STR(I1),I
                        IPF=0
                        ENDIF
                    ENDIF
19                  FORMAT(2F6.2,I4)
                    ENDDO
          ENDIF
              ENDDO
       ENDIF

20     CONTINUE
       DO KK=0,NT
       WRITE(IFFU1,30) (UWC_OUT(JJ,KK,1), JJ=0,NX)
       WRITE(IFFW1,30) (UWC_OUT(JJ,KK,2), JJ=0,NX)
       WRITE(IFFC1,30) (UWC_OUT(JJ,KK,3), JJ=0,NX)
       WRITE(IFFU2,30) (UWC_OUT(JJ,KK,4), JJ=0,NX)
       WRITE(IFFW2,30) (UWC_OUT(JJ,KK,5), JJ=0,NX)
       WRITE(IFFC2,30) (UWC_OUT(JJ,KK,6), JJ=0,NX)
       WRITE(IFHU1,30) (UWC_OUT(JJ,KK,7), JJ=0,NX)
       WRITE(IFHW1,30) (UWC_OUT(JJ,KK,8), JJ=0,NX)
       WRITE(IFHC1,30) (UWC_OUT(JJ,KK,9), JJ=0,NX)
       WRITE(IFHU2,30) (UWC_OUT(JJ,KK,10), JJ=0,NX)
       WRITE(IFHW2,30) (UWC_OUT(JJ,KK,11), JJ=0,NX)
       WRITE(IFHC2,30) (UWC_OUT(JJ,KK,12), JJ=0,NX)
30     FORMAT(201E12.3E3)
40     FORMAT(F10.6,70F10.1)
       ENDDO
       STR_OUT(0,0,0)=0.0
       STS_OUT(0,0,0)=0.0
       WRITE(IFSTR,*) 'MicroStrain OutPut'
       WRITE(IFSTS,*) 'Stress Output (MPa)'
       DO I1=0,N_STR
       WRITE(IFSTR,45) X_STR(I1)
       WRITE(IFSTS,45) X_STR(I1)
45     FORMAT('Station= ',F5.3)
       WRITE(IFSTR,46)
46     FORMAT(20X,'First Order Results Shear Deformation',
     &   20X,'Higher Order Shear Deformation Results')
       WRITE(IFSTR,47)
47     FORMAT(20X,'Axial Strain of each layer',
     &   20X,'Shear Strain of Each layer',
     &   20X,'Axial Strain of each layer',
     &   20X,'Shear Strain of Each layer')
```

```
      WRITE(IFSTR,48) (I+100, I=0,LAYERS),(I+200,I=0,LAYERS),
     &          (I+300, I=0,LAYERS),(I+400,I=0,LAYERS)
48    FORMAT(2X,'time', 4X, 60I10)
      WRITE(IFSTS,56)
56    FORMAT(20X,'First Order Results Shear Deformation',
     &  20X,'Higher Order Shear Deformation Results')
      WRITE(IFSTS,57)
57    FORMAT(20X,'Axial Stress of each layer',
     &  20X,'Shear Stress of Each layer',
     &  20X,'Axial Stress of each layer',
     &  20X,'Shear Stress of Each layer')
      WRITE(IFSTS,58) (I+100, I=1,LAYERS),(I+200,I=0,LAYERS),
     &          (I+300, I=1,LAYERS),(I+400,I=0,LAYERS)
58    FORMAT(2X,'time', 4X, 60I10)
      DO KK=0,NT
      WRITE(IFSTR,60) (STR_OUT(KK,I,I1),I=0,NOUT)
      WRITE(IFSTS,60) (STS_OUT(KK,I,I1),I=0,NOUT-2)
      WRITE(IFFC,70) (FFC_OUT(KK,I,I1),I=0,NOUTF)
      WRITE(IFHC,70) (FHC_OUT(KK,I,I1),I=0,NOUTF)
60    FORMAT(E10.4E1,80E12.3E3)
70    FORMAT(F6.3,' ',80F6.2)
      NDDO
      ENDDO
      DO I=1,23
      CLOSE(I)
      ENDDO
      END

      SUBROUTINE X_ABC(J,K,XA,XB,XC)
      INCLUDE 'COMMON.INC'
      REAL(8) UJ(-1:1),CJ(-1:1),WJ(-2:2),W0(-2:2),UK_1,WK_1,CK_1
            REAL(8)
     TEMP0,TEMP1,TEMP2,TEMP3,TEMP4,TEMP5,TEMP6,TEMP7,TEMP8,TEM
     P9
      REAL(8) XA(20,4),XB(7,4),XC(9,4),TEMP10
      DO 30 I=1,4
      DO 10 I1=-1,1
      UJ(I1)=UWCK_2(J+I1,I*3-2)
      CJ(I1)=UWCK_2(J+I1,I*3)
10    ONTINUE
      DO 15 I1=-2,2
      WJ(I1)=UWCK_2(J+I1,I*3-1)
      W0(I1)=W_INI(J+I1)
15    CONTINUE
```

```
IF((IMP_TYPE.EQ.1).AND.(BND_TYPE.EQ.1)) THEN
        IF(J.EQ.0) THEN
                UJ(-1)=-UJ(1)
                CJ(-1)=-CJ(1)
                UJ(0)=0.0
                CJ(0)=0.0
                WJ(-2)=WJ(2)
                WJ(-1)=WJ(1)
                WJ(0)=0.0
                W0(-2)=W0(2)
                W0(-1)=W0(1)
        ELSEIF(J.EQ.NX_STEP) THEN
                UJ(1)=-UJ(-1)
                CJ(1)=-CJ(-1)
                CJ(0)=0.0
                WJ(2)=WJ(-2)
                WJ(1)=WJ(-1)
                WJ(0)=0.0
                W0(2)=W0(-2)
                W0(1)=W0(-1)
        ELSEIF(J.EQ.1) THEN
                UJ(-1)=0.0
                CJ(-1)=0.0
                WJ(-2)=WJ(0)
                WJ(-1)=0.0
                W0(-2)=W0(0)
                W0(-1)=0.0

        ELSEIF(J.EQ.NX_STEP-1) THEN
                WJ(2)=WJ(0)
                WJ(1)=0.0
                W0(2)=W0(0)
                W0(1)=0.0
        ENDIF
ENDIF
IF((IMP_TYPE.EQ.1).AND.(BND_TYPE.EQ.2)) THEN
        IF(J.EQ.0) THEN
                UJ(-1)=-UJ(1)
                CJ(-1)=CJ(1)
                WJ(-2)=2.0*WJ(0)-WJ(2)
                WJ(-1)=2.0*WJ(0)-WJ(1)
                W0(-2)=2.0*W0(0)-W0(2)
                W0(-1)=2.0*W0(0)-W0(1)
```

```
        ELSEIF(J.EQ.NX_STEP) THEN
                CJ(1)=CJ(-1)
                WJ(2)=2.0*WJ(0)-WJ(-2)
                WJ(1)=2.0*WJ(0)-WJ(-1)
                W0(2)=2.0*W0(0)-W0(-2)
                W0(1)=2.0*W0(0)-W0(-1)
        ELSEIF(J.EQ.1) THEN
                WJ(-2)=2.0*WJ(-1)-WJ(0)
                W0(-2)=2.0*W0(-1)-W0(0)
        ELSEIF(J.EQ.NX_STEP-1) THEN
                WJ(2)=2.0*WJ(1)-WJ(0)
                W0(2)=2.0*W0(1)-W0(0)
        ENDIF
ENDIF
IF((IMP_TYPE.EQ.2).AND.(BND_TYPE.EQ.1)) THEN
        IF(J.EQ.0) THEN
                UJ(-1)=-UJ(1)
                CJ(-1)=-CJ(1)
                UJ(0)=0.0
                CJ(0)=0.0
                WJ(-2)=WJ(2)
                WJ(-1)=WJ(1)
                WJ(0)=0.0
                W0(-2)=W0(2)
                W0(-1)=W0(1)
        ELSEIF(J.EQ.NX_STEP) THEN
                CJ(1)=-CJ(-1)
                CJ(0)=0.0
                WJ(2)=WJ(-2)
                WJ(1)=WJ(-1)
                W0(2)=W0(-2)
                W0(1)=W0(-1)
        ELSEIF(J.EQ.1) THEN
                UJ(-1)=0.0
                CJ(-1)=0.0
                WJ(-2)=WJ(0)
                WJ(-1)=0.0
                W0(-2)=W0(0)
                W0(-1)=0.0

        ELSEIF(J.EQ.NX_STEP-1) THEN
                WJ(2)=WJ(0)
                WJ(1)=0.0
                W0(2)=W0(0)
```

```
                W0(1)=0.0
            ENDIF
        ENDIF
        IF((IMP_TYPE.EQ.2).AND.(BND_TYPE.EQ.2)) THEN
            IF(J.EQ.0) THEN
                UJ(-1)=-UJ(1)
                CJ(-1)=CJ(1)
                WJ(-2)=2.0*WJ(0)-WJ(2)
                WJ(-1)=2.0*WJ(0)-WJ(1)
                W0(-2)=2.0*W0(0)-W0(2)
                W0(-1)=2.0*W0(0)-W0(1)
            ELSEIF(J.EQ.NX_STEP) THEN
                CJ(1)=CJ(-1)
                WJ(2)=2.0*WJ(0)-WJ(-2)
                WJ(1)=2.0*WJ(0)-WJ(-1)
                W0(2)=2.0*W0(0)-W0(-2)
                W0(1)=2.0*W0(0)-W0(-1)
            ELSEIF(J.EQ.1) THEN
                WJ(-2)=2.0*WJ(-1)-WJ(0)
                W0(-2)=2.0*W0(-1)-W0(0)
            ELSEIF(J.EQ.NX_STEP-1) THEN
          WJ(2)=2.0*WJ(1)-WJ(0)
                W0(2)=2.0*W0(1)-W0(0)
            ENDIF
        ENDIF
    IF (K.EQ.1) THEN
        UK_1=UWCK_2(J,I*3-2)
        WK_1=UWCK_2(J,I*3-1)
        CK_1=UWCK_2(J,I*3)
        ELSE
        UK_1=UWCK_1(J,I*3-2)
        WK_1=UWCK_1(J,I*3-1)
        CK_1=UWCK_1(J,I*3)
        ENDIF
        XA(1,I)=(UJ(1)-UJ(-1))/(2.0*GX)
        XA(2,I)=(UJ(1)-2*UJ(0)+UJ(-1))/(GX*GX)
        XA(3,I)=(WJ(1)-WJ(-1))/(2.0*GX)
        XA(4,I)=(WJ(1)-2*WJ(0)+WJ(-1))/(GX*GX)
        XA(5,I)=(W0(1)-W0(-1))/(2.0*GX)
        XA(6,I)=(W0(1)-2*W0(0)+W0(-1))/(GX*GX)
        XA(7,I)=(CJ(1)-CJ(-1))/(2.0*GX)
        XA(8,I)=(CJ(1)-2*CJ(0)+CJ(-1))/(GX*GX)
        XA(9,I)=-2.0*UJ(0)+UK_1
        XA(10,I)=-2.0*WJ(0)+WK_1
```

```
      XA(11,I)=-2.0*CJ(0)+CK_1
      XA(12,I)=CJ(0)
      XA(13,I)=(WJ(2)-2*WJ(1)+2*WJ(-1)-WJ(-2))/(2*GX**3)
      XA(14,I)=(W0(2)-2*W0(1)+2*W0(-1)-W0(-2))/(2*GX**3)
      XA(15,I)=4.0*E(1,1)/(3.0*A(1,1)*A_LEN*H_THK**2)
      XA(16,I)=4.0*G(2,2)/(A(1,1)*H_THK**2)
      XA(17,I)=4.0*H(1,1)/(3.0*A_LEN*H_THK**2)
      XA(18,I)=A(1,1)*DI2/DI1
      XA(19,I)=A_LEN*(F(2,2)-4.0*G(2,2)/H_THK**2)
      XA(20,I)=4.0*G(2,2)/(H_THK**2)
      XB(1,I)=XA(2,I)+XA(3,I)*XA(4,I)-XA(5,I)*XA(6,I)
      XB(2,I)=XA(8,I)+XA(13,I)-XA(14,I)
      XB(3,I)=-XA(12,I)+XA(5,I)
      XB(4,I)=-XA(7,I)+XA(6,I)
      XB(5,I)=XA(7,I)+XA(4,I)-XA(6,I)
      XB(6,I)=XA(12,I)+XA(3,I)-XA(5,I)
      XB(7,I)=XA(1,I)+0.5*XA(3,I)*XA(3,I)-0.5*XA(5,I)*XA(5,I)
      XC(1,I)=B(1,1)/(A(1,1)*A_LEN)
      XC(2,I)=F(2,2)/A(1,1)
      XC(3,I)=B(1,1)*A_LEN
      XC(4,I)=D(1,1)
      XC(5,I)=F(2,2)*A_LEN**2
      XC(6,I)=XA(20,I)*A_LEN**2
      XC(7,I)=((UJ(0)-UK_1)/HT)*CL*SQRT(A(1,1)/DI1)*A_LEN/A(1,1)
      XC(8,I)=((WJ(0)-WK_1)/HT)*CT*SQRT(A(1,1)/DI1)*A_LEN/A(1,1)
      XC(9,I)=((CJ(0)-CK_1)/HT)*CR*A_LEN/(SQRT(A(1,1)/DI1)*DI2)
30    CONTINUE
      END

      SUBROUTINE BND_INI
      INCLUDE 'COMMON.INC'
      IF (IMP_TYPE.EQ.1) THEN
      V_END=VEL_0
      SELECT CASE (BND_TYPE)
      CASE (1)
        DO 111 I=1,12
111     UWC(0,I)=0.0
            DO 112 I=1,NX_STEP
        DO 112 J=0,3
        UWC(I,3*J+1)=0.0
        UWC(I,3*J+2)=W_INI(I)
            IF(I.EQ.NX_STEP) THEN
                  UWC(I,3*J+3)=0.0
            ELSE
```

```
                UWC(I,3*J+3)=0.0
            ENDIF
112         CONTINUE
        CASE (2)
            DO 122 I=0,NX_STEP
          DO 122 J=0,3
          UWC(I,3*J+1)=0.0
          UWC(I,3*J+2)=W_INI(I)
            IF(I.EQ.0) THEN
              UWC(I,3*J+3)=(W_INI(I)-W_INI(I+1))/GX
            ELSEIF(I.EQ.NX_STEP) THEN
              UWC(I,3*J+3)=(W_INI(I-1)-W_INI(I))/GX
            ELSE
              UWC(I,3*J+3)=(W_INI(I-1)-W_INI(I+1))/(2*GX)
            ENDIF
122         CONTINUE
        END SELECT
        ELSEIF (IMP_TYPE.EQ.2) THEN
        SELECT CASE (BND_TYPE)
        CASE (1)
          DO 211 I=1,12
211       UWC(0,I)=0.0
            DO 212 I=1,NX_STEP
          DO 212 J=0,3
          UWC(I,3*J+1)=0.0
          UWC(I,3*J+2)=W_INI(I)
            IF(I.EQ.NX_STEP) THEN
                UWC(I,3*J+3)=0.0
            ELSE
                UWC(I,3*J+3)=(W_INI(I-1)-W_INI(I+1))/(2*GX)
            ENDIF
212         CONTINUE
        CASE (2)
            DO 222 I=0,NX_STEP
          DO 222 J=0,3
          UWC(I,3*J+1)=0.0
          UWC(I,3*J+2)=W_INI(I)
            IF(I.EQ.0) THEN
              UWC(I,3*J+3)=(W_INI(I)-W_INI(I+1))/GX
            ELSEIF(I.EQ.NX_STEP) THEN
              UWC(I,3*J+3)=(W_INI(I-1)-W_INI(I))/GX
            ELSE
              UWC(I,3*J+3)=(W_INI(I-1)-W_INI(I+1))/(2*GX)
            ENDIF
```

```
222          CONTINUE
      END SELECT
      ELSEIF (IMP_TYPE.EQ.3) THEN
      SELECT CASE (BND_TYPE)
      CASE (1)
      CASE (2)
      CASE (3)
      CASE (4)
      CASE (5)
      END SELECT
      ENDIF
      END

      SUBROUTINE NON_DIMENSION
      INCLUDE 'COMMON.INC'
      REAL(8) C
      C=SQRT(A(1,1)/DI1)
      GX=1.0/NX_STEP
      HT=T_END/NT_STEP
      HT=C*HT/A_LEN
      W_INI=W_INI/A_LEN
      VEL_0=VEL_0/C
      END

      SUBROUTINE LEFTENDU(I,K)
      INCLUDE 'COMMON.INC'
     REAL(8) TEMP1,TEMP2,TEMP3
      SELECT CASE (IMP_TYPE)
      CASE (1)
      IF (K.EQ.1) THEN
            TEMP1=V_END*HT
            TEMP2=0.5*HT*B_WID*DI1*A_LEN/MASS
            UWC(NX_STEP,I*3-2)=TEMP1*(1.0-TEMP2)
      ELSE
        IF(ICONTACT.EQ.1) THEN
            TEMP1=DI1*A_LEN*B_WID*HT*HT/(MASS*GX)
            TEMP2=-UWCK_2(NX_STEP,I*3-2)+UWCK_2(NX_STEP-1,I*3-2)
            IF(TEMP2.GT.0.0) THEN
            TEMP3=2.0*UWCK_2(NX_STEP,I*3-2)-UWCK_1(NX_STEP,I*3-2)
                        UWC(NX_STEP,I*3-2)=TEMP3+TEMP1*TEMP2
      ELSE
            ICONTACT=0
      ENDIF
      ENDIF
```

```
    IF(ICONTACT.EQ.0) THEN
          UWC(NX_STEP+1,I*3-2)=UWC(NX_STEP-1,I*3-2)
          UWC(NX_STEP,I*3-2)=UWC(NX_STEP-1,I*3-2)
     ENDIF
    ENDIF
    CASE (2)
   ALL FORCE_TIME(K,FORCE)
    TEMP1=2.0*(FORCE/(A(1,1)*B_WID))*GX
    UWC(NX_STEP+1,I*3-2)=TEMP1+UWC(NX_STEP-1,I*3-2)
    END SELECT
    END
    SUBROUTINE FORCE_TIME(ITSTEP,FORC)
    INCLUDE 'COMMON.INC'
    REAL(8) STIFF,PI,OMEGA,T,DELTA_T,TIME,FORC,C
    ELECT CASE (IFORCE)
    CASE (1)
          DELTA_T=T_END/NT_STEP
          TIME=ITSTEP*DELTA_T
          IF(TIME.GE.F_DUR) THEN
                FORC=0.0
          ELSE
        FORC=F_MAG
          ENDIF
    CASE (2)
          PI=3.141592654
          STIFF=A(1,1)*B_WID/A_LEN
          OMEGA=SQRT(STIFF/MASS)
          T=PI/OMEGA
          DELTA_T=T_END/NT_STEP
          TIME=ITSTEP*DELTA_T
          IF(TIME.GE.T) THEN
                FORC=0.0
          ELSE
        C=SQRT(A(1,1)/DI1)
        X=((VEL_0*C)/OMEGA)*SIN(OMEGA*TIME)
                FORC=STIFF*X
          ENDIF
    END SELECT
END


        REAL(8) A(3,3),B(3,3),D(3,3),E(3,3),F(2,2),G(2,2),H(3,3),DI1,DI2
        REAL(8) FORCE,FORCE_T(0:20000),F_TIME(0:20000),F_MAG, F_DUR
        REAL(8) VEL(0:20),V_TIME(0:20)
```

```
      REAL(8) UWC(-2:2501,1:12),UWCK_1(-2:2501,1:12),UWCK_2(-
2:2501,1:12)
      REAL(8) V_END,UMK_2(4),W_INI(-2:2501)
      REAL(8)
L_ANG(0:48),L_MAT(50),MAT(0:48,10),MASS,BETA,X_STR(0:20)
&          INTEGER, BND_TYPE,IMP_TYPE,NX_OUT_STEP,NT_OUT_STEP,
&          IFORCE,ICONTACT
     REAL(8) A_LEN,B_WID,H_THK,HZ(48),VEL_0
      REAL(8) CIL,CIT,CIR,CL,CT,CR
      COMMON/ELAS1/A,B,D,E,F,G,H,DI1,DI2
      COMMON/IMPLOAD/FORCE,FORCE_T,F_TIME,VEL,V_TIME,F_MAG,
&                F_DUR
      COMMON/DVA/UWC,UWCK_1,UWCK_2,V_END,UMK_2,W_INI
      COMMON/STACK/L_ANG,L_MAT,MAT,MASS,BETA,X_STR
      COMMON/BNDINI/BND_TYPE,IMP_TYPE,IFORCE,ICONTACT
      COMMON/OUTCTL/NX_OUT_STEP,NT_OUT_STEP,N_STR
      COMMON/ANA/NX_STEP,NT_STEP,T_END,GX,HT
      COMMON/GEO/MM,NN,A_LEN,B_WID,H_THK,HZ,VEL_0,N_FSTEPS
      COMMON/FILE1/IFINP,IFDIS,IFVEL,IFACC,IFSTS,IFSTR,IFCMP,
     &                  IFOUT
      COMMON/FILE2/IFFU1,IFFW1,IFFC1,IFFU2,IFFW2,IFFC2
      COMMON/FILE3/IFHU1,IFHW1,IFHC1,IFHU2,IFHW2,IFHC2
      COMMON/FILE4/IFFC,IFHC,IPOS
      COMMON/OTHERS01/N_STACK,Q0,LAYERS
      COMMON/DAMPING/CIL,CIT,CIR,CL,CT,CR

SUBROUTINE SOLVE
INCLUDE 'COMMON.INC'
INTEGER status, INDEX_DLM
REAL(8) XA(19),XB(7),XC(3),Q(3,3),QQ(2,2),GRF(4)
REAL(8) DGROTHB,DGROTHE,DGROTHT
NX=INT((NX_STEP-1)/NX_OUT_STEP)+1
NT=INT((NT_STEP-1)/NT_OUT_STEP)+1
NOUT=4*(LAYERS+1)
NOUTF=2*LAYERS-1
TEMP_W=0.0
UWC=0.0
UWCK_1=0.0
UWCK_2=0.0
UWC_S=0.0
UWCK_1_S=0.0
UWCK_2_S=0.0
UJK_1=0.0
GX=A_LEN/NX_STEP
```

```
      HT=T_END/NT_STEP
      H2=HT**2
      ICONTACT=1
      IPF=1
      IF(MOD(LAYERS,2).EQ.0) THEN
            LAYERS_HALF=LAYERS/2
      ELSE
        LAYERS_HALF=0
      ENDIF
      CALL BND_INI
      N=NT_STEP
      M=NX_STEP
      IB=0
      DO 10 JJ=0,NX-1
      DO 10 I=1,3
      IF(I.EQ.2) THEN
      UWC_OUT(JJ,I)=UWC(JJ*NX_OUT_STEP,I)-W_INI(JJ*NX_OUT_STEP)
            UWC_OUT_S(JJ,I)=UWC(JJ*NX_OUT_STEP,I)-
      W_INI(JJ*NX_OUT_STEP)
      ELSE
        UWC_OUT(JJ,I)=UWC(JJ*NX_OUT_STEP,I)
            UWC_OUT_S(JJ,I)=UWC(JJ*NX_OUT_STEP,I)
      ENDIF
10    CONTINUE
       DO 15 I=1,3
      UWC_OUT(NX,I)=UWC(NX_STEP,I)
15    UWC_OUT_S(NX,I)=UWC_S(NX_STEP,I)
      J_DLM_B=INT(X_DLM/GX)+1
      J_DLM_L=INT(XL_DLM/GX)+1
      J_DLM_E=J_DLM_B+J_DLM_L
      J_DLM_B1=J_DLM_B
      J_DLM_E1=J_DLM_E
      WRITE(IFDLM,*) ' CTIME J_DLM_B J_DLM_E J_DLM_L'
      CALL WRITETITLES()
      DO 22 K=1,N
      UMK_2(1)=UWCK_1(NX_STEP,1)
     UWCK_1=UWCK_2
      UWCK_2=UWC
      UWCK_1_S=UWCK_2_S
      UWCK_2_S=UWC_S
      RATIOB=0.0
      RATIOE=0.0
      INDEX_DLM=0
      DO 20 J=IB,M
```

```
      IF(J.GE.J_DLM_E) THEN
            CALL X_ABC(J,K,XA,XB,XC,1)
            CALL UWCM(J,K,XA,XB,XC,1)
            CALL UWCSM(J)
      ELSEIF(J.LE.J_DLM_B) THEN
            CALL X_ABC(J,K,XA,XB,XC,4)
            CALL UWCM(J,K,XA,XB,XC,4)
            CALL UWCSM(J)
      ELSE
            CALL X_ABC(J,K,XA,XB,XC,2)
            CALL UWCM(J,K,XA,XB,XC,2)
            CALL X_ABC(J,K,XA,XB,XC,3)
            CALL UWCS(J,K,XA,XB,XC,3)
     IF(UWC_S(J,2).GT.UWC(J,2)) THEN
                  DLT=UWC_S(J,2)-UWC(J,2)
                  DLTS=DLT*DM(1,1)/(DS(1,1)+DM(1,1))
                  DLTM=DLT*DS(1,1)/(DS(1,1)+DM(1,1))
                  UWC_S(J,2)=UWC_S(J,2)-DLTS
                  UWC(J,2)=UWC(J,2)+DLTM
            ENDIF
      ENDIF
      IF(J.EQ.0) THEN
      UWC(J,1)=0.0
      UWC_S(J,1)=0.0
      ENDIF
      IF((J.EQ.M).OR.(J.EQ.0)) THEN
      UWC(J,2)=0.0
      UWC_S(J,2)=0.0
      ENDIF
      IF (J.EQ.M) THEN
      CALL LEFTENDU(K)
      ENDIF
20    CONTINUE
      CALL DLM_STRERR(GRF)
      RATIOB=(GRF(1)/GC1)**2+(GRF(2)/GC2)**2
      RATIOE=(GRF(3)/GC1)**2+(GRF(4)/GC2)**2
      IF(RATIOB.GE.1.0) THEN
      J_DLM_B=J_DLM_B-1
      J_DLM_L=J_DLM_L+1
      ENDIF
      IF(RATIOE.GE.1.0) THEN
      J_DLM_E=J_DLM_E+1
      J_DLM_L=J_DLM_L+1
      ENDIF
```

```
      IF((RATIOB.GE.1.0).OR.(RATIOE.GE.1.0)) THEN
            INDEX_DLM=1
      ENDIF
      CTIME=K*HT
      DGROTHB=(J_DLM_B1-J_DLM_B)*GX
      DGROTHE=(J_DLM_E-J_DLM_E1)*GX
      DGROTHT=DGROTHE+DGROTHB
      IF((MOD(K,10).EQ.0).OR.(INDEX_DLM.EQ.1)) THEN
            WRITE(IFVEL,23) GRF(1),GRF(2),GRF(3),GRF(4)
            WRITE(IFDLM,21) CTIME, J_DLM_B, J_DLM_E, J_DLM_L,
                              RATIOB,RATIOE,
     &      DGROTHB,DGROTHE,DGROTHT
21          FORMAT(E14.5E3, 3I8, 5F14.7)
      ENDIF
      IF(INDEX_DLM.EQ.1) THEN
            CALL WRTDLMFM(K)
      ENDIF
      IF (MOD(K,NT_OUT_STEP).EQ.0) THEN
            CALL WRTOUT(K,M,NX,NT)
      ENDIF
22    CONTINUE
23    FORMAT(4E14.5E3)
      DO I=1,25
      CLOSE(I)
      ENDDO
      END


      SUBROUTINE X_ABC(J,K,XA,XB,XC,IDLM)
      INCLUDE 'COMMON.INC'
      REAL(8) UJ(-1:1),CJ(-1:1),WJ(-2:2),W0(-2:2),UK_1,WK_1,CK_1
      REAL(8) XA(17),XB(7),XC(3)
      REAL(8) TE,TF,TG,TH,TH_THK
      XA=0.0
      XB=0.0
      XC=0.0
      CALL DAMP_MS(IDLM)
      SELECT CASE (IDLM)
      CASE (1)
            DO 10 I1=-1,1
            UJ(I1)=UWCK_2(J+I1,1)
            CJ(I1)=UWCK_2(J+I1,3)
10        CONTINUE
            DO 15 I1=-2,2
```

```
                WJ(I1)=UWCK_2(J+I1,2)
                W0(I1)=W_INI(J+I1)
15              CONTINUE
          IF(J.EQ.J_DLM_E+1) THEN
                      WJ(-2)=UWCK_2(J-2,2)*DM(1,1)/(DM(1,1)+DS(1,1))
     &          +UWCK_2_S(J-2,2)*DS(1,1)/(DM(1,1)+DS(1,1))
                ELSEIF(J.EQ.J_DLM_E) THEN
              UJ(-1)=UWCK_2(J-1,1)*AM(1,1)/(AM(1,1)+AS(1,1))
     &          +UWCK_2_S(J-1,1)*AS(1,1)/(AM(1,1)+AS(1,1))
              CJ(-1)=UWCK_2(J-1,3)*DIM2/(DIM2+DIS2)
     &          +UWCK_2_S(J-1,3)*DIS2/(DIM2+DIS2)
                      WJ(-1)=UWCK_2(J-1,2)*DM(1,1)/(DM(1,1)+DS(1,1))
     &          +UWCK_2_S(J-1,2)*DS(1,1)/(DM(1,1)+DS(1,1))
                      WJ(-2)=UWCK_2(J-2,2)*DM(1,1)/(DM(1,1)+DS(1,1))
     &          +UWCK_2_S(J-2,2)*DS(1,1)/(DM(1,1)+DS(1,1))
        ENDIF
                TE=E(1,1)
                TF=F(2,2)
                TG=G(2,2)
                TH=H(1,1)
                TH_THK=H_THK
         CASE (2)
                DO 20 I1=-1,1
                UJ(I1)=UWCK_2(J+I1,1)
                CJ(I1)=UWCK_2(J+I1,3)
20              CONTINUE
                DO 25 I1=-2,2
                WJ(I1)=UWCK_2(J+I1,2)
                W0(I1)=W_INI(J+I1)
25              CONTINUE

                TE=EM(1,1)
                TF=FM(2,2)
                TG=GM(2,2)
                TH=HM(1,1)
                TH_THK=H_THK*(1.0-LAY_DLM/LAYERS)
         CASE (3)
                DO 30 I1=-1,1
                UJ(I1)=UWCK_2_S(J+I1,1)
                CJ(I1)=UWCK_2_S(J+I1,3)
30          CONTINUE
                DO 35 I1=-2,2
                WJ(I1)=UWCK_2_S(J+I1,2)
                W0(I1)=W_INI(J+I1)
```

```
35              CONTINUE
                TE=ES(1,1)
                TF=FS(2,2)
                TG=GS(2,2)
                TH=HS(1,1)
                TH_THK=H_THK*LAY_DLM/LAYERS
        CASE (4)
                DO 40 I1=-1,1
                UJ(I1)=UWCK_2(J+I1,1)
                CJ(I1)=UWCK_2(J+I1,3)
40              CONTINUE
                DO 45 I1=-2,2
                WJ(I1)=UWCK_2(J+I1,2)
                W0(I1)=W_INI(J+I1)
45              CONTINUE
                IF(J.EQ.J_DLM_B-1) THEN
                        WJ(2)=UWCK_2(J+2,2)*DM(1,1)/(DM(1,1)+DS(1,1))
     &           +UWCK_2_S(J+2,2)*DS(1,1)/(DM(1,1)+DS(1,1))
                ELSEIF(J.EQ.J_DLM_B) THEN
               UJ(1)=UWCK_2(J+1,1)*AM(1,1)/(AM(1,1)+AS(1,1))
     &           +UWCK_2_S(J+1,1)*AS(1,1)/(AM(1,1)+AS(1,1))
               CJ(1)=UWCK_2(J+1,3)*DIM2/(DIM2+DIS2)
     &           +UWCK_2_S(J+1,3)*DIS2/(DIM2+DIS2)
                        WJ(1)=UWCK_2(J+1,2)*DM(1,1)/(DM(1,1)+DS(1,1))
     &           +UWCK_2_S(J+1,2)*DS(1,1)/(DM(1,1)+DS(1,1))
                        WJ(2)=UWCK_2(J+2,2)*DM(1,1)/(DM(1,1)+DS(1,1))
     &           +UWCK_2_S(J+2,2)*DS(1,1)/(DM(1,1)+DS(1,1))
       ENDIF
                TE=E(1,1)
                TF=F(2,2)
                TG=G(2,2)
                TH=H(1,1)
                TH_THK=H_THK
        END SELECT
        IF(J.EQ.0) THEN
                UJ(-1)=-UJ(1)
                CJ(-1)=-CJ(1)
                UJ(0)=0.0
                CJ(0)=0.0
                WJ(-2)=WJ(2)
                WJ(-1)=WJ(1)
                WJ(0)=0.0
                W0(-2)=W0(2)
                W0(-1)=W0(1)
```

```
ELSEIF(J.EQ.NX_STEP) THEN
        UJ(1)=-UJ(-1)
        CJ(1)=-CJ(-1)
        CJ(0)=0.0
        WJ(2)=WJ(-2)
        WJ(1)=WJ(-1)
        WJ(0)=0.0
        W0(2)=W0(-2)
        W0(1)=W0(-1)
ELSEIF(J.EQ.1) THEN
        UJ(-1)=0.0
        CJ(-1)=0.0
  WJ(-2)=WJ(0)
  WJ(-1)=0.0
        W0(-2)=W0(0)
        W0(-1)=0.0
ELSEIF(J.EQ.NX_STEP-1) THEN
  WJ(2)=WJ(0)
        WJ(1)=0.0
        W0(2)=W0(0)
        W0(1)=0.0
ENDIF
 IF (K.EQ.1) THEN
        UK_1=UWCK_2(J,1)
        WK_1=UWCK_2(J,2)
        CK_1=UWCK_2(J,3)
ELSEIF(IDLM.EQ.3) THEN
        UK_1=UWCK_1_S(J,1)
        WK_1=UWCK_1_S(J,2)
        CK_1=UWCK_1_S(J,3)
ELSE
        UK_1=UWCK_1(J,1)
        WK_1=UWCK_1(J,2)
        CK_1=UWCK_1(J,3)
ENDIF
XA(1)=(UJ(1)-UJ(-1))/(2.0*GX)
XA(2)=(UJ(1)-2*UJ(0)+UJ(-1))/(GX*GX)
XA(3)=(WJ(1)-WJ(-1))/(2.0*GX)
XA(4)=(WJ(1)-2*WJ(0)+WJ(-1))/(GX*GX)
XA(5)=(W0(1)-W0(-1))/(2.0*GX)
XA(6)=(W0(1)-2*W0(0)+W0(-1))/(GX*GX)
XA(7)=(CJ(1)-CJ(-1))/(2.0*GX)
XA(8)=(CJ(1)-2*CJ(0)+CJ(-1))/(GX*GX)
XA(9)=-2.0*UJ(0)+UK_1
```

```
XA(10)=-2.0*WJ(0)+WK_1
XA(11)=-2.0*CJ(0)+CK_1
XA(12)=CJ(0)
XA(13)=(WJ(2)-2*WJ(1)+2*WJ(-1)-WJ(-2))/(2*GX**3)
XA(14)=(W0(2)-2*W0(1)+2*W0(-1)-W0(-2))/(2*GX**3)
XA(15)=4.0*BETA*TE/(3.0*TH_THK**2)
XA(16)=TF-4.0*TG*BETA/TH_THK
XA(17)=4.0*TH*BETA/(3.0*TH_THK**2)
XB(1)=XA(2)+XA(3)*XA(4)-XA(5)*XA(6)
XB(2)=XA(8)+XA(13)-XA(14)
XB(3)=-XA(12)+XA(5)
XB(4)=-XA(7)+XA(6)
XB(5)=XA(7)+XA(4)-XA(6)
XB(6)=XA(12)+XA(3)-XA(5)
XB(7)=XA(1)+0.5*XA(3)*XA(3)-0.5*XA(5)*XA(5)
XC(1)=((UJ(0)-UK_1)/HT)*CL
XC(2)=((WJ(0)-WK_1)/HT)*CT
XC(3)=((CJ(0)-CK_1)/HT)*CR
END

SUBROUTINE UWCM(J,K,XA,XB,XC,IDLM)
INCLUDE 'COMMON.INC'
REAL(8) XA(19),XB(7),XC(3)
SELECT CASE (IDLM)
CASE (1)
        TA=A(1,1)
        TB=B(1,1)
        TD=D(1,1)
        TDI1=DI1
        TDI2=DI2
CASE (4)
       TA=A(1,1)
        TB=B(1,1)
        TD=D(1,1)
        TDI1=DI1
        TDI2=DI2
CASE (2)
        TA=AM(1,1)
        TB=BM(1,1)
        TD=DM(1,1)
        TDI1=DIM1
        TDI2=DIM2
END SELECT
```

```
      UWC(J,1)=((TA*XB(1)+TB*XA(8)-XA(15)*XB(2)-XC(1))/TDI1)*H2-XA(9)
      UWC(J,2)=(((TA*XB(1)+TB*XA(8)-XA(15)*XB(2))*XB(3)
     &     +(TA*XB(7)+TB*XA(7)-XA(15)*XB(5))*XB(4)
     &     +XA(16)*XB(5)-XC(2))/TDI1)*H2-XA(10)
      UWC(J,3)=((TB*XB(1)+TD*XA(8)-XA(17)*XB(2)-XA(16)*XB(6)-XC(3))
     &    /TDI2)*H2-XA(11)
      END

      SUBROUTINE UWCS(J,K,XA,XB,XC,IDLM)
      INCLUDE 'COMMON.INC'
      REAL(8) XA(19),XB(7),XC(3)
      SELECT CASE (IDLM)
      CASE (3)
      TA=AS(1,1)
            TB=BS(1,1)
            TD=DS(1,1)
            TDI1=DIS1
            TDI2=DIS2
      END SELECT
      UWC_S(J,1)=((TA*XB(1)+TB*XA(8)-XA(15)*XB(2)-XC(1))/TDI1)*H2-XA(9)
      UWC_S(J,2)=(((TA*XB(1)+TB*XA(8)-XA(15)*XB(2))*XB(3)
     &     +(TA*XB(7)+TB*XA(7)-XA(15)*XB(5))*XB(4)
     &     +XA(16)*XB(5)-XC(2))/TDI1)*H2-XA(10)
      UWC_S(J,3)=((TB*XB(1)+TD*XA(8)-XA(17)*XB(2)-XA(16)*XB(6)-XC(3))
     &    /TDI2)*H2-XA(11)
      END
      SUBROUTINE UWCSM(J)
      INCLUDE 'COMMON.INC'
      INTEGER J1
      DO JI=1,3
            UWC_S(J,JI)=UWC(J,JI)
      ENDDO
      END
      SUBROUTINE WRTOUT(K,M,NX,NT)
      INCLUDE 'COMMON.INC'
      INTEGER JJ,ITEMP
      DO JJ=0,NX-1
      J=JJ*NX_OUT_STEP
      UWC_OUT(JJ,1)=UWC(J,1)
      UWC_OUT(JJ,2)=(UWC(J,2)-W_INI(J))
      UWC_OUT(JJ,3)=UWC(J,3)
      UWC_OUT_S(JJ,1)=UWC_S(J,1)
      UWC_OUT_S(JJ,2)=(UWC_S(J,2)-W_INI(J))
      UWC_OUT_S(JJ,3)=UWC_S(J,3)
```

```
      ENDDO
      J=M
      UWC_OUT(NX,1)=UWC(J,1)
      UWC_OUT(NX,2)=(UWC(J,2)-W_INI(J))
      UWC_OUT(NX,3)=UWC(J,3)

      UWC_OUT_S(NX,1)=UWC_S(J,1)
      UWC_OUT_S(NX,2)=(UWC_S(J,2)-W_INI(J))
      UWC_OUT_S(NX,3)=UWC_S(J,3)
      WRITE(IFHU1,30) (UWC_OUT(JJ,1), JJ=0,NX)
      WRITE(IFHW1,30) (UWC_OUT(JJ,2), JJ=0,NX)
      WRITE(IFHC1,30) (UWC_OUT(JJ,3), JJ=0,NX)
      WRITE(IFHU2,30) (UWC_OUT_S(JJ,1), JJ=0,NX)
      WRITE(IFHW2,30) (UWC_OUT_S(JJ,2), JJ=0,NX)
      WRITE(IFHC2,30) (UWC_OUT_S(JJ,3), JJ=0,NX)
30    FORMAT(201E12.3E3)
      END

      SUBROUTINE WRTDLMFM(K)
      INCLUDE 'COMMON.INC'
      REAL(8) CTIME
      INTEGER JDLM
      CTIME=K*HT
      DO JDLM=0,NX_STEP
            TEMP_W(JDLM)=UWC(JDLM,2)-W_INI(JDLM)
      ENDDO
      WRITE(IFDDM,21) CTIME, (TEMP_W(JDLM),JDLM=0,NX_STEP)
      DO JDLM=0,NX_STEP
            TEMP_W(JDLM)=UWC_S(JDLM,2)-W_INI(JDLM)
      ENDDO
      WRITE(IFDDM,21) CTIME, (TEMP_W(JDLM),JDLM=0,NX_STEP)
21    FORMAT(E14.5E3, 201E12.3E3)
      END

      SUBROUTINE WRITETITLES()
      INCLUDE 'COMMON.INC'
      WRITE(IFSTR,*) 'MicroStrain OutPut'
      WRITE(IFSTS,*) 'Stress Output (MPa)'
      WRITE(IFSTR,46)
46    FORMAT(20X,'First Order Results Shear Deformation',
     &   20X,'Higher Order Shear Deformation Results')
      WRITE(IFSTR,47)
47    FORMAT(20X,'Axial Strain of each layer',
     &   20X,'Shear Strain of Each layer',
```

```
     &     20X,'Axial Strain of each layer',
     &     20X,'Shear Strain of Each layer')
           WRITE(IFSTS,56)
56         FORMAT(20X,'First Order Results Shear Deformation',
     &     20X,'Higher Order Shear Deformation Results')
           WRITE(IFSTS,57)
57         FORMAT(20X,'Axial Stress of each layer',
     &     20X,'Shear Stress of Each layer',
     &     20X,'Axial Stress of each layer',
     &     20X,'Shear Stress of Each layer')
      END

           SUBROUTINE DAMP_MS(IDLM)
           INCLUDE 'COMMON.INC'
           REAL(8) OMEGA_T,OMEGA_L,TH_THK,TA_LEN,TD,TA,TDI1
           SELECT CASE (IDLM)
           CASE (1)
                 TH_THK=H_THK
                 TA_LEN=A_LEN*(1.0-J_DLM_E/NX_STEP)
                 TD=D(1,1)
                 TA=A(1,1)
                 TDI1=DI1
                 CIT1=CIT
                 CIL1=CIL
           CASE (2)
                 TH_THK=H_THK*(1.0-LAY_DLM/LAYERS)
                 TA_LEN=A_LEN*J_DLM_L/NX_STEP
                 TD=DM(1,1)
                 TA=AM(1,1)
                 TDI1=DIM1
                 CIT1=CIT/DR
                 CIL1=CIL/DR
           CASE (3)
                 TH_THK=H_THK*LAY_DLM/LAYERS
                 TA_LEN=A_LEN*J_DLM_L/NX_STEP
                 TD=DS(1,1)
                 TA=AS(1,1)
                 TDI1=DIS1
                 CIT1=CIT/DR
                 CIL1=CIL/DR

           CASE (4)
                 TH_THK=H_THK
                 TA_LEN=A_LEN*J_DLM_B/NX_STEP
```

```
            TD=D(1,1)
            TA=A(1,1)
            TDI1=DI1
            CIT1=CIT
            CIL1=CIL
        END SELECT
        OMEGA_T=4.0*3.14159**2*SQRT((TD)/(MAT(1,7)*TH_THK))/TA_LEN**2
        CT=2.0*CIT1*OMEGA_T*TDI1
        OMEGA_L=SQRT(2.0*TA/(TH_THK*MAT(1,7)))/TA_LEN
        CL=2.0*CIL1*OMEGA_L*TDI1
        CR=0.5*CT
        END

        SUBROUTINE DLM_STRERR(GRF)
        INCLUDE 'COMMON.INC'
        REAL(8) GRF(4),FMI,FMII
        CALL MODE_SEPARATE(FMI,FMII)
        J=J_DLM_B
        FI=DS(1,1)/(DS(1,1)+DM(1,1))
        FIP=2.0*AS(1,1)/(AS(1,1)+AM(1,1))
        FIV=2.0*FS(1,1)/(FS(1,1)+FM(1,1))
        FIW=2.0*DS(1,1)/(DS(1,1)+DM(1,1))
        FFI=25.0
        TEMP01=(UWC(J,1)-UWC(J-2,1))/(2.0*GX)
        TEMP02=(UWC(J,2)-UWC(J-2,2))/(2.0*GX)
        TEMP03=(UWC(J,3)-UWC(J-2,3))/(2.0*GX)
        TEMP04=(W_INI(J)-W_INI(J-2))/(2.0*GX)
        TEMP05=(UWC(J,2)-2*UWC(J-1,2)+UWC(J-2,2))/(GX*GX)
        TEMP06=(W_INI(J)-2*W_INI(J-1)+W_INI(J-2))/(GX*GX)
        TH_THK=H_THK*LAY_DLM/LAYERS
        P1=A(1,1)*(TEMP01+0.5*TEMP02**2-0.5*TEMP04**2)+B(1,1)*TEMP03
     &  -4.0*E(1,1)*BETA*(TEMP03+TEMP05-TEMP06)/(3.0*H_THK**2)
        V1=(F(1,1)-4.0*G(1,1)*BETA/H_THK**2)*(UWC(J-1,3)+TEMP02-TEMP04)
        W1=B(1,1)*(TEMP01+0.5*TEMP02**2-0.5*TEMP04**2)+D(1,1)*TEMP03
     &  -4.0*H(1,1)*BETA*(TEMP03+TEMP05-TEMP06)/(3.0*H_THK**2)
        TH_THK1=0.5*H_THK-H_THK*LAY_DLM/LAYERS
        P1=P1*FIP
        V1=V1*FIV
        W1=W1*FIW
        W1=W1+P1*TH_THK1/FFI
        TEMP01=(UWC(J,1)-UWC(J-1,1))/(1.0*GX)
        TEMP02=(UWC(J,2)-UWC(J-1,2))/(1.0*GX)
        TEMP03=(UWC(J,3)-UWC(J-1,3))/(1.0*GX)
        TEMP04=(W_INI(J)-W_INI(J-1))/(1.0*GX)
```

```
      TEMP15=(UWC(J+1,2)-2*UWC(J,2)+UWC(J-1,2))/(GX*GX)
      TEMP25=(UWC_S(J+1,2)-2*UWC_S(J,2)+UWC_S(J-1,2))/(GX*GX)
      TEMP05=FI*TEMP15+(1.0-FI)*TEMP25
      TEMP06=(W_INI(J+1)-2*W_INI(J)+W_INI(J-1))/(GX*GX)

      P2=A(1,1)*(TEMP01+0.5*TEMP02**2-0.5*TEMP04**2)+B(1,1)*TEMP03
     & -4.0*E(1,1)*BETA*(TEMP03+TEMP05-TEMP06)/(3.0*H_THK**2)
      V2=(F(1,1)-4.0*G(1,1)*BETA/H_THK**2)*(UWC(J,3)+TEMP02-TEMP04)
      W2=B(1,1)*(TEMP01+0.5*TEMP02**2-0.5*TEMP04**2)+D(1,1)*TEMP03
     & -4.0*H(1,1)*BETA*(TEMP03+TEMP05-TEMP06)/(3.0*H_THK**2)
      P2=P2*FIP
      V2=V2*FIV
      W2=W2*FIW
      W2=W2+P2*TH_THK1/FFI
      U3=UWC_S(J+1,1)-UWC(J+1,1)
      U4=UWC_S(J+2,1)-UWC(J+2,1)
      W3=UWC_S(J+1,2)-UWC(J+1,2)
      W4=UWC_S(J+2,2)-UWC(J+2,2)
      C31=FI*UWC_S(J+1,3)+(1.0-FI)*UWC(J+1,3)-UWC(J,3)
      C41=FI*UWC_S(J+2,3)+(1.0-FI)*UWC(J+2,3)
     & -FI*UWC_S(J+1,3)-(1.0-FI)*UWC(J+1,3)
      C3=UWC_S(J+1,3)-UWC(J+1,3)
      C4=UWC_S(J+2,3)-UWC(J+2,3)
      GRF(1)=(abs(V1*W3)+abs(V2*W4)+abs(FMI*(W1*C3+W2*C4)))*0.25/GX
      GRF(2)=(abs(P1*U3)+abs(P2*U4)+abs(FMII*(W1*C31+W2*C41)))*0.25/GX
      TEMP01=(UWC(J+2,1)-UWC(J,1))/(2.0*GX)
      TEMP02=(UWC(J+2,2)-UWC(J,2))/(2.0*GX)
      TEMP03=(UWC(J+2,3)-UWC(J,3))/(2.0*GX)
      TEMP04=(W_INI(J+2)-W_INI(J))/(2.0*GX)
      TEMP05=(UWC(J+2,2)-2*UWC(J+1,2)+UWC(J,2))/(GX*GX)
      TEMP06=(W_INI(J+2)-2*W_INI(J+1)+W_INI(J))/(GX*GX)
      P2=A(1,1)*(TEMP01+0.5*TEMP02**2-0.5*TEMP04**2)+B(1,1)*TEMP03
     & -4.0*E(1,1)*BETA*(TEMP03+TEMP05-TEMP06)/(3.0*H_THK**2)
      V2=(F(1,1)-4.0*G(1,1)*BETA/H_THK**2)*(UWC(J+1,3)+TEMP02-TEMP04)
      W2=B(1,1)*(TEMP01+0.5*TEMP02**2-0.5*TEMP04**2)+D(1,1)*TEMP03
     & -4.0*H(1,1)*BETA*(TEMP03+TEMP05-TEMP06)/(3.0*H_THK**2)
      P2=P2*FIP
      V2=V2*FIV
      W2=W2*FIW
      W2=W2+P2*TH_THK1/FFI
      TEMP01=(UWC(J+1,1)-UWC(J,1))/(1.0*GX)
      TEMP02=(UWC(J+1,2)-UWC(J,2))/(1.0*GX)
      TEMP03=(UWC(J+1,3)-UWC(J,3))/(1.0*GX)
      TEMP04=(W_INI(J+1)-W_INI(J))/(1.0*GX)
```

```
      TEMP15=((UWC(J+1,2)-2*UWC(J,2)+UWC(J-1,2))/(GX*GX))/A_LEN
      TEMP25=((UWC_S(J+1,2)-2*UWC_S(J,2)+UWC_S(J-1,2))/(GX*GX))/A_LEN
      TEMP05=FI*TEMP15+(1.0-FI)*TEMP25
      TEMP06=((W_INI(J+1)-2*W_INI(J)+W_INI(J-1))/(GX*GX))/A_LEN

      P1=A(1,1)*(TEMP01+0.5*TEMP02**2-0.5*TEMP04**2)+B(1,1)*TEMP03
     &  -4.0*E(1,1)*BETA*(TEMP03+TEMP05-TEMP06)/(3.0*H_THK**2)
      V1=(F(1,1)-4.0*G(1,1)*BETA/H_THK**2)*(UWC(J,3)+TEMP02-TEMP04)
      W1=B(1,1)*(TEMP01+0.5*TEMP02**2-0.5*TEMP04**2)+D(1,1)*TEMP03
     &  -4.0*H(1,1)*BETA*(TEMP03+TEMP05-TEMP06)/(3.0*H_THK**2)
      P1=P1*FIP
      V1=V1*FIV
      W1=W1*FIW
      W1=W1+P1*TH_THK1/FFI
      U3=UWC_S(J-2,1)-UWC(J-2,1)
      U4=UWC_S(J-1,1)-UWC(J-1,1)
      W3=UWC_S(J-2,2)-UWC(J-2,2)
      W4=UWC_S(J-1,2)-UWC(J-1,2)
      C31=FI*UWC_S(J-1,3)+(1.0-FI)*UWC(J-1,3)
     &  -FI*UWC_S(J-2,3)-(1.0-FI)*UWC(J-2,3)
      C41=UWC(J,3)-FI*UWC_S(J-1,3)-(1.0-FI)*UWC(J-1,3)
      C3=UWC_S(J-2,3)-UWC(J-2,3)
      C4=UWC_S(J-1,3)-UWC(J-1,3)
      GRF(3)=(abs(V1*W3)+abs(V2*W4)+abs(FMI*(W1*C3+W2*C4)))*0.25/GX
      GRF(4)=(abs(P1*U3)+abs(P2*U4)+abs(FMII*(W1*C31+W2*C41)))*0.25/GX
      END
      SUBROUTINE MODE_SEPARATE(FMI,FMII)
      INCLUDE 'COMMON.INC'
      REAL(8) FMI,FMII
      THKS=H_THK*LAY_DLM/LAYERS
      THKM=H_THK-THKS
      ETA=THKS/H_THK
      EV=1.0/(12.0*(1.0+3.0*ETA**3))
      EU=1.0/(1.0+4*ETA+6*ETA**2+3*ETA**3)
      EOMEGA=3.14159*(52.1-3.0*ETA)/180.0
      EGAMA=ASIN(SQRT(EU*EV)*6.0*ETA**2*(1.0+ETA))
      EA2=SIN(EOMEGA+EGAMA)
      EB2=COS(EOMEGA+EGAMA)
      FMI=EA2/(EA2+EB2)
      FMII=EB2/(EA2+EB2)
      END
```

Appendix D: Typical Test Results of Physical properties

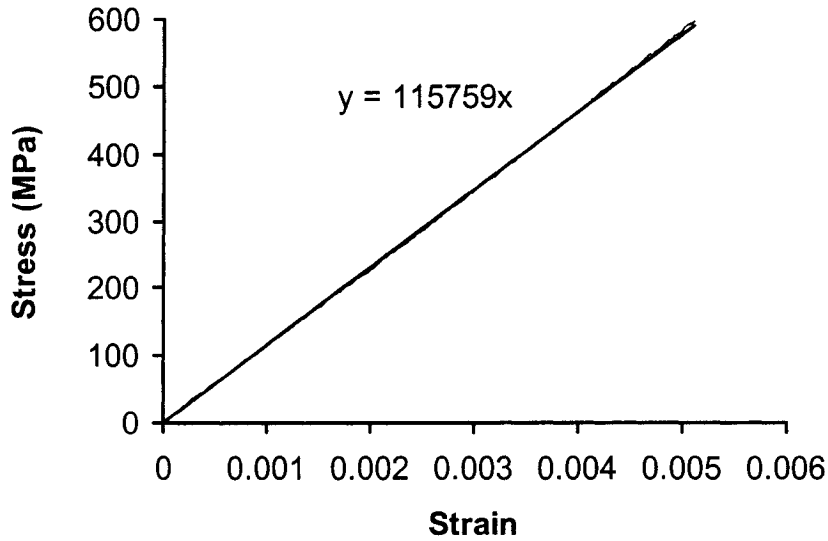

Figure D-1 Typical tensile property E_{11} test results of carbon/epoxy laminate.

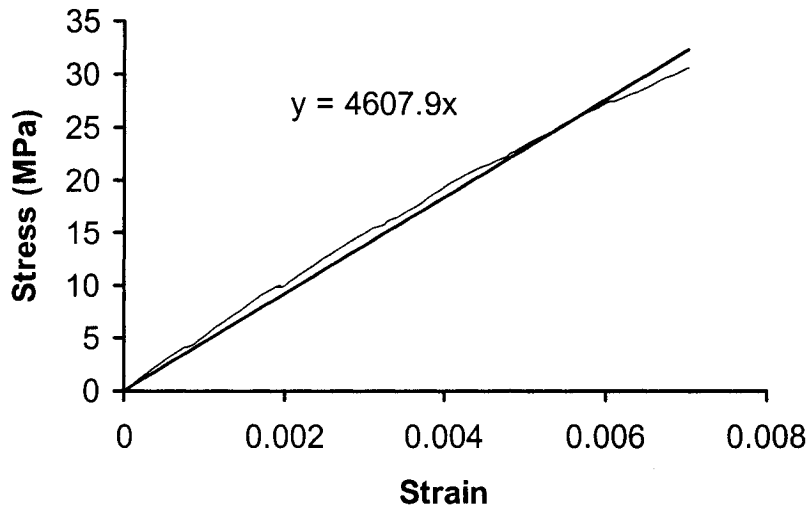

Figure D-2 Typical tensile property E_{22} test results of carbon/epoxy laminate.

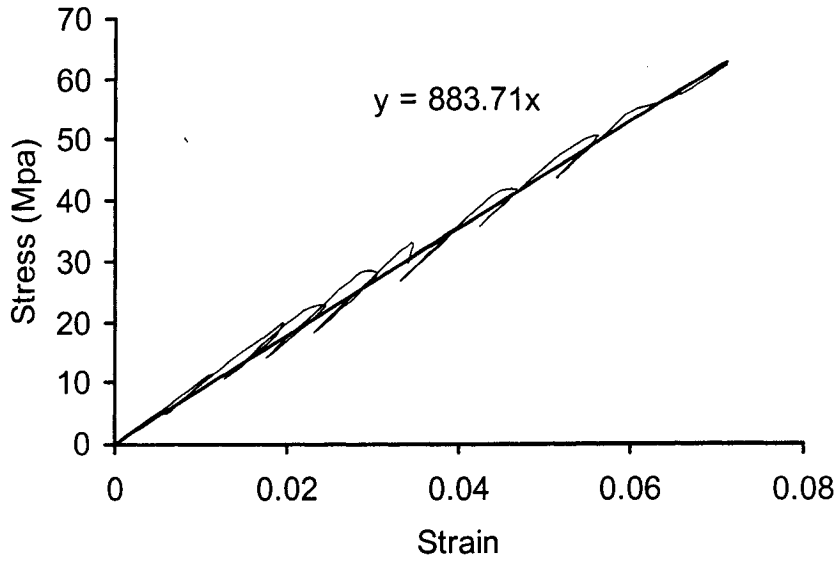

Figure D-3 Typical tensile property G_{12} test results of carbon/epoxy laminate.

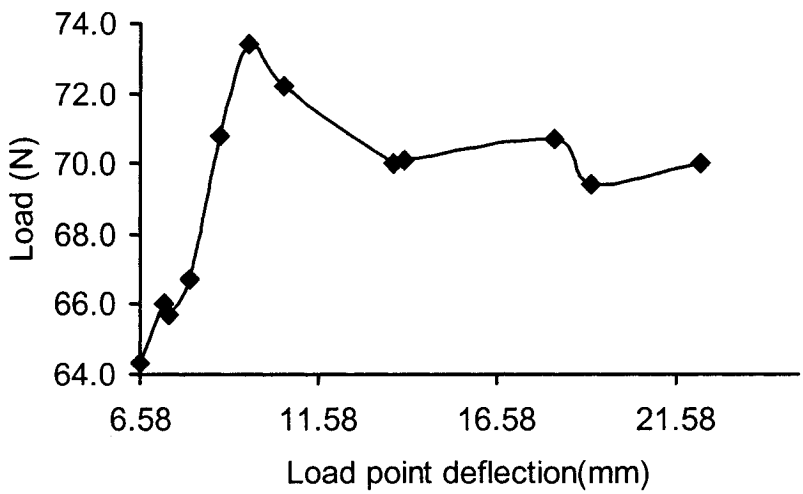

Figure D-4 Typical load deflection curve of double cantilever beam (DCB) for G_{IC} test.

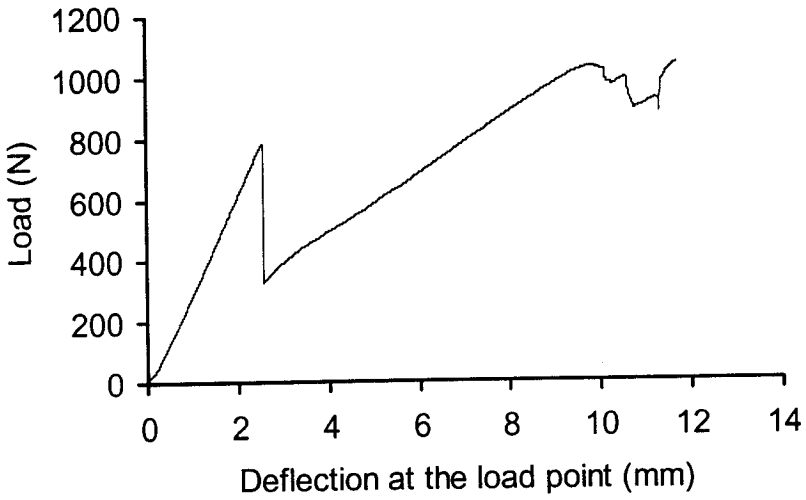

Figure D-5 Typical load deflection curve of end notched flexure (ENF) for G_{IIC} test.